E-ISSN: 2147-1959

MIRT

Molecular Imaging and Radionuclide Therapy

June 2022 Volume 31 Issue 2 www.tsnm.org

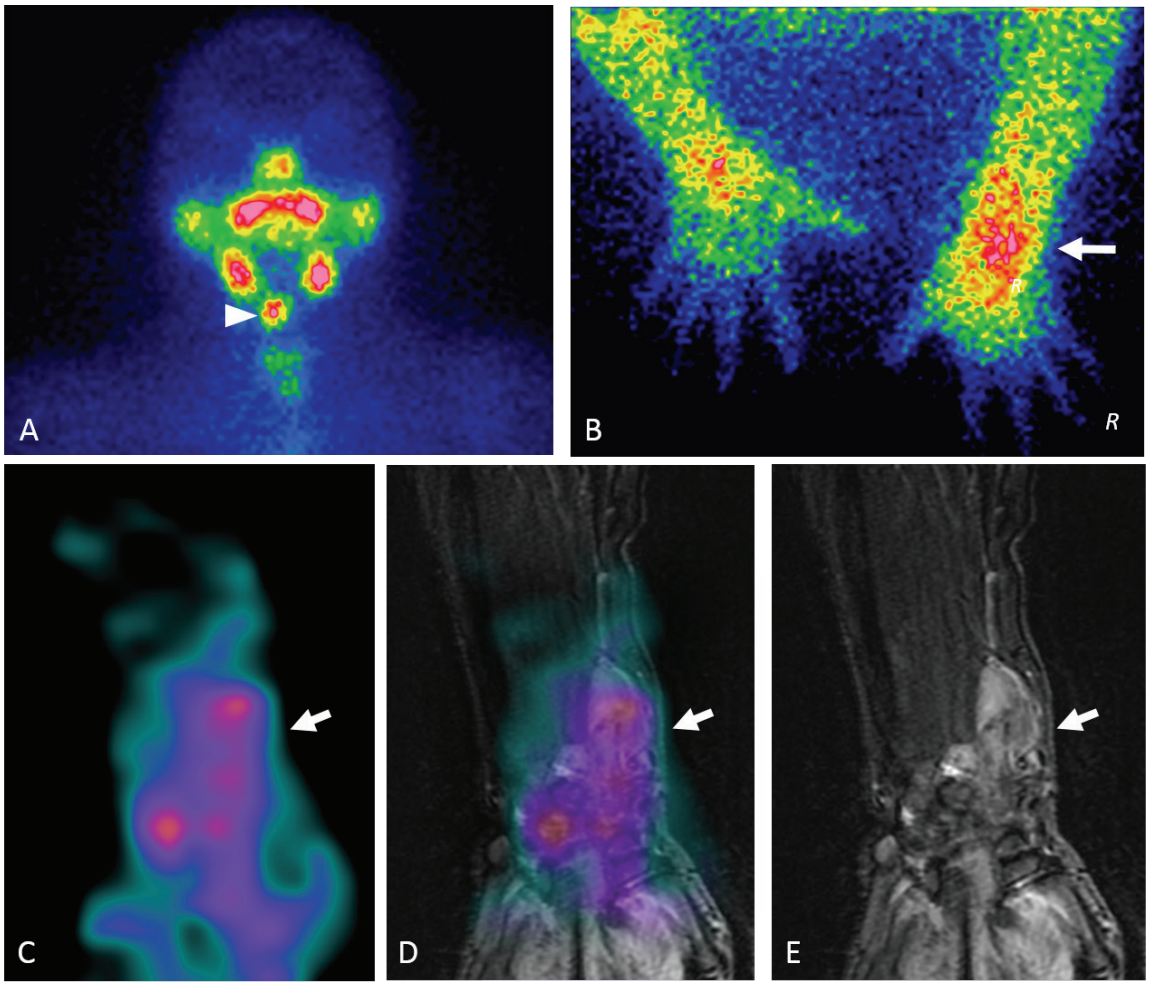

"Official Journal of the Turkish Society of Nuclear Medicine"

galenos yayınevi

TURKISH SOCIETY OF NUCLEAR MEDICINE 1975

MIRT

Molecular Imaging and Radionuclide Therapy

MIRT

Molecular Imaging and Radionuclide Therapy

Turkish Society of Nuclear Medicine
Cinnah Caddesi Pilot Sokak No: 10/12 Çankaya 06650 Ankara, Turkey **Phone:** +90 312 441 00 45 **Fax:** +90 312 441 12 95 **Web:** www.tsnm.org **E-mail:** dernekmerkezi@tsnm.org
"Formerly Turkish Journal of Nuclear Medicine"

Reviewing the articles' conformity to the publishing standards of the Journal, typesetting, reviewing and editing the manuscripts and abstracts in English, creating links to source data, and publishing process are realized by Galenos.

Galenos Publishing House
Owner and Publisher
Derya Mor
Erkan Mor

Publication Coordinator
Burak Sever

Web Coordinators
Fuat Hocalar
Turgay Akpınar

Graphics Department
Ayda Alaca
Çiğdem Birinci
Gülşah Özgül
Gülay Saday

Finance Coordinator
Sevinç Çakmak
Emre Kurtulmuş

Project Coordinators
Aysel Balta
Gamze Aksoy
Gülay Akın
Hatice Sever
Melike Eren
Özlem Çelik Çekil
Pınar Akpınar
Rabia Palazoğlu
Sümeyye Karadağ

Research&Development
Melisa Yiğitoğlu
Nihan Karamanlı

Digital Marketing Specialist
Ümit Topluoğlu

Publisher Contact
Address: Molla Gürani Mah. Kaçamak Sk. No: 21/1
34093 İstanbul, Turkey
Phone: +90 (212) 621 99 25 **Fax:** +90 (212) 621 99 27
E-mail: info@galenos.com.tr/yayin@galenos.com.tr
Web: www.galenos.com.tr
Publisher Certificate Number: 14521

Online Publication Date: June 2022
ISSN: 2146-1414 **E-ISSN:** 2147-1959
International scientific journal published quarterly.

MIRT

Molecular Imaging and Radionuclide Therapy

ABOUT US

Molecular Imaging and Radionuclide Therapy (formerly Turkish Journal of Nuclear Medicine) is the official publication of Turkish Society of Nuclear Medicine.

Focus and Scope

Molecular Imaging and Radionuclide Therapy (Mol Imaging Radionucl Ther, MIRT) is a double-blind peer-review journal published in English language. It publishes original research articles, invited reviews, editorials, short communications, letters, consensus statements, guidelines and case reports with a literature review on the topic, in the field of molecular imaging, multimodality imaging, nuclear medicine, radionuclide therapy, radiopharmacy, medical physics, dosimetry and radiobiology. MIRT is published three times a year (February, June, October). Audience: Nuclear medicine physicians, medical physicists, radiopharmaceutical scientists, radiobiologists.

The editorial policies are based on the "Recommendations for the Conduct, Reporting, Editing, and Publication of Scholarly Work in Medical Journals (ICMJE Recommendations)" by the International Committee of Medical Journal Editors (2016, archived at http://www.icmje.org/) rules.

Molecular Imaging and Radionuclide Therapy is indexed in **Pubmed, Pubmed Central (PMC), Emerging Sources Citation Index (ESCI), TUBITAK-ULAKBIM, DOAJ, Scopus, Gale/Cengage Learning, EBSCO databases, Embase, ProQuest Health & Medical Complete, CINAHL, Index Copernicus, J-Gate, IdealOnline, ROOT INDEXING, Türkiye Atıf Dizini-Turkiye Citation Index, Turk Medline, EuroPub, Hinari, GOALI, ARDI, OARE** and **AGORA.**

Open Access Policy

This journal provides immediate open access to its content on the principle that making research freely available to the public supports a greater global exchange of knowledge.

Open Access Policy is based on rules of Budapest Open Access Initiative (BOAI) (http://www.budapestopenaccessinitiative.org/). By "open access" to [peer-reviewed research literature], we mean its free availability on the public internet, permitting any users to read, download, copy, distribute, print, search, or link to the full texts of these articles, crawl them for indexing, pass them as data to software, or use them for any other lawful purpose, without financial, legal, or technical barriers other than those inseparable from gaining access to the internet itself. The only constraint on reproduction and distribution, and the only role for copyright in this domain, should be to give authors control over the integrity of their work and the right to be properly acknowledged and cited.

Subscription Information

Manuscripts can only be submitted electronically through the Journal Agent website (http://www.journalagent.com/mirt/?plng=eng) after creating an account. This system allows online submission and review.

All published volumes in full text can be reached free of charge through the website http://mirt.tsnmjournals.org

Copyright Statement

Turkish Society of Nuclear Medicine holds the international copyright of all the content published in the journal.

Republication and reproduction of images or tables in any published material should be done with proper citation of source providing authors names; article title; journal title; year (volume) and page of publication; copyright year of the article.

The author(s) hereby affirms that the manuscript submitted is original, that all statement asserted as facts are based on author(s) careful investigation and research for accuracy, that the manuscript does not, in whole or part, infringe any copyright, that it has not been published in total or in part and is not being submitted or considered for publication in total or in part elsewhere.

Completed Copyright Statement form should be submitted to the online article system.

By signing this form,

1. Each author acknowledge that he/she participated in the work in a substantive way and is prepared to take public responsibility for the work.

2. Each author further affirms that he or she has read and understands the "Ethical Guidelines for Publication of Research".

3. The author(s), in consideration of the acceptance of the manuscript for publication, does hereby assign and transfer to the Molecular Imaging and Radionuclide Therapy all of the rights and interest in and the copyright of the work in its current form and in any form subsequently revised for publication and/or electronic dissemination.

Instructions for Authors

Instructions for authors are published in the journal and on the website http://mirt.tsnmjournals.org

Material Disclaimer

Scientific and legal responsibilities pertaining to the papers belong to the authors. Contents of the manuscripts and accuracy of references are also the author's responsibility. The Turkish Society of Nuclear Medicine, the Editor, the Editorial Board or the publisher do not accept any responsibility for opinions expressed in articles.

Financial expenses of the journal are covered by Turkish Society of Nuclear Medicine.

Correspondence Address

Editor in Chief Prof. Murat Fani Bozkurt, MD, FEBNM Hacettepe University, Medical School, Department of Nuclear Medicine, Ankara, Turkey

E-mail: fanibozkurt@gmail.com

Web page: http://mirt.tsnmjournals.org/

Publisher Corresponding Address

Galenos Yayınevi Tic. Ltd. Şti.
Address: Molla Gürani Mah. Kaçamak Sk. No: 21/1 34093 Fındıkzade, İstanbul, Turkey
Phone: +90 212 621 99 25
Fax: +90 212 621 99 27
E-mail: info@galenos.com.tr

MIRT

Molecular Imaging and Radionuclide Therapy

INSTRUCTIONS TO AUTHORS

Molecular Imaging and Radionuclide Therapy (Mol Imaging Radionucl Ther, MIRT) publishes original research articles, short communications, invited reviews, editorials, case reports with a literature review on the topic, interesting images, consensus statements, guidelines, letters in the field of molecular imaging, multimodality imaging, nuclear medicine, radionuclide therapy, radiopharmacy, medical physics, dosimetry and radiobiology. MIRT is published by the Turkish Society of Nuclear Medicine three times a year (February, June, October).

Molecular Imaging and Radionuclide Therapy does not charge any article submission or processing fees.

GENERAL INFORMATION

MIRT commits to rigorous peer review, and stipulates freedom from commercial influence, and promotion of the highest ethical and scientific standards in published articles. Neither the Editor(s) nor the publisher guarantees, warrants or endorses any product or service advertised in this publication. All articles are subject to review by the editors and peer reviewers. If the article is accepted for publication, it may be subjected to editorial revisions to aid clarity and understanding without changing the data presented.

Manuscripts must be written in English and must meet the requirements of the journal. The journal is in compliance with the uniform requirements for manuscripts submitted to biomedical journals published by the International Committee of Medical Journal Editors (NEJM 1997; 336:309-315, updated 2016). Manuscripts that do not meet these requirements will be returned to the author for necessary revision before the review. Authors of manuscripts requiring modifications have a maximum of two months to resubmit the revised text. Manuscripts returned after this deadline will be treated as new submissions.

It is the authors' responsibility to prepare a manuscript that meets ethical criteria. The Journal adheres to the principles set forth in the Helsinki Declaration October 2013 (https://www.wma.net/policies-post/wma-declaration-of-helsinki-ethical-principles-for-medical-research-involving-human-subjects/) and holds that all reported research involving "Human beings" conducted in accordance with such principles.

Reports describing data obtained from research conducted in human participants must contain a statement in the MATERIALS AND METHODS section indicating approval by the ethical review board (including the approval number) and affirmation that INFORMED CONSENT was obtained from each participant.

All manuscripts reporting experiments using animals must include a statement in the MATERIALS AND METHODS section giving assurance that all animals have received humane care in compliance with the Guide for the Care and Use of Laboratory Animals (www.nap.edu) and indicating approval by the ethical review board.

If the study should have ethical approval, authors asked to provide ethical approval in order to proceed the review process. If they provide approval, review of the manuscript will continue.

In case report(s) and interesting image(s) a statement regarding the informed consent of the patients should be included in the manuscript and the identity of the patient(s) should be hidden.

Subjects must be identified only by number or letter, not by initials or names. Photographs of patients' faces should be included only if scientifically relevant. Authors must obtain written consent from the patient for use of such photographs. In cases of image media usage that potentially expose patients' identity requires obtaining permission for publication from the patients or their parents/guardians.

If the proposed publication concerns any commercial product, the author must include in the cover letter a statement indicating that the author(s) has (have) no financial or other interest with the product or explaining the nature of any relations (including consultancies) between the author(s) and editor the manufacturer or distributor of the product.

All submissions will be screened by Crossref Smilarity Check powered by "iThenticate". Manuscripts with an overall similarity index of greater than 25%, or duplication rate at or higher than 5% with a single source will be returned back to authors.

MANUSCRIPT CATEGORIES

1. Original Articles

2. Short Communications are short descriptions of focused studies with important, but very straightforward results.

3. Reviews address important topics in the field. Authors considering the submission of uninvited reviews should contact the editor in advance to determine if the topic that they propose is of current potential interest to the Journal. Reviews will be considered for publication only if they are written by authors who have at least three published manuscripts in the international peer reviewed journals and these studies should be cited in the review. Otherwise only invited reviews will be considered for peer review from qualified experts in the area.

4. Editorials are usually written by invitation of the editor by the editors on current topics or by the reviewers involved in the evaluation of a submitted manuscript and published concurrently with that manuscript.

5. Case Report and Literature Reviews are descriptions of a case or small number of cases revealing a previously undocumented disease process, a unique unreported manifestation or treatment of a known disease process, unique unreported complications of treatment regimens or novel and important insights into a condition's pathogenesis, presentation, and/or management. The journal's policy is to accept case reports only if it is accompanied by a review of the literature on the related topic. They should include an adequate number of images and figures.

6. Interesting Image

One of the regular parts of Molecular Imaging and Radionuclide Therapy is a section devoted to interesting images. Interesting image(s) should describe case(s) which are unique and include interesting findings adding insights into the interpretation of patient images, a condition's pathogenesis, presentation, and/or management.

7. Consensus Statements or Guidelines may be submitted by professional societies. All such submissions will be subjected to peer review, must be modifiable in response to criticisms, and will be published only if they meet the Journal's usual editorial standards.

8. Letters to the Editor may be submitted in response to work that has been published in the Journal. Letters should be short commentaries related to specific points of agreement or disagreement with the published work.

Note on Prior Publication

Articles are accepted for publication on the condition that they are original, are not under consideration by another journal, or have not been previously published. Direct quotations, tables, or illustrations that have appeared in

MIRT
Molecular Imaging and Radionuclide Therapy

copyrighted material must be accompanied by written permission for their use from the copyright owner and authors. Materials previously published in whole or in part shall not be considered for publication. At the time of submission, authors must report that the manuscript has not been published elsewhere. Abstracts or posters displayed at scientific meetings need not be reported.

MANUSCRIPT SUBMISSION PROCEDURES

MIRT only accepts electronic manuscript submission at the web site http://www.journalagent.com/mirt/. After logging on to the website Click the 'online manuscript submission' icon. All corresponding authors should be provided with a password and a username after entering the information required. If you already have an account from a previous submission, enter your username and password to submit a new or revised manuscript. If you have forgotten your username and/or password, please send an e-mail to the editorial office for assistance. After logging on to the article submission system please read carefully the directions of the system to give all needed information and attach the manuscript, tables and figures and additional documents.

All Submissions Must Include:

1. Completed Copyright Assignment & Disclosure of Potential Conflict of Interest Form; This form should be downloaded from the website (provided in the author section), filled in thoroughly and uploaded to the website during the submission.
2. All manuscripts describing data obtained from research conducted in human participants must be accompanied with an approval document by the ethical review board.
3. All manuscripts reporting experiments using animals must include approval document by the animal ethical review board.
4. All submissions must include the authorship contribution form which is signed by all authors.

Authors must complete all online submission forms. If you are unable to successfully upload the files please contact the editorial office by e-mail.

MANUSCRIPT PREPARATION

General Format

The Journal requires that all submissions be submitted according to these guidelines:

- Text should be double spaced with 2.5 cm margins on both sides using 12-point type in Times Roman font.
- All tables and figures must be placed after the text and must be labeled.
- Each section (abstract, text, references, tables, figures) should start on a separate page.
- Manuscripts should be prepared as a word document (*.doc) or rich text format (*.rtf).
- Please make the tables using the table function in Word.
- Abbreviations should be defined in parenthesis where the word is first mentioned and used consistently thereafter.
- Results should be expressed in metric units. Statistical analysis should be done accurately and with precision. Please consult a statistician if necessary.
- Authors' names and institutions should not be included in the manuscript text and should be written only in the title page.

Title Page

The title page should be a separate form from the main text and should include the following:

- Full title (in English and in Turkish). Turkish title will be provided by the editorial office for the authors who are not Turkish speakers.
- Authors' names and institutions.
- Short title of not more than 40 characters for page headings.
- At least three and maximum eight keywords. (in English and in Turkish). Do not use abbreviations in the keywords. Turkish keywords will be provided by the editorial office for the authors who are not Turkish speakers. If you are not a native Turkish speaker, please reenter your English keywords to the area provided for the Turkish keywords. English keywords should be provided from http://www.nlm.nih.gov/mesh (Medical Subject Headings) while Turkish keywords should be provided from http://www.bilimterimleri.com.
- Word count (excluding abstract, figure legends and references).
- Corresponding author's e-mail and address, telephone and fax numbers.
- Name and address of person to whom reprint requests should be addressed.

Original Articles

Authors are required to state in their manuscripts that ethical approval from an appropriate committee and informed consents of the patients were obtained.

Original Articles should be submitted with a structured abstract of no more than 250 words. All information reported in the abstract must appear in the manuscript. The abstract should not include references. Please use complete sentences for all sections of the abstract. Structured abstract should include background, objective, methods, results and conclusions. Turkish abstract will be provided by the editorial office for the authors who are not Turkish speakers. If you are not a native Turkish speaker, please reenter your English abstract to the area provided for the Turkish abstract.

- Introduction
- Materials and Methods
- Results
- Discussion
- Study Limitations
- Conclusion

May be given for contributors who are not listed as authors, or for grant support of the research.

References should be cited in numerical order (in parentheses) in the text and listed in the same numerical order at the end of the manuscript on a separate page or pages. The author is responsible for the accuracy of references. Examples of the reference style are given below. Further examples will be found in the articles describing the Uniform Requirements for Manuscripts Submitted to Biomedical Journals (Ann Intern Med.1988; 208:258-265, Br Med J. 1988; 296:401-405). The titles of journals should be abbreviated according to the style used in the Index Medicus. Journal Articles and Abstracts: Surnames and initials of author's name, title of the article, journal name, date, volume number, and pages. All authors should be listed regardless of number. The citation of unpublished papers, observations or personal communications is not permitted. Citing an abstract is not recommended. Books: Surnames and initials of author's names, chapter title, editor's name, book title, edition, city, publisher, date and pages.

MIRT
Molecular Imaging and Radionuclide Therapy

Sample References

Journal Article: Sayit E, Söylev M, Capa G, Durak I, Ada E, Yilmaz M. The role of technetium-99m-HMPAO-labeled WBC scintigraphy in the diagnosis of orbital cellulitis. Ann Nucl Med 2001;15:41-44.

Erselcan T, Hasbek Z, Tandogan I, Gumus C, Akkurt I. Modification of Diet in Renal Disease equation in the risk stratification of contrast induced acute kidney injury in hospital inpatients. Nefrologia 2009 doi: 10.3265/Nefrologia.2009.29.5.5449.en.full.

Article in a journal published ahead of print: Ludbrook J. Musculovenous pumps in the human lower limb. Am Heart J 2009;00:1-6. (accessed 20 February 2009).

Lang TF, Duryea J. Peripheral Bone Mineral Assessment of the Axial Skeleton: Technical Aspects. In: Orwoll ES, Bliziotes M (eds). Osteoporosis: Pathophsiology and Clinical Management. New Jersey, Humana Pres Inc, 2003;83-104.

Books: Greenspan A. Orthopaedic Radiology a Pratical Approach. 3th ed. Philadelphia, Lippincott Williams Wilkins 2000, 295-330.

Website: Smith JR. 'Choosing Your Reference Style', Online Referencing 2(3), http://orj.sagepub.com (200, accessed October 2008).

- Tables

Tables must be constructed as simply as possible. Each table must have a concise heading and should be submitted on a separate page. Tables must not simply duplicate the text or figures. Number all tables in the order of their citation in the text. Include a title for each table (a brief phrase, preferably no longer than 10 to 15 words). Include all tables in a single file following the manuscript.

– Figure Legends

Figure legends should be submitted on a separate page and should be clear and informative.

– Figures

Number all figures (graphs, charts, photographs, and illustrations) in the order of their citation in the text. At submission, the following file formats are acceptable: AI, EMF, EPS, JPG, PDF, PPT, PSD, TIF. Figures may be embedded at the end of the manuscript text file or loaded as separate files for submission. All images MUST be at or above intended display size, with the following image resolutions: Line Art 800 dpi, Combination (Line Art + Halftone) 600 dpi, Halftone 300 dpi. Image files also must be cropped as close to the actual image as possible.

Short Communications:

Short communications should be submitted with a structured abstract of no more than 200 words. These manuscripts should be no longer than 2000 words, and include no more than two figures and tables and 20 references. Other rules which the authors are required to prepare and submit their manuscripts are the same as described above for the original articles.

Invited Review Articles:

- Title page (see above)
- Abstract: Maximum 250 words; without structural divisions; in English and in Turkish . Turkish abstract will be provided by the editorial office for the authors who are not Turkish speakers. If you are not a native Turkish speaker, please reenter your English abstract to the area provided for the Turkish abstract.
- Text
- Conclusion
- Acknowledgements (if any)
- References

Editorial:

- Title page (see above)
- Abstract: Maximum 250 words; without structural divisions; in English and in Turkish. Turkish abstract will be provided by the editorial office for the authors who are not Turkish speakers. If you are not a native Turkish speaker, please re enter your English abstract to the area provided for the Turkish abstract.
- Text
- References

Case Report and Literature Review

- Title page (see above)
- Abstract: Approximately 100-150 words; without structural divisions; in English and in Turkish. Turkish abstract will be provided by the editorial office for the authors who are not Turkish speakers. If you are not a native Turkish speaker, please re-enter your English abstract to the area provided for the Turkish abstract.
- Introduction
- Case report
- Literature Review and Discussion
- References

Interesting Image:

No manuscript text is required. Interesting Image submissions must include the following:

Title Page: (see Original article section)

Abstract: Approximately 100-150 words; without structural divisions; in English and in Turkish. Turkish abstract will be provided by the editorial office for the authors who are not Turkish speakers. If you are not a native Turkish speaker, please re-enter your English abstract to the area provided for the Turkish abstract.

Image(s): The number of images is left to the discretion of the author. (See Original article section)

Figure Legend: Reference citations should appear in the legends, not in the abstract. Since there is no manuscript text, the legends for illustrations should be prepared in considerable detail but should be no more than 500 words total. The case should be presented and discussed in the Figure legend section.

References: Maximum eight references (see original article section).

Letters to the Editor:

- Title page (see above)
- Short comment to a published work, no longer than 500 words, no figures or tables.
- References no more than five.

Consensus Statements or Guidelines: These manuscripts should typically be no longer than 4000 words and include no more than six figures and tables and 120 references.

Proofs and Reprints

Proofs and a reprint orders are sent to the corresponding author. The author should designate by footnote on the title page of the manuscript the name and

MIRT
Molecular Imaging and Radionuclide Therapy

address of the person to whom reprint requests should be directed. The manuscript when published will become the property of the journal.

Archiving

The editorial office will retain all manuscripts and related documentation (correspondence, reviews, etc.) for 12 months following the date of publication or rejection.

Submission Preparation Checklist

As part of the submission process, authors are required to check off their submission's compliance with all of the following items, and submissions may be returned to authors that do not adhere to these guidelines.

1. The submission has not been previously published, nor is it before another journal for consideration (or an explanation has been provided in Comments to the Editor).
2. The submission file is in Microsoft Word, RTF, or WordPerfect document file format. The text is double-spaced; uses a 12-point font; employs italics, rather than underlining (except with URL addresses); and the location for all illustrations, figures, and tables should be marked within the text at the appropriate points.
3. Where available, URLs for the references will be provided.
4. All authors should be listed in the references, regardless of the number.
5. The text adheres to the stylistic and bibliographic requirements outlined in the Author Guidelines, which is found in About the Journal.
6. English keywords should be provided from http://www.nlm.nih.gov/mesh(Medical Subject Headings), while Turkish keywords should be provided fromhttp://www.bilimterimleri.com
7. The title page should be a separate document from the main text and should be uploaded separately.
8. The "Affirmation of Originality and Assignment of Copyright/The Disclosure Form for Potential Conflicts of Interest Form" and Authorship Contribution Form should be downloaded from the website, filled thoroughly and uploaded during the submission of the manuscript.

TO AUTHORS

Copyright Notice

The author(s) hereby affirms that the manuscript submitted is original, that all statement asserted as facts are based on author(s) careful investigation and research for accuracy, that the manuscript does not, in whole or part, infringe any copyright, that it has not been published in total or in part and is not being submitted or considered for publication in total or in part elsewhere. Completed Copyright Assignment & Affirmation of Originality Form will be uploaded during submission. By signing this form;

1. Each author acknowledges that he/she participated in the work in a substantive way and is prepared to take public responsibility for the work.
2. Each author further affirms that he or she has read and understands the "Ethical Guidelines for Publication of Research".
3. The author(s), in consideration of the acceptance of the manuscript for publication, does hereby assign and transfer to the Molecular Imaging and Radionuclide Therapy all of the rights and interest in and the copyright of the work in its current form and in any form subsequently revised for publication and/or electronic dissemination.

Privacy Statement

The names and email addresses entered in this journal site will be used exclusively for the stated purposes of this journal and will not be made available for any other purpose or to any other party.

Peer Review Process

1. The manuscript is assigned to an editor, who reviews the manuscript and makes an initial decision based on manuscript quality and editorial priorities.
2. For those manuscripts sent for external peer review, the editor assigns at least two reviewers to the manuscript.
3. The reviewers review the manuscript.
4. The editor makes a final decision based on editorial priorities, manuscript quality, and reviewer recommendations.
5. The decision letter is sent to the author.

Contact Address

All correspondence should be directed to the Editorial Office:
Cinnah Caddesi Pilot Sokak No:10/12 06650 Çankaya / Ankara, Turkey
Phone: +90 312 441 00 45
Fax: +90 312 441 12 97
E-mail: info@tsnmjournals.org

MIRT
Molecular Imaging and Radionuclide Therapy

CONTENTS

Original Articles

75 Investigation of the Presence of Integrin Alpha-3 and Beta-1 Receptors on Tumor Tissue, Metastatic Lymph Node and Normal Tissue in Thyroid Cancer

Tiroid Kanseri Tümör Dokusu, Metastatik Lenf Nodu ve Normal Doku Üzerinde İntegrin Alfa-3 ve Beta-1 Reseptörlerinin Varlığının Araştırılması

Esra Arslan, Tamer Aksoy, Taha Cumhan Şavlı, Didem Can Trabulus, Ahmet Volkan Sünter, Tevfik Fikret Çermik; İstanbul, Turkey

82 Diagnostic Performance of Machine Learning Models Based on ^{18}F-FDG PET/CT Radiomic Features in the Classification of Solitary Pulmonary Nodules

Soliter Pulmoner Nodüllerin Sınıflandırılmasında ^{18}F-FDG PET/BT Radyomik Özelliklerine Dayalı Makine Öğrenme Modellerinin Tanısal Performansı

Yavuz Sami Salihoğlu, Rabiye Uslu Erdemir, Büşra Aydur Püren, Semra Özdemir, Çağlar Uyulan, Türker Tekin Ergüzel, Hüseyin Ozan Tekin; Çanakkale, Zonguldak, İzmir, İstanbul, Turkey; Sharjah, United Arab Emirates

89 Correlation of Morphological and Functional Cardiac Images: Fusion of Myocardial Perfusion SPECT and CT Angiography

Morfolojik ve Fonksiyonel Kardiyak Görüntülerin Korelasyonu: Miyokard Perfüzyon SPECT ve BT Anjiyografi Füzyonu

Hüseyin Şan, Alper Özgür Karaçalıoğlu, Uğur Bozlar, Semra İnce, Engin Alagöz, Mustafa Özdeş Emer, Mustafa Taşar, Nuri Arslan; Ankara, Turkey

96 Prevalence and Clinical Significance of Incidental Focal ^{18}F-FDG Uptake in Colon on PET/CT Imaging

PET/BT Görüntülemede Kolonda İnsidental Fokal ^{18}F-FDG Tutulumunun Prevalansı ve Klinik Önemi

Yasemin Gökden, Filiz Özülker, Tamer Özülker; İstanbul, Turkey

104 The Prognostic Value of ^{18}F-FDG PET/CT Metabolic Parameters in Predicting Treatment Response Before EGFR TKI Treatment in Patients with Advanced Lung Adenocarcinoma

İlerlemiş Akciğer Adenokarsinomu Olan Hastalarda EGFR TKI Tedavisi Öncesi Tedavi Yanıtını Öngörmede ^{18}F-FDG PET/BT Metabolik Parametrelerinin Prognostik Değeri

Nurşin Agüloğlu, Murat Akyol, Halil Kömek, Nuran Katgı; İzmir, Diyarbakır, Turkey

114 Elevated Angiogenic Factor Levels After Transarterial Radioembolization for Colorectal Cancer Liver Metastases May Predict a Poor Prognosis

Yüksek Anjiyojenik Faktör Seviyeleri Kolorektal Kanser Karaciğer Metastazları İçin Transarteriyel Radyoembolizasyon Sonrası Kötü Prognozu Öngörebilir

Çiğdem Soydal, Mine Araz, Mustafa Durmaz, Elgin Özkan, Berrin İmge Ergüder, Nuriye Özlem Küçük, Sadık Bilgiç, Atilla Halil Elhan, İbrahim Ethem Geçim; Ankara, Turkey

123 The Value of ^{18}F-FDG PET/CT Imaging in the Evaluation of Interim Neoadjuvant Chemotherapy Response in Locally Advanced Breast Cancer

Lokal İleri Meme Kanserinde Neoadjuvan İnterim Kemoterapi Yanıtının Değerlendirilmesinde ^{18}F-FDG PET/BT Görüntülemenin Değeri

Gamze Tatar, Özlem Özkul, Göksel Alçin; İstanbul, Turkey

130 Comparison of the Diagnostic Performance of Myocardial Perfusion Scintigraphy with and Without Attenuation Correction

Atenüasyon Düzeltmeli ve Düzeltmesiz Miyokard Perfüzyon Sintigrafisinin Tanısal Performansının Karşılaştırılması

Sira Vachatimanont, Sasitorn Sirisalipoch, Maythinee Chantadisai; Bangkok, Thailand

MIRT
Molecular Imaging and Radionuclide Therapy

CONTENTS

Interesting Images

139 Almost Complete Response with a Single Administration ^{225}Ac-DOTATATE in a Patient with a Metastatic Neuroendocrine Tumor of Unknown Primary

Primeri Bilinmeyen Metastatik Nöroendokrin Tümörlü Hastaya Tek Doz ^{225}Ac-DOTATATE Uygulaması Sonrası Tam/Tama Yakın Yanıt

Nalan Alan Selçuk, Emre Demirci, Meltem Ocak, Türkay Toklu, Selçuk Ergen, Levent Kabasakal; İstanbul, Turkey

142 "Picture-in-Picture" Artifact in Post-therapeutic ^{131}I Whole-body Survey: Deceiving Spot View but Unraveling Whole-body Scanning

Tedavi Sonrası ^{131}I Tüm Vücut Taramada "Resim-İçinde-Resim" Artefaktı: Spot Görüntülemedeki Yanıltıcılığın Tüm Vücut Görüntülemede Ortaya Çıkarılması

Mohsen Qutbi, Reyhane Ahmadi; Tehran, Hamadan, Iran

145 Unusual Uptake of [^{131}I] in a Tenosynovial Giant Cell Tumour Relapse in a Patient with Differentiated Thyroid Cancer

Diferansiye Tiroid Kanserli Bir Hastada Tenosinovyal Dev Hücreli Tümör Nüksünde Olağandışı [^{131}I] Tutulumu

Francisco Manuel Cañete Sánchez, Leonardo Gabriel Romero Robles, Xavier Louis Boulvard Chollet, María Mangas Losada, Puy Garrastachu, Antonio Cabrera Villegas, Rafael Ramírez Lasanta, Roberto Delgado Bolton; Logroño, Spain

148 A Rare Case of Primary Cardiac Diffuse Large B-cell Lymphoma Imaged with ^{18}F-FDG PET/CT

^{18}F-FDG PET/BT ile Görüntülenen Nadir Bir Primer Kardiyak Diffüz Büyük B-hücreli Lenfoma Olgusu

Seval Erhamamcı, Nesrin Aslan; İstanbul, Turkey

151 A Rare Case of Pulmonary Alveolar Microlithiasis with Diffuse Lung Uptake on Bone Scintigraphy

Kemik Sintigrafisinde Diffüz Akciğer Tutulumu Olan Nadir Bir Pulmoner Alveolar Mikrolitiazis Olgusu

Ahmet Eren Şen, Özlem Şahin, Zeynep Aydın, Buğra Kaya, Çağlagül Erol; Konya, Turkey

154 Mesenteric Panniculitis Appears as Metastatic Disease on ^{18}F-FDG-PET/CT Scan

^{18}F-FDG-PET/BT Görüntülemesinde Metastaz Düşündüren Mezenterik Pannikülit Olgusu

Özgül Ekmekçioğlu, Selim Bakan, Kerim Sönmezoğlu; İstanbul, Turkey

157 Multiple Subcutaneous ^{18}F-FDG-avid Granulomas Due to Enoxaparin Injection

Enoksaparin Enjeksiyonuna Bağlı Gelişen Yoğun ^{18}F-FDG Tutan Multipl Subkütan Granülomlar

Özge Erol Fenercioğlu, Nurhan Ergül, Ediz Beyhan, Rahime Şahin, Tevfik Fikret Çermik; İstanbul, Turkey

160 Two Cases of Acrometastasis from Lung Cancer Revealed on ^{18}F-FDG PET/CT

^{18}F-FDG PET/BT ile Gösterilen Akciğer Kanserine Bağlı İki Akrometastaz Olgusu

Rahime Şahin, Özge Erol Fenercioğlu, Ediz Beyhan, Nurhan Ergül, Tevfik Fikret Çermik; İstanbul, Turkey

163 Imaging Features of Breast Plasmacytoma

Meme Plazmositomunun Görüntüleme Özellikleri

Şeyma Babaoğlu, Necdet Poyraz, Buğra Kaya, Sıddıka Fındık, Sinan Demircioğlu; Konya, Turkey

166 Metabolic Activity of Neurogenic Heterotopic Ossification on ^{18}F-FDG PET/CT Matching with Ongoing Osteoblastic Activity on Bone Scan

^{18}F-FDG PET/BT'de Nörojenik Heterotopik Ossifikasyonun Metabolik Aktivitesi ile Kemik Taramasında Devam Eden Osteoblastik Aktivite Eşleşmesi

Matthieu Dietz, Jeremie Tordo; Lyon, France

169 Increased ^{18}F-FDG Uptake in the Axillary Lymph Nodes of the Vaccinated Side Associated with COVID-19 Vaccination

COVID-19 Aşılaması ile İlişkili Aşılı Tarafın Aksiller Lenf Nodlarında Artan ^{18}F-FDG Tutulumu

Yoichi Otomi, Saho Irahara, Hiroaki Inoue, Takayoshi Shinya, Hideki Otsuka, Masafumi Harada; Tokushima, Japan

Original Article
Mol Imaging Radionucl Ther 2022;31:75-81 DOI:10.4274/mirt.galenos.2021.71501

Investigation of the Presence of Integrin Alpha-3 and Beta-1 Receptors on Tumor Tissue, Metastatic Lymph Node and Normal Tissue in Thyroid Cancer

Tiroid Kanseri Tümör Dokusu, Metastatik Lenf Nodu ve Normal Doku Üzerinde İntegrin Alfa-3 ve Beta-1 Reseptörlerinin Varlığının Araştırılması

Esra Arslan[1], Tamer Aksoy[1], Taha Cumhan Şavlı[2], Didem Can Trabulus[3], Ahmet Volkan Sünter[4], Tevfik Fikret Çermik[1]

[1]*University of Health and Sciences Turkey, İstanbul Training and Research Hospital, Clinic of Nuclear Medicine, İstanbul, Turkey*
[2]*University of Health and Sciences Turkey, İstanbul Training and Research Hospital, Clinic of Pathology, İstanbul, Turkey*
[3]*University of Health and Sciences Turkey, İstanbul Training and Research Hospital, Clinic of Surgery of Pathology, İstanbul, Turkey*
[4]*University of Health and Sciences Turkey, İstanbul Training and Research Hospital, Clinic of Otorhinolaryngology, Division of Head and Neck Surgery, İstanbul, Turkey*

Abstract

Objectives: The important roles of integrins in tumor invasion, migration and proliferation are well known. In this study, we investigated the presence of integrin α3 and β1 receptors in tumor tissue, metastatic lymph node (LN) and normal thyroid tissue of patients diagnosed with thyroid cancer (TCa) and showed the prognostic and diagnostic value of these molecules as well as peptide-receptor.

Methods: Sixty-one patients with TCa were included in this study. The presence of integrin α3 and β1 expression was investigated by immunohistochemical methods from tumor tissue after total thyroidectomy. TNM system was used in tumor staging. The relationship between prognostic properties such as tumor size, LN metastasis, capsular invasion and the presence of integrin α3 and β1 expression was investigated.

Results: Classical type papillary TCa was the most common subtype in our study group with 31.1%. Integrin β1 was expressed in 4.9% (n=3) of normal tissue, 57.4% (n=35) of tumor tissue and 16.4% (n=10) of metastatic LN; integrin α3 was expressed in 50.8% (n=31) of normal tissue, 67.2% (n=41) of tumor tissue and 9.8% (n=6) metastatic LN. Integrin β1 expression was observed 21.3% (n=13), integrin α3 in 14.8% (n=9) and integrin α3 and β1 expression in 36.1% (n=22). Integrin β1 expression increased statistically significantly in the presence of LN metastasis and capsular invasion (p=0.022, 0.014, respectively). Furthermore, the expression of integrin α3 was found to be statistically significant in primary tumors of patients with LN metastasis (p=0.045).

Conclusion: Our study showed a significant increase in integrin α3 and β1 expression in LN metastasis or thyroid capsule invasion in tumor. Thus, it appears that the demonstration of the presence of integrin α3 and β1 expression in TCa is not only a prognostic biomarker but also has value as a potential theranostic target with peptide-bound radioactive agents.

Keywords: Thyroid cancer, papillary thyroid cancer, integrin alpha-3, integrin beta-1

Öz

Amaç: İntegrinlerin tümör invazyon, migrasyon ve proliferasyonu üzerindeki önemli rolleri iyi bilinmektedir. Çalışmamızda tiroid kanseri (TCa) tanılı hastaların tümör dokusunda, metastatik lenf nodunda (LN) ve normal tiroid dokusunda integrin α3 ve β1 reseptör varlığını araştırarak moleküllerin

Address for Correspondence: Esra Arslan Assoc. Prof., University of Health and Sciences Turkey, İstanbul Training and Research Hospital, Clinic of Nuclear Medicine, İstanbul, Turkey
Phone: +90 212 459 68 02 **E-mail:** dresraarslan@gmail.com ORCID ID: orcid.org/0000-0002-9222-8883
Received: 17.05.2021 **Accepted:** 26.08.2021

prognostik ve diagnostik değerini gösterme yanında ayrıca peptit-reseptör bağlı radyonüklidler ile TCa teranostik potansiyelini değerlendirmeyi amaçladık.

Yöntem: Çalışmaya TCa tanılı 61 hasta prospektif olarak dahil edilmiştir. Total tiroidektomi sonrasında tümör dokusu preparatlarından immünohistokimyasal yöntemler ile integrin α3 ve β1 ekspresyonu varlığı araştırıldı. Evrelemede TNM sistemi kullanılarak tiplendirme histopatolojik olarak yapıldı. Tümör boyutu, LN metastazı, kapsüler invazyon gibi prognostik özellikler integrin α3 ve β1 ekspresyon varlığı ile karşılaştırılarak incelendi.

Bulgular: Klasik tip papiller TCa %31,1 ile en sık bulunan alt tiptir. İntegrin β1'in normal dokuda %4,9 (n=3), tümörlü dokuda %57,4 (n=35) ve metastatik LN'de %16,4 (n=10) eksprese edildiği; integrin α3'ün; normal dokuda %50,8 (n=31), tümörlü dokuda %67,2 (n=41) ve metastatik LN'de %9,8 (n=6) eksprese edildiği gözlenmiştir. Hastaların %21,3'ünde (n=13) integrin β1, %14,8'inde (n=9) integrin α3 ve %36,1'inde (n=22) ise integrin α3 + β1 ekspresyonu birlikte gözlenmiştir. İntegrin β1 ekspresyonunun azalan tümör çapı, LN metastazı ve kapsüler invazyon varlığında istatistiksel olarak anlamlı şekilde arttığı saptanmıştır (sırasıyla p değerleri= 0,014, 0,022 ve 0,014). Ayrıca integrin α3 ekspresyonunun LN metastazlı olguların primer tümör odağında istatistiksel olarak anlamlı olacak şekilde yüksek oranda eksprese edildiği saptanmıştır (p=0,045).

Sonuç: Çalışmamızda tümör dokusu yanında LN metastazı ve tiroid kapsül invazyonu varlığında integrin α3 ve β1 ekspresyonundaki anlamlı artış gösterilmiştir. Böylece TCa'da integrin α3 ve β1 ekspresyon varlığının gösterilmesinin prognostik biomarker olması yanında, peptit bağlı radyoaktif ajanlar ile görüntülemede kullanılabilecek potansiyel diagnostik ve terapötik hedef olarak değeri ortaya konulmuştur.

Anahtar kelimeler: Tiroid kanseri, papiller tiroid kanseri, integrin alfa-3, integrin beta-1

Introduction

Thyroid cancers (TCa) with high incidence among endocrine system neoplasms, are the most common malignant tumors of the head and neck region. Papillary TCa (PTCa) is the most common and least aggressive type of TCa (1). Five-year survival rates more than 95% have been shown in TCa, which generally shows a good prognosis (2). However, 2-5% of these tumors lose their differentiated phenotype and the chance of radionuclide treatment with ^{131}I is eliminated since there is be no radioiodine uptake (3).

Integrins are heterodimeric transmembrane receptors that regulate cell-to-cell and cell extracellular matrix (ECM) interactions. The human genome encodes 24 integrin receptors with restricted combinations of 18α and 8β subunits. The functions of integrins are generally focused on ECM interactions and adhesion regulation; alpha 3 integrin has been associated with cellular motility, while beta 1 integrin has been associated with adhesion in stromal cells (4). The α3β1 integrin heterodimer that acts as a laminin receptor has been reported to be closely related to the migration of tumor cells. Studies have shown that integrins increase the aggressive property of the tumor due to their important role in tumor invasion, migration, proliferation, drug resistance and angiogenesis in many types of cancer, including TCa (5,6).

Although the incidence of TCa has increased due of easy and early diagnosis, mortality rates have decreased, especially in developed countries (7). However, the detection and treatment of indolent, asymptomatic TCa with population-based screening programs is a controversial issue because it does not cause a significant change in long-term mortality rates, increased complications and healthcare costs (8). This study provides the presence and ratio of integrin α3 and β1 in tumor tissue, metastatic lymph node (LN), and normal tissue in patients with TCa. Thus, it was investigated the potentials of integrin α3 and β1 as indicators in the differential diagnosis of aggressive subtypes of TCa.

Materials and Methods

Patients

Resection materials of 61 TCa patients [mean ± standard deviation (SD) age: 49.0±13.3, range: 25-80 years, 48 female, 13 male] were included in this retrospective study. Approval from the Institutional Review Board, University of Health and Sciences Turkey, Istanbul Training and Research Hospital Ethics Committee of our hospital was obtained (2670/2021). Additionally, the medical findings of all patients can be used for research through oral and written consent is obtained. TNM system was used in tumor staging.

Immunohistochemical Staining

In our study, resection materials of 61 patients diagnosed with TCa were retrospectively re-evaluated at our pathology clinic between 2015 and 2018. Immunohistochemical study auto-staining (Ventana Bench Mark ULTRA, Ventana Medical Systems, Inc., Tucson, AZ) was performed out in accordance with the manufacturer's protocols. The Ventana ultraviolet dab Detection kit for detection (Ventana Medical Systems, Inc.) was used. 2 sections of 2 µm thick were taken from the paraffin blocks of tissue samples. Sections EZ Prep solution (Ventana Medical Systems, Inc.) was deparaffinized with heat-induced antigen recovery (heat-induced antigen retrieval) cell conditioning 1 solution at 98 °C for 20 min for integrin β1 (4B7R) antibody (Ventana Medical Systems, Inc.) for Integrin α3 (a-3) antibody with

cell conditioning 2 solution at 98 °C for 56 min (Ventana Medical Systems, Inc.) performed. Endogenous peroxidase activity in 3% H_2O_2 for 4 min is an ultraviolet inhibitor (Ventana Medical Systems, Inc.) using blocked. Then a section β1 integrin (4B7R) (1:50 dilution, Santa Cruz biotechnology, Dallas, TX, USA, catalog no: sc-9970) and the other Integrin α3 (A-3): (1:100 dilution, Santa Cruz biotechnology, Dallas, TX, USA, catalog no: sc-374242) with, respectively, 1 h, 40 min and 20 min for periods of 1 h at 37 °C were incubated. It was then incubated at 37 °C with diaminobenzidine tetrahydrochloride and H_2O_2 for 8 min. After incubation, preparations were prepared by first painting with hematoxylin for 16 min and bluing reagent for 4 min.

Scoring;

Score 0: No staining,

Score 1: 1-25% staining in cells,

Score 2: 26-50% staining in cells,

Score 3: More than 50% staining was revealed in the cells.

According to this scoring system, patients with a score of 0 were defined as having negative receptor expression, and patients with a score of 1, 2, and 3 were defined as having positive receptor expression.

Laboratory Analysis

Three months after ablation of radioactive iodine 131 (RAI), serum thyroglobulin (Tg) levels were checked. Reactions for Tg detection were measured and reported using electro-chemiluminescence method in Roche brand, Cobas 6000 model (Tokyo, Japan) immunological autoanalyzer system with test kits manufactured in polystyrene wells suitable for chemiluminescent method.

Statistical Analysis

All data were evaluated using the SPSS software for Windows (v21.0; IBM, Armonk, NY, USA) program. All data were evaluated on the basis of mean, standard derivation, median (minimum-maximum), distribution frequencies, and percentages. The normalization of data distribution was evaluated by Kolmogorov-Smirnov test The Mann-Whitney U and Kruskal-Wallis tests were used to compare non-normal distribution variables. The chi-square test was used to evaluate categorizable variables. Results were considered statistically significant when the p value was <0.05.

Results

In the study group, 60.7% (n=37) of the patients were 45 years of age or older and 39.3% (n=24) were under 45 years of age. When histological variants are examined, classical PTCa with a ratio of 31.1% (n=19) is observed most frequently, while other common subgroups are 27.9% (n=17) multiple variant types, 14.8% (n=9) follicular TCa, and 11.5% (n=7) oncocytic PTCa. All subtypes of other tumors are presented in Table 1.

The average diameter of the largest tumor was 1.8±1.3 (range: 0.5-7.0) cm, 67.2% of lesions (n=41) are multicentric. 31.1% (n=19) were right lobes, 31.1% (n=19) were left lobes, and 37.7% (n=23) were bilateral placement. The thyroid capsule invasion was observed in 49.2% (n=30) and LN metastasis was observed in 16.4% (n=10). Three months after RAI in the postoperative period, the mean ± SD Tg levels were 79.9±469.7 (distribution range: 0.0-3649.0) ng/mL.

Integrin α3 expression was found to be 50.8% (n=31) in normal tissue, 67.2% (n=41) in tumor tissue (Figure 1, 2) and 9.8% (n=6) in metastatic LN. The expression of integrin β1 was evaluated in 4.9% (n=3) of normal tissue, 57.4% (n=35) of tumor tissue (Figure 3) and 16.4% (n=10) of metastatic LN. No statistically significant difference was observed in classic type PTCa (57.9%) and other poor differential variants (57.1%) when the expression of integrin β1 in tumor tissue was compared with clinical features (p=0.956). When the tumor diameters were less than 4 cm (n=57, 93.4%) and more 4 cm (n=4, 6.6%), no statistically significant difference was detected in terms of the presence of integrin β1 expression (p=0.203). Integrin β1 expression (25.7%) in primary tumors of patients with LN metastasis was found to be statistically significantly higher (p=0.022). Significantly higher integrin β1 expression [62.9% (positive) & 37.1% (negative)] was detected in the primary tumor of the patients with capsule invasion (p=0.014). The increase in postoperative Tg levels in the presence of integrin β1 expression was not statistically significant (p=0.555) (Table 2).

Table 1. Distribution of TCa tumor variants in the cases

Tumor variants	n (%)
Classic PTCa	19 (31.1)
Multiple variants	17 (27.9)
Follicular TCa	9 (14.8)
Oncocytic PTCa	7 (11.5)
Tall cell variant PTCa	3 (4.9)
Solid variant of PTCa	3 (4.9)
Warthin-like PTCa	2 (3.3)
Clear cell PTCa	1 (1.6)
Total	61 (100)

PTCa: Papillary thyroid cancer, TCa: Thyroid cancer

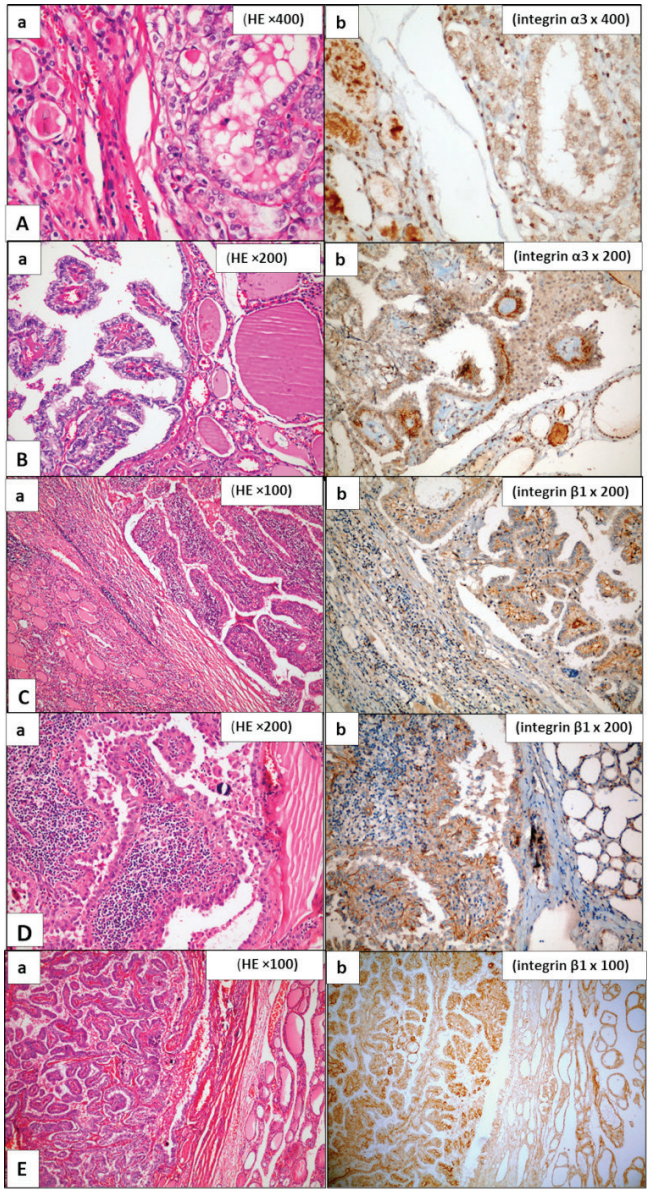

Figure 1. (A) a. Thyroid papillary carcinoma, classic variant (HE × 400). b. Poor cytoplasmic and membranous staining with integrin α3 in carcinoma cells (score 1) (integrin α3 x 400). (B) a. Thyroid papillary carcinoma, classic variant (HE × 200). b. Cytoplasmic membranous staining with integrin α3 in carcinoma cells compared to surrounding non-neoplastic thyroid tissue (score 2) (integrin α3 x 200). (C) a. Warthin-like variant of papiller thyroid carcinoma (HE × 100). b. Membranous staining with integrin β1 (4B7R) in a small number of carcinoma cells (score 1) [integrin β1 (4B7R) x 200]. (D) a. Warthin-like variant of papiller thyroid carcinoma (HE × 200). b. Significant membranous staining with integrin β1 (4B7R) in carcinoma cells compared to surrounding non-neoplastic thyroid tissue (score 2) [integrin β1 (4B7R) x 200]. (E) a. Thyroid papillary carcinoma, classic variant (HE × 100). b. Strong membranous staining with integrin β1 (4B7R) in most carcinoma cells (score 3) [integrin β1 (4B7R) x 100]
HE: Hematoxylin and eosin

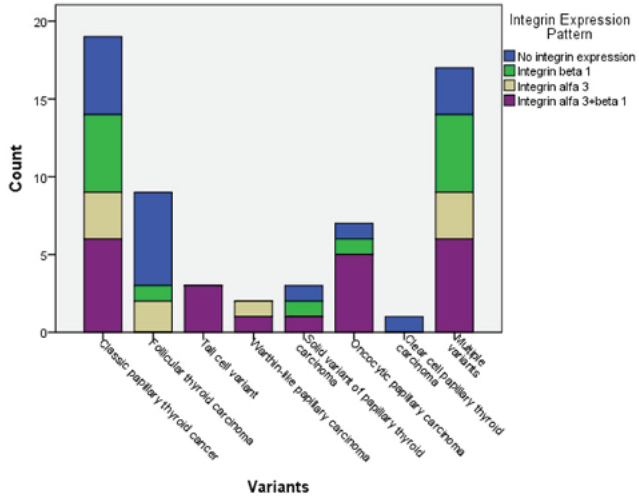

Figure 2. Integrin α3 and β1 expression distribution between all variants

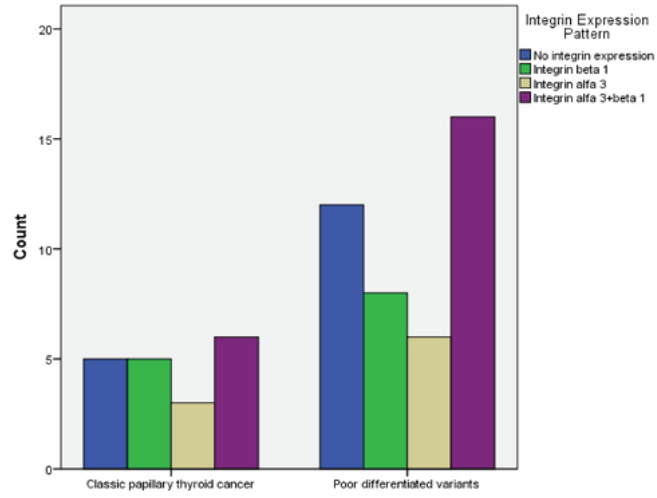

Figure 3. Distribution of integrin α3 and β1 expression between classic PTCa and poor differentiated variants
PTCa: Papillary thyroid cancer

When clinical features and expression of integrin α3 in primary tumor tissue were compared, no statistically significant difference was observed in the classic PTCa and poor differential variants (p=0.717). However, integrin α3 expression (25.8%) was found to be statistically significantly higher in primary tumor in LN metastases (p=0.045). The increase in postoperative Tg levels was not statistically significant in the presence of Integrin α3 expression (p=0.655) (Table 3).

In 27.9% (n=17) of the cases, both types of integrin expression were not observed, while in 21.3% (n=13) only integrin β1, in 14.8% (n=9) only integrin α3 and in 36.1% (n=22) integrin α3 and β1 expression were both observed.

However, the distributions of these groups on variants were not statistically significant (p=0.764) (Figure 2, 3). In primary tumor and lymph node metastasis, both integrin β1 and integrin α3 receptors were negative in 9 patients. The subtype distribution of these patients was as follows; 2 follicular (Tg: 0.43-2.38), 1 tall cell + classic (Tg: 3.85), 1 oncocytic (Tg: 3.51), 1 clear cell (Tg: 8.85) and 4 classical variants of papillary cancer (Tg: 0.39-213.24). There were multiple bone metastases in one of the patients with a classical variant with a serum Tg value of 213.24.

Discussion

Integrins regulate complex cellular behavior, such as intracellular signaling, survival, proliferation, migration, and transition. To date, pancreatic cancer, melanoma, prostate cancer, ovarian cancer, and many other cancer types including ECM signal TCa through provocation, especially in regulation; tumor progression, invasion, metastasis E-cadherin plays an important role in the processes is known (9). Integrins are formed in various combinations of α and β subunits and are expressed at varying rates in both normal and tumoral tissues. In normal thyroid tissue, especially α3β1 and αvβ3 integrin expression is restricted rates and their expression increases when cell-cell signaling intensifies and tumor transformation (10). While integrin α1β1 and α6β1 subunits are expressed in both normal and tumor tissues; integrin α6β4 subunit has never been observed in normal and adenomatous follicular cells of the thyroid, only intense expression of the thyroid in malignant forms such as follicular and PTCa has been reported and integrin α6β4 expression has been associated with aggressive tumoral behavior and poor prognosis (11). Liu et al. (12) in a study conducted with 150 TCa patients, integrin αvβ6 expression was never found in normal thyroid tissue; they reported its expression in tumor tissue and metastatic LN and determined the sensitivity of integrin αvβ6 expression to separating normal tissue from TCa at 78.9% and specificity at 62%. In our study, integrin β1 was expressed 4.9% in normal tissue, 57.4% in tumor tissue and 16.4% in metastatic LN. However, the expression of integrin α3 was found to be 50.8% in normal tissue, 67.2% in tumor tissue and 9.8% in metastatic LN. Integrin β1 was observed in 21.3% of cases, integrin α3 in 14.8% and integrin α3 + β1 expression in 36.1%.

Integrin αvβ3 is also known to be expressed at different rates in tumor cells and dividing vascular cells. The role of the thyroid hormone-tetrac (tetra-iodo-thyro-acetic-acid) receptor site on this molecule was determined by angiogenesis, cancer cell proliferation, metastasis and cancer cell resistance pathways (13). Chernaya et al. (14) investigated integrin expression in 70 TCa patients and showed a statistically significant increase in integrin α2 (p=0.037), integrin α3 (p=0.041) and integrin α5 (p=0.048) expression in PTC. Increased expression of integrin α3

Table 2. Relation between integrin β1 expression in tumor tissue and clinical, histopathological features of the patients

	Clinical variables	Integrin β1 expression		p value
		Negative n (%)	Positive n (%)	
Gender	Female Male	20 (76.9%) 6 (23.1%)	28 (80.0%) 7 (20.0%)	0.772
Age	<45 year ≥45 year	9 (34.6%) 17 (65.4%)	15 (42.9%) 20 (57.1%)	0.515
Variant	Classic PTC Poor differentiated variants	8 (42.1%) 18 (42.9%)	11 (57.9%) 24 (57.1%)	0.956
Tumor size	<4 cm ≥4 cm	23 (88.5%) 3 (11.5%)	34 (97.1%) 1 (2.9%)	0.203
Multicentric	Absent Present	9 (34.6%) 17 (65.4%)	11 (31.4%) 24 (68.6%)	0.793
Lobe	Unilateral Bilateral	17 (65.4%) 9 (34.6%)	21 (60.0%) 14 (40.0%)	0.668
LN involvement	Absent Present	25 (96.2%) 1 (3.8%)	26 (74.3%) 9 (25.7%)	0.022*
Thyroid capsular invasion	Absent Present	18 (69.2%) 8 (30.8%)	13 (37.1%) 22 (62.9%)	0.014*
Postoperative thyroglobulin levels	Mean ± SD	12.39±41.24	130.11±618.08	0.555

*p<0.05 statistically significant. PTCa: Papillary thyroid cancer, LN: Lymph node, SD: Standard deviation

Table 3. Relation between integrin α3 expression in tumor tissue and clinical, histopathological features of the patients

	Clinical variables	Integrin α3 expression		
		Negative n (%)	Positive n (%)	p value
Gender	Female Male	24 (80.0%) 6 (20.0%)	24 (77.4%) 7 (22.6%)	0.806
Age	<45 year ≥45 year	10 (33.3%) 20 (66.7%)	14 (45.2%) 17 (54.8%)	0.344
Variant	Classic PTC Poor differentiated variants	0 (52.6%) 20 (47.6%)	9 (47.4%) 22 (52.4%)	0.717
Tumor size	<4 cm ≥4 cm	27 (90.0%) 3 (10.0%)	30 (96.8%) 1 (3.2%)	0.294
Multicentric	Absent Present	11 (36.7%) 19 (63.3%)	9 (29.0%) 22 (71.0%)	0.525
Lobe	Unilateral Bilateral	19 (63.3%) 11 (36.7%)	19 (61.3%) 12 (38.7%)	0.869
LN involvement	Absent Present	28 (93.3%) 2 (6.7%)	23 (74.2%) 8 (25.8%)	0.045*
Thyroid capsular invasion	Absent Present	17 (56.7%) 13 (43.3%)	14 (45.2%) 17 (54.8%)	0.369
Postoperative thyroglobulin levels	Mean ± SD	32.40±97.42	25.94±653.95	0.655

*p<0.05 statistically significant. PTCa: Papillary thyroid cancer, LN: Lymph node, SD: Standard deviation

(p=0.017), integrin α6 (p=0.028) and integrin α9 (p=0.026) was also reported to be statistically significantly higher in patients with T3-T4 stages compared with T1-T2 stages. He et al. (15) in a study conducted with 181 patients with PTCa diagnosis, it was reported that integrin α3 expression showed 96.5% sensitivity and 77.3% specificity. Although the postoperative serum Tg levels were significantly higher in both integrin β1 and α3 expression positive patients than in patients with negative, no statistically significant differences were found in our study (respectively p=0.555, p=0.655). We think that these results are due to the small number of the study groups, as well as large SD values. In our study, we observed a statistically significant increase in integrin β1 expression in the presence of LN metastasis and capsular invasion, and a statistically significant increase in integrin α3 expression in the presence of LN metastasis.

Conclusion

In conclusion, in addition to the increase in integrin α3 and β1 expression in TCa primary tumor tissue, significantly increased expression of integrins in the presence of LN metastasis and capsular invasion was demonstrated. Thus, we think that the expression of integrin α3 and β1 in TCa can be used as diagnostic and prognostic biomarkers.

Ethics

Ethics Committee Approval: Approval from the Institutional Review Board, University of Health and Sciences Turkey, Istanbul Training and Research Hospital Ethics Committee of our hospital was obtained (2670/2021).

Informed Consent: Written informed consent.

Peer-review: Externally peer-reviewed.

Authorship Contributions

Surgical and Medical Practices: T.C.Ş., D.C.T., A.V.S., Concept: E.A., T.F.Ç., Design: E.A., T.A., T.C.Ş., D.C.T., A.V.S., T.F.Ç., Data Collection or Processing: E.A., T.A., Analysis or Interpretation: E.A., T.A., Literature Search: E.A., T.A., Writing: E.A., T.A., T.F.Ç.

Conflict of Interest: No conflict of interest was declared by the authors.

Financial Disclosure: The authors declared that this study has received no financial support.

References

1. Kitahara CM, Sosa JA. The changing incidence of thyroid cancer. Nat Rev Endocrinol 2016;12:646-653.
2. Fugazzola L, Elisei R, Fuhrer D, Jarzab B, Leboulleux S, Newbold K, Smit J. 2019 European Thyroid Association Guidelines for the Treatment and Follow-Up of Advanced Radioiodine-Refractory Thyroid Cancer. Eur Thyroid J 2019;8:227-245.
3. Rivera M, Ghossein RA, Schoder H, Gomez D, Larson SM, Tuttle RM. Histopathologic characterization of radioactive iodine-refractory fluorodeoxyglucose-positron emission tomography-positive thyroid carcinoma. Cancer 2008;113:48-56.
4. Kadry YA, Calderwood DA. Chapter 22: Structural and signaling functions of integrins. Biochim Biophys Acta Biomembr 2020;1862:183206.

5. Seguin L, Desgrosellier JS, Weis SM, Cheresh DA. Integrins and cancer: regulators of cancer stemness, metastasis, and drug resistance. Trends Cell Biol 2015;25:234-240.
6. Klubo-Gwiezdzinska J, Chen X. Targeting integrins with radiolabeled RGD analogues for radiotheranostics of metastatic radioactive iodine nonresponsive thyroid cancer: new avenues in personalized medicine. Thyroid 2020;30:476-478.
7. Lortet-Tieulent J, Franceschi S, Dal Maso L, Vaccarella S. Thyroid cancer "epidemic" also occurs in low- and middle-income countries. Int J Cancer 2019;144:2082-2087.
8. Rahman ST, McLeod DSA, Pandeya N, Neale RE, Bain CJ, Baade P, Youl PH, Jordan SJ. Understanding pathways to the diagnosis of thyroid cancer: are there ways we can reduce over-diagnosis? Thyroid 2019;29:341-348.
9. Cooper J, Giancotti FG. Integrin signaling in cancer: mechanotransduction, stemness, epithelial plasticity, and therapeutic resistance. Cancer Cell 2019;35:347-367.
10. Salzano M, Russo E, Postiglione L, Guerra A, Marotta V, Esposito S, Vitale M. Interferon-γ inhibits integrin-mediated adhesion to fibronectin and survival signaling in thyroid cells. J Endocrinol 2012;215:439-444.
11. Stewart RL, O'Connor KL. Clinical significance of the integrin α6β4 in human malignancies. Lab Invest 2015;95:976-986.
12. Liu S, Liang B, Gao H, Zhang F, Wang B, Dong X, Niu J. Integrin αvβ6as a novel marker for diagnosis and metastatic potential of thyroid carcinoma. Head Neck Oncol 2013;16;5-7.
13. Davis PJ, Glinsky GV, Lin HY, Leith JT, Hercbergs A, Tang HY, Ashur-Fabian O, Incerpi S, Mousa SA. Cancer cell gene expression modulated from plasma membrane integrin αvβ3 by thyroid hormone and nanoparticulate tetrac. Front Endocrinol (Lausanne) 2015;5:240.
14. Chernaya G, Mikhno N, Khabalova T, Svyatchenko S, Mostovich L, Shevchenko S, Gulyaeva L. The expression profile of integrin receptors and osteopontin in thyroid malignancies varies depending on the tumor progression rate and presence of BRAF V600E mutation. Surg Oncol 2018;27:702-708.
15. He M, Zhao Y, Yi H, Sun H, Liu X, Ma S. The combination of TP53INP1, TP53INP2 and AXIN2: potential biomarkers in papillary thyroid carcinoma. Endocrine 2015;48:712-717.

Original Article
Mol Imaging Radionucl Ther 2022;31:82-88 DOI:10.4274/mirt.galenos.2021.43760

Diagnostic Performance of Machine Learning Models Based on ^{18}F-FDG PET/CT Radiomic Features in the Classification of Solitary Pulmonary Nodules

Soliter Pulmoner Nodüllerin Sınıflandırılmasında ^{18}F-FDG PET/BT Radyomik Özelliklerine Dayalı Makine Öğrenme Modellerinin Tanısal Performansı

Yavuz Sami Salihoğlu[1], Rabiye Uslu Erdemir[2], Büşra Aydur Püren[1], Semra Özdemir[1], Çağlar Uyulan[3], Türker Tekin Ergüzel[4], Hüseyin Ozan Tekin[5]

[1]Çanakkale Onsekiz Mart University Faculty of Medicine, Department of Nuclear Medicine, Çanakkale, Turkey
[2]Zonguldak Bülent Ecevit University Faculty of Medicine, Department of Nuclear Medicine, Zonguldak, Turkey
[3]İzmir Katip Çelebi University Faculty of Engineering and Architecture, Department of Mechanical Engineering, İzmir, Turkey
[4]Üsküdar University Faculty of Natural Sciences, Department of Software Engineering, İstanbul, Turkey
[5]University of Sharjah, College of Health Sciences, Department of Medical Diagnostic Imaging, Sharjah, United Arab Emirates

Abstract

Objectives: This study aimed to evaluate the ability of ^{18}fluorine-fluorodeoxyglucose (^{18}F-FDG) positron emission tomography/computed tomography (PET/CT) radiomic features combined with machine learning methods to distinguish between benign and malignant solitary pulmonary nodules (SPN).

Methods: Data of 48 patients with SPN detected on ^{18}F-FDG PET/CT scan were evaluated retrospectively. The texture feature extraction from PET/CT images was performed using an open-source application (LIFEx). Deep learning and classical machine learning algorithms were used to build the models. Final diagnosis was confirmed by pathology and follow-up was accepted as the reference. The performances of the models were assessed by the following metrics: Sensitivity, specificity, accuracy, and area under the receiver operator characteristic curve (AUC).

Results: The predictive models provided reasonable performance for the differential diagnosis of SPNs (AUCs ~0.81). The accuracy and AUC of the radiomic models were similar to the visual interpretation. However, when compared to the conventional evaluation, the sensitivity of the deep learning model (88% vs. 83%) and specificity of the classic learning model were higher (86% vs. 79%).

Conclusion: Machine learning based on ^{18}F-FDG PET/CT texture features can contribute to the conventional evaluation to distinguish between benign and malignant lung nodules.

Keywords: Solitary pulmonary nodule, PET/CT, radiomic, machine learning

Öz

Amaç: Bu çalışmada, ^{18}flor-florodeoksiglukoz (^{18}F-FDG) pozitron emisyon tomografisi/bilgisayarlı tomografi (PET/BT) radyomik özelliklerinin makine öğrenme yöntemleriyle birleştirilmesinin benign ve malign soliter pulmoner nodülleri (SPN) ayırt etme yeteneğini değerlendirmeyi amaçladık.

Yöntem: ^{18}F-FDG PET/BT taramasında SPN saptanan 48 hastanın verileri geriye dönük olarak değerlendirildi. PET/BT görüntülerinden doku özelliği çıkarımı, açık kaynaklı bir uygulama (LIFEx) kullanılarak yapıldı. Modelleri oluşturmak için derin öğrenme ve klasik makine öğrenme algoritmaları

Address for Correspondence: Yavuz Sami Salihoğlu Asst. Prof., Çanakkale Onsekiz Mart University Faculty of Medicine, Department of Nuclear Medicine, Çanakkale, Turkey
Phone: +90 286 263 59 50-2034 **E-mail:** yssalihoglu@hotmail.com ORCID ID: orcid.org/0000-0003-2465-9128
Received: 03.09.2021 **Accepted:** 26.12.2021

kullanıldı. Patoloji ve izlem ile kesinleşen tanı referans olarak kabul edildi. Modellerin performansları şu metriklerle değerlendirildi: Duyarlılık, özgüllük, doğruluk ve alıcı operatör özellikleri eğrisi altındaki alan (EAA).

Bulgular: Tahmine dayalı modeller, SPN'lerin ayırıcı tanısı için makul performans sağlandı (EAA'ler ~0,81). Radyomik modellerin doğruluğu ve EAA'sı görsel yorumlamaya benzerdi. Ancak geleneksel değerlendirme ile karşılaştırıldığında, derin öğrenme modelinin duyarlılığı (%88'e karşı %83) ve klasik öğrenme modelinin özgüllüğü (%86'ya karşı %79) daha yüksekti.

Sonuç: ^{18}F-FDG PET/BT doku özelliklerine dayalı makine öğrenimi, iyi huylu ve kötü huylu akciğer nodüllerini ayırt etmek için geleneksel değerlendirmeye katkıda bulunabilir.

Anahtar kelimeler: Soliter pulmoner nodül, PET/BT, radyomik, makine öğrenmesi

Introduction

Lung cancer is an important health problem, representing about a quarter of all cancers (1). Early-stage lung cancer may manifest as pulmonary nodules with several distinct features on medical imaging. A solitary pulmonary nodule (SPN) is defined as a well-marginated, rounded parenchymal lesion less than 30 mm in diameter, not associated with other lung pathologies. Common causes of SPN include benign diseases such as infectious granulomas and hamartomas, as well as primary or metastatic lung cancers (2). The management of patients with SPN includes periodic follow-up or further imaging and histopathological examination, considering the malignancy risk (3,4). Positron emission tomography/computed tomography (PET/CT) are widely preferred imaging techniques to detect and characterize SPN, however their diagnostic efficacy does not fully meet clinical needs (5,6).

Radiomics is defined as obtaining high-throughput quantitative features and information from medical images and is a promising approach that has received widespread attention recently (7,8,9,10). Previously, classical machine learning methods and more recently, artificial intelligence applications have been explored for a wide variety of potential uses in lung cancer imaging (11,12,13). Deep learning algorithms using large datasets, such as those from lung cancer screening trials, detect and classify pulmonary nodules with high diagnostic accuracy (13,14).

Several predictive models with generally high diagnostic accuracy based on a combination of radiomic features from lung CT and PET/CT have been proposed for different clinical goals (15,16,17,18,19). Preliminary evidence from these studies is promising however more research is needed to verify these results before clinical application. In this study, we aimed to develop predictive models based on ^{18}fluorine-fluorodeoxyglucose (^{18}F-FDG) PET/CT texture features for the differential diagnosis of SPN and to evaluate the diagnostic performance of these models.

Materials and Methods

Study Populations

The data of patients who underwent ^{18}F-FDG PET/CT between January 2014 and December 2018 were analyzed retrospectively. The patients included had all the criteria following: (i) ^{18}F-FDG avid SPN detected on PET/CT (n=108); (ii) availability of pathological evidence or at least one-year follow-up (n=80) for the final diagnosis of nodules, as a reference standard. The exclusion criteria are as follows: (i) Nodules at the base of the lungs likely to cause respiratory artifacts (n=15); (ii) nodules with too small metabolic volume to allow adequate tissue features to be extracted (n=17). Finally, the data of 48 patients were evaluated under the above criteria. The Local Ethics Committee of Canakkale Onsekiz Mart University Faculty of Medicine approved this study under the decision number: 09.12.2020/2020-14 and patient informed consent was waived.

PET/CT Acquisition Procedure

^{18}F-FDG PET/CT scans were performed using an integrated PET/CT system (Gemini TF16 PET/CT; Philips Medical Systems). PET images were acquired 60±5 minutes after the intravenous injection of ^{18}F-FDG at a dose of 350-550 MBq in patients who fasted for at least 6 hours and had blood glucose <150 mg/dL. First, a low-dose CT scan (120 kVp peak voltage, of 60-150 mA automated tube current, and 5 mm slice thickness) without contrast enhancement was acquired from the skull vertex to the proximal thigh. Then, PET images were acquired for 2-3 minutes per bed position in 3D mode. PET images were reconstructed using the line-of-response row-action maximum likelihood algorithm (LOR-RAMLA; Philips Astonish TF).

PET/CT Image Interpretation

The PET images were reviewed by two experienced nuclear medicine specialists blinded by the final diagnosis, and the final decision was reached by consensus. The decision for benign and malignant nodules was based on ^{18}F-FDG avidity on PET, along with CT features such as size, margin, density, and calcification (20).

Feature Extraction

An open-source application (LIFEx version 6.30) was used for texture analysis from PET/CT images (21). This application declares Image Biomarker Standardization Initiative compliance. A fixed relative thresholding technique was applied for the tumor delineation on images. A 3-D spherical volume of interest (VOI) was initially placed on the entire lesion. A 40% maximum standardized uptake value (SUV_{max}) threshold was applied to (semi)automatically delineation the VOI of the target lesion on the PET images. All volumes were spatially resampled of 4×4×4 mm in size; absolute resampling was used for intensity rescaling with bounds from 0 to 20 SUV (64 bins, 0.32 fixed bin width); and 64 gray levels were applied for intensity discretization. Radiomic features derived from PET images included conventional indices; first-order features-histogram; shape features; second-order texture features [gray-level co-occurrence matrix (GLCM), gray-level run-length matrix (GLRLM), gray-level zone length matrix (GLZLM) and neighborhood gray-tone different matrix (NGLDM)]. A detailed description of the texture parameters can be found at http://www.lifexsoft.org.

Model Establishment

First, feature selection and dimensionality reduction were applied to the feature dataset using the recursive feature elimination (RFE) method. The RFE is a feature selection method that fits a model and removes the weakest features until the specified number of features is reached (22). We build two prediction models based on supervised machine learning classification algorithms selected feature sets: Extreme gradient boosting (XGB) and deep neural network (DNN) to distinguish between benign and malignant nodules. XGB is a tree-based algorithm under the supervised branch of machine learning. XGB, which ensembles the decision tree methods, uses a computationally efficient descent algorithm to minimize errors while adding new trees (19). Deep learning is multi-layer feed-forward neural network that accepts images as input and can be trained end-to-end in a supervised method while learning highly discriminative image features. The opportunity to use large databases has paved the way for the wider adoption of machine/deep learning techniques, particularly in lung cancer assessment (14).

For all models, the dataset was randomly split into two sets using 70% of the samples for training/validating the models and the remaining 30% for testing the results. The models were evaluated using k-fold cross-validation, with three repeats and 10 folds. Figure 1 illustrates the workflow of the radiomic analysis.

Statistical Analysis

We used IBM SPSS statistics software (version 23.0; SPSS Inc.) and Python software to perform statistical analyses. We investigated the performance of predictive models and compared them with the visual evaluation. The following metrics obtained through the confusion matrix were used to compare the performance of the models: Sensitivity, specificity, accuracy, and area under the receiver operator characteristic curve.

Results

In total, the records of 80 patients with SPN were reviewed. Thirty-two patients were excluded under the exclusion criteria. As a result, the study group consisted of 48 patients (31 males, 17 females) with a mean age of 62.38±11.27 years. All of the malignant nodules and 12 of the benign lesions were pathologically proven; the diagnosis of benign lesions was confirmed by follow-up in 5 patients. Thirty-one lesions were malignant nodules, and 17 lesions were benign. The most common malignant diagnosis was adenocarcinoma (58%), while the benign disease was a granulomatous change (53%). The diagnosis and subtypes of SPNs are summarized in Table 1. The majority of malignant nodules (71%) occurred in the upper lobes, whereas about half of the benign nodules (48%) occurred in the lower lobes. Central calcification was observed in four of the benign nodules and punctual calcification was observed in one of the malignant nodules. While most benign nodules tend to have well-defined edges, about half of the malignant nodules have irregular and poorly defined margins. The average diameter of malignant nodules was 20.32 mm (range 16.1-30) and that of benign nodules was 16.9 mm (range 14.2-30). The average SUV_{max} of malignant nodules was 5.46 (range 1.88-10.33) and that of benign nodules was 2.06 (range 1.12-6.77). While SUV_{max} was <2.5 in 24% (4/17) of malignant nodules, SUV_{max} was >2.5 in 23% (7/31) of benign nodules.

The ten most relevant PET features obtained after feature selection and used to develop predictive models are represented in Table 2. The three features with the highest score by the assessment of feature importance were GLZLM_SZLGE (n=30), HISTO_Energy (n=21), and SUV_{bwmean} (n=21). A few of the second-order features (D_HISTO_Energy, GLCM_Homogeneity, NGLDM_Busyness) were higher in benign nodules, while conventional SUV-related features and other second-order features were higher in the malignant group. Texture features that differ significantly between malignant and benign nodules are shown in Table 3.

Table 4 shows the performance of radiomic models and visual interpretation in the differential diagnosis of SPN.

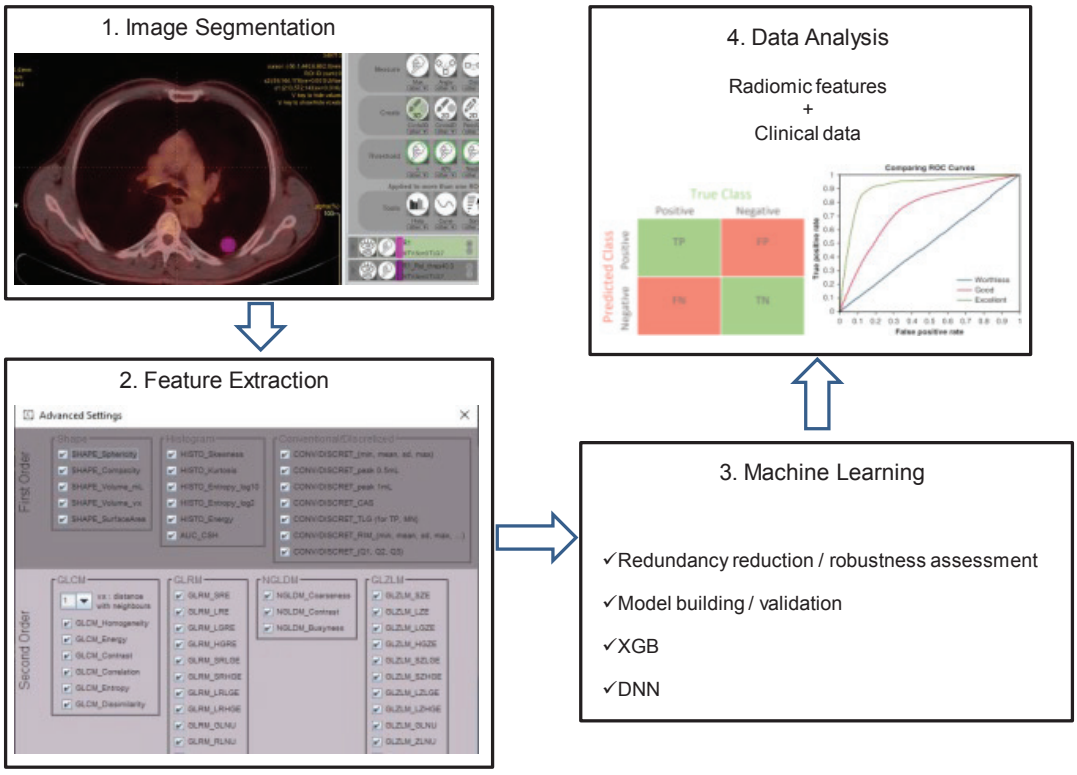

Figure 1. The flowchart of radiomics. 1) The VOI was (semi)automatically defined on PET/CT images with a threshold of 40% of the SUV_{max}. 2) Radiomic features from the VOI were extracted, including first-order and second-order features. 3) Predictive models were established by feature selection methods and classification methods. 4) The model's performance was evaluated by appropriate statistical methods
VOI: Volume of interest, PET/CT: Positron emission tomography/computed tomography, SUV_{max}: Maximum standardized uptake value

Table 1. The diagnosis and subtypes of the SPNs

Type	Diagnosis	Number
Benign (n=17)	Infectious granuloma	9
	Hamartoma	3
	Not specified*	5
Malignant (n=31)	Adenocarcinoma	18
	Squamous cell carcinoma	7
	Metastasis	2
	Small cell carcinoma	2
	Carcinoid tumor	2

*Diagnosed by follow-up, SPNs: Solitary pulmonary nodules

Table 2. The most relevant PET features obtained after feature selection

f score	Texture features
f0	C_SUV_{bwmean}
f1	D_HISTO_Energy
f2	GLCM_Energy
f3	GLCM_Dissimilarity
f4	GLRLM_HGRE
f5	GLRLM_SRHGE
f6	GLRLM_LRHGE
f7	NGLDM_Busyness
f8	GLZLM_SZLGE
f9	GLZLM_SZHGE

SUV: Standardized uptake value, GLCM: Gray-level co-occurrence matrix, GLRLM: Gray-level run-length matrix, NGLDM: Neighborhood gray-tone different matrix, GLZLM: Gray-level zone length matrix

The overall diagnostic performances of both models were close to each other. The DNN model improved sensitivity, while the XGB model increased specificity compared to visual assessment.

Discussion

In this study, we evaluated the performance of machine learning models based on ^{18}F-FDG PET/CT radiomic features for SPN classification. We have shown that the diagnostic accuracy of predictive models is higher than that of commonly used clinical metrics and visual interpretation. The improved diagnostic performance could benefit by

Table 3. Texture features with significant differences between malignant benign nodules

Features	Benign SPN	Malign SPN	p
C_SUV$_{bwmin}$	1.19±0.75	2.61±1.27	0.0003
C_SUV$_{bwmean}$	2.52±1.63	6.53±2.62	<0.0001
C_SUV$_{bwmax}$	4.11±2.56	10.85±4.52	<0.0001
D_HISTO_Energy	0.22±0.14	0.08±0.03	<0.0001
GLCM_Homogeneity	0.54±0.17	0.33±0.11	<0.0001
GLCM_Energy	0.081±0.19	0.014±0.011	<0.0001
GLCM_Dissimilarity	1.27±1.21	4.72±2.13	<0.0001
GLRLM_HGRE	124±104	567±232	<0.0001
GLRLM_SRHGE	95±121	543±423	<0.0001
GLRLM_LRHGE	148.95±137.49	672.55±470.7	<0.0001
NGLDM_Busyness	0.87±0.52	0.24±0.23	<0.0001
GLZLM_SZLGE	0.013±0.013	0.004±0.008	<0.0001
GLZLM_SZHGE	48.75±45.77	342.91±306.06	<0.0001

SPN: Solitary pulmonary nodule, SUV: Standardized uptake value, GLCM: Gray-level co-occurrence matrix, GLRLM: Gray-level run-length matrix, NGLDM: Neighborhood gray-tone different matrix, GLZLM: Gray-level zone length matrix

Table 4. The estimated performances of radiomic models and visual interpretation

Model	SN	SP	ACC	AUC
DNN	88%	82%	0.80	0.81
XGB	81%	86%	0.79	0.80
VI	83%	79%	0.80	0.80

SN: Sensitivity, SP: Specificity, ACC: Accuracy, AUC: Area under the curve, DNN: Deep neural network, XGB: Extreme gradient boosting, VI: Visual interpretation

preventing unnecessary invasive tests following false-positive findings or providing an earlier diagnosis of malignant disease.

^{18}F-FDG PET/CT has reasonable sensitivity to differentiate benign from malignant pulmonary nodules but has lower specificity due to granulomatous diseases (5,6,23,24). Many recent studies have concluded that medical image radiomic features improve clinical or imaging outcomes in many cancers. Although the results available in the literature are promising, they have not yet been sufficiently introduced into clinical practice due to well-known limitations such as the lack of use of standardized methods in the workflow and the lack of external validation (9,10,13).

PET/CT radiomics in lung cancer have been investigated for clinical goals such as characterization of nodules, histological subtyping, prediction of survival, and response to therapy (11,12). Few studies that focused on the characterization of pulmonary nodules demonstrated the ability of PET/CT radiography to distinguish between malign and benign lesions (15,16,17,18,19,25,26,27). In the studies, the results of machine learning models trained with texture features derived from ^{18}F-FDG PET/CT were compared with standard metrics [SUV, metabolic tumor volume (MTV), and total lesion glycolysis] and/or visual interpretation evaluation. Studies with dual time point ^{18}F-FDG PET/CT, particularly the results obtained with tissue properties in delayed images, provided important improvements for classifying SPNs (14,15,27,28). Texture features that reflect intra-lesional heterogeneity, termed second-order texture features in this study, showed significant differences between the malignant and benign groups, as reported in studies.

Our predictive models showed reasonable diagnostic performance with balanced sensitivity and specificity for the differential diagnosis of SPNs. Compared with the conventional evaluation results, the deep learning model increased sensitivity, while the classic machine learning model increased specificity. The overall performance of our models was consistent with the results of the cited studies; however, the improvement in diagnostic accuracy was less than the reported results (15,16,17,18,19). This difference may be due to the small size of our cohort and the fact that the diagnosis of all nodules was not confirmed by pathology. Additionally, most investigators created models with tissue features from dual time-point PET/CT, and higher diagnostic accuracy was reported, particularly from delayed images.

In standard PET/CT scans, respiratory motion adversely affects both alignment and image sharpness, resulting in reduced tracer uptake and an overestimation of MTV (29). Several PET/CT radiomics articles have reported that respiratory motion significantly affects the values of texture features of lung lesions (30,31). These effects differ according to the location of the lesion in the lung; for example, it is more prominent in the lower lobes. Therefore, nodules located in the lower lobes of the lungs were excluded from the radiomic analysis in our study.

It is difficult to compare the results of machine learning studies reported on PET/CT imaging of lung cancer, as researchers have chosen different materials and methods to construct their models. We performed PET/CT radiomic analysis with two models based on classifiers and feature selection methods to improve the quality score of our study, as suggested by Lambin et al. (32). Zhou et al. (19) compared the performance of machine learning models based on PET/CT radiomics for the classification of lung lesions (16). They reported that most classifiers combined with appropriate feature selection methods showed excellent discrimination. They suggested that gradient

boosting decision tree and random forest are the best classification methods. In another study, the deep learning method was compared with classical machine learning methods to classify mediastinal lymph node metastasis in PET/CT images (33). The authors reported that there was no significant difference between the results of deep learning and classical methods, however, machine learning methods have higher sensitivity but lower specificity than doctors.

Study Limitations

Several limitations should be considered in our study. First, this study was a retrospective analysis and inherent selection bias existed. Secondly, the small size of our study population may have adversely affected the performance of machine learning algorithms. Thirdly, the study's lack of external validation limits the generalizability of our results.

Conclusion

In this study, we performed a machine learning-based analysis of pulmonary nodules using PET/CT images. We found that ^{18}F-PET/CT-based radiomic features can provide added value in differentiating SPNs. The method should be further confirmed in large-scale multicenter, ideally prospective studies so that it can be applied in routine clinical practice.

Ethics

Ethics Committee Approval: The Local Ethics Committee of Canakkale Onsekiz Mart University Faculty of Medicine approved this study under the decision number: 09.12.2020/2020-14.

Informed Consent: Patient informed consent was waived.

Peer-review: Externally peer-reviewed.

Authorship Contributions

Design: Y.S.S., Data Collection or Processing: R.U.E., B.A.P., Y.S.S., Ç.U., T.T.E., H.O.T., Analysis or Interpretation: Y.S.S., S.Ö., R.U.E., Literature Search: Y.S.S., R.U.E., Writing: Y.S.S., S.Ö.

Conflict of interest: No conflict of interest was declared by the authors.

Financial Disclosure: The authors declare that this study has received no financial support.

References

1. Siegel RL, Miller KD, Jemal A. Cancer statistics, 2019. CA Cancer J Clin 2019;69:7-34.
2. Nasim F, Ost DE. Management of the solitary pulmonary nodule. Curr Opin Pulm Med 2019;25:344-353.
3. Bai C, Choi CM, Chu CM, Anantham D, Chung-Man Ho J, Khan AZ, Lee JM, Li SY, Saenghirunvattana S, Yim A. Evaluation of pulmonary nodules: clinical practice consensus guidelines for Asia. Chest 2016;150:877-893.
4. MacMahon H, Naidich DP, Goo JM, Lee KS, Leung ANC, Mayo JR, Mehta AC, Ohno Y, Powell CA, Prokop M, Rubin GD, Schaefer-Prokop CM, Travis WD, Van Schil PE, Bankier AA. Guidelines for management of incidental pulmonary nodules detected on CT images: from the Fleischner Society 2017. Radiology 2017;284:228-243.
5. Jia Y, Gong W, Zhang Z, Tu G, Li J, Xiong F, Hou H, Zhang Y, Wu M, Zhang L. Comparing the diagnostic value of ^{18}F-FDG-PET/CT versus CT for differentiating benign and malignant solitary pulmonary nodules: a meta-analysis. J Thorac Dis 2019;11:2082-2098.
6. Divisi D, Barone M, Bertolaccini L, Zaccagna G, Gabriele F, Crisci R. Diagnostic performance of fluorine-18 fluorodeoxyglucose positron emission tomography in the management of solitary pulmonary nodule: a meta-analysis. J Thorac Dis 2018;10(Suppl 7):S779-S789.
7. Zwanenburg A. Radiomics in nuclear medicine: robustness, reproducibility, standardization, and how to avoid data analysis traps and replication crisis. Eur J Nucl Med Mol Imaging 2019;46:2638-2655.
8. Mayerhoefer ME, Materka A, Langs G, Häggström I, Szczypi ski P, Gibbs P, Cook G. Introduction to Radiomics. J Nucl Med 2020;61:488-495.
9. Hatt M, Cheze Le Rest C, Antonorsi N, Tixier F, Tankyevych O, Jaouen V, Lucia F, Bourbonne V, Schick U, Badic B, Visvikis D. Radiomics in PET/CT: current status and future AI-based evolutions. Semin Nucl Med 2021;51:126-133.
10. Piñeiro-Fiel M, Moscoso A, Pubul V, Ruibal Á, Silva-Rodríguez J, Aguiar P. A Systematic review of pet textural analysis and radiomics in cancer. Diagnostics (Basel) 2021;11:380.
11. Bianconi F, Palumbo I, Spanu A, Nuvoli S, Fravolini ML, Palumbo B. PET/CT radiomics in lung cancer: an overview. Appl Sci 2020;10:1718.
12. Manafi-Farid R, Karamzade-Ziarati N, Vali R, Mottaghy FM, Beheshti M. 2-[(18)F]FDG PET/CT radiomics in lung cancer: an overview of the technical aspect and its emerging role in management of the disease. Methods 2021;188:84-97.
13. Krarup MMK, Krokos G, Subesinghe M, Nair A, Fischer BM. Artificial intelligence for the characterization of pulmonary nodules, lung tumors and mediastinal nodes on PET/CT. Semin Nucl Med 2021;51:143-156.
14. Avanzo M, Stancanello J, Pirrone G, Sartor G. Radiomics and deep learning in lung cancer. Strahlenther Onkol 2020;196:879-887.
15. Chen S, Harmon S, Perk T, Li X, Chen M, Li Y, Jeraj R. Diagnostic classification of solitary pulmonary nodules using dual time ^{18}F-FDG PET/CT image texture features in granuloma-endemic regions. Sci Rep 2017;7:9370.
16. Chen S, Harmon S, Perk T, Li X, Chen M, Li Y, Jeraj R. Using neighborhood gray tone difference matrix texture features on dual time point PET/CT images to differentiate malignant from benign FDG-avid solitary pulmonary nodules. Cancer Imaging 2019;19:56.
17. Zhang J, Ma G, Cheng J, Song S, Zhang Y, Shi LQ. Diagnostic classification of solitary pulmonary nodules using support vector machine model based on 2-[18F]fluoro-2-deoxy-D-glucose PET/computed tomography texture features. Nucl Med Commun 2020;41:560-566.
18. Palumbo B, Bianconi F, Palumbo I, Fravolini ML, Minestrini M, Nuvoli S, Stazza ML, Rondini M, Spanu A. Value of shape and texture features from ^{18}F-FDG PET/CT to discriminate between benign and malignant solitary pulmonary nodules: an experimental evaluation. Diagnostics (Basel) 2020;10:696.
19. Zhou Y, Ma XL, Zhang T, Wang J, Zhang T, Tian R. Use of radiomics based on ^{18}F-FDG PET/CT and machine learning methods to aid clinical decision-making in the classification of solitary pulmonary lesions: an innovative approach. Eur J Nucl Med Mol Imaging 2021;48:2904-2913.
20. Cruickshank A, Stieler G, Ameer F. Evaluation of the solitary pulmonary nodule. Intern Med J 2019;49:306-315.

21. Nioche C, Orlhac F, Boughdad S, Reuzé S, Goya-Outi J, Robert C, Pellot-Barakat C, Soussan M, Frouin F, Buvat I. LIFEx: a freeware for radiomic feature calculation in multimodality imaging to accelerate advances in the characterization of tumor heterogeneity. Cancer Res 2018;78:4786-4789.
22. Jeon H, Oh S. Hybrid-recursive feature elimination for efficient feature selection. Applied Sciences 2020;10:3211.
23. Taralli S, Scolozzi V, Foti M, Ricciardi S, Forcione AR, Cardillo G, Calcagni ML. ^{18}F-FDG PET/CT diagnostic performance in solitary and multiple pulmonary nodules detected in patients with previous cancer history: reports of 182 nodules. Eur J Nucl Med Mol Imaging 2019;46:429-436.
24. Deppen SA, Blume JD, Kensinger CD, Morgan AM, Aldrich MC, Massion PP, Walker RC, McPheeters ML, Putnam JB Jr, Grogan EL. Accuracy of FDG-PET to diagnose lung cancer in areas with infectious lung disease: a meta-analysis. JAMA 2014;312:1227-1236.
25. Du D, Gu J, Chen X, Lv W, Feng Q, Rahmim A, Wu H, Lu L. Integration of PET/CT radiomics and semantic features for differentiation between active pulmonary tuberculosis and lung cancer. Mol Imaging Biol 2021;23:287-298.
26. Hu Y, Zhao X, Zhang J, Han J, Dai M. Value of ^{18}F-FDG PET/CT radiomic features to distinguish solitary lung adenocarcinoma from tuberculosis. Eur J Nucl Med Mol Imaging 2021;48:231-240.
27. Nakajo M, Jinguji M, Aoki M, Tani A, Sato M, Yoshiura T. The clinical value of texture analysis of dual-time-point ^{18}F-FDG-PET/CT imaging to differentiate between 18F-FDG-avid benign and malignant pulmonary lesions. Eur Radiol 2020;30:1759-1769.
28. Teramoto A, Tsujimoto M, Inoue T, Tsukamoto T, Imaizumi K, Toyama H, Saito K, Fujita H. Automated classification of pulmonary nodules through a retrospective analysis of conventional CT and two-phase PET images in patients undergoing biopsy. Asia Ocean J Nucl Med Biol 2019;7:29-37.
29. Vaidya M, Creach KM, Frye J, Dehdashti F, Bradley JD, El Naqa I. Combined PET/CT image characteristics for radiotherapy tumor response in lung cancer. Radiother Oncol 2012;102:239-245.
30. Oliver JA, Budzevich M, Zhang GG, Dilling TJ, Latifi K, Moros EG. Variability of image features computed from conventional and respiratory-gated PET/CT images of lung cancer. Transl Oncol 2015;8:524-534.
31. Grootjans W, Tixier F, van der Vos CS, Vriens D, Le Rest CC, Bussink J, Oyen WJ, de Geus-Oei LF, Visvikis D, Visser EP. The Impact of optimal respiratory gating and image noise on evaluation of intratumor heterogeneity on 18F-FDG PET imaging of lung cancer. J Nucl Med 2016;57:1692-1698.
32. Lambin P, Leijenaar RTH, Deist TM, Peerlings J, de Jong EEC, van Timmeren J, Sanduleanu S, Larue RTHM, Even AJG, Jochems A, van Wijk Y, Woodruff H, van Soest J, Lustberg T, Roelofs E, van Elmpt W, Dekker A, Mottaghy FM, Wildberger JE, Walsh S. Radiomics: the bridge between medical imaging and personalized medicine. Nat Rev Clin Oncol 2017;14:749-762.
33. Wang H, Zhou Z, Li Y, Chen Z, Lu P, Wang W, Liu W, Yu L. Comparison of machine learning methods for classifying mediastinal lymph node metastasis of non-small cell lung cancer from ^{18}F-FDG PET/CT images. EJNMMI Res 2017;7:11.

Original Article
Mol Imaging Radionucl Ther 2022;31:89-95 DOI:10.4274/mirt.galenos.2022.00377

Correlation of Morphological and Functional Cardiac Images: Fusion of Myocardial Perfusion SPECT and CT Angiography

Morfolojik ve Fonksiyonel Kardiyak Görüntülerin Korelasyonu: Miyokard Perfüzyon SPECT ve BT Anjiyografi Füzyonu

Hüseyin Şan[1], Alper Özgür Karaçalıoğlu[2], Uğur Bozlar[3], Semra İnce[2], Engin Alagöz[2], Mustafa Özdeş Emer[2], Mustafa Taşar[3], Nuri Arslan[2]

[1]University of Health Sciences Turkey, Ankara City Hospital, Clinic of Nuclear Medicine, Ankara, Turkey
[2]University of Health Sciences Turkey, Gülhane Training and Research Hospital, Clinic of Nuclear Medicine, Ankara, Turkey
[3]University of Health Sciences Turkey, Gülhane Training and Research Hospital, Clinic of Radiology, Ankara, Turkey

Abstract

Objectives: The current study evaluates the value of cardiac hybrid imaging (CHI), performed by the fusion of functional and anatomic cardiac images, in the detection of hemodynamically significant coronary stenosis in cases with multiple coronary stenosis.

Methods: A total of 36 patients (10 female, 26 male) in whom ischemia or infarction was detected on gated myocardial perfusion single photon emission computed tomography (gMPS) and multiple coronary stenosis were concomitantly detected on coronary computed tomography angiography (CCTA) and undergone invasive coronary angiography (ICA) was included in this study. Statistical analyses were performed using SPSS 22 Windows software. McNemar test was applied to show concordance between coronary CT angiography, ICA and CHI in the detection of anatomically or hemodynamically significant stenosis in three major coronary arteries. Comparison results of coronary arteries responsible for perfusion defects on CHI and gMPS are presented as percentages (%).

Results: There was total accordance between coronary arteries leading to perfusion defects detected by gMPS and CHI in 50% of patients. It was observed a partial accordance in 36.1% of the patients. Additionally, it was also detected perfusion defects originated from side branches in 25% of the patients. Between results of CCTA and ICA, no statistically significant difference was noted in the detection of anatomically significant stenoses in the left main coronary artery, left anterior descending artery (LAD), left circumflex artery (LCx) and right coronary artery (RCA) (p=1.000, 0.070, 0.549, and 1.000, respectively). In addition, no statistically significant difference was found in the detection of anatomically and hemodynamically significant stenoses in LAD, LCx and RCA by CCTA and CHI (p=0.344, 0.629, and 0.219, respectively). No statistically significant difference was observed in the detection of anatomically and hemodynamically significant stenoses in LAD, LCx and RCA by ICA and CHI (p=0.804, 1.000, and 0.344, respectively).

Conclusion: It is possible to detect hemodynamically significant coronary stenosis directly by CHI modality in patients with multiple coronary stenosis, wide perfusion defects.

Keywords: Cardiac hybrid imaging, coronary stenosis, myocardial perfusion scintigraphy, coronary CT angiography

Öz

Amaç: Bu çalışmanın amacı, fonksiyonel ve anatomik kardiyak görüntülerin füzyonu ile gerçekleştirilen kardiyak hibrid görüntülemenin (KHG), multipl koroner darlıkları ve perfüzyon defektleri olan olgularda, hemodinamik olarak ciddi koroner darlıkları saptamadaki katkısını değerlendirmektir.

Address for Correspondence: Hüseyin Şan MD, University of Health Sciences Turkey, Ankara City Hospital, Clinic of Nuclear Medicine, Ankara, Turkey
Phone: +90 312 552 60 00 **E-mail:** dr.huseyinsan@yahoo.com ORCID ID: orcid.org/0000-0002-2264-5446
Received: 14.09.2021 **Accepted:** 03.01.2022

Yöntem: Çalışmaya gated miyokard perfüzyon sintigrafisi tek foton emisyonlu bilgisayarlı tomografi (gMPS) tetkikinde iskemi veya enfarkt ve koroner bilgisayarlı tomografi anjiyografi (KBTA) tetkikinde birden fazla koroner darlık saptanarak girişimsel koroner anjiyografi (GKA) yapılan toplam 36 hasta (10 kadın, 26 erkek) dahil edildi. Anatomik ve fonksiyonel görüntüler CardIQ Fusion yazılımı (GE Healthcare, IL, ABD) ile birleştirildi. İstatistiksel analizler SPSS 22 yazılımı kullanılarak yapıldı. Üç ana koroner arterde anatomik ve hemodinamik olarak ciddi koroner darlık tespitinde, KBTA, GKA ve KHG arasındaki uyumu göstermek için McNemar testi uygulandı. KHG ve gMPS'de perfüzyon defektlerinden sorumlu koroner arterlerin karşılaştırıldığı sonuçlar yüzde olarak sunuldu.

Bulgular: Hastaların %50'sinde, gMPS ve KHG ile perfüzyon defektlerinden sorumlu olduğu düşünülen koroner arterler arasında tam bir uyum vardı. Hastaların %36,1'inde kısmi uyum gözlenirken, %13,9'unda ise gMPS ile KHG tamamen uyumsuzdu. Hastaların %25'inde, KHG sayesinde, perfüzyon defektlerinden koroner yan dallardaki darlıkların sorumlu olduğu saptandı. Sol ana koroner arter, sol ön inen arter, sol sirkumfleks arter ve sağ koroner arterde anatomik olarak ciddi darlıkların saptanmasında; KBTA ve GKA sonuçları arasında istatistiksel olarak anlamlı bir fark saptanmadı (sırasıyla; p=1,000, 0,070, 0,549 ve 1,000). Ayrıca sol ön inen arter, sol sirkumfleks arter ve sağ koroner arterde; anatomik ve hemodinamik olarak ciddi darlıkların saptanmasında, KBTA ve KHG sonuçları arasında istatistiksel olarak anlamlı fark bulunmadı (sırasıyla; p=0,344, 0,629 ve 0,219). Ayrıca sol ön inen arter, sol sirkumfleks arter ve sağ koroner arterde; anatomik ve hemodinamik olarak ciddi darlıkların saptanmasında, GKA ve KHG arasında istatistiksel olarak anlamlı bir fark gözlenmedi (sırasıyla; p=0,804, 1,000 ve 0,344).

Sonuç: Multipl koroner darlıkları ve geniş perfüzyon defektleri olan hastalarda, KHG yöntemi ile iskemiden sorumlu olan, hemodinamik olarak ciddi koroner darlıkların doğrudan tespit edilmesi mümkündür.

Anahtar kelimeler: Kardiyak hibrid görüntüleme, koroner stenoz, miyokard perfüzyon sintigrafisi, koroner BT anjiyografi

Introduction

Coronary artery diseases (CAD) are the most common causes of mortality worldwide (1,2). COURAGE and FAME studies have shown that coronary revascularization should be performed by targeting ischemia in stable CAD (3,4). Moreover, it is crucial to detect or rule out hemodynamically significant stenosis and to verify left ventricular ischemic burden using non-invasive methods to decrease risks associated with invasive interventions (5).

In patients with multiple coronary atherosclerotic plaques, history of previous percutaneous coronary intervention (PCI) and coronary artery by-pass grafting (CABG), gated myocardial perfusion scintigraphy (gMPS) usually detect perfusion defects. However, because of differences in individual coronary anatomy and the complexity of multiple coronary stenoses, detection of coronary stenosis responsible for perfusion defects that requires clinical intervention has become increasingly difficult. In such cases, cardiac hybrid imaging (CHI) is a precious approach to localize the hemodynamically significant stenosis (6). Otherwise, discrepancies between gMPS and invasive coronary angiography (ICA) may cause difficulties in patient management and usage of unnecessary and risky invasive interventions (5). CHI is a modality that fuses myocardial perfusion single photon emission computed tomography (SPECT)/positron emission tomography (PET) and coronary computed tomography angiography (CCTA) images using automatic software. CHI provides more diagnostic data compared with separately or side-by-side evaluation of these two tests (7).

Objectives

With the above background, this retrospective study investigated the potential benefits of CHI in detecting hemodynamically significant coronary stenosis in patients with a medical history of multiple coronary stenosis, CABG and PCI.

Materials and Methods

Patient Sample

Data of patients who underwent CCTA, Tc-99m-Sestamibi gMPS and ICA between 2011 and 2016 were reviewed from the archives of the tertiary hospital. CCTA was performed 1 month before or after gMPS. A total of 36 patients (10 female, 26 male) were enrolled in this retrospective study. The inclusion criteria of the study were as follows: (i) patients who had perfusion defects at gMPS; (ii) patients who had coronary stenosis at CCTA. Patients with valvular heart disease, morbid obesity and cardiac arrhythmias were excluded from this study.

Evaluation of gMPS imaging: For exercise imaging, cardiac vasodilatation was achieved by following the standard Bruce protocol (stepwise increments of velocity and slope every 3 min) or maximum coronary hyperemia was pharmacologically achieved by 6-min intravenous infusion of adenosine (140 mcg/kg/min). The imaging started 25±5 min after injection of 7±1 mCi (259±37 mBq) Tc-99m sestamibi (Cardio-SPECT Medi-Radiopharma, Hungary). According to the two-day protocol, the "rest-condition imaging" was performed again 24±2 h after exercise imaging by the same protocol. Before the first day of the imaging study, daily quality control of the gamma was conducted routinely. A dedicated cardiac gamma camera

(Discovery NM 530c, GE Healthcare, Haifa, Israel) was used for both the stress and rest imaging. The dedicated cardiac gamma camera was equipped with a multiple pinhole collimator and 19 stationary cadmium-zinc-telluride detectors, with each detector containing 32×32 pixel 5-mm thick (2.46×2.46 mm) elements. A window of 15% was centered on the 140 keV gamma peak and the gating was conducted with 16 frames per RR cycle. List mode files were obtained and stored. Images were reconstructed with SPECT acquisition (Xeleris II, GE Healthcare, Israel) using a dedicated iterative algorithm. A Butterworth post-processing filter (frequency 0.37, order 7) was applied to these constructed slices. The images were reconstructed without scatter or attenuation correction. All two-day evaluations were done by the automated software Quantitative Gated SPECT/Quantitative Perfusion SPECT (Cedars-SinaiMedical Center, Los Angeles, CA). The left ventricle was divided into 20 segments using an apical, mid-ventricular and basal short-axis slice as well as a mid-vertical long-axis view for visual analysis. Each segment was scored qualitatively using a 5-point scoring scale (0, normal; 1, mild; 2, moderate; 3, severe reduction in photon activity; 4, absence of photon activity). The summed stress score (SSS) and summed rest score (SRS) were calculated by adding the scores for all 20 segments and within each vascular territory [left anterior descending artery (LAD) and left circumflex artery (LCx) and right coronary artery (RCA)] for each image. The classification "reversible" was used for images with an SSS greater than the respective SRS.

Evaluation of Coronary Computed Tomography Angiography

Before the workup, pulse rates were checked and controlled with β-blocker if necessary (maximum 60/minimum). Nitroglycerin (0.4 mg) was administered sublingual 1-3 times for coronary vasodilatation and pulse rates were continuously monitored. Moreover, 70-80 mL contrast medium was infused (4.5-5 mL/s), a 320-detector CT device was used (Aquilion One, Toshiba Medical System, Japan) and imaging was performed by prospective electrocardiograph triggering with 100-120 Kvp phantom and patient-based modified tube voltage. Reconstructed images were evaluated by Vitrea FX version 6.2 (VitalImages, MN, USA) and artifacts were minimized by further investigation. Stenosis in coronary arteries and/or their branches was divided into four groups as follows: 0-24%, 25-49%, 50-74%, and >75%. Stenosis >50% was defined as "anatomically significant."

Invasive Coronary Angiography

Imaging was performed through the right femoral approach using the Judkins technique, standard 6-7 French catheters and a Siemens Axiom Artis FC device (Siemens Medical Solutions, Germany). After intubation of the left coronary artery, right anterior oblique caudal, anteroposterior axis cranial, left anterior oblique caudal and right anterior oblique caudal (spider) views were evaluated. Further investigations were performed as necessary. ICA images were evaluated retrospectively and the same stenosis classification was applied. Stenosis >50% was defined as "anatomically significant".

Cardiac Hybrid Imaging Fusion Phase

All anatomic and functional images were fused by CardIQ Fusion software (Advantage Workstation 4.3, GE Healthcare, IL, USA). All axes from two separate imaging techniques were interlaced and optimized automatically. A perfusion map that was inserted into three-dimensional (3D) CCTA images of the left ventricle was assessed and discrepancies were rectified. After the exclusion of pulmonary arteries and veins, the "coronary artery tree" was created and software fused 3D images of the left ventricle and coronary artery were interlaced to create a CHI (Figure 1, 2, 3). Evaluation of gMPS and CHI results was

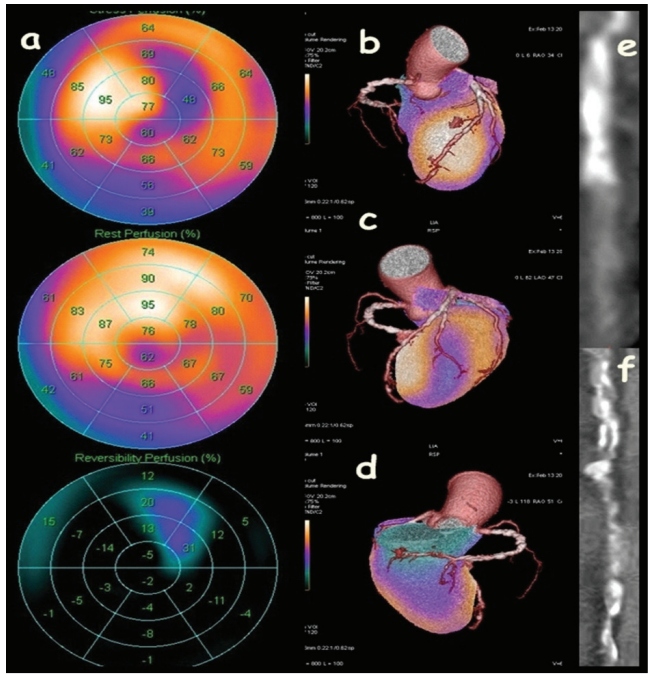

Figure 1. gMPS and CHI findings a) gMPS polar map images; top: Stress perfusion, medium: Rest perfusion, bottom: Reversibility perfusion. b) Fusion image; normal perfusion areas at LAD vascularization zone. c) Fusion image; reversible perfusion defects at diagonal artery vascularization zone. d) Fusion image; fixed perfusion defects at RCA vascularization zone. e) CCTA image; severe calcified stenosis at diagonal artery. f) CCTA image; severe calcified stenosis at main body of RCA
gMPS: Gated myocard perfusion scintigraphy, CHI: Cardiac hybrid imaging, LAD: Left anterior descending artery, RCA: Right coronary artery, CCTA: Coronary computed tomography angiography

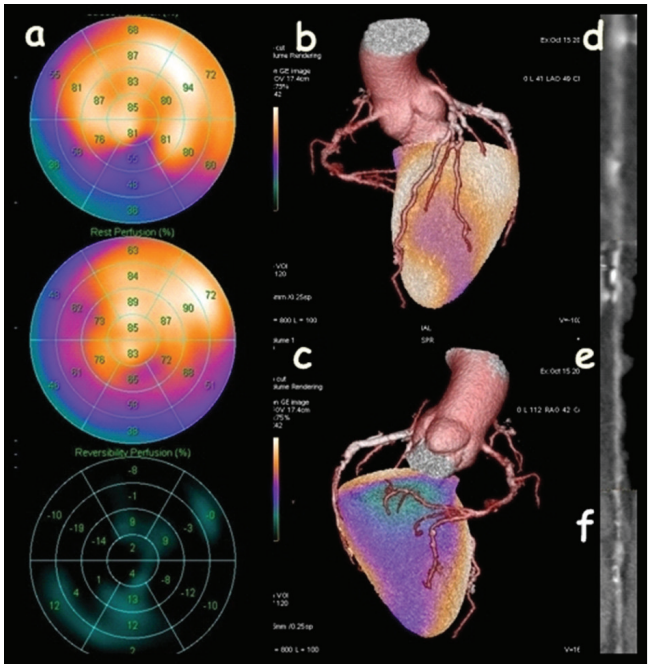

Figure 2. gMPS and CHI findings a) gMPS polar map images; top: Stress perfusion, medium: Rest perfusion, bottom: Reversibility perfusion. b) Fusion image; hypoperfusion areas at 2nd and 3rd diagonal artery vascularization zone. c) Fusion image; perfusion defects at RCA vascularization zone. d) CCTA image; severe calcified stenosis at 3rd diagonal artery. e) CCTA image; severe calcified stenosis at 2nd diagonal artery. f) CCTA image; severe calcified stenosis at main body of RCA
gMPS: Gated myocard perfusion scintigraphy, CHI: Cardiac hybrid imaging, LAD: Left anterior descending artery, RCA: Right coronary artery, CCTA: Coronary computed tomography angiography

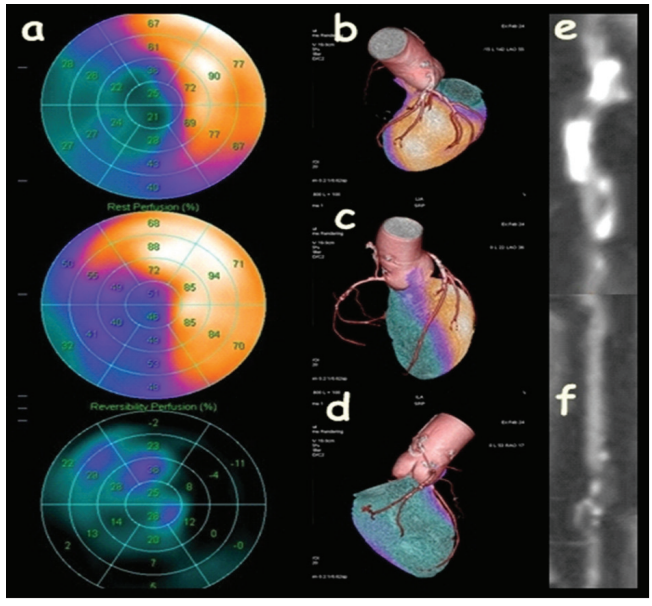

Figure 3. gMPS and CHI findings a) gMPS polar map images; top: Stress perfusion, medium: Rest perfusion, bottom: Reversibility perfusion. b) Fusion image; normal perfusion areas of diagonal branch and LCx vascularization zone. c) Fusion image; partially reversible perfusion defects at LAD vascularization zone. d) Fusion image; wide perfusion defects at RCA vascularization zone. e) CCTA image; severe calcified stenosis at LAD. f) CCTA image; severe calcified and mixed type stenosis at main body of RCA
gMPS: Gated myocard perfusion scintigraphy, CHI: Cardiac hybrid imaging, LCx: Left circumflex artery, LAD: Left anterior descending artery, RCA: Right coronary artery, CCTA: Coronary computed tomography angiography

blinded. Atherosclerotic stenosis in the coronary arteries and/or their branches with normal perfusion was defined as "hemodynamically insignificant" but perfusion defects with stenosis >50% were defined as "hemodynamically significant." Gulhane Military Medical Academy Command Local Ethics Committee granted approval for the study (approval number: 05.01.2016/25).

Statistical Analysis

Statistical consistency between CCTA, ICA and CHI results on significant anatomic and hemodynamic stenoses in three major coronary arteries were evaluated using the McNemar test. SPSS Statistics version 22 (IBM Corp., Armonk, NY, USA) was used. Comparison results of the coronary arteries responsible for the perfusion defects on CHI, gMPS and other comparisons were presented as percentages (%).

Results

The median age of the patients was 60.1±10.9 (38-82) years, 10 (27.8%) of them were female and 26 (72.2%) were male. Among the participants, thirteen patients had a history of PCI and/or CABG and twenty-three patients had native coronary arteries. Patient characteristics are presented in Table 1.

Coronary arteries responsible for perfusion defects that were detected by gMPS and CHI were totally compatible in 50% of the patients (18 of 36); however, they were partially compatible in 36.1% of the patients (13 of 36). In 46.2% (n=6/13) of partially compatible cases, additional stenoses in different coronary arteries causing the same perfusion defects were observed by CHI, apart from the coronary arteries considered responsible by gMPS. By contrast, in 53.8% (n=7/13) of the cases, CHI revealed that some coronary arterial stenosis considered responsible for the perfusion defects detected by gMPS were not the causative ones. Furthermore, 13.9% of the cases (n=5/36) were completely incompatible because the coronary arteries identified by gMPS as responsible for the perfusion defects were not actually the ones that created them

because these perfusion defects were caused by different coronary arteries or branches. Moreover, in 25% (n=9) of cases, perfusion defects were actually sourced from stenosis in the side branches by CHI evaluation.

Between results of CCTA and ICA, no statistically significant difference was noted in the detection of anatomically significant stenoses in the LMCA, LAD, LCx and RCA (p=1.000, 0.070, 0.549, and 1.000, respectively). In addition, no statistically significant difference was found in the detection of anatomically and hemodynamically significant stenoses in the LAD, LCx and RCA by CCTA and CHI (p=0.344, 0.629 and 0.219, respectively). Furthermore, no statistically significant difference was observed in the detection of anatomically and hemodynamically significant stenoses in the LAD, LCx and RCA by ICA and CHI (p=0.804, 1.000, and 0.344, respectively). The distributions of anatomically and hemodynamically significant stenosis in three major coronary arteries are presented in Table 2.

Table 1. The characteristics of the participants

	Mean (SD)
Age	60.10±10.90
Ejection fraction (%) (gMPS)	58.89±2.08
Myocardial perfusion defect extent	15.22±1.93
Summed stress score	11.69±1.62
Summed rest score	5.58±0.93
Gender	**n**
Female	10
Male	26
History of treatment for coronary arteries	**n**
PCI	1
CABG	9
PCI + CABG	3
Native coronary artery	23

SD: Standard deviation, n: Number of patients, PCI: Percutaneous coronary intervention, CABG: Coronary artery bypass greft, gMPS: Gated myocardial perfusion scintigraphy

Discussion

In the last few decades, CAD has become one of the most common causes of mortality and morbidity; while diagnostic approaches have been modified according to new developments and patient populations. For diagnosis, minimally invasive methods are generally preferred, particularly when the patient has multiple comorbidities. This study focused on patients who had multiple coronary atherosclerotic plaques, history of PCI or CABG. Identification of the hemodynamically significant stenosis that causes myocardial ischemia is a challenge; thus, multidisciplinary diagnostic approaches are often preferred. CHI appears beneficial in such cases by demonstrating a hemodynamically significant stenosis directly. In this study, no statistically significant difference was noted in the detection of anatomically and hemodynamically significant stenoses in the LAD, LCx, and RCA by CCTA, ICA, and CHI. Although concepts of anatomically and hemodynamically significant stenosis are different, we suppose that most of the anatomically significant stenoses were also hemodynamically significant in our study.

In separate evaluations using gMPS and CHI, coronary arteries which were considered responsible for perfusion defects by gMPS and CHI, were completely compatible in 50%, partially compatible in 36.1% and totally incompatible in 13.9% of the patients. In partially compatible and totally incompatible groups, in addition to the coronary artery, which is thought responsible for the perfusion defects detected by gMPS, CHI revealed that perfusion defects are actually caused by stenosis in a different coronary artery and that some coronary arteries considered responsible for the perfusion defects in gMPS are not actually responsible for them. The anatomy of the coronary arteries may vary among individuals, which sometimes creates discordance with standard myocardial segmentation maps in gMPS (8). This condition suggests the superiority of CHI over separately or side-by-side evaluations performed by gMPS

Table 2. The distribution of anatomically and hemodinamically significant stenosis in three major coronary arteries

	Coronary CT angiography			**Invasive coronary angiography**			**Cardiac hybrid imaging**		
	Stenosis severity <%50	**Stenosis severity ≥%50**	**Total number of patients**	**Stenosis severity <%50**	**Stenosis severity ≥%50**	**Total number of patients**	**Hemodinamically insignificant stenosis**	**Hemodinamically significant stenosis**	**Total number of patients**
LAD	12	24	36	18	18	36	16	20	36
Cx	11	25	36	14	22	36	14	22	36
RCA	16	20	36	16	20	36	20	16	36

LAD: Left anterior descending artery, Cx: Circumflex artery, RCA: Right coronary artery

and CCTA. CHI enables direct 3D observation of coronary arteries that cause perfusion defects (7). Javadi et al. (9) reported that this discordance was observed between PET and CHI for at least one segmentation in 72% of the patients, with a total discordance rate of 9% (n=112/1207 segmentations). In the "EVINCI" study of Liga et al. (8), 25% (n=146/1004) of the perfusion defects detected by gMPS and PET did not show actual concordance with individual anatomical evaluations performed by CHI. By CHI, 18% of the perfusion defects were detected to originate in a totally different coronary artery; thus, diagnoses in 42% of the cases were modified (8).

Studies have indicated that CHI plays a major role in patients with intermediate to high risk of CAD who have unclear gMPS and CCTA findings (7,10,11). In a prospective study, Schaap et al. (10) found that CHI had a positive predictive value of 91% [95% confidence interval (CI): 72-98] and negative predictive value of 90% (95% CI: 60-98) in cases with non-conclusive gMPS and CCTA findings. Researchers claimed that the fusion of functional and anatomical imaging data provides a "synergistic" approach to compensate for their own weaknesses, especially potential false-positive results by CCTA and false-negative results by gMPS (10). In our study, CCTA was reported as suboptimal due to intense coronary calcifications and motion artifacts in one patient. CHI revealed that stenosis at the LAD and the third obtuse marginali branch of the LCx were responsible for perfusion defects; however, stenoses at the first diagonal branch of the LAD and RCA were hemodynamically insignificant in this patient. Another patient had a perfusion defect at inferior cardiac wall that was suspected as a potentially false-positive result at gMPS, due to the gastrointestinal activity. False-positive result at gMPS was confirmed by CHI since there was no coronary stenosis in the RCA. In addition, perfusion defects that are not accompanied by coronary stenosis might have resulted from a microvascular disease or endothelial dysfunction. Certain diagnosis of these diseases can be made by quantitative evaluation of regional absolute myocardial blood flow with Rb-82, N-13-ammonium, and O-15 PET radionuclides (12). By this modality, anatomically insignificant but with impaired blood flow CAD, such as a microvascular disease or endothelial dysfunction may be also detected (12).

In this study, with CHI, 25% (n=9) of the detected perfusion defects were caused by hemodynamically significant stenosis at the side branches. It is impossible to specify and differentiate whether the major coronary arteries or the side branch is responsible for perfusion defects detected by gMPS, particularly when there are multiple stenosis. CHI can guide targeted revascularization by direct observation of hemodynamically significant stenosis at the side branches responsible for ischemia (13).

Study Limitations

The retrospective design, lack of routine measurement of fractional flow reserve during the gold standard ICA and absence of a statistical design for the correlation between CCTA and gMPS are the limitations of our study.

Conclusion

In patients with high risk of CAD, multiple coronary stenoses, history of PCI or CABG and wide perfusion defects, specifying the location of hemodynamically significant stenosis becomes challenging. In such cases, CHI appears beneficial by providing fused data of the 3D coronary anatomy and myocardial perfusion map with high spatial accuracy, which enables direct observation of hemodynamically significant stenosis. CHI can guide ischemia-targeted revascularization procedures. In addition, CHI can prevent unnecessary interventions to hemodynamically insignificant stenosis.

Acknowledgment

In this article, we thank to Atila İyisoy MD, Turgay Çelik MD for their permission during data collection and Ali Korhan Sığ MD for his support.

Ethics

Ethics Committee Approval: Gulhane Military Medical Academy Command Local Ethics Committee granted approval for the study (approval number: 05.01.2016/25).

Informed Consent: Since the study had been designed as a "retrospective study"; no informed consent was required.

Peer-review: Externally peer-reviewed.

Authorship Contributions

Surgical and Medical Practices: H.Ş., A.Ö.K., U.B., S.İ., E.A., M.Ö.E., Concept: H.Ş. A.Ö.K., U.B., M.T., N.A., Design: H.Ş., A.Ö.K., U.B., M.T., N.A., Data Collection or Processing: H.Ş., A.Ö.K., U.B., S.İ., E.A., M.Ö.E., M.T., N.A., Analysis or Interpretation: H.Ş., A.Ö.K., A.Ö.K., U.B., Literature Search: H.Ş., S.İ., E.A., M.Ö.E., A.Ö.K., U.B., Writing: H.Ş., A.Ö.K., U.B.

Conflict of Interest: No conflict of interest was declared by the authors.

Financial Disclosure: The authors declared that this study has received no financial support.

References

1. Lee AK, Qutub MA, Aljizeeri A, Chow BJ. Integrating anatomical and functional imaging for the assessment of coronary artery disease. Expert Rev Cardiovasc Ther 2013;11:1301-1310.
2. Roger VL, Go AS, Lloyd-Jones DM, Adams RJ, Berry JD, Brown TM, Carnethon MR, Dai S, de Simone G, Ford ES, Fox CS, Fullerton HJ, Gillespie C, Greenlund KJ, Hailpern SM, Heit JA, Ho PM, Howard VJ, Kissela BM, Kittner SJ, Lackland DT, Lichtman JH, Lisabeth LD, Makuc DM, Marcus GM, Marelli A, Matchar DB, McDermott MM, Meigs JB, Moy CS, Mozaffarian D, Mussolino ME, Nichol G, Paynter NP, Rosamond WD, Sorlie PD, Stafford RS, Turan TN, Turner MB, Wong ND, Wylie-Rosett J; American Heart Association Statistics Committee and Stroke Statistics Subcommittee. Heart disease and stroke statistics–2011 update: a report from the American Heart Association. Circulation 2011;123:e18-e209.
3. Shaw LJ, Berman DS, Maron DJ, Mancini GB, Hayes SW, Hartigan PM, Weintraub WS, O'Rourke RA, Dada M, Spertus JA, Chaitman BR, Friedman J, Slomka P, Heller GV, Germano G, Gosselin G, Berger P, Kostuk WJ, Schwartz RG, Knudtson M, Veledar E, Bates ER, McCallister B, Teo KK, Boden WE; COURAGE Investigators. Optimal medical therapy with or without percutaneous coronary intervention to reduce ischemic burden: results from the Clinical Outcomes Utilizing Revascularization and Aggressive Drug Evaluation (COURAGE) trial nuclear substudy. Circulation 2008;117:1283-1291.
4. Tonino PA, Fearon WF, De Bruyne B, Oldroyd KG, Leesar MA, Ver Lee PN, Maccarthy PA, Van't Veer M, Pijls NH. Angiographic versus functional severity of coronary artery stenoses in the FAME study fractional flow reserve versus angiography in multivessel evaluation. J Am Coll Cardiol 2010;55:2816-2821.
5. Tonino PA, De Bruyne B, Pijls NH, Siebert U, Ikeno F, van' t Veer M, Klauss V, Manoharan G, Engstrøm T, Oldroyd KG, Ver Lee PN, MacCarthy PA, Fearon WF; FAME Study Investigators. Fractional flow reserve versus angiography for guiding percutaneous coronary intervention. N Engl J Med 2009;360:213-224.
6. Zamorano JL, Bax J, Knuuti J, Lancellotti P, Pinto F, Popescu BA, Sechtem U. The ESC Textbook of Cardiovascular Imaging: Oxford University Press, USA; 2015.
7. Gaemperli O, Bengel FM, Kaufmann PA. Cardiac hybrid imaging. Eur Heart J 2011;32:2100-2108.
8. Liga R, Vontobel J, Rovai D, Marinelli M, Caselli C, Pietila M, Teresinska A, Aguadé-Bruix S, Pizzi MN, Todiere G, Gimelli A, Chiappino D, Marraccini P, Schroeder S, Drosch T, Poddighe R, Casolo G, Anagnostopoulos C, Pugliese F, Rouzet F, Le Guludec D, Cappelli F, Valente S, Gensini GF, Zawaideh C, Capitanio S, Sambuceti G, Marsico F, Filardi PP, Fernández-Golfín C, Rincón LM, Graner FP, de Graaf MA, Stehli J, Reyes E, Nkomo S, Mäki M, Lorenzoni V, Turchetti G, Carpeggiani C, Puzzuoli S, Mangione M, Marcheschi P, Giannessi D, Nekolla S, Lombardi M, Sicari R, Scholte AJ, Zamorano JL, Underwood SR, Knuuti J, Kaufmann PA, Neglia D, Gaemperli O; EVINCI Study Investigators. Multicentre multi-device hybrid imaging study of coronary artery disease: results from the Evaluation of Integrated Cardiac Imaging for the Detection and Characterization of Ischaemic Heart Disease (EVINCI) hybrid imaging population. Eur Heart J Cardiovasc Imaging 2016;17:951-960.
9. Javadi MS, Lautamäki R, Merrill J, Voicu C, Epley W, McBride G, Bengel FM. Definition of vascular territories on myocardial perfusion images by integration with true coronary anatomy: a hybrid PET/CT analysis. J Nucl Med 2010;51:198-203.
10. Schaap J, Kauling RM, Boekholdt SM, Nieman K, Meijboom WB, Post MC, Van der Heyden JA, de Kroon TL, van Es HW, Rensing BJ, Verzijlbergen JF. Incremental diagnostic accuracy of hybrid SPECT/CT coronary angiography in a population with an intermediate to high pre-test likelihood of coronary artery disease. Eur Heart J Cardiovasc Imaging 2013;14:642-649.
11. Flotats A, Knuuti J, Gutberlet M, Marcassa C, Bengel FM, Kaufmann PA, Rees MR, Hesse B; Cardiovascular Committee of the EANM, the ESCR and the ECNC. Hybrid cardiac imaging: SPECT/CT and PET/CT. A joint position statement by the European Association of Nuclear Medicine (EANM), the European Society of Cardiac Radiology (ESCR) and the European Council of Nuclear Cardiology (ECNC). Eur J Nucl Med Mol Imaging 2011;38:201-212.
12. Dilsizian V, Narula J. Atlas of nuclear cardiology: Springer Science & Business Media; 2013.
13. Gaemperli O, Kaufmann PA, Alkadhi H. Cardiac hybrid imaging. Eur J Nucl Med Mol Imaging 2014;41(Suppl 1):S91-S103.

Original Article
Mol Imaging Radionucl Ther 2022;31:96-103 DOI:10.4274/mirt.galenos.2022.38247

Prevalence and Clinical Significance of Incidental Focal ^{18}F-FDG Uptake in Colon on PET/CT Imaging

PET/BT Görüntülemede Kolonda İnsidental Fokal ^{18}F-FDG Tutulumunun Prevalansı ve Klinik Önemi

Yasemin Gökden[1], Filiz Özülker[2], Tamer Özülker[2]

[1]University of Health Sciences Turkey, Prof. Dr. Cemil Taşcıoğlu City Hospital, Clinic of Internal Medicine, İstanbul, Turkey
[2]University of Health Sciences Turkey, Prof. Dr. Cemil Taşcıoğlu City Hospital, Clinic of Nuclear Medicine, İstanbul, Turkey

Abstract

Objectives: The present study aimed to identify the prevalence of focal uptake in the colon on ^{18}fluorine-fluorodeoxyglucose (^{18}F-FDG) positron emission tomography/computed tomography (PET/CT) studies performed for the evaluation of malignancies other than colon, to detect the rate of malignancy in incidental focal ^{18}F-FDG avid colonic lesions and to investigate if any possible role of maximum standardized uptake value (SUV_{max}) values in the discrimination of malignant lesions from premalignant and benign ones exist.

Methods: We retrospectively reviewed the files of 8,017 patients with known or suspected malignancy, who underwent whole-body ^{18}F-FDG PET/CT at our institution during the period November 2017 to November 2019. Patients showing a single site of focally increased colonic ^{18}F-FDG uptake that was more intense compared to liver uptake on ^{18}F-FDG PET studies and referred to colonoscopy were enrolled in the study.

Results: Fifty two patients (83.8%) had at least 1 corresponding lesion on colonoscopy, whereas in 10 patients no lesion was detected. Subsequent histopathological examinations revealed no corresponding lesion in 13 (13.7%), a benign lesion in 18 (18.9%), hyperplastic polyp in 10 (10.5%), low-grade polyp in 16 (16.8%), high-grade polyp in 29 (30.5%) and malignant lesion in 9 (9.5%) of the focal ^{18}F-FDG uptake sites. According to histopathology results, statistically no significant difference was found between the SUV_{max} measurements of malignant and benign cases ($p>0.05$) but the average SUV_{max} measurements of malignant cases were found to be significantly higher than lower + high-grade cases ($p<0.05$) and hyperplastic polyp cases ($p<0.01$).

Conclusion: In conclusion, any unexpected focal ^{18}F-FDG uptake in ^{18}F-FDG PET/CT studies is suspicious for malignancy and should be clarified by colonoscopy. The intensity of ^{18}F-FDG uptake does not preclude the application of colonoscopy and histopathological verification of the lesion if there is any.

Keywords: Gastrointestinal tract, incidentally detected lesions, colon, incidental ^{18}F-FDG uptake

Öz

Amaç: Bu çalışmanın amaçları kolon dışındaki malignitelerin değerlendirilmesi için yapılan ^{18}flor-florodeoksiglukoz (^{18}F-FDG) pozitron emisyon tomografisi/bilgisayarlı tomografi (PET/BT) çalışmalarında kolonda fokal tutulum prevalansını, tesadüfi fokal ^{18}F-FDG avid kolonik lezyonlarda malignite oranını belirlemek ve maksimum standardize alım değeri (SUV_{maks}) değerlerinin, malign lezyonların premalign ve iyi huylu olanlardan ayırt edilmesindeki olası rolünü araştırmaktı.

Yöntem: Kasım 2017-Kasım 2019 döneminde kurumumuzda tüm vücut ^{18}F-FDG PET/BT uygulanan, malignitesi bilinen veya şüphelenilen 8.017 hastanın dosyalarını geriye dönük olarak inceledik. ^{18}F-FDG PET çalışmalarında kolonda, karaciğer tutulumuna göre daha yoğun tek bir fokal ^{18}F-FDG tutulumu gösteren ve kolonoskopiye yönlendirilen hastalar olan çalışmaya alındı.

Address for Correspondence: Filiz Özülker Assoc. Prof., University of Health Sciences Turkey, Prof. Dr. Cemil Taşcıoğlu City Hospital, Clinic of Nuclear Medicine, İstanbul, Turkey
Phone: +90 506 302 61 57 **E-mail:** fozulker@gmail.com ORCID ID: orcid.org/0000-0003-2075-1429
Received: 27.10.2021 **Accepted:** 07.01.2022

Bulgular: Elli iki hastada (%83,8) kolonoskopide buna karşılık gelen en az 1 lezyon bulunurken, 10 hastada lezyon saptanmadı. Sonraki histopatolojik incelemelerde fokal ^{18}F-FDG tutulum bölgelerinin 13'ünde (%13,7) karşılık gelen lezyon izlenmedi, 18'inde (%18,9) benign lezyon, 10'unda hiperplastik polip (%10,5), 16'sında düşük dereceli polip (%16,8), 29'unda (%30,5) yüksek dereceli polip, 9'unda (%9,5) malign lezyon saptandı. Histopatoloji sonuçlarına göre malign ve benign olguların SUV_{maks} ölçümleri arasında istatistiksel olarak anlamlı fark bulunmazken (p>0,05), malign olguların ortalama SUV_{maks} ölçümleri düşük + yüksek gradlı olgulara (p<0,05) ve hiperplastik polip olgularına (p<0,01) göre anlamlı derecede yüksek bulundu.

Sonuç: Sonuç olarak, ^{18}F-FDG PET/BT çalışmalarında herhangi bir beklenmeyen fokal ^{18}F-FDG tutulumu malignite açısından şüphelidir ve kolonoskopi ile netleştirilmelidir. ^{18}F-FDG tutulumunun yoğunluğu kolonoskopi yapılmasını ve varsa lezyonun histopatolojik olarak doğrulanmasını engellemez.

Anahtar kelimeler: Gastrointestinal sistem, insidental olarak saptanan lezyonlar, kolon, insidental ^{18}F-FDG tutulumu

Inroduction

In imaging studies, an incidental finding, which is commonly named as "incidentaloma," is a lesion which is detected serendipitously and is of indeterminate clinical significance. ^{18}Fluorine-fluorodeoxyglucose (^{18}F-FDG) positron emission tomography/computed tomography (PET/CT) is increasingly being used as an imaging modality in oncology and this has led to an increasing number of focal ^{18}F-FDG-avid lesions in several organs including the thyroid gland, adrenal gland gastrointestinal tract, pituitary gland, prostate gland (1,2,3,4,5). Although identification of some of these findings may provide a chance to treat a secondary primary malignancy, in many cases, further studies done for exploration of these lesions might cause unnecessary anxiety in patients, complications from additional medical interventions and economic burden (6,7).

Physiologic colonic ^{18}F-FDG uptake is a commonly seen variant on PET scans and can be distinguished from malignant processes with its diffuse pattern. Segmental involvement of the colon in ^{18}F-FDG PET studies is suggestive for inflammatory process. Focal involvement of the colon leaves the interpreter with a dilemma since it has the potential for malignancy, while some of the benign lesions also show ^{18}F-FDG uptake. The prevalence of focal colonic incidentalomas detected by ^{18}F-FDG PET or PET/CT was found as 3.6% pooled risk of malignant or premalignant lesions was 68% (8). It can be deduced from all these facts that it is crucial to know the malignancy rates of these lesions and distinguishing features on ^{18}F-FDG PET/CT, in order to make further management properly.

The aims of the present study were to identify the prevalence of focal uptake in the colon on ^{18}F-FDG PET/CT studies done for the evaluation of malignancies other than colon, rate of malignancy in incidental focal ^{18}F-FDG avid colonic lesions and to investigate any possible role of maximum standardized uptake value (SUV_{max}) values in the discrimination of malignant lesions from premalignant and benign ones.

Materials and Methods

Patient Population

We retrospectively reviewed the files of 8,017 patients with known or suspected malignancy, who underwent whole-body ^{18}F-FDG PET/CT at our institution during the period November 2017 to November 2019. Patients with a previous history of colorectal cancer and inflammatory bowel disease, were excluded from our study. Patients showing a single site of focally increased colonic ^{18}F-FDG uptake that was more intense compared to liver uptake on ^{18}F-FDG PET studies and referred to colonoscopy were enrolled in the study. Of the 8,017 patients, 62 (30 men, 32 women; age range, 19-88 y; mean age, 63.66±10.09 y) met these criteria. The type and frequencies of primary malignancies are given in Table 1. Ethical approval was obtained from the Ethics Committee of University of Health Sciences Turkey, Prof. Dr. Cemil Tascioglu City Hospital (protocol number: E-48670771-514.10).

PET/CT Protocol: Imaging and Interpretation

Patients were imaged using an integrated PET/CT scanner that consisted of a full-ring HI-REZ LSO PET and a six-slice CT scanner (Siemens Biograph 6, Chicago, IL, USA).

Patients were instructed to fast, for 4-6 h before the injection of 370-555 MBq (10-15 mCi) of ^{18}F-FDG. All patients were administered oral contrast starting 4 h before the study. Blood glucose levels were measured before the study and ^{18}F-FDG was injected only when the blood glucose level was below 11.11 mmol/L. At 60 min post-injection, PET/CT scan was conducted with an emission time of 3 min per bed position from the vertex to the upper thigh. Before emission images, a low-dose CT scan was performed for attenuation correction and anatomical localization with the following parameters: 50 mA, 140 kV, and 5 mm section thickness. Image analysis was carried out on the Esoft multimodality computer platform (Siemens Medical Solutions, Erlangen, Germany). All images were reassessed by two experienced nuclear medicine physicians who were unaware of the endoscopic and histopathologic results.

Table 1. Baseline features of the patients and their incidental lesions

		n (%)
Age (year)	Min-max	19-88 (64.5)
	Mean ± SD	62.84±11.54
Sex (n=62)	Male	32 (51.6)
	Female	30 (48.4)
Location in colon	Rectum	24 (25.3)
	Sigmoid colon	22 (23.2)
	Descending colon	13 (13.7)
	Transverse colon	12 (12.6)
	Ascending colon	13 (13.7)
	Cecum	7 (7.4)
	Anal region	4 (4.2)
SUV_{max}	Min-max	0-49.8
	Mean ± SD	7.51±8.05
Histopathology	Physiologic	13 (13.7)
	Benign	18 (18.9)
	Hyperplastic polyp	10 (10.5)
	Low grade	16 (16.8)
	High grade	29 (30.5)
	Malignant	9 (9.5)
Size	<1 cm	25 (26.3)
	1-3 cm	37 (38.9)
	3-5 cm	4 (4.2)
	>5 cm	18 (18.9)
	N/A	11 (11.6)
Primary malignancy	Endometrium carcinoma	6 (9.7)
	Breast carcinoma	12 (19.4)
	Carcinoma of unknown primary	9 (14.5)
	Lymphoma	6 (9.7)
	Lung cancer	9 (14.5)
	Neuroendocrine tumor	1 (1.6)
	Testis carcinoma	2 (3.2)
	Gastric carcinoma	2 (3.2)
	Renal cell carcinoma	1 (1.6)
	Pancreas carcinoma	3 (4.8)
	Cholangiocarcinoma	1 (1.6)
	Larynx carcinoma	2 (3.2)
	Cervix carcinoma	2 (3.2)
	Ovarian carcinoma	1 (1.6)
	Skin cancer	4 (6.4)
	Multiple myeloma	1 (1.6)

Min: Minimum, Max: Maximum, SD: Standard deviation, SUV_{max}: Maximum standardized uptake value

Focal suspicious colorectal ^{18}F-FDG uptake sites showing intense activity compared with the liver were recorded, whereas diffuse and segmental uptake sites were excluded.

Regions of interest were manually drawn in transaxial slices encircling the focal activity to measure the SUV_{max} as a semiquantitative index. The colon was divided into 7 anatomical segments as the rectum, sigmoid colon, descending colon, transverse colon, ascending colon, cecum, anal region. The lesions are classified according to their locations in these segments by using the body low-dose CT component.

We accepted a findings in PET/CT results as true-positive when focal ^{18}F-FDG uptake corresponded to a certain lesion in endoscopic or surgical evaluation. When no solid lesion was detected with these evaluations, the cause of the ^{18}F-FDG uptake was attributed to physiologic accumulation of activity and the result was interpreted as false-positive. The true-positive lesions were further categorized as benign, premalignant and malignant.

Colonoscopic and Histopathological Evaluation

Histopathologic evaluation of the lesions following colonoscopy was used as the gold standard and performed in all patients within 60 days of the PET/CT scan. Biopsy or excision of the 95 lesions corresponding to the focal ^{18}F-FDG uptake sites was performed. The descriptions of the lesions were also done morphologically during colonoscopy and the lesions were reported as polyp, mass lesion, diverticulum, hemorrhoid, ulcerovegetative mass, radiation colitis, rectovaginal fistula and ulcer. Any ^{18}F-FDG uptake focus without a corresponding lesion on colonoscopy and negative histopathological result was considered as physiological.

On histopathological evaluation, the lesions are categorized as physiological; benign; hyperplastic polyp; low-grade polyp; high-grade polyp and malignant. The lesions were also categorized according to their dimensions as 1 cm >; 1-3 cm; 3-5 cm; 5 cm <.

Statistical Analysis

Number Cruncher Statistical System 2007 & PASS (Power Analysis and Sample Size) 2008 Statistical Software (Utah, USA) program was used for statistical analysis. While evaluating the study data, in addition to descriptive statistical methods (mean, standard deviation, median, frequency, ratio), Shapiro-Wilk test and box plot graphs were used for the normal distribution of variables. Mann-Whitney U test was used for intergroup comparisons of parameters not showing normal distribution. Spearman's correlation analysis was used to evaluate the relationships between variables. Receiver operating characteristic (ROC)

curve analysis and diagnostic screening tests were used to determine the cut off for the SUV_{max} value. Significance was evaluated at the $p<0.05$ level.

Results

Of the 8,017 PET/CT scans performed during the study period, 95 focally increased colonic ^{18}F-FDG uptake was found in 62 (0.77%) patients. Among these 62 patients showing focal ^{18}F-FDG uptake, 52 patients (83.8%) had at least 1 corresponding lesion in colonoscopy, whereas in 10 patients no lesion was detected. Of the 95 hypermetabolic foci, 7 were in the cecum, 13 in the ascending colon, 12 in the transverse colon, 13 in the descending colon, 22 in the sigmoid colon, 24 in the rectum and 4 in the anal region. Subsequent histopathological examinations revealed no corresponding lesion in 13 (13.7%), a benign lesion in 18 (18.9%), hyperplastic polyp in 10 (10.5%), low-grade polyp in 16 (16.8%), high-grade polyp in 29 (30.5%) and malignant lesion in 9 (9.5%) of the focal ^{18}F-FDG uptake sites. So a premalignant lesion (high grade polyp + low grade polyp) and a malignant lesion were detected in totally 54 (56.8%) of the suspicious hypermetabolic foci.

Malignant and Premalignant Lesions

The malignant lesions were found in the descending colon in 3 (33.3%), transverse colon in 3 (33.3%), rectum in 2 (22.2%) and the sigmoid colon in 1 (11.1%) cases (Figure 1). SUV_{max} in malignant lesions was 14.41±14.4 (0-49.8) on average. The size of the malignant lesions was 4.56±1.32 (2.5-5.5) cm on average. The distribution of 45 premalignant lesions detected on colonoscopy were 14 in sigmoid (31.1%), 7 in the rectum (15.5%), 8 in the ascending colon (17.7%), 7 in the descending colon (15.5%), 6 in transverse colon (13.3%), 3 in the cecum (6.6%). Histopathologic examination revealed 29 high-grade and 16 low-grade polyps (n=24 tubuler adenoma; n=21 tubulovillous adenoma) showing ^{18}F-FDG uptake with an average SUV_{max} of 6.54±7.87 (0-27) and size of 1.41±1.13 (0.5-5.5) (Figure 2).

Hyperplastic Polyps

The distribution of 10 hyperplastic polyps among the colon segments was as follows: 5 lesions in the rectum (50%), 2 in the ascending colon (20%), 1 in the cecum (10%), one in the descending colon (10%) and 1 in sigmoid (10%). SUV_{max} in hyperplastic polyps was 2.76±5.12 (0-16.3) on average.

Physiologic Uptake and Benign Lesions

Histopathologic examinations revealed benign inflammatory pathologies in 18 of the lesions. Activated ulcerative colitis was the cause in 2 lesions (11.1%). Granulation was detected in the ulcerous ground in 5 lesions (27.7%). In 2 patients who had undergone radiotherapy for gynecological malignancies, radiation colitis was detected (11.1%). Diverticula was detected in the descending colons of 2 patients (11.1%). Hemorrhoids in the lower rectum was seen in 4 patients and rectovaginal fistulas in 1 patient (5.5%). Tuberculous ulcers were the cause in two incidental ^{18}F-FDG uptake sites (11.1%) (Figure 3). SUV_{max} in

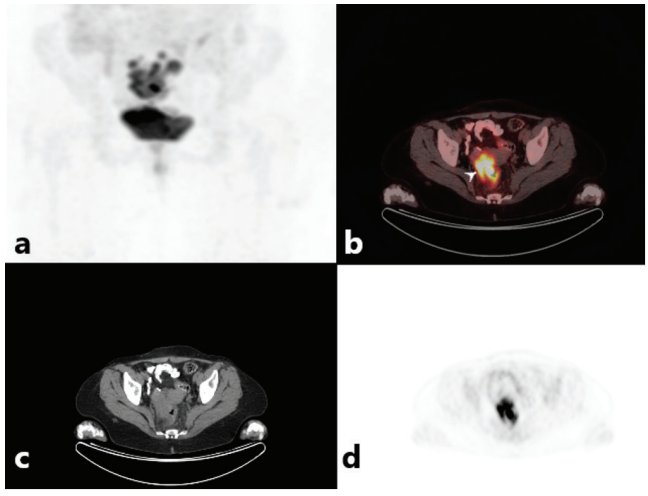

Figure 1. MIP (a), axial fusion, CT and PET (b, c, d) images of a 31-year-old female patient who underwent ^{18}F-FDG PET/CT scanning for breast cancer revealed intense ^{18}F-FDG avid mass (SUV_{max}: 12.7) in sigmoid colon (arrow head) which turned out to be an adenocarcinoma of the colon
CT: Computed tomography, PET: Positron emission tomography, ^{18}F-FDG: ^{18}Fluorine-fluorodeoxyglucose, SUV_{max}: Maximum standardized uptake value

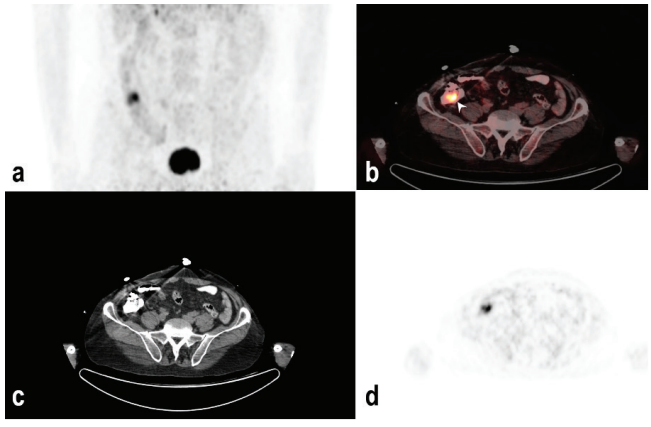

Figure 2. MIP (a), axial fusion, CT and PET (b, c, d) images of a 61-year-old male patient who underwent ^{18}F-FDG PET/CT scanning for malignant melanoma, revealed incidental focal ^{18}F-FDG uptake (SUV_{max}: 8.1) in ascending colon (arrow head). It was a polyp 4 cm in diameter and after excision histopathology of the lesion turned out to be a polyp with high grade dysplasia
CT: Computed tomography, PET: Positron emission tomography, ^{18}F-FDG: ^{18}Fluorine-fluorodeoxyglucose, SUV_{max}: Maximum standardized uptake value

these benign lesions was 7.88±5.09 (2.9-24.6) on average. In 13 of the hypermetabolic foci, colonoscopy revealed no corresponding lesions and the activity accumulations at these sites are attributed to physiologic uptake. The average SUV_{max} values at these false positive uptake sites were 9.22±4.88 (3.8-18.4). The average SUV_{max} in all lesions was 7.51±8.05 (0-49.8) (Figure 4).

According to histopathology results, statistically no significant difference was found between the SUV_{max} measurements of malignant and benign cases ($p>0.05$). The average SUV_{max} measurements of malignant cases were found to be significantly higher than low + high-grade cases ($p<0.05$) and hyperplastic polyp cases ($p<0.01$).

Based on this significance, it was considered to determine the cut-off point for SUV_{max} in detecting malignant cases. ROC analysis was used to determine the cut off point according to the groups.

For the 5.2 cut-off value of SUV_{max} measurement; sensitivity, specificity, positive predictive value (PPV), negative predictive value and accuracy in the discrimination between malignant and low + high-grade groups were 88.9%, 62.2%, 32%, 96.6%, 85.2% respectively. The ODDS rate for SUV_{max} measurement is 12.00 [95% confidance interval (CI): 1.38-104.3] that means that the risk of malignancy is 12 times higher in patients with SUV_{max} level of 5.2 and above.

When discrimination between malignant and hyperplastic polyp groups was concerned, for the 5.2 cut-off value of SUV_{max} measurement; sensitivity, specificity, PPV, negative predictive value and accuracy were 88.9%, 90%, 88.9%, 90%, 84.2% respectively.

A statistically significant difference was found between SUV_{max} measurements according to lesion size ($p<0.01$). SUV_{max} measurement of cases with a lesion size less than 1 cm was found to be statistically significantly lower than other dimensions.

According to histopathology results, size measurements of malignant cases were found to be significantly higher than premalignant cases ($p<0.05$).

Discussion

Focal incidental ^{18}F-FDG uptake is a commonly encountered finding in PET/CT studies done of various oncologic diseases. Sone et al. (9) reported that in 6.7% of the PET/CT studies incidental finding is seen and in 2.2% of all patients, histopathology revealed malignancy in incidental lesions. The most commonly detected sites for these incidental lesions were the colon, lung and stomach (9).

In patients with more than one malignancies, although the prognosis becomes poorer, early detection of the second primary cancer improves the overall outcome (10,11). Adams et al. (6) reported that at least 1 incidental finding was reported in the findings section of 74.9% of PET/CT reports, resulting in a substantial additional cost per PET/CT study. So it becomes crucial to decide when to make suggestions for further investigations in the evaluation of incidental findings instead of follow-up and this requires knowledge of its differential diagnosis, the possibility of malignancy and other PET/CT criteria, which can be used in the characterization of the finding (12).

In our study, incidental colorectal uptake of ^{18}F-FDG was found in 62 of 8,017 patients who underwent ^{18}F-FDG PET/CT studies. In a meta-analysis comprising 32 studies,

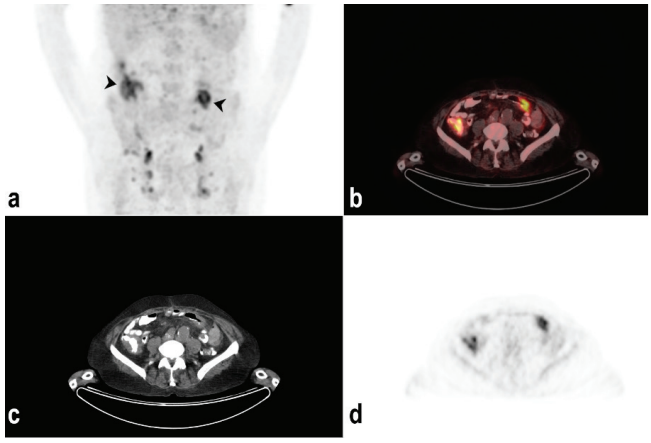

Figure 3. MIP (a), axial fusion, CT and PET (b, c, d) images of a 74-year-old male patient who underwent ^{18}F-FDG PET/CT scanning for search of carcinoma of unknown primary, revealed focal ^{18}F-FDG uptake in walls of cecum (SUV_{max}: 6.6) and transverse colon (SUV_{max}: 7.5) (arrow heads). Histopathological evaluation done following endoscopy showed that the lesions were tuberculous ulcers

CT: Computed tomography, PET: Positron emission tomography, ^{18}F-FDG: ^{18}Fluorine-fluorodeoxyglucose, SUV_{max}: Maximum standardized uptake value

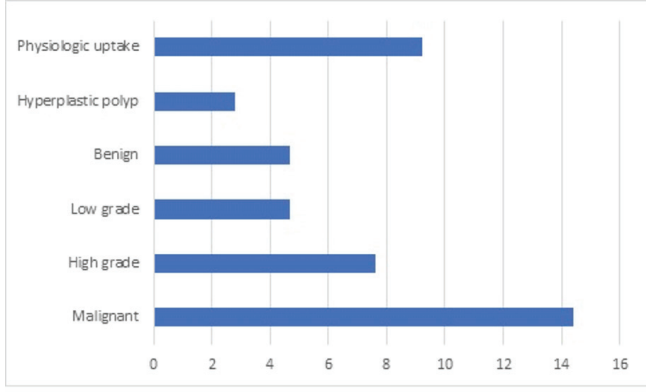

Figure 4. Distribution of SUV_{max} values according to histopathology

SUV_{max}: Maximum standardized uptake value

a pooled prevalence of 3.6% (0.4-16.3%) was reported for focal incidental colonic uptake (8). Initial detection rate of incidental colonic findings might be as high as 10% due to the high mean age of the patients included (13). Lower levels of incidental detection rate of 1.17% was also reported, which is attributed to the inclusion criteria of the study that restricted patients only to meet the strict criteria for focal colonic uptake (14).

In our study, among the patients showing focal ^{18}F-FDG uptake, 83.8% had at least 1 corresponding lesion in colonoscopy, either benign or malign, whereas in 10 patients (16.2%) no lesion was detected. On lesion-based analysis 13 of the 95 (13.7%) focal uptake sites represented physiologic accumulation with no corresponding lesion. Although physiological activities are generally seen in diffuse pattern and therefore not included in studies on incidental ^{18}F-FDG uptake, they can also be seen as a focal involvement. In the past studies, no correlative lesions were detected at endoscopy in 13.7-56% of patients with focal colorectal uptake of ^{18}F-FDG who underwent colonoscopy (13,15,16,17,18). Although the mechanisms of this physiologic intestinal activity are not established clearly, several studies have suggested that the gut microbiota, peristaltic activity in muscles, presence of lymphoid tissue, high concentration of WBCs in the bowel wall, ^{18}F-FDG secreting cells in the wall of the intestines, is responsible (18,19,20,21,22).

A premalignant lesion (high grade polyp + low grade polyp) and a malignant lesion were detected in totally 54 (56.8%) of suspicious hypermetabolic foci. This finding was consistent with the literature; Treglia et al. (8) conducted a systematic review and meta-analysis of incidental focal colonic uptake among 89,061 patients evaluated by ^{18}F-FDG PET or PET/CT and they found the pooled risk of malignant or premalignant lesions as 68% [95% CI (60-75%)]. Another study conducted by Treglia et al. (17), reported malignant or premalignant lesions in 64% of the patients who underwent further investigations. The rate of false positivity can be related to the reference activity chosen for comparison to accept a lesion as positive. Liu et al. (23) reported colon cancer in 10 out of 24 (PPV: 42%) patients who showed incidental focal ^{18}F-FDG uptake in ^{18}F-FDG PET/CT studies, which means that 58% of lesions were false positive. They explained this relatively high false positivity by taking the comparison of focal ^{18}F-FDG activity with blood pool activity as criteria for positive focal ^{18}F-FDG (23). The authors compared their results with Cho et al.'s (24) study in which also low levels of PPV were reported (51.6%) and they attributed this to the definition of a positive criterion on imaging findings with SUV_{max} >3.5.

In our study, focal suspicious colorectal ^{18}F-FDG uptake sites showing intense activity compared with the liver were accepted as positive focal ^{18}F-FDG. So given that mean SUV_{max} value of liver is 2.89±1.26 (1.30-5.2) in our study, we can postulate that the false positivity rate (43.2%) could be lower if we accepted a higher reference SUV_{max} value.

As an indicator of metabolic activity, SUV_{max} value of lesions has been proposed as a semiquantitative index that can be helpful in the discrimination of benign and malignant lesions in oncologic PET/CT studies. When the colonic incidentalomas concerned, previous studies report that SUV_{max} value is unreliable enough to be used in the differentiation of malignant, premalignant and benign lesions because of significant overlap between SUV_{max} of benign and malignant lesions. Indeed, some of these previous studies have reported differences in SUV_{max} measurements between malignant and benign lesions or physiologic uptake, but none of them claimed that this difference in SUV_{max} precludes colonoscopy (18,25,26,27,28). Several studies have shown no statistical differences in SUV_{max} between true and false positive uptake sites (17,29,30). There have been made to determine a certain cut-off value for SUV_{max} in the discrimination of malignant and benign lesions; Luboldt et al. (28) proposed optimal SUV_{max} threshold of 5. However, their results were not confirmed by a study by Rigault et al. (31) in which they reported 14 advanced neoplasias with SUV_{max} values ≤5.

Hoeij et al. (25) reported sensitivity 80%, specificity 82%, PPV 34%, negative predictive value 98% in the discrimination of malignant and benign incidental colonic lesions when the optimal cut-off value was taken as 11.4. Although the authors stated that all incidental focal lesions showing ^{18}F-FDG uptake with a SUV_{max} ≥11.4 should be examined by colonoscopy without delay, they concluded that SUV_{max} alone is not sufficiently discriminative to differentiate malignant, premalignant and benign lesions (25).

We could not find any significant difference between the SUV_{max} measurements of malignant and benign cases. When these benign lesions were overviewed; activated ulcerative colitis was the cause in 2 lesions of a patient, radiation colitis was detected in two patients who had undergone radiotherapy for gynecological malignancies and diverticula were detected in the descending colon of 2 patients. Although these lesions are not discriminated from malignancies due to their metabolic activity, when the morbidity of these lesions is regarded, early detection of them with ^{18}F-FDG PET/CT becomes crucial (32).

Depending on the statistically significant high values of SUV_{max} in malignant cases compared with low + high grade cases and hyperplastic polyp cases, we tried assessing the threshold of SUV_{max} to differentiate the malignant cases and we found that above 5.2 the malignancy is detected with a sensitivity and specificity of 88.9% and 62.2% compared with low + high grade groups and 88.9% and 90%, when compared with hyperplastic polyp groups. Although these values seem to be high, given that 12 out of 18 benign lesions and 10 out of 13 physiologic uptake sites exhibit SUVmax values more than 5.2, in line with the literature, this cut-off value cannot be set as a strict threshold for the discrimination of malignant lesions.

Study Limitations

Our study has some limitations. First, it was limited by its retrospective and single center design. We couldn't detect the sensitivity of ^{18}F-FDG PET/CT in the identification of colonic neoplasms since whole lesions found in colonoscopy whether they were ^{18}F-FDG avid or not are not recorded. All patients were administered oral contrast before the study as a part of routine applications in our PET/CT studies in our department. This might be mentioned as a limitation since it might have caused artefacts in the PET images, but these artefacts were distinguished from unusual focal ^{18}F-FDG uptake with their diffuse patterns, and any misinterpretations were avoided. Administration of negative contrast material like water to improve bowel distention might have been more appropriate in this kind of study.

Conclusion

In conclusion, any unexpected focal ^{18}F-FDG uptake in ^{18}F-FDG PET/CT studies is suspicious for malignancy and should be clarified by colonoscopy. The intensity of ^{18}F-FDG uptake does not preclude the application of colonoscopy and histopathological verification of the lesion if there is any. SUV_{max} values more than 5.2 might only alert the physician to the higher risk of malignancy and force for urgent intervention.

Ethics

Ethics Committee Approval: Ethical approval was obtained from the Ethics Committee of University of Health Sciences Turkey, Prof. Dr. Cemil Tascioglu City Hospital (protocol number: E-48670771-514.10).

Informed Consent: Retrospective study.

Peer-review: Externally peer-reviewed.

Authorship Contributions

Surgical and Medical Practices: Y.G., F.Ö., Concept: Y.G., F.Ö., T.Ö., Design: Y.G., F.Ö., Data Collection or Processing: Y.G., F.Ö., Analysis or Interpretation: Y.G., F.Ö., Literature Search: Y.G., T.Ö., Writing: Y.G., F.Ö., T.Ö.

Conflict of Interest: No conflict of interest was declared by the authors.

Financial Disclosure: The authors declared that this study has received no financial support.

References

1. Kamakshi K, Krishnamurthy A, Karthik V, Vinodkumar P, Kumar RK, Lakshmipathy KM. Positron emission tomography-computed tomography-associated incidental neoplasms of the thyroid gland. World J Nucl Med 2020;19:36-40.
2. Akkuş G, Güney IB, Ok F, Evran M, Izol V, Erdoğan Ş, Bayazıt Y, Sert M, Tetiker T. Diagnostic efficacy of 18F-FDG PET/CT in patients with adrenal incidentaloma. Endocr Connect 2019;8:838-845.
3. Servente L, Gigirey V, García Fontes M, Alonso O. Incidental focal colonic uptake in studies (18)F-FDG PET/CT. Rev Esp Med Nucl Imagen Mol 2018;37:15-19.
4. Miljić D, Manojlović-Gačić E, Skender-Gazibara M, Milojević T, Bogosavljević V, Kozarević N, Petrović N, Stojanović M, Pekić S, Doknić M, Petakov M, Popović V. All that glitters on PET is not cancer! 18F-deoxy-glucose avidity versus tumor biology: pituitary incidentaloma in a survivor of two previous unrelated malignancies. Endokrynol Pol 2017;68:352-359.
5. Mannas MP, Lee T, Pourghiasian M, Wilson DC, Black PC. Incidentalomas of the prostate detected by 18-fluoro-2-deoxy-D-glucose positron emission tomography/computed tomography. Can Urol Assoc J 2020;14:180-184.
6. Adams SJ, Rakheja R, Bryce R, Babyn PS. Incidence and economic ımpact of ıncidental findings on 18 F-FDG PET/CT imaging.Can Assoc Radiol J 2018;69:63-70.
7. Ding A, Eisenberg JD, Pandharipande PV. The economic burden of incidentally detected findings. Radiol Clin North Am 2011;49:257-265.
8. Treglia G, Taralli S, Salsano M, Muoio B, Sadeghi R, Giovanella L. Prevalence and malignancy risk of focal colorectal incidental uptake detected by (18)F-FDG-PET or PET/CT:a meta-analysis. Radiol Oncol 2014;48:99-104.
9. Sone Y, Sobajima A, Kawachi T, Kohara S, Kato K, Naganawa S. Ability of 18-fludeoxyglucosepositron emission tomography/CT to detect incidental cancer. Br J Radiol 2014;87:20140030.
10. Choy AT, van Hasselt CA, Chisholm EM, Williams SR, King WW, Lİ AK. Multiple primary cancers in Hong Kong Chinese patients with squamous cell cancer of the head or neck. Cancer 1992;70:815-820.
11. Wu B, Cui Y, Tian J, Song X, Hu P, Wei S. Effect of second primary cancer on the prognosis of patients with non-small cell lung cancer. Thorac Dis 2019;11:573-582.
12. Pencharz D, Nathan M, Wagner TL. Evidence-based management of incidental focal uptake of fluorodeoxyglucose on PET-CT. Br J Radiol 2018;91:20170774.
13. Farquharson AL, Chopra A, Ford A, Matthews S, Amin SN, Noronha RD. Incidental focal colonic lesions found on (18)fluorodeoxyglucose positron emission tomography/computed tomography scan: further support for a national guideline on definitive management. Colorectal Dis 2012;14:56-63.
14. Fuertes J, Montagut C, Bullich S, Coma MI, Mestre-Fusco A, Suárez-Piñera M, Trampal C, Bellmunt J. Incidental focal uptake in colorectal location on oncologic ^{18}FDG PET and PET/CT studies: histopathological findings and clinical significances. Rev Esp Med Nucl Imagen Mol 2015;34:95-101.

15. Putora PM, Müller J, Borovicka J, Plasswilm L, Schmidt F. Relevance of incidental colorectal FDG-PET-CT-enhanced lesions. Onkologie 2013;36:200-204.
16. Peng J, He Y, Xu J, Sheng J, Cai S, Zhang Z. Detection of incidental colorectal tumours with 18F-labelled 2-fluoro-2- deoxyglucose positron emission tomography/computed tomography scans: results of a prospective study. Colorectal Dis 2011;13:374-378.
17. Treglia G, Calcagni ML, Rufini V, Leccisotti L, Meduri GM, Spitilli MG,Dambra DP, De Gaetano AM, Giordano A. Clinical significance of incidental focal colorectal (18)F-fluorodeoxyglucose uptake: our experience and a review of the literature. Colorectal Dis 2012;14:174-180.
18. Gutman F, Alberini JL, Wartski M, Vilain D, Le Stanc E, Sarandi F. Incidental colonic focal lesions detected by FDG PET-CT. AJR Am J Roentgenol 2005;185:495-500.
19. Kang JY, Kim H , Chang Y, Yun Y, Ryu S, Shin H, Kim HL. Gut microbiota and physiologic bowel (18)F-FDG uptake. EJNMMI Res 2017;7:72.
20. Delbeke D. Oncological applications of FDG PET imaging: brain tumors, colorectal cancer, lymphoma and melanoma. J Nucl Med 1999;40:591-603.
21. Engel H, Steinert H, Buck A, Berthold T, Böni HRA, von Schulthess GK. Whole-body PET: physiological and artifactual fluorodeoxyglucose accumulations. J Nucl Med 1996;37:441-446.
22. Strauss LG. Fluorine-18 deoxyglucose and falsepositive results: a major problem in the diagnosticsof oncological patients. Eur J Nucl Med 1996;23:1409-1415.
23. Liu T, Behr S, Khan S, Osterhoff R, Aparici CM. Focal colonic FDG activity with PET/CT: guidelines for recommendation of colonoscopy. World J Nucl Med 2015;14:25-30.
24. Cho SH, Kim SW, Kim WC, Park JM, Yoo IeR, Kim SH, Oh ST. Incidental focal colorectal 18F-fluorodeoxyglucose uptake on positron emission tomography/computed tomography. World J Gastroenterol 2013;19:3453-3458.
25. Hoeij FB, Keijsers RG, Loffeld BC, Dun G, Stadhouders PH, Weusten BL. Incidental colonic focal FDG uptake on PET/CT: can the maximum standardized uptake value (SUVmax) guide us in the timing of colonoscopy? Eur J Nucl Med Mol Imaging 2015;42:66-71.
26. Weston BR, Iyer RB, Qiao W, Lee JH, Bresalier RS, Ross WA. Ability of integrated positron emission and computed tomography to detect significant colonic pathology: the experience of a tertiary cancer center. Cancer 2010;116:1454-1461.
27. Oh JR, Min JJ, Song HC, Chong A, Kim GE, Choi CSeo JH, Bom HS. A stepwise approach using metabolic volume and SUVmax to differentiate malignancy and dysplasia from benign colonic uptakes on 18F-FDG PET/CT. Clin Nucl Med 2012;37:134-140.
28. Luboldt W, Volker T, Wiedemann B, Zöphel K, Wehrmann U, Koch A, Toussaint T, Abolmaali N, Middendorp M, Aust D, Kotzerke J, Grünwald F, Vogl TJ, Luboldt HJ. Detection of relevant colonic neoplasms with PET/CT: promising accuracy with minimal CT dose and a standardised PET cut-off. Eur Radiol 2010;20:2274-2285.
29. Kei PL, Vikram R, Yeung HW, Stroehlein JR, Macapinlac HA. Incidental finding of focal FDG uptake in the bowel during PET Ğ CT: CT features and correlation with histopathologic results. AJR Am J Roentgenol 2010;194:401-406.
30. Israel O, Yefremov N, Bar-Shalom R, Kagana O, Frenkel A, Keidar Z, Fischer D. PET/CT detection of unexpected gastrointestinal foci of 18F-FDG uptake: incidence, localization patterns, and clinical significance. J Nucl Med 2005;46:758-762.
31. Rigault E, Lenoir L, Bouguen G, M, Lièvre A , Garin E, Siproudhis L, Bretagne JF. Incidental colorectal focal 18 F-FDG uptake: a novel indication for colonoscopy. Endosc Int Open 2017;5:924-930.
32. Kamel EM, Thumshirn M, Truninger K, Schiesser M, Fried M, Padberg B. Significance of incidental 18F-FDG accumulations in the gastrointestinal tract in PET/CT: correlation with endoscopic and histopathologic results. J Nucl Med 2004;45:1804-1810.

Original Article
Mol Imaging Radionucl Ther 2022;31:104-113 DOI:10.4274/mirt.galenos.2022.24650

The Prognostic Value of ^{18}F-FDG PET/CT Metabolic Parameters in Predicting Treatment Response Before EGFR TKI Treatment in Patients with Advanced Lung Adenocarcinoma

İlerlemiş Akciğer Adenokarsinomu Olan Hastalarda EGFR TKI Tedavisi Öncesi Tedavi Yanıtını Öngörmede ^{18}F-FDG PET/BT Metabolik Parametrelerinin Prognostik Değeri

Nurşin Agüloğlu[1], Murat Akyol[2], Halil Kömek[3], Nuran Katgı[4]

[1]*University of Health Sciences Turkey, Dr. Suat Seren Chest Diseases and Surgery Hospital, Clinic of Nuclear Medicine, İzmir, Turkey*
[2]*İzmir Bakırçay University Faculty of Medicine, Department of Medical Oncology, İzmir, Turkey*
[3]*Gazi Yaşargil Training and Research Hospital, Clinic of Nuclear Medicine, Diyarbakır, Turkey*
[4]*University of Health Sciences Turkey, Dr. Suat Seren Chest Diseases and Surgery Hospital, Clinic of Chest Diseases, İzmir, Turkey*

Abstract

Objectives: This study makes a retrospective examination of exploring the prognostic value of ^{18}fluorine-fluorodeoxyglucose (^{18}F-FDG) positron emission tomography/computed tomography (PET/CT) related metabolic-volumetric variables, nutritional status, and immune and inflammatory markers on progression-free survival (PFS) and overall survival (OS) in advanced adenocarcinoma patients with positive epidermal growth factor receptor (EGFR) mutations undergoing EGFR tyrosine kinase inhibitor (TKI) therapy.

Methods: A retrospective examination was made of patients diagnosed with lung adenocarcinoma who underwent ^{18}F-FDG PET/CT imaging for staging maximum four weeks before starting treatment, between January 2015 and July 2020. Included in the study were 68 patients identified histopathologically to have locally advanced/metastatic EGFR mutation-positive adenocarcinoma, and who underwent EGFR TKI therapy. The laboratory data of the patients, obtained 15 days before imaging performed for PET/CT staging, were evaluated.

Results: Metabolic tumor volume, modified Glasgow prognostic score and locally advanced disease were identified as independent prognostic parameters for PFS (p=0.004, p=0.029, p=0.016, respectively). A univariate Cox regression analysis revealed albumin/alkaline phosphatase and tumor size to be significant parameters for prognosis (p=0.033, p=0.043, respectively). A multivariate Cox regression analysis revealed that none of the parameters were predictive or OS.

Conclusion: The parameters of ^{18}F-FDG PET/CT, especially the volumetric parameters, were found to be strong prognostic factors with statistical significance for predicting PFS. We believe that these parameters are important prognostic markers that should be evaluated together in the management and follow-up of patients with EGFR mutation-positive adenocarcinoma.

Keywords: ^{18}F-FDG PET/CT, lung cancer, adenocarcinoma, EGFR, progression-free survival, overall survival

Öz

Amaç: Çalışmamızda, epidermal büyüme faktörü reseptörü (EGFR) tirozin kinaz inhibitörü (TKI) tedavisi gören pozitif EGFR mutasyonları olan ileri adenokarsinom hastalarında progresyonsuz sağkalım (PFS) ve genel sağkalım (OS) üzerindeki ^{18}flor-florodeoksiglukoz (^{18}F-FDG) pozitron emisyon tomografisi/bilgisayarlı tomografi (PET/BT) ile ilişkili metabolik-hacimsel değişkenlerin, nutrisyonel durumunun ve immün ve enflamasyon belirteçlerin prognostik değerini retrospektif bir incelemesini yapmaktadır.

Address for Correspondence: Nurşin Agüloğlu MD, University of Health Sciences Turkey, Dr. Suat Seren Chest Diseases and Surgery Hospital, Clinic of Nuclear Medicine, İzmir, Turkey
Phone: +90 505 273 33 41 **E-mail:** aguloglunursin@gmail.com ORCID ID: orcid.org/0000-0003-3976-2064
Received: 04.10.2021 **Accepted:** 10.02.2022

Yöntem: Ocak 2015 ile Temmuz 2020 tarihleri arasında küçük hücreli dışı akciğer kanseri tanısı alan ve tedavi almadan en fazla dört hafta önce evreleme için ^{18}F-FDG PET/BT görüntülemesi yapılan hastalar geriye dönük olarak incelendi. Histopatolojik olarak adenokarsinom EGFR mutasyonu saptanan lokal ileri/metastatik TKI tedavisi alan 68 hasta çalışmaya dahil edildi. Hastaların PET/BT evrelemesi için yapılan görüntülemeden 15 gün önce alınan laboratuvar verileri değerlendirildi.

Bulgular: Metabolik tümör hacmi, modifiye Glasgow prognostik skoru ve lokal ileri hastalık, PFS için bağımsız prognostik parametreler olarak tanımlandı (sırasıyla; p=0,004, p=0,029, p=0,016). Tek değişkenli Cox regresyon analizi, albümin/alkalin fosfataz ve tümör boyutunun prognoz için önemli parametreler olduğunu ortaya koydu (sırasıyla; p=0,033, p=0,043). Çok değişkenli Cox regresyon analizi, hiçbir parametrenin OS için öngörücü olmadığını gösterdi.

Sonuç: ^{18}F-FDG PET/BT parametreleri, özellikle volümetrik parametreler, PFS'nin öngörülmesi için istatistiksel anlamlılığı olan güçlü prognostik faktörler olarak bulundu. Bu parametrelerin EGFR mutasyon pozitif adenokarsinomlu hastaların yönetimi ve takibinde birlikte değerlendirilmesi gereken önemli prognostik belirteçler olduğuna inanıyoruz.

Anahtar kelimeler: ^{18}F-FDG PET/BT, akciğer kanseri, EGFR, progresyonsuz sağkalım, genel sağkalım

Introduction

Non-small cell lung cancer (NSCLC), triggered by the activation of epidermal growth factor receptor (EGFR) mutations, accounts for approximately 10% of all NSCLC cases (1). Tyrosine kinase inhibitor (TKI) therapy is the first-line treatment for metastatic NSCLC with an EGFR mutation (2). EGFR signaling regulates the pathways of glucose metabolism in EGFR-mutated cancer cells, and EGFR TKIs reduce lactate production and glucose consumption (3). TKIs have been associated with longer progression-free survival (PFS) than chemotherapy in advanced NSCLC with EGFR mutations (2,4). The approved agents for TKI therapy include first-generation EGFR TKIs, erlotinib and gefitinib, and second-generation EGFR TKI, afatinib. The objective response rates to these agents in randomized clinical trials range from 56-74%, and the median time to progression is 9-13 months (5,6,7).

Recently, simple and accessible biomarkers related to systemic inflammation and nutritional status have been developed for predicting prognosis in various cancers (8). While the modified Glasgow prognostic score (mGPS), which is based on serum C-reactive protein (CRP) and albumin (ALB) concentrations, is considered a prognostic factor for most cancers (9), the prognostic nutritional index (PNI), which is calculated on the basis of ALB and total lymphocyte count, is more useful for predicting overall survival (OS) (10).

Lactate dehydrogenase (LDH) is another serum enzyme that is mainly involved in the conversion of pyruvate to lactate, and that has been linked to tumor metabolism (11). Several studies have established elevated LDH levels in various types of cancer, including NSCLC (12,13).

Immune and inflammatory responses have a characteristic significance for developing tumors in the body. Homeostasis and inflammation are among the numerous physiological and pathological pathways in which platelets are involved. There have been many studies associating an elevated platelet count with poor prognosis for various solid cancers, including those of the lung (14). The neutrophil-to-lymphocyte ratio (NLR) and platelet-to-lymphocyte ratio (PLR), which are systemic inflammatory markers, play a prognostic role in many malignancies, such as malignant melanoma, esophageal cancer, prostate cancer, diffuse large B-cell lymphoma, breast cancer, nasopharyngeal cancer and NSCLC (15). There have also been many recent publications reporting the systemic immune-inflammation index (SII), which is based on platelet, lymphocyte and neutrophil counts, to be another important prognostic marker for various cancers (16).

^{18}Fluorine-fluorodeoxyglucose (^{18}F-FDG) positron emission tomography/computed tomography (PET/CT) is an imaging method that is used to diagnose and stage lung cancer and is based on the elevated glucose metabolism of tumor cells with increased expression of glucose transporter protein and hexokinase activity. In addition to diagnosis and staging, ^{18}F-FDG-PET is being increasingly used to assess treatment response and to predict outcomes (17). Some studies recommend early assessment with ^{18}F-FDG PET/CT as a criterion in the modification of tumor response during treatment (18,19). The volumetric parameters; metabolic tumor volume (MTV) and total lesion glycolysis (TLG) have been used to reflect the disease burden and tumor aggressiveness in NSCLC (20). The standardized uptake value (SUV) is a semi-quantitative determination of the normalized concentration of radioactivity, and maximum SUV (SUV_{max}) is the most widely applied parameter in clinical practice (21).

This study is conducted to explore the prognostic value of inflammatory markers and metabolic- and volume-based parameters related to ^{18}F-FDG PET/CT on treatment response assessment and outcome prediction, while also establishing the prognostic value of these parameters in adenocarcinoma patients with EGFR mutations.

Materials and Methods

Patients diagnosed with NSCLC who underwent ^{18}F-FDG PET/CT imaging for staging max four weeks before starting treatment between January 2015 and July 2020 were reviewed retrospectively. Subsequently, 68 patients who were found histopathologically to have locally advanced/metastatic EGFR mutation-positive adenocarcinoma and who underwent EGFR TKI therapy were included in the study. Patients were staged based on the TNM classification, according to the 8th edition staging system recommended by the International Association for the Study of Lung Cancer. The final surveillance program will be conducted in December 2020. Excluded from the study were: 1-) Patients with diagnoses other that concurrent cancer; 2-) Patients who underwent surgery or received any treatment (e.g. chemotherapy, radiotherapy) before imaging; 3-) Patients with missing hospital records; 4-) Patients without ^{18}F-FDG uptake at the site of the primary tumor; 5-) Patients with unknown status of EGFR gene mutation; and 6-) Patients who were followed up by an external center. In our retrospective study, the informed consent form was not documented, it was prepared in accordance with the local Clinical Practices guide and the current legislation, approval for the use of the patient data for publication was obtained from University of Health Sciences Turkey, Dr. Suat Seren Chest Diseases and Surgery Hospital Institutional Ethics Committee (approval no: 49109414-604.02).

Assessments

Age, gender and laboratory data [complete blood count, LDH, CRP, alkaline phosphatase (ALP), ALB obtained 15 days before ^{18}F-FDG PET/CT imaging was retrieved from the electronic hospital records. The NLR, PLR, CRP-to-ALB ratio, and serum ALB-to-serum ALP ratio were calculated. The formulas used to calculate the SII and PNI were as follows: SSI = platelet count × neutrophil count/lymphocyte count; PNI = 10 × serum ALB level + 0.5 × lymphocyte count. PNI score was recorded as 0 if PNI ≥45, and 1 if PNI was <45; mGPS was recorded as 0 if CRP was ≤10 mg/L, one if CRP was >10 mg/L and ALB ≥35 g/L, and 2 if CRP was >10 mg/L and alb <35 g/L. The recorded parameters related to ^{18}F-FDG PET/CT imaging included the longest diameter (mm) of the primary mass, MTV (cm^3), TLG (g/mL × cm^3), SUV_{max} and SUV_{mean}.

Positron Emission Tomography/Computed Tomography Protocol

Imaging was performed in a Philips Gemini TF 16-slice combined PET/CT scanner, with the same scanner used for all patients. Following a min 6 hours of fasting, 8-15 mCi ^{18}F-FDG (2.5 MBq/kg body weight) was administered intravenously and the time between intravenous injection and scans was 60±5 minutes. The patient did an intravenous contrast agent. The first CT images (140 kV, 100 mAs, 5 mm sections) and then PET images were acquired. Attenuation-corrected emission data were obtained using non-contrast-enhanced data, extrapolated to 511 keV. PET images were acquired through emission scanning for 1.5 min per bed position, and a wholebody scan from skull vertex to the proximal thigh using 9 or 10 bed positions. The images were reconstructed with iterative algorithms over a 128x128 matrix.

Image Analysis

Hybrid images of the ^{18}F-FDG PET/CT data were analyzed independently by two nuclear medicine specialists. The pattern and degree of primary mass uptake were evaluated and located. A 3D isocontour region of interest was drawn automatically on the lesion with the primary mass uptake in all three planes. While calculating the SUV_{max}, SUV_{mean} and the MTV included in the volume of interest, the area related to the 40% threshold was calculated automatically. TLG was calculated by multiplying MTV by the SUV_{mean}.

EGFR Mutation Assessment

Tissue samples acquired from paraffin-embedded specimens were collected in 1.5 mL vials, and DNA was extracted using a DNA Sample Preparation Kit (Cobas, Roche Molecular Systems, USA) and reverse transcription-polymerase chain reaction was performed. All procedures were conducted according to the manufacturer's instructions (Cobas EGFR Mutation Test v2, Roche Molecular Systems, USA).

Statistical Analysis

Data were analyzed using the IBM SPSS Statistics (Version 26.0. Armonk, NY: IBM Corp.) and MedCalc Statistical Software version 16.4.3 (MedCalc Software BV, Ostend, Belgium; https://www.medcalc.org; 2016) software packages. Descriptive statistics were expressed as the unit number (n), percentage (%), mean ($\bar{x}$), standard deviation, standard error, median (M), minimum (min) and max values. The performance of prognostic markers in predicting recurrence and survival was evaluated by a receiver operating characteristic curve (ROC) analysis. The survival times of the patients were compared using the log-rank (Mantel-Cox) test of the Kaplan-Meier analysis, based on the optimum cut-off point for the markers found significant in the ROC analysis. Univariate and multivariate Cox regression analyses were used to determine the factors affecting PFS and OS. p values of <0.05 were considered statistically significant.

Results

Patient Characteristics

Among the 68 patients with advanced EGFR-mutated adenocarcinoma were 40 (58.8%) female and 28 (41.2%) male patients, with a median age of 64.5 (31.0-85.0) years. 43 (63.2%) patients of 68 were non-smoker. Of the patients with advanced adenocarcinoma, 15 (22.1%) were classified as locally advanced and 53 (77.9%) as metastatic. Of the total, five (7.3%) patients had mutations in exon 18, 47 (69.1%) in exon 19, and 16 (23.5%) in exon 21. For EGFR TKI, 27 (39.7%) patients underwent afatinib therapy, 35 (51.5%) erlotinib therapy and six (8.8%) gefitinib therapy. During the follow-up, 66.2% of the patients experienced local or metastatic relapse and 13 (19.1%) died from disease progression. Patient characteristics are presented in Table 1.

^{18}F-FDG PET/CT Parameters

Of 68 patients with advanced EGFR mutation adenocarcinoma, the median SUV_{max} value was 9.81 (3.50-38.10), the median MTV value was 25.66 (1.66-461.12), and the median TLG value was 158.19 (5.88-1826.04). The metabolic and volumetric parameters of the patients, as well as their immune and inflammatory parameters, are presented in Table 1.

Progression-free Survival Analysis

The median PFS was 13.9 (1.9-99.8) months overall. When the continuous variables were evaluated on the ROC curve drawn to determine progression, the analysis results revealed that the parameters with a significant area under the curve (AUC) values were MTV 0.725 [95% confidence interval (CI): 0.630-0.826, p=0.001], TLG 0.728 (95% CI: 0.606-0.828, p<0.001) and NLR 0.653 (95% CI: 0.528-0.765, p=0.019), which were predictive of progression (Table 2). MTV >7.04, TLG >78.68, NLR >4.73, an mGPS score of two and metastatic disease had statistically significantly high sensitivity and specificity in predicting of progression (Table 2). Optimum values were determined for MTV, TLG and NLR for use in the determination of progression, and patients were divided into groups based on these values. A Kaplan-Meier analysis revealed MTV, TLG, NLR, gender and locally advanced disease to be significant parameters, and further showing that PFS was significantly shorter in patients with MTV >7.04, TLG >78.68 and NLR >4.73 than in those with low values of these parameters (p=0.001, p=0.003, p=0.001, respectively). Metastatic patients had a shorter PFS than locally advanced patients (p=0.003); and those with an mGPS score of two were found to have a shorter PFS than those with a score of 0 (p=0.009) (Table 3). The univariate Cox regression analysis

Table 1. Patient characteristics

Characteristics	n (%)	
Gender		
Female	40 (58.8)	
Male	28 (41.2)	
Age (years)		
Mean ± SD	63.2±11.2	
M (min-max)	64.5 (31.0-85.0)	
Stage		
Local advanced stage	15 (22.1)	
Metastatic	53 (77.9)	
Pharmaceutical group		
Afatinib	27 (39.7)	
Erlotinib	35 (51.5)	
Gefitinib	6 (8.8)	
Exon 18	5 (7.3)	
Exon 19	47 (69.1)	
Exon 21	16 (23.5)	
Relapse		
No	23 (33.8)	
Yes	45 (66.2)	
Survival		
Alive	55 (80.9)	
Ex	13 (19.1)	
mGPS score		
0	33 (51.5)	
2	33 (48.5)	
PNI score		
<45	26 (38.2)	
>45	42 (61.8)	
	Mean ± SD	**M (min-max)**
Progression-free survival	19.9±17.5	13.9 (1.9-99.8)
Overall survival	25.7±19.1	21.9 (2.9-99.8)
SUV_{max}	10.87±5.71	9.81 (3.50-38.10)
SUV_{mean}	5.89±3.28	5.33 (1.20-20.50)
MTV	60.57±90.75	25.66 (1.66-461.12)
TLG	294.14±362.41	158.19 (5.88-1826.04)
LDH	225.1±79.8	208.0 (117.0-475.0)
CRP/ALB	8.05±13.59	2.21 (0.13-70.47)
ALB/ALP	0.047±0.021	0.047 (0.021-0.174)
NLR	5.08±5.56	3.33 (1.00-29.20)
PLR	238.27±190.65	192.48 (37.37-1385.00)
Size (cm)	4.14±1.82	4.00 (1.30-10.50)
SII	1587.2±1825.5	1008.4 (253.4-9956.0)
PNI	46.28±10.04	48.00 (8.50-80.60)

SD: Standard deviation, min: Minimum, max: Maximum, mGPS: Modified Glasgow prognostic score, PNI: Prognostic nutritional index, SUVmax: Maximum standardized uptake value, MTV: Metabolic tumor volume, TLG: Total lesion glycolysis, LDH: Lactate dehydrogenase, CRP: C-reactive protein, ALB: Albumin, ALP: Alkaline phosphatase, NLR: Neutrophil-to-lymphocyte ratio, SII: Systemic immune-inflammation index, PLR: Platelet-to-lymphocyte ratio

Table 2. ROC analysis results of prognostic markers according to recurrence and survival status					
Recurrence status	**AUC (95% CI)**	**p**	**Cut-off value**	**Sensitivity (95% CI)**	**Specificity (95% CI)**
MTV	0.725 (0.630-0.826)	0.001	>7.04	95.56 (84.9-99.5)	43.48 (23.2-65.5)
TLG	0.728 (0.606-0.828)	<0.001	>78.68	73.33 (58.1-85.4)	60.87 (38.5-80.3)
N/L	0.653 (0.528-0.765)	0.019	>4.733	35.56 (21.9-51.2)	100.0 (85.2-100.0)
Survival status					
MTV	0.715 (0.594-0.817)	0.007	>41.02	69.23 (38.6-90.9)	75.00 (61.6-85.6)
TLG	0.701 (0.578-0.805	0.017	>384.8	61.54 (31.6-86.1)	80.36 (67.6-89.8)
LDH	0.678 (0.554-0.787)	0.031	>222	69.23 (38.6-90.9)	69.09 (55.2-80.9)
CRP/ALB	0.729 (0.607-0.829)	0.007	>3.956	76.92 (46.2-95.0)	72.73 (59.0-83.9)
PNI	0.776 (0.658-0.868)	0.001	≤41.3	76.92 (46.2-95.0)	83.64 (71.2-92.2)

ROC: Receiver operating characteristic curve, AUC: Area under curve, CI: Confidence interval, MTV: Metabolic tumor volume, TLG: Total lesion glycolysis, LDH: Lactate dehydrogenase, CRP: C-reactive protein, ALB: Albumin, PNI: Prognostic nutritional index, CI: Confidence interval

for systemic inflammation, and nutritional and volumetric parameters identified PLR, SII and tumor size was predictive of PFS (p=0.001, p=0.001, p=0.007, respectively) (Table 3). The Multivariate Cox regression analysis, in turn, identified MTV, mGPS and stage as independent prognostic factors for PFS (p=0.004, p=0.029, p=0.016, respectively) (Table 4). Among the volumetric parameters, MTV was determined to be a representative volumetric parameter; and among the general patient characteristics, age and gender had no statistically significant effect on PFS.

Overall Survival Analysis

The median OS was 21.9 (2.9-99.8) months. Among the general patient characteristics, age and gender had no statistically significant effect on OS.

When the continuous variables were evaluated on the ROC curve drawn according to survival, the parameters with a significant AUC values were MTV 0.715 (95% CI: 0.594-0.817, p=0.007), TLG 0.701 (%95 CI: 0.578-0.805, p=0.017), LDH 0.678 (%95 CI: 0.554-0.787, p=0.031), CRP/ALB 0.729 (95% CI: 0.607-0.829, p=0.007) and PNI 0.776 (95% CI: 0.658-0.868, p=0.001), which were predictive of survival MTV >41.02, TLG >384.8, LDH >222, CRP/ALB >3.956, and PNI >41.3 had statistically significantly high sensitivity and specificity in predicting survival (Table 2).

The Kaplan-Meier analysis for survival showed OS to be significantly shorter in patients with MTV >41.02, TLG >384.8, LDH >222 and CRP/ALB >3.956 than in those with low values of these parameters (p=0.001, p=0.002, p=0.040, p<0.001, p<0.001, p=0.001, respectively) (Table 4). A multivariate Cox regression analysis for systemic inflammation, and nutritional and volumetric parameters identified ALB/ALP and tumor size as significant parameters (p=0.033, p=0.043, respectively) (Table 4). The multivariate Cox regression analysis demonstrated that none of the parameters were predictive or OS (Table 4).

Discussion

This study found MTV, a volumetric parameter of ^{18}F-FDG PET/CT performed for staging in 68 patients with advanced EGFR-mutated adenocarcinoma, to be an independent prognostic factor for PFS. We further identified the scoring method for mGPS according to CRP and ALB levels as another significant prognostic factor for PFS. ROC analysis results revealed MTV, TLG and NLR to have statistically high sensitivity and specificity in predicting progression. We believe that these parameters are important prognostic markers that should be evaluated together in the treatment management and follow-up of patients with EGFR mutation-positive advanced adenocarcinomas.

EGFR mutations play a decisive role in the systematic treatment of NSCLC. The treatment of EGFR-mutated NSCLC has improved significantly in recent years, with EGFR-TKIs being the primary therapy for patients with advanced EGFR-mutated NSCLC (22,23). Previous studies have clearly demonstrated the dramatic response of patients with advanced adenocarcinoma to treatment with EGFR TKIs (gefitinib, erlotinib and afatinib). The presence of somatic mutations in the EGFR gene is deemed the best predictor of the response to TKIs (5,24). Gefitinib, erlotinib, afatinib and osimertinib have significantly prolonged the PFS of patients with untreated advanced EGFR-mutated NSCLC, although discussions of the optimal sequence are continuing (25). Patients who are to benefit from EGFR TKI therapy should be selected carefully to avoid such critical side effects as interstitial lung disease (26).

The variation in the survival of patients with advanced adenocarcinoma is associated with multiple factors (EGFR mutations, metabolism changes, serum markers and gender). ^{18}F-FDG PET/CT is a promising method and may reveal specific differences in metabolism in contrast to

Table 3. Univariant analysis of factors affecting progression-free survival					
	Recurrence		Estimate progression-free time (m)	Estimate proportion surviving at the 1/3 year	p value
	Present	Absent			
	n (%)	n (%)	Mean ± SE		
MTV					
≤7.04	2	10	79.873±12.27	100/75	**0.001[k]**
>7.04	43	13	21.20±2.45	62.7/49.9	
TLG					
≤78.68	12	14	48.73±9.522	78.6/45.3	**0.003[k]**
>78.68	33	9	19.47±2.53	63.2/7.0	
NLR					
≤4.73	29	23	37.02±6.03	79.4/49.8	**0.001[k]**
>4.73	16	0	14.55±3.74	37.5/6.3	
Gender					
Female	24	16	36.53±6.70	100/55.9	**0.187[k]**
Male	21	7	22.64±3.98	59.4/14.3	
Stage					
Local advanced stage	6	9	56.18±11.87	83.3/31.3/0.0	**0.003[k]**
Metastatic	39	14	20.98±2.78	93.3/52.3/43.6	
mGPS score					
0	20	15	36.65±6.56	80.7/33	0.009[k]
2	25	8	19.54±3.42	57/9.2	
Multivariate analysis of factors affecting progression-free survival					
	Odss ratio	**95% CI for Odss ratio**			
		Lower bound	**Upper bound**	**p**	
SUV_{max}	0.995	0.946	1.046	0.839[c]	
SUV_{mean}	0.98	0.897	1.071	0.654[c]	
LDH	0.998	0.994	1.002	0.379[c]	
CRP/ALB	1.014	0.998	1.031	0.095[c]	
ALB/ALP	0.001	0	7938.969	0.392[c]	
PLR	1.002	1.001	1.003	0.001[c]	
Size (cm)	1.225	1.057	1.419	0.007[c]	
SII	1	1	1	0.001[c]	
PNI	0.966	0.932	1.001	0.059[c]	
Age	1.01	0.985	1.035	0.437[c]	
MTV	11.474	2.191	60.096	0.004	
TLG	0.675	0.286	1.595	0.371	
NLR	0.617	0.216	1.764	0.367	
Stage	3.313	1.251	8.771	0.016	
mGPS score	1.496	1.042	2.146	0.029	
PLR	1.002	0.999	1.004	0.231	
Size (cm)	1.127	0.938	1.354	0.202	
SII	1	1	1	0.686	

k: Kaplan Meier test, log rank (Mantel-Cox), c: Cox regression-enter method, SE: Standard Error, CI: Confidence interval, MTV: Metabolic tumor volume, TLG: Total lesion glycolysis, NLR: Neutrophil-to-lymphocyte ratio, SII: Systemic immune-inflammation index, mGPS: Modified Glasgow prognostic score, PNI: Prognostic nutritional index, SUVmax: Maximum standardized uptake value, LDH: Lactate dehydrogenase, CRP: C-reactive protein, ALB: Albumin, ALP: Alkaline phosphatase, PLR: Platelet-to-lymphocyte ratio

Table 4. Univariate analysis of factors affecting overall survival					
	Dead	Alive	Estimate survival (m)	Estimate proportion surviving at the 1/3 year	p value
	n (%)	n (%)	Mean ± SE		
MTV					
≤41.02	4	41	2682,80±150,13	92/85.9	0.001[k]
>41.02	9	14	880.10±106.26	69.5/27.8	
TLG					
≤384.8	5	44	85.77±6.21	89.8/83.3	0.002[k]
>384.8	8	11	26.58±4.51	71.8/28.7	
LDH					
≤222	4	38	60.57±3.32	88.2/88.2	0.040[k]
>222	9	17	57.44±10.45	79.1/48	
CRP/ALB					
≤3.956	3	40	91.82±4.44	91.1/91.1	<0.001[k]
>3.956	10	15	21.52±2.10	73.2/15.2	
PNI					
≤41.3	10	9	19.07±2.7	62.6/0.0	<0.001[k]
>41.3	3	46	93.12±3.75	95.1/92.6	
Stage					
Local advanced stage	1	14	89.49±9.60	85.7	0.065[k]
Metastatic	12	41	47.05±5.10	79.2	
mGPS score					
0	2	33	93.32±4.45	92.7/92.7	0.001[k]
2	11	22	32.43±6.66	76.2/26.1	
Multivariate analysis of factors affecting overall survival					
	Odss ratio	95% CI for Odss ratio			
		Lower bound	Upper bound	p	
SUV_{max}	0.976	0.884	1.077	0.624[c]	
SUV_{mean}	0.956	0.806	1.134	0.602[c]	
LDH	1.003	0.998	1.009	0.258[c]	
ALB/ALP	0	0	0.028	0.033[c]	
NLR	1.017	0.928	1.115	0.72[c]	
PLR	1.001	0.998	1.003	0.674[c]	
Size (cm)	1.282	1.008	1.629	0.043[c]	
SII	1	1	1	0.29[c]	
Age	0.991	0.94.8	1.035	0.674[c]	
MTV	2.503	0.34	18.416	0.368	
TLG	0.357	0.042	3.057	0.347	
LDH	1.719	0.326	9.073	0.523	
Stage	3.003	0.343	26.249	0.32	
mGPS score	1.735	0.458	6.562	0.417	
Size (cm)	1.416	0.939	2.135	0.097	
ALB/ALP	0	0	449.598	0.088	
CRP/ALB	1.896	0.138	26.072	0.633	
PNI	0.431	0.064	2.888	0.386	

[k]: Kaplan Meier test, log rank (Mantel-Cox), [c]: Cox regression-enter method, SE: Standard Error, CI: Confidence interval, MTV: Metabolic tumor volume, TLG: Total lesion glycolysis, NLR: Neutrophil-to-lymphocyte ratio, SII: Systemic immune-inflammation index, mGPS: Modified Glasgow prognostic score, PNI: Prognostic nutritional index, SUV_{max}: Maximum standardized uptake value, LDH: Lactate dehydrogenase, CRP: C-reactive protein, ALB: Albumin, ALP: Alkaline phosphatase

conventional methods when selecting patients with a better prognosis. ^{18}F-FDG PET/CT has been increasingly identified as a prognostic biomarker for various malignancies in the assessment of early responses to treatment (27). Studies have shown that assessment with ^{18}F-FDG PET/CT in NSCLC can predict PFS and OS in patients treated with TKIs in the early period (18,28). In another study, early ^{18}F-FDG PET/CT was reported to predict the histopathological response in NSCLC patients treated with TKIs as neoadjuvant therapy (29).

Several studies (28,29) to date have evaluated the significance of ^{18}F-FDG uptake in the prediction of EGFR mutations in NSCLC, some of which have focused on SUV_{max}, identifying low SUV_{max} as an independent predictor of EGFR mutations (30,31,32,33); while in another study, it was emphasized that a high SUV_{max} was a significant predictor of EGFR mutations (31). It has been suggested that these differences may be attributable to clinicopathological features, and so this study evaluated the metabolic and volumetric parameters from PET/CT with immune, inflammatory and nutritional parameters for assessing PFS and OS, and investigated the effects of these parameters on each other, with MTV and mGPS being identified as the most valuable prognostic parameters for PFS. Compared to other studies, we think that evaluating ^{18}F-FDG PET/CT volumetric-metabolic and immune-inflammatory parameters in patients with NSCLC is more effective in determining the prognosis of the disease.

A recent study emphasized the important role of the systemic inflammation and the immune status of patients in cancer progression. Immune suppression and systemic inflammation at the onset of the disease are associated with a poor prognosis (34), and NLR, PLR, and LDH are the most effective and easily accessible markers for assessing inflammation and immune status (15).

There have been many studies reporting the prognostic value of ^{18}F-FDG PET/CT based on metabolic parameters, not only in lung cancer treated with TKIs (35,36), but also in other lung cancers in general (37,38). Unlike SUV_{max}, MTV and TLG include metabolic load and disease extent, and thus can have a higher predictive value (39,40,41). Similar to our study, another study reported that ^{18}F-FDG PET/CT volumetric parameters reflect both metabolic and tumor burdens, and thus had higher prognostic value than the metabolic activity values obtained by PET/CT (42,43) and tumor size (44) in lung cancers. Volumetric parameters, such as MTV and TLG, have been extensively studied in recent years. The prognostic role of MTV and TLG was meta-analyzed in patients with NSCLC at different stages (44). Volume-based parameters exhibit advantages in the measurement of metabolic tumor burden. Parameters obtained ^{18}F-FDG PET/CT can be used to select patients at high risk of death and who may benefit from subsequent more aggressive treatments.

Furthermore, our study identified mGPS and NLR as significant prognostic factors for PFS. There have been other studies demonstrating that other available blood-based biomarkers, such as NLR, PLR and mGPS, reflect the inflammatory status associated with cancer, and can be used as prognostic factors in lung cancer (21,45). mGPS, which assesses both systemic inflammation and nutritional status, has been identified as a potential prognostic predictor of lung cancer, as evaluated in many studies (46,47). The utility of NLR as a predictor in cancer patients has not been well studied, although there is increasing evidence that molecular and cellular pathways involve inflammations that contribute to the proliferation, angiogenesis and metastasis of neoplastic cells (48,49). Moreover, circulating neutrophils release various inflammatory cytokines, including tumor necrosis factor-α and interleukin-6, leading to cancer progression (50). It may therefore be reasonable to claim that treatment with EGFR-TKI is more effective in EGFR-mutated NSCLC patients with low NLR than in those with high NLR. Our analysis also suggests that NLR may be associated with PFS in NSCLC patients.

Study Limitations

Our study had certain limitations. The study protocol could not be strictly controlled because to its retrospective nature, although a standard imaging protocol was followed for all patients, and there was no difference due to homogeneous clinical management.

Conclusion

The aim in this study was to determine the optimum prognostic factors for assessing treatment response in advanced EGFR-mutated adenocarcinoma patients treated with TKIs. ^{18}F-FDG PET/CT volumetric parameters were found to have statistical significance in predicting PFS. We believe that these parameters are important prognostic markers that should be evaluated together in the management and follow-up of patients with EGFR-mutated adenocarcinoma. ^{18}F-FDG PET/CT may be considered an appropriate guide when making treatment decisions.

Ethics

Ethics Committee Approval: University of Health Sciences Turkey, Dr. Suat Seren Chest Diseases and Surgery Hospital Institutional Ethics Committee (approval no: 49109414-604.02).

Informed Consent: Consent was received.

Peer-review: Externally peer-reviewed.

Authorship Contributions

Surgical and Medical Practices: M.A., Concept: N.A., Design: N.A., Data Collection or Processing: N.A., H.K., N.K., Analysis or Interpretation: N.A., H.K., Literature Search: N.A., M.A., N.K., Writing: N.A.

Conflict of Interest: No conflict of interest was declared by the authors.

Financial Disclosure: The author declared that this study has received no financial support.

References

1. Shigematsu H, Lin L, Takahashi T, Nomura M, Suzuki M, Wistuba II, Fong KM, Lee H, Toyooka S, Shimizu N, Fujisawa T, Feng Z, Roth JA, Herz J, Minna JD, Gazdar AF. Clinical and biological features associated with epidermal growth factor receptor gene mutations in lung cancers. J Natl Cancer Inst 2005;97:339-346.
2. Mok TS, Wu YL, Thongprasert S, Yang CH, Chu DT, Saijo N, Sunpaweravong P, Han B, Margono B, Ichinose Y, Nishiwaki Y, Ohe Y, Yang JJ, Chewaskulyong B, Jiang H, Duffield EL, Watkins CL, Armour AA, Fukuoka M. Gefitinib or carboplatin-paclitaxel in pulmonary adenocarcinoma. N Engl J Med 2009;361:947-957.
3. Makinoshima H, Takita M, Matsumoto S, Yagishita A, Owada S, Esumi H, Tsuchihara K. Epidermal growth factor receptor (EGFR) signaling regulates global metabolic pathways in EGFR-mutated lung adenocarcinoma. J Biol Chem 2014;289:20813-20823.
4. Pao W, Miller V, Zakowski M, Doherty J, Politi K, Sarkaria I, Singh B, Heelan R, Rusch V, Fulton L, Mardis E, Kupfer D, Wilson R, Kris M, Varmus H. EGF receptor gene mutations are common in lung cancers from "never smokers" and are associated with sensitivity of tumors to gefitinib and erlotinib. Proc Natl Acad Sci USA 2004;101:13306-13311.
5. Mitsudomi T, Morita S, Yatabe Y, Negoro S, Okamoto I, Tsurutani J, Seto T, Satouchi M, Tada H, Hirashima T, Asami K, Katakami N, Takada M, Yoshioka H, Shibata K, Kudoh S, Shimizu E, Saito H, Toyooka S, Nakagawa K, Fukuoka M; West Japan Oncology Group. Gefitinib versus cisplatin plus docetaxel in patients with non-small-cell lung cancer harbouring mutations of the epidermal growth factor receptor (WJTOG3405): an open label, randomised phase 3 trial. Lancet Oncol 2010;11:121-128.
6. Zhou C, Wu YL, Chen G, Feng J, Liu XQ, Wang C, Zhang S, Wang J, Zhou S, Ren S, Lu S, Zhang L, Hu C, Hu C, Luo Y, Chen L, Ye M, Huang J, Zhi X, Zhang Y, Xiu Q, Ma J, Zhang L, You C. Erlotinib versus chemotherapy as first-line treatment for patients with advanced EGFR mutation-positive non-small-cell lung cancer (OPTIMAL, CTONG-0802): a multicentre, open-label, randomised, phase 3 study. Lancet Oncol 2011;12:735-742.
7. Rosell R, Carcereny E, Gervais R, Vergnenegre A, Massuti B, Felip E, Palmero R, Garcia-Gomez R, Pallares C, Sanchez JM, Porta R, Cobo M, Garrido P, Longo F, Moran T, Insa A, De Marinis F, Corre R, Bover I, Illiano A, Dansin E, de Castro J, Milella M, Reguart N, Altavilla G, Jimenez U, Provencio M, Moreno MA, Terrasa J, Muñoz-Langa J, Valdivia J, Isla D, Domine M, Molinier O, Mazieres J, Baize N, Garcia-Campelo R, Robinet G, Rodriguez-Abreu D, Lopez-Vivanco G, Gebbia V, Ferrera-Delgado L, Bombaron P, Bernabe R, Bearz A, Artal A, Cortesi E, Rolfo C, Sanchez-Ronco M, Drozdowskyj A, Queralt C, de Aguirre I, Ramirez JL, Sanchez JJ, Molina MA, Taron M, Paz-Ares L; Spanish Lung Cancer Group in collaboration with Groupe Français de Pneumo-Cancérologie and Associazione Italiana Oncologia Toracica. Erlotinib versus standard chemotherapy as first-line treatment for European patients with advanced EGFR mutation-positive non-small-cell lung cancer (EURTAC): a multicentre, open-label, randomised phase 3 trial. Lancet Oncol 2012;13:239-246.
8. Minami S, Ogata Y, Ihara S, Yamamoto S, Komuta K. Pretreatment Glasgow prognostic score and prognostic nutritional index predict overall survival of patients with advanced small cell lung cancer. Lung Cancer (Auckl) 2017;8:249-257.
9. Laird BJ, Kaasa S, McMillan DC, Fallon MT, Hjermstad MJ, Fayers P, Klepstad P. Prognostic factors in patients with advanced cancer: a comparison of clinicopathological factors and the development of an inflammation-based prognostic system. Clin Cancer Res 2013;19:5456-5464.
10. Zhou T, Zhao Y, Zhao S, Yang Y, Huang Y, Hou X, Zhao H, Zhang L. Comparison of the prognostic value of systemic inflammation response markers in small cell lung cancer patients. J Cancer 2019;10:1685-1692.
11. Ferreira LM, Hebrant A, Dumont JE. Metabolic reprogramming of the tumor. Oncogene 2012;31:3999-4011.
12. Zhang X, Guo M, Fan J, Lv Z, Huang Q, Han J, Wu F, Hu G, Xu J, Jin Y. Prognostic significance of serum LDH in small cell lung cancer: a systematic review with meta-analysis. Cancer Biomark 2016;16:415-423.
13. Lee DS, Park KR, Kim SJ, Chung MJ, Lee YH, Chang JH, Kang JH, Hong SH, Kim MS, Kim YS. Serum lactate dehydrogenase levels at presentation in stage IV non-small cell lung cancer: predictive value of metastases and relation to survival outcomes. Tumour Biol 2016;37:619-625.
14. Buergy D, Wenz F, Groden C, Brockmann MA. Tumor-platelet interaction in solid tumors. Int J Cancer 2012;130:2747-2760.
15. Deng M, Ma X, Liang X, Zhu C, Wang M. Are pretreatment neutrophil-lymphocyte ratio and platelet-lymphocyte ratio useful in predicting the outcomes of patients with small-cell lung cancer? Oncotarget 2017;8:37200-37207.
16. Hong X, Cui B, Wang M, Yang Z, Wang L, Xu Q. Systemic immune-inflammation index, based on platelet counts and neutrophil-lymphocyte ratio, is useful for predicting prognosis in small cell lung cancer. Tohoku J Exp Med 2015;236:297-304.
17. Dose Schwarz J, Bader M, Jenicke L, Hemminger G, Jänicke F, Avril N. Early prediction of response to chemotherapy in metastatic breast cancer using sequential 18F-FDG PET. J Nucl Med 2005;46:1144-1150.
18. Mileshkin L, Hicks RJ, Hughes BG, Mitchell PL, Charu V, Gitlitz BJ, Macfarlane D, Solomon B, Amler LC, Yu W, Pirzkall A, Fine BM. Changes in 18F-fluorodeoxyglucose and 18F-fluorodeoxythymidine positron emission tomography imaging in patients with non-small cell lung cancer treated with erlotinib. Clin Cancer Res 2011;17:3304-3315.
19. Edet-Sanson A, Dubray B, Doyeux K, Back A, Hapdey S, Modzelewski R, Bohn P, Gardin I, Vera P. Serial assessment of FDG-PET FDG uptake and functional volume during radiotherapy (RT) in patients with non-small cell lung cancer (NSCLC). Radiother Oncol 2012;102:251-257.
20. Davison J, Mercier G, Russo G, Subramaniam RM. PET-based primary tumor volumetric parameters and survival of patients with non-small cell lung carcinoma. AJR Am J Roentgenol 2013;200:635-640.
21. Paidpally V, Chirindel A, Lam S, Agrawal N, Quon H, Subramaniam RM. FDG-PET/CT imaging biomarkers in head and neck squamous cell carcinoma. Imaging Med 2012;4:633-647.
22. Miyawaki M, Naoki K, Yoda S, Nakayama S, Satomi R, Sato T, Ikemura S, Ohgino K, Ishioka K, Arai D, Namkoong H, Otsuka K, Miyazaki M, Tani T, Kuroda A, Nishino M, Yasuda H, Kawada I, Koh H, Nakamura M, Terashima T, Sakamaki F, Sayama K, Betsuyaku T, Soejima K. Erlotinib as second- or third-line treatment in elderly patients with advanced non-small cell lung cancer: Keio Lung Oncology Group Study 001 (KLOG001). Mol Clin Oncol 2017;6:409-414.
23. Ramalingam SS, Vansteenkiste J, Planchard D, Cho BC, Gray JE, Ohe Y, Zhou C, Reungwetwattana T, Cheng Y, Chewaskulyong B, Shah R, Cobo M, Lee KH, Cheema P, Tiseo M, John T, Lin MC, Imamura F, Kurata T, Todd

A, Hodge R, Saggese M, Rukazenkov Y, Soria JC; FLAURA Investigators. Overall survival with osimertinib in untreated, EGFR-mutated advanced NSCLC. N Engl J Med 2020;382:41-50.

24. Maemondo M, Inoue A, Kobayashi K, Sugawara S, Oizumi S, Isobe H, Gemma A, Harada M, Yoshizawa H, Kinoshita I, Fujita Y, Okinaga S, Hirano H, Yoshimori K, Harada T, Ogura T, Ando M, Miyazawa H, Tanaka T, Saijo Y, Hagiwara K, Morita S, Nukiwa T; North-East Japan Study Group. Gefitinib or chemotherapy for non-small-cell lung cancer with mutated EGFR. N Engl J Med 2010;362:2380-2388.
25. Takeda M, Nakagawa K. First- and second-generation EGFR-TKIs are all replaced to osimertinib in chemo-Naive EGFR mutation-positive non-small cell lung cancer? Int J Mol Sci 2019;20:146.
26. Cersosimo RJ. Gefitinib: an adverse effects profile. Expert Opin Drug Saf 2006;5:469-479.
27. Vansteenkiste J, Fischer BM, Dooms C, Mortensen J. Positron-emission tomography in prognostic and therapeutic assessment of lung cancer: systematic review. Lancet Oncol 2004;5:531-540.
28. Zander T, Scheffler M, Nogova L, Kobe C, Engel-Riedel W, Hellmich M, Papachristou I, Toepelt K, Draube A, Heukamp L, Buettner R, Ko YD, Ullrich RT, Smit E, Boellaard R, Lammertsma AA, Hallek M, Jacobs AH, Schlesinger A, Schulte K, Querings S, Stoelben E, Neumaier B, Thomas RK, Dietlein M, Wolf J. Early prediction of nonprogression in advanced non-small-cell lung cancer treated with erlotinib by using [(18)F]fluorodeoxyglucose and [(18)F]fluorothymidine positron emission tomography. J Clin Oncol 2011;29:1701-1708.
29. Aukema TS, Kappers I, Olmos RA, Codrington HE, van Tinteren H, van Pel R, Klomp HM; NEL Study Group. Is 18F-FDG PET/CT useful for the early prediction of histopathologic response to neoadjuvant erlotinib in patients with non-small cell lung cancer? J Nucl Med 2010;51:1344-1348.
30. Lv Z, Fan J, Xu J, Wu F, Huang Q, Guo M, Liao T, Liu S, Lan X, Liao S, Geng W, Jin Y. Value of 18F-FDG PET/CT for predicting EGFR mutations and positive ALK expression in patients with non-small cell lung cancer: a retrospective analysis of 849 Chinese patients. Eur J Nucl Med Mol Imaging 2018;45:735-750.
31. Lee EY, Khong PL, Lee VH, Qian W, Yu X, Wong MP. Metabolic phenotype of stage IV lung adenocarcinoma: relationship with epidermal growth factor receptor mutation. Clin Nucl Med 2015;40:e190-e195.
32. Gu J, Xu S, Huang L, Li S, Wu J, Xu J, Feng J, Liu B, Zhou Y. Value of combining serum carcinoembryonic antigen and PET/CT in predicting EGFR mutation in non-small cell lung cancer. J Thorac Dis 2018;10:723-731.
33. Guan J, Xiao NJ, Chen M, Zhou WL, Zhang YW, Wang S, Dai YM, Li L, Zhang Y, Li QY, Li XZ, Yang M, Wu HB, Chen LH, Liu LY. 18F-FDG uptake for prediction EGFR mutation status in non-small cell lung cancer. Medicine (Baltimore) 2016;95:e4421.
34. Pinkerton JW, Kim RY, Robertson AAB, Hirota JA, Wood LG, Knight DA, Cooper MA, O'Neill LAJ, Horvat JC, Hansbro PM. Inflammasomes in the lung. Mol Immunol 2017;86:44-55.
35. van Gool MH, Aukema TS, Schaake EE, Rijna H, Codrington HE, Valdés Olmos RA, Teertstra HJ, van Pel R, Burgers SA, van Tinteren H, Klomp HM. (18)F-fluorodeoxyglucose positron emission tomography versus computed tomography in predicting histopathological response to epidermal growth factor receptor-tyrosine kinase inhibitor treatment in resectable non-small cell lung cancer. Ann Surg Oncol 2014;21:2831-2837.
36. Benz MR, Herrmann K, Walter F, Garon EB, Reckamp KL, Figlin R, Phelps ME, Weber WA, Czernin J, Allen-Auerbach MS. (18)F-FDG PET/CT for monitoring treatment responses to the epidermal growth factor receptor inhibitor erlotinib. J Nucl Med 2011;52:1684-1689.
37. Higashi K, Ueda Y, Arisaka Y, Sakuma T, Nambu Y, Oguchi M, Seki H, Taki S, Tonami H, Yamamoto I. 18F-FDG uptake as a biologic prognostic factor for recurrence in patients with surgically resected non-small cell lung cancer. J Nucl Med 2002;43:39-45.
38. Imamura Y, Azuma K, Kurata S, Hattori S, Sasada T, Kinoshita T, Okamoto M, Kawayama T, Kaida H, Ishibashi M, Aizawa H. Prognostic value of SUVmax measurements obtained by FDG-PET in patients with non-small cell lung cancer receiving chemotherapy. Lung Cancer 2011;71:49-54.
39. Chen HH, Chiu NT, Su WC, Guo HR, Lee BF. Prognostic value of whole-body total lesion glycolysis at pretreatment FDG PET/CT in non-small cell lung cancer. Radiology 2012;264:559-566.
40. Olivier A, Petyt G, Cortot A, Scherpereel A, Hossein-Foucher C. Higher predictive value of tumour and node [18F]-FDG PET metabolic volume and TLG in advanced lung cancer under chemotherapy. Nucl Med Commun 2014;35:908-915.
41. Liao S, Penney BC, Wroblewski K, Zhang H, Simon CA, Kampalath R, Shih MC, Shimada N, Chen S, Salgia R, Appelbaum DE, Suzuki K, Chen CT, Pu Y. Prognostic value of metabolic tumor burden on 18F-FDG PET in nonsurgical patients with non-small cell lung cancer. Eur J Nucl Med Mol Imaging 2012;39:27-38.
42. Oh JR, Seo JH, Chong A, Min JJ, Song HC, Kim YC, Bom HS. Whole-body metabolic tumour volume of 18F-FDG PET/CT improves the prediction of prognosis in small cell lung cancer. Eur J Nucl Med Mol Imaging 2012;39:925-935.
43. Yoo SW, Kim J, Chong A, Kwon SY, Min JJ, Song HC, Bom HS. Metabolic tumor volume measured by F-18 FDG PET/CT can further stratify the prognosis of patients with Stage IV non-small cell lung cancer. Nucl Med Mol Imaging 2012;46:286-293.
44. Im HJ, Pak K, Cheon GJ, Kang KW, Kim SJ, Kim IJ, Chung JK, Kim EE, Lee DS. Prognostic value of volumetric parameters of (18)F-FDG PET in non-small-cell lung cancer: a meta-analysis. Eur J Nucl Med Mol Imaging 2015;42:241-251.
45. Klemm F, Joyce JA. Microenvironmental regulation of therapeutic response in cancer. Trends Cell Biol 2015;25:198-213.
46. Wang J, Wang B, Chu H, Yao Y. Intrinsic resistance to EGFR tyrosine kinase inhibitors in advanced non-small-cell lung cancer with activating EGFR mutations. Onco Targets Ther 2016;9:3711-3726.
47. Igawa S, Sasaki J, Otani S, Ishihara M, Takakura A, Katagiri M, Masuda N. Impact of smoking history on the efficacy of gefitinib in patients with non-small cell lung cancer harboring activating epidermal growth factor receptor mutations. Oncology 2015;89:275-280.
48. Colotta F, Allavena P, Sica A, Garlanda C, Mantovani A. Cancer-related inflammation, the seventh hallmark of cancer: links to genetic instability. Carcinogenesis 2009;30:1073-1081.
49. Mantovani A, Allavena P, Sica A, Balkwill F. Cancer-related inflammation. Nature 2008;454:436-444.
50. Balkwill F, Mantovani A. Inflammation and cancer: back to Virchow? Lancet 2001;357:539-545.

Original Article
Mol Imaging Radionucl Ther 2022;31:114-122 DOI:10.4274/mirt.galenos.2022.73636

Elevated Angiogenic Factor Levels After Transarterial Radioembolization for Colorectal Cancer Liver Metastases May Predict a Poor Prognosis

Yüksek Anjiyojenik Faktör Seviyeleri Kolorektal Kanser Karaciğer Metastazları İçin Transarteriyel Radyoembolizasyon Sonrası Kötü Prognozu Öngörebilir

Çiğdem Soydal[1], Mine Araz[1], Mustafa Durmaz[2], Elgin Özkan[1], Berrin İmge Ergüder[2], Nuriye Özlem Küçük[1], Sadık Bilgiç[3], Atilla Halil Elhan[4], İbrahim Ethem Geçim[5]

[1]*Ankara University Faculty of Medicine, Department of Nuclear Medicine, Ankara, Turkey*
[2]*Ankara University Faculty of Medicine, Department of Biochemistry, Ankara, Turkey*
[3]*Ankara University Faculty of Medicine, Department of Radiology, Ankara, Turkey*
[4]*Ankara University Faculty of Medicine, Department of Biostatistics, Ankara, Turkey*
[5]*Ankara University Faculty of Medicine, Department of Surgery, Ankara, Turkey*

Abstract

Objectives: To analyze the change in circulating angiogenic factor levels after transarterial radioembolization (TARE) for colorectal cancer liver metastases (CRCLMs) and its prognostic significance.

Methods: Blood samples immediately before TARE and on 1 day, 1 week and 6 weeks after were collected for angiogenic factor analysis in 23 patients.

Results: Patients with elevated serum basic fibroblast growth factor and platelet-derived growth factor levels in the 1st week and vascular endothelial growth factor (VEGF) levels in the 6th week after TARE had significantly shorter median overall survival (OS) times.

Conclusion: Some early increases in serum angiogenic factor levels and in serum VEGF in the 6th week after TARE for CRCLMs are related to short OS and progression-free survival.

Keywords: Colorectal cancer, liver metastasis, transarterial radioembolization, serum angiogenic factors

Öz

Amaç: Kolorektal kanser metastazları için transarteriyel radyoembolizasyon (TARE) sonrası dolaşımda anjiyojenik faktörlerin seviyelerindeki değişikliklerin analiz edilmesidir.

Yöntem: Anjiyojenik faktör analizi için 23 hastada TARE'den hemen önce, 1. günde, 1. haftada ve 6 hafta sonra kan örnekleri toplandı.

Bulgular: TARE sonrası 1. haftada bazik fibroblast büyüme faktörü ve platelet kaynaklı büyüme faktörü seviyelerinde ve 6. haftada vasküler endotelyal büyüme faktörü (VEGF) seviyelerinde artış olan hastalarda medyan genel sağkalım süreleri istatistiksel olarak daha kısaydı.

Sonuç: Bazı anjiyojenik faktör seviyelerinde erken yükselişler ve kolorektal kanser metastazları için TARE sonrası 6. haftada serum VEGF seviyelerinde artış olması kısa genel sağkalım ve progresyonsuz sağkalım ile ilişkilidir.

Anahtar kelimeler: Kolorektal kanser, karaciğer metastazı, transarteriyel radyoembolizasyon, serum anjiyojenik faktörler

Address for Correspondence: Mine Araz MD, Ankara University Faculty of Medicine, Department of Nuclear Medicine, Ankara, Turkey
Phone: +90 532 666 73 13 **E-mail:** minesoylu@yahoo.com ORCID ID: orcid.org/0000-0001-6467-618X
Received: 09.12.2021 **Accepted:** 20.02.2022

Introduction

The liver is the most common metastasis site of colorectal cancer (CRC) and a major cause of death (1). The only curative treatment choice is surgery; however, it is impossible for most patients, and palliative options such as systemic treatments may be administered instead (2). Local treatment options should be considered for patients for whom systemic treatments fail. Specifically, transarterial radioembolization (TARE) might be an alternative for these patient groups (3).

Ideal candidates for TARE for colorectal cancer liver metastases (CRCLMs) are those with liver-dominant, unresectable, and chemorefractory tumors (4,5). Resin microspheres with diameters of 30-40 μm embedded with Yttrium-90 (Y-90) are delivered to the hepatic artery via a catheter. The microspheres become lodged in the arteriolar system of the tumor and cause necrosis due to radiation and embolic effects (6,7,8). Despite the promising outcomes for CRCLM, not all patients show a good response to TARE. Moreover, some patients experience rapid progression of extrahepatic disease following TARE. One of the possible explanations is an increase in circulating angiogenic factor levels after TARE and their effects on extrahepatic progression. Because both radiation and embolization promote angiogenesis, it has been hypothesized that increases in proangiogenic cytokines or decreases in cytokines that inhibit angiogenesis may affect the response to TARE (9,10,11). Measuring these markers might therefore have predictive value for treatment response to TARE. If increases in circulating angiogenic factor levels can be proven to be related to prognosis, concomitant use of anti-angiogenic treatments with TARE may improve patient outcomes.

To date, only three studies have focused on angiogenic markers after TARE (9,12,13,14), and one included only hepatocellular cancer (HCC) patients (12). Considering the limited data on this topic, in our pilot study, we included patients with CRCLM and measured circulating angiogenic factors and baseline levels at different time points after TARE. The primary goal of this study was to determine whether there is a change in circulating angiogenic factor levels after TARE with resin microspheres and to investigate possible prognostic importance. We also compared the baseline circulating angiogenic factor levels of patients with and without extrahepatic disease as a secondary objective.

Materials and Methods

This prospective study was approved by the Ankara University Faculty of Medicine, Local Institutional Ethical Committee (decision number: 01-14-16) and supported by a research grant from the Nevin Baykent Health and the Education Foundation. Inclusion criteria were as follows: Older than 18 years, the existence of inoperable CRCLM, fit the criteria for TARE, and provided informed consent for the trial. The exclusion criteria were as follows: Younger than 18 years, prior history of bevacizumab therapy, coexistence of a secondary malignancy, and any contraindications for TARE. Written informed consent was obtained from all participants. All patients who fitted the inclusion criteria and received TARE between March 2016 and May 2019 for the treatment of CRCLM were included in the analysis. Pretreatment tumor load of the liver was evaluated by computed tomography (CT) or magnetic resonance imaging of the liver. Pretreatment ^{18}fluorine-fluorodeoxyglucose (^{18}F-FDG) positron emission tomography (PET)/CT was performed to assess the extrahepatic tumor load. After the TARE, none of the patients received additional treatment until the 6th week. Treatment response and extrahepatic disease progression were evaluated using ^{18}F-FDG PET/CT using the PERCIST 1.1 criteria, which is based on the percent change in metabolic activity at the 6th week of follow-up. The outline of the study design is given in Figure 1.

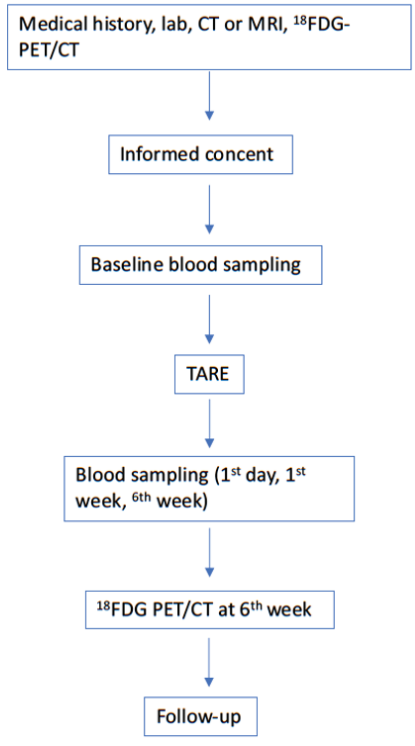

Figure 1. Outline of the clinical evaluations and study procedures
CT: Computed tomography, MRI: Magnetic resonance imaging, ^{18}F-FDG: ^{18}Fluorine-fluorodeoxyglucose, PET: Positron emission tomography, TARE: Transarterial radioembolization

Transarterial Radioembolization

The widely accepted parameters of liver reserve, bone marrow reserve (granulocytes >1500/μL, platelets >60000/μL), and hepatic vascularity were used as inclusion and exclusion criteria for TARE. Liver reserve was assessed on serum bilirubin, aspartate transaminase (AST), alanine transaminase (ALT), gamma glutamyl transferase (GGT), and alkaline phosphatase (ALP) levels. For radioembolization, bilirubin levels below 2 mg/dL AST, ALT and ALP levels less than five times the standard upper limit was required. The candidate patient provided written informed consent. The Y-90 dose was adjusted according to the following body surface area (BSA) method: Activity (GBq) = (BSA -0.2) + tumor volume/total liver volume. Tumor and liver volumes were calculated from CT images. The lung shunt fraction was calculated from hepatic artery perfusion scintigraphic images. Mean absorbed dose thresholds were accepted as 120 Gy for tumors, 50 Gy for non-tumorous liver tissue and 20 Gy for the lung. The Y-90 resin microspheres (Sirtex Medical) were injected through selective catheterization of the hepatic artery catheter under intermittent fluoroscopic visualization. A right femoral puncture was performed using the landmark technique, where the maximal pulse was palpated; left femoral puncture was performed if right femoral access could not be achieved because of underlying vascular pathology. For hepatic arterial catheterizations, either the celiac truncus or superior mesenteric artery was selectively catheterized with an appropriate 5 F catheter (Sim2, C2, RDC, or sim 1; Imager II Boston Scientific Corp., Natick, MA, USA or Terumo Medical Corp., Tokyo, Japan). After selective catheterization of the artery, a 2.7 F microcatheter set with a 0.021-inch guidewire (Progreat; Terumo Medical Corp., Tokyo, Japan) was used for superselective catheterization of the tumor feeders coaxial. Subsegmental, selective right, or selective left hepatic arterial catheterization decisions were made according to the vascularity patterns of the tumors on DSA images. If <2 hepatic segments were involved in diagnostic images, subsegmental catheterization was performed for ablative purposes. Within 1-24 hours after microsphere infusion, Bremsstrahlung images were obtained to confirm that Y-90 was deposited only in the liver. For patients with bilobar disease, TARE was applied in two separate sequences. All patients were hospitalized overnight, and medications (e.g., analgesics, antiemetic, H_2 antagonists) were administered if necessary. All patients were closely monitored until acute or late toxicities were resolved.

Angiogenic Factor Measurements

Blood samples immediately before TARE and on 1 day, 1 week and 6 weeks after were collected for angiogenic factor analysis. Serum vascular endothelial growth factor (VEGF), angiopoietin-2 (Ang-2), basic fibroblast growth factor (bFGF), hepatocyte growth factor (HGF) and platelet-derived growth factor (PDGF) measurements were performed by ELISA using the quantitative sandwich enzyme immunoassay technique.

Statistical Analysis

Descriptive data are expressed as median [minimum (min)-maximum (max)] or mean ± standard deviation (SD) values. The Mann-Whitney U test was used to compare the difference between the two groups in terms of non-normally distributed variables. Differences among the four time points for circulating angiogenic factor levels were evaluated by the Friedman test. When the p value from the Friedman test showed statistical significance, Bonferroni correction was applied for multiple comparisons. Nominal variables were tested by Fisher's Exact test. Survival estimations were performed using the Kaplan-Meier algorithm, and comparison between groups was evaluated with the log-rank test. A p value less than 0.05 was considered significant. SPSS version 20.0 (IBM, Chicago, Illinois, USA) was used for the statistical analysis.

Results

Patients

Twenty-three patients (median age: 64, min-max: 45-78; 3 female and 20 male) with inoperable CRCLM were included in the study. All patients had inoperable liver-dominant or liver-only metastases and fitted the inclusion criteria. While the primary tumor was operable in 21 patients, it was inoperable in 2 patients. All patients had received chemotherapy and had chemorefractory or recurrent disease before TARE. Primary tumors were located in the right, left colon and rectum in 12 (52%), 8 (35%) and 3 (13%) patients, respectively. Surgical liver resection was performed in 4 (17%) patients; transarterial chemoembolization (TACE) was applied in 16 (70%) cases before the TARE. All patients had received one-line systemic chemotherapy for liver metastases before consideration for TARE; 16 (70%) patients received FOLFOX and 7 (30%) the FOLFIRI regimen. The median time between the last cycle of chemotherapy and TARE was (3 months, min-max: 1-5 months). The number of liver tumors was 1-5 in 5 (22%), 6-10 in 8 (35%) and >10 in 10 (43%) patients. The mean tumor diameter was calculated as 34.6±12.7 mm. The pretreatment mean levels of serum ALT, AST, GGT and ALP were 44.13±37.7 IU/L, 35.56±29.3 IU/L, 217.5±264.5IU/L, and 231.86±182.1IU/L, respectively. Before the TARE,

extrahepatic disease was detected in 12 (52%) patients, located in the lymph nodes, lungs and bones in 8 (35%), 3 (13%) and 1 (4%), respectively. TARE was administered to both the right and left liver lobes in 5 (22%), 15 (65%) and 3 (13%) patients, respectively.

Angiogenic Factor Analyses

Baseline measurements of median serum angiogenic factor levels of patients with and without extrahepatic disease were not significant (Table 1). In the entire patient group, a slight increase in the median values of several angiogenic factors in the 1st day or in the 1st week after TARE was observed. While at the 1st day median values of all angiogenic factors except HGF were elevated, at the 1st week only median values of VEGF and Ang-2 were done. By the 6th week, serum VEGF levels were significantly decreased compared to on the 1st day and in the 1st week (Figure 2). An increase in any angiogenic factor level was seen in 21 (91%) patients on the 1st day, and increases were found in 21 (91%) and 17 (74%) patients in the 1st and 6th weeks. In three patients, all of the angiogenic factor levels were elevated on the 1st day and in the 1st week. Changes in the median values of serum angiogenic factor levels are summarized in Table 2.

Follow-up and Survival Analyses

The survivors in this study had a minimum follow-up time of 4 months. There was an insignificant difference between baseline median angiogenic factor levels of those patients with overall survival (OS) longer than 6 months and those with OS shorter than 6 months (Table 3).

By the 6th week of follow-up, disease progression in the treated liver lobe was seen in 7 (30%) patients, and extrahepatic metastases were detected in 12 (52%). Some of the mean ± SD values of circulating angiogenic factor levels of the patients with and without progression in the treated liver lobe in the 6th week of follow-up were significantly different (Table 4, Figure 3); mean ± SD Ang-2 levels on the 1st day for patients with and without extrahepatic disease progression in the 6th week also differed significantly (Figure 4).

In the follow-up period, 16 (70%) patients had died by the median 20 months follow-up period (min: 3, max: 43). Patients with elevated serum bFGF and PDGF levels in the 1st week after TARE had significantly shorter median OS times than those without elevated levels [for FGF; 5.0±0.7 (95% confidance interval (CI); 3.7-6.3) months vs. 11.0±2.1 (95% CI; 7.0-15.0) months, p=0.004; for

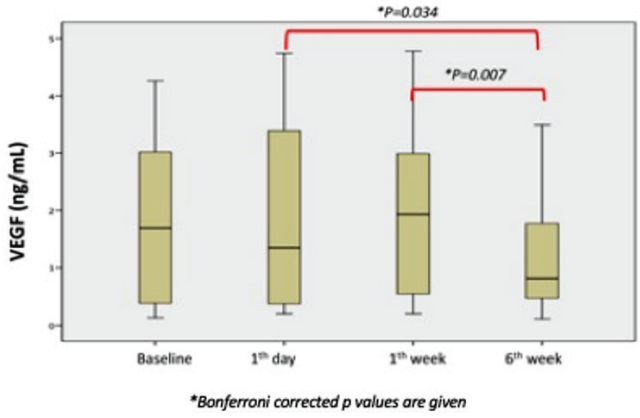

Figure 2. Boxplots of median serum VEGF levels after transarterial radioembolization for different time points
VEGF: Vascular endothelial growth factor, ng/mL: Nanogram per milliliter

Table 1. Descriptive data of baseline angiogenic factor levels of patients with and without extrahepatic disease

Extrahepatic disease		VEGF		Ang-2		bFGF		HGF		PDGF	
Absent	N	11	*p=0.087	11	*p=0.83	11	*p=0.074	11	*p=0.68	11	*p=0.95
	Mean	2.30		2.70		39.17		1.76		12.96	
	SD	1.56		1.96		20.89		1.51		5.57	
	Median	2.79		2.24		34.11		1.11		10.37	
	Minimum	0.30		0.34		18.25		0.50		7.43	
	Maximum	4.26		7.24		92.46		5.64		23.34	
Present	N	12		12		12		12		12	
	Mean	1.13		2.39		25.45		1.20		15.26	
	SD	1.08		1.56		10.68		0.48		11.45	
	Median	0.93		2.06		23.42		1.09		13.50	
	Minimum	0.13		0.73		10.00		0.57		2.20	
	Maximum	3.93		6.47		45.50		2.11		42.29	

*Mann-Whitney U test, N: Number, SD: Standard deviation, VEGF: Vascular endothelial growth factor, Ang-2: Angiopoietin-2, bFGF: Basic fibroblast growth factor, HGF: Hepatocyte growth factor, PDGF: Platelet-derived growth factor

Table 2. Change in median serum levels of different angiogenic factors at different time points

Angiogenic factor	Baseline (median, min-max)	1st day (median, min-max)	1st week (median, min-max)	6th week (median, min-max)	*p value
VEGF (ng/mL)	1.20 (0.13-4.26)	1.35 (0.20-4.74)	1.65 (0.20-4.58)	0.82 (0.11-3.38)	0.006
Ang-2 (ng/mL)	2.10 (0.34-7.24)	2.36 (0.63-6.83)	2.86 (0.30-7.13)	2.43 (0.06-7.26)	0.25
bFGF (ng/mL)	27.93 (10.00-92.46)	30.06 (6.5-63.38)	27.31 (8.1-64.92)	30.35 (4.86-77.81)	0.67
HGF (ng/mL)	1.11 (0.50-5.64)	1.04 (0.53-8.49)	1.09 (0.45-4.17)	1.04 (0.33-3.85)	0.79
PDGF (ng/mL)	11.34 (2.2-42.29)	12.98 (2.35-32.31)	11.37 (3.36-43.12)	10.79 (1.74-38.99)	0.53

*Bonferroni-corrected p values are given. VEGF: Vascular endothelial growth factor, Ang-2: Angiopoietin-2, bFGF: Basic fibroblast growth factor, HGF: Hepatocyte growth factor, PDGF: Platelet-derived growth factor, N: number, min: Minimum, max: Maximum

Table 3. Descriptive data of baseline angiogenic factor levels of patients who did or did not have overall survival longer than 6 months

Overall survival		VEGF		Ang-2		bFGF		HGF		PDGF	
<6 months	N	10	*p=0.95	10	*p=0.13	10	*p=0.75	10	p=0.44	10	*p=0.15
	Mean	1.8		3.3		36		1.56		17.1	
	SD	1.5		2.2		23.8		0.84		10.4	
	Median	1.8		2.9		29.7		1.63		16	
	Minimum	0.1		0.7		10.3		0.5		6.12	
	Maximum	4.3		7.2		92.5		2.72		42.3	
>6 months	N	13		13		13		13		13	
	Mean	1.6		1.9		28.9		1.4		11.9	
	SD	1.4		0.9		1.3		1.3		7.35	
	Median	1.1		1.9		1.04		1.04		9.93	
	Minimum	0.3		0.3		0.61		0.61		2.2	
	Maximum	3.9		3.4		5.64		5.64		30.9	

*Mann-Whitney U test. VEGF: Vascular endothelial growth factor, Ang-2: Angiopoietin-2, bFGF: Basic fibroblast growth factor, HGF: Hepatocyte growth factor, PDGF: Platelet-derived growth factor, N; Number, SD: Standard deviation

Table 4. Significant difference in circulating angiogenic factor levels of patients with and without progression of the treated liver lobe at the 6th week of follow-up

Progression on the treated liver lobe at the 6th week follow-up	Circulating VEGF (mean ± SE, ng/mL) level at the 6th week	Circulating PDFG (mean ± SE, ng/mL) level at the baseline	Circulating PDGF (mean ± SE, ng/mL) level at the 24th hour	Circulating PDGF (mean ± SE, ng/mL) level at the 1st week	Circulating PDGF (mean ± SE, ng/mL) level at the 6th week
Negative	3.1±0.2	12.5±1.6	12.3±1.5	11.7±1.7	11.0±1.3
Positive	3.3±0.5	16.2±5.4	16.2±4.2	16.9±5.6	15.1±4.7
*p value	0.031	0.007	0.007	0.007	0.022

*Mann-Whitney U test, negative and positive not descriptive. VEGF: Vascular endothelial growth factor, PDGF: Platelet-derived growth factor, SE: Standard error

PGDF; 5.0±2.2 (95% CI; 0.8-9.2) months vs. 16.0±3.3 (95% CI: 9.4-22.6) months, p=0.013] (Figure 5). Patients who had elevated serum VEGF levels in the 6th week also had significantly shorter median OS times than those who did not [11.0±0.0 months vs. 16.0±1.2 (95% CI; 13.7-18.3) months, p=0.034] (Figure 5). Moreover, patients with elevations of all of the angiogenic factors in the 1st week had shorter median OS times than those who did not [5.0±0.0 months vs. 11.0±0.8 (95% CI; 9.5-12.5) months, p=0.007] (Figure 5).

Disease progression occurred in 16 (70%) patients. Patients with elevated bFGF levels in the 1st week after TARE had

significantly shorter median progression-free survival (PFS) than those without elevated bFGF levels [2.0±0.1 (95% CI, 2.0-2.1) months vs. 5.2±1.5 (95% CI, 1.6-9.0) months, p=0.050].

Discussion

Angiogenesis is a complex process that is still not fully understood. Antiangiogenic drugs have been developed for cancer treatment because the activation of the angiogenic process responds to hypoxia. Several studies have focused on angiogenic factors after transarterial treatments of liver tumors (9,14,15,16,17,18,19). However, most of them have been designed to evaluate the angiogenic response after TACE for HCC (16,17,18,19). In contrast, data on the angiogenic response after TARE for CRC liver metastases are limited to two studies (9,13). For this reason, in this

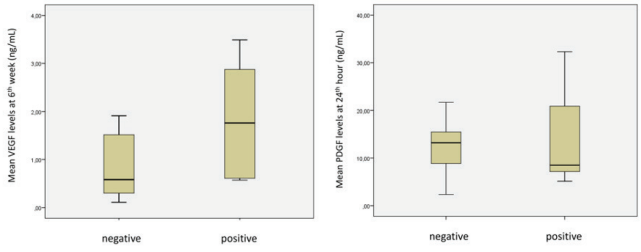

Figure 3. Boxplots representing significant distributions of median serum VEGF and PDGF levels of patients who had progression on treated liver lobe in the 6th week of follow-up
VEGF: Vascular endothelial growth factor, PDGF: Platelet-derived growth factor, Negative: No progression, Positive: Progression

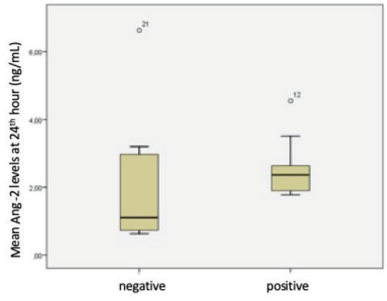

Figure 4. Boxplots representing significant distributions of mean Ang-2 levels of patients who had extrahepatic disease progession in the 6th week of follow-up
Ang-2: Angiopoietin-2, Negative: No progression, Positive: Progression

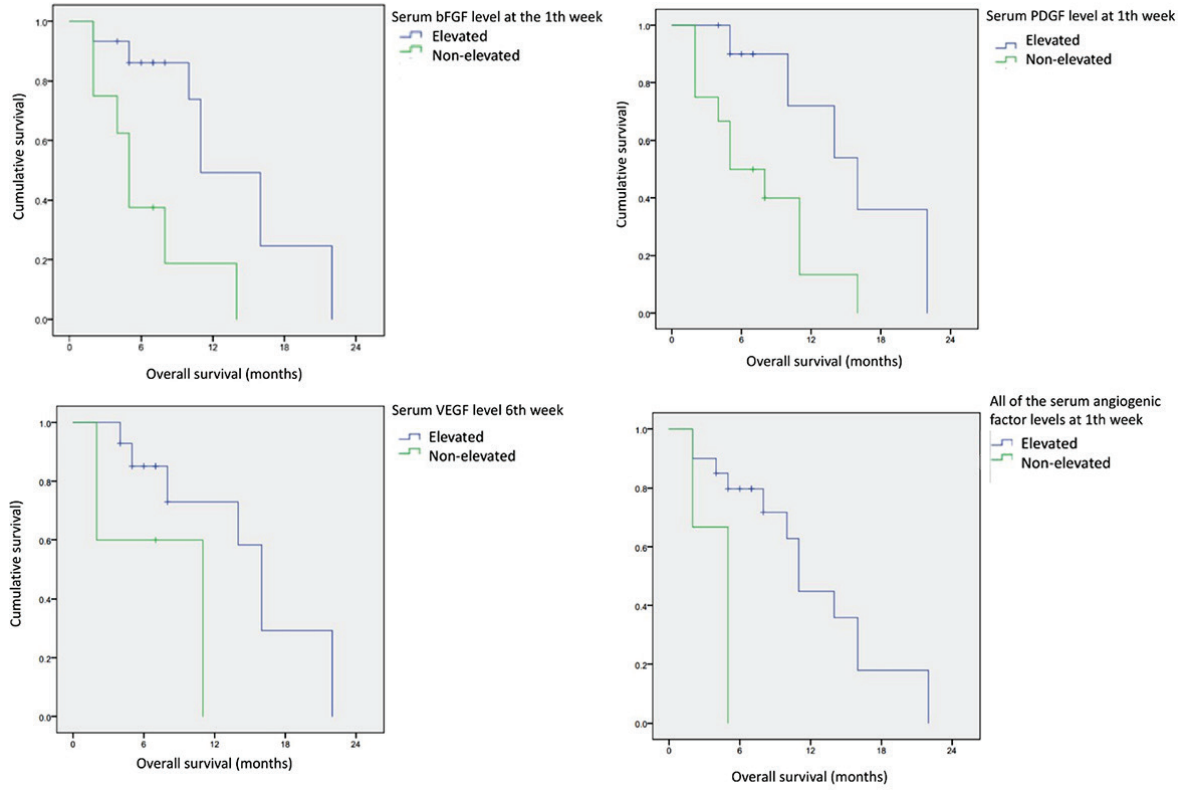

Figure 5. Kaplan-Meier survival curves of patient groups with significant overall survival differences according to elevated and non-elevated levels of different angiogenic factors at different time points. You have studied 5 angiogenic factors, but why only 2 parameters are included. why some week 1 and some week 6. It might be more descriptive if you elaborate more in the results section
bFGF: Basic fibroblast growth factor, VEGF: Vascular endothelial growth factor, PDGF: Platelet-derived growth factor

pilot study, we analyzed the angiogenic response after TARE in CRCLM patients.

First, we evaluated the change in circulating angiogenic factor levels after TARE. An increase in most of the angiogenic factor levels was observed on the 1st day or in the 1st week after TARE. Moreover, in 91% of patients, at least one angiogenic factor level was increased on the 1st day and in the 1st week after treatment. Additionally, serum levels of circulating VEGF and PDGF for different time points were significantly different among patients who responded and did not respond to treatment. Similarly, Rosenbaum et al. (13) found a significant increase in serum VEGF, HGF and Ang-2 levels after TARE in 42 CRCLM patients. Carpizo et al. (9) also reported an increase >50% over the baseline in serum angiogenic factor levels in patients who received TARE for HCC and CRCLMs. Consideration of the results of these three studies reveals that an angiogenic response after TARE is observed in at least one group of patients, and it seems to be related to treatment response. Antiangiogenic treatment combinations might be a valuable option for these patients. Antiangiogenic treatment may help prevent early progression by increasing oxygenation of the tumor via the normalization of the blood supply. In three large prospective trials, TARE was combined with antiangiogenic treatments in subgroups of patients (20,21). However, subgroup analysis of patients who received or did not receive bevacizumab has not yet been reported. Moreover, when considering the elevation of different angiogenic factor levels, multitarget agents might be more beneficial than bevacizumab.

Similar to our study, Carpizo et al. (9) evaluated the prognostic importance of circulating angiogenic factors in CRCLM patients and found that baseline cytokine levels in patients with OS <6 months differed significantly from those with longer survival. In our analysis, we did not find any difference between baseline angiogenic factor levels of patients with longer and shorter (<6 months) OS. In contrast to a previous report, we performed Kaplan-Meier analysis of patient groups based on the elevation of angiogenic factor levels after TARE. We observed that the elevation of serum bFGF and PDGF levels in the 1st week and in serum VEGF levels in the 6th week of treatment has a prognostic value in the prediction of OS after TARE. Moreover, we performed PFS analysis and found that the elevation of serum bFGF levels in the 1st week seemed to predict PFS after TARE.

Lastly, we analyzed the difference in baseline circulating angiogenic factor levels of patients with and without extrahepatic disease. Although the finding was not statistically significant, some of the baseline levels of circulating angiogenic factors were higher in patients with extrahepatic disease; this difference in baseline VEGF and bFGF levels was nearly significant. A small number of patients included in our analysis might account for the low significance; therefore, a larger patient population may improve the significance of these differences.

Study Limitations

A major limitation of our study was the relatively small number of patients included. Some calculated values that did not reach the significance level may have been proven to be significant if applied to data for a larger study population. Additionally, if the frequency of blood samples collected was higher, the trend of the angiogenic response depending on time might be demonstrated more precisely. We cannot reach the details of the previously given TACE procedures. compared with the TARE, TACE has significant hypoxic effects, especially if larger particles are used; furthermore, some professionals attempt to achieve complete arterial blockage for success. Therefore, previous procedures might have affected the baseline levels of angiogenic factor levels. Last, additional different angiogenic factors should be examined to allow for documentation of a wide profile of angiogenic factor changes following TARE.

Despite its limitations; differently from previous analyses, our study demonstrated a relationship between elevation of different serum angiogenic factor levels and overall and progression free survival times after TARE in patients with CRCLMs. Based on the results of our analysis, which contributes to the limited data in the literature, various circulating angiogenic factors seem to have prognostic importance for patients who receive TARE for CRCLMs. An early elevation of circulating angiogenic factor levels was found in most of the patients after treatment. Some of these elevations seem to be related to treatment response, OS and PFS. Future larger prospective studies would help clarify the relationship between angiogenic response and prognosis of patients with CRCLMs. Combined treatment with antiangiogenic agents and TARE might be a suitable option to improve patient outcomes in the future.

Conclusion

Some early increases in serum PDGF, bFGF and Ang-2 levels and increases in serum VEGF in the 6th week after TARE are related to a poor treatment response and short overall and progression-free survival times for patients with CRCLMs. If outcomes of our analyses would be supported with

further studies, combined treatment options would be standardized to improve survival of patients with CRCLMs.

Ethics

Ethics Committee Approval: This prospective study was approved by the Ankara University Faculty of Medicine, Local Institutional Ethical Committee (decision number: 01-14-16).

Informed Consent: Written informed consent was obtained from all participants.

Peer-review: Externally peer-reviewed.

Authorship Contributions

Surgical and Medical Practices: İ.E.G., S.B., N.Ö.K., E.Ö., Concept: İ.E.G., Ç.S., N.Ö.K., S.B., Design: Ç.S., Data Collection or Processing: M.D., B.İ.E., Analysis or Interpretation: Ç.S., A.H.E., Literature Search: Ç.S., Writing: Ç.S., M.A.

Conflict of Interest: No conflict of interest was declared by the authors.

Financial Disclosure: The author declared that this study has received no financial support.

REFERENCES

1. Ferlay J, Soerjomataram I, Dikshit R, Eser S, Mathers C, Rebelo M, Parkin DM, Forman D, Bray F. Cancer incidence and mortality worldwide: sources, methods and major patterns in GLOBOCAN 2012. Int J Cancer 2015;136:E359-E386.
2. Silberhumer GR, Paty PB, Temple LK, Araujo RL, Denton B, Gonen M, Nash GM, Allen PJ, DeMatteo RP, Guillem J, Weiser MR, D'Angelica MI, Jarnagin WR, Wong DW, Fong Y. Simultaneous resection for rectal cancer with synchronous liver metastasis is a safe procedure. Am J Surg 2015;209:935-942.
3. Van Cutsem E, Cervantes A, Adam R, Sobrero A, Van Krieken JH, Aderka D, Aranda Aguilar E, Bardelli A, Benson A, Bodoky G, Ciardiello F, D'Hoore A, Diaz-Rubio E, Douillard JY, Ducreux M, Falcone A, Grothey A, Gruenberger T, Haustermans K, Heinemann V, Hoff P, Köhne CH, Labianca R, Laurent-Puig P, Ma B, Maughan T, Muro K, Normanno N, Österlund P, Oyen WJ, Papamichael D, Pentheroudakis G, Pfeiffer P, Price TJ, Punt C, Ricke J, Roth A, Salazar R, Scheithauer W, Schmoll HJ, Tabernero J, Taïeb J, Tejpar S, Wasan H, Yoshino T, Zaanan A, Arnold D. ESMO consensus guidelines for the management of patients with metastatic colorectal cancer. Ann Oncol 2016;27:1386-1422.
4. Tsitskari M, Filippiadis D, Kostantos C, Palialexis K, Zavridis P, Kelekis N, Brountzos E. The role of interventional oncology in the treatment of colorectal cancer liver metastases. Ann Gastroenterol 2019;32:147-155.
5. Boas FE, Bodei L, Sofocleous CT. Radioembolization of colorectal liver metastases: indications, technique, and outcomes. J Nucl Med 2017;58(Suppl 2):104S-111S.
6. Gray B, Van Hazel G, Hope M, Burton M, Moroz P, Anderson J, Gebski V. Randomised trial of SIR-Spheres plus chemotherapy vs. chemotherapy alone for treating patients with liver metastases from primary large bowel cancer. Ann Oncol 2001;12:1711-1720.
7. Hendlisz A, Van den Eynde M, Peeters M, Maleux G, Lambert B, Vannoote J, De Keukeleire K, Verslype C, Defreyne L, Van Cutsem E, Delatte P, Delaunoit T, Personeni N, Paesmans M, Van Laethem JL, Flamen P. Phase III trial comparing protracted intravenous fluorouracil infusion alone or with Yttrium-90 resin microspheres radioembolization for liver-limited metastatic colorectal cancer refractory to standard chemotherapy. J Clin Oncol 2010;28:3687-3694.
8. Van Hazel G, Blackwell A, Anderson J, Price D, Moroz P, Bower G, Cardaci G, Gray B. Randomised phase 2 trial of SIR-Spheres plus fluorouracil/leucovorin chemotherapy versus fluorouracil/leucovorin chemotherapy alone in advanced colorectal cancer. J Surg Oncol 2004;88:78-85.
9. Carpizo DR, Gensure RH, Yu X, Gendel VM, Greene SJ, Moore DF, Jabbour SK, Nosher JL. Pilot study of angiogenic response to yttrium-90 radioembolization with resin microspheres. J Vasc Interv Radiol 2014;25:297-306.e1.
10. Gorski DH, Beckett MA, Jaskowiak NT, Calvin DP, Mauceri HJ, Salloum RM, Seetharam S, Koons A, Hari DM, Kufe DW, Weichselbaum RR. Blockage of the vascular endothelial growth factor stress response increases the antitumor effects of ionizing radiation. Cancer Res 1999;59:3374-3378.
11. Korse CM, Bonfrer JM, Prevoo W, Baas P, Taal BG. Increase of angiogenic growth factors after hepatic artery embolization in patients with neuroendocrine tumours. Tumour Biol 2011;32:647-652.
12. Lewandowski RJ, Andreoli JM, Hickey R, Kallini JR, Gabr A, Baker T, Kircher S, Salem R, Kulik L. Angiogenic response following radioembolization: results from a randomized pilot study of Yttrium-90 with or without sorafenib. J Vasc Interv Radiol 2016;27:1329-1336.
13. Rosenbaum CE, van den Hoven AF, Braat MN, Koopman M, Lam MG, Zonnenberg BA, Verkooijen HM, van den Bosch MA. Yttrium-90 radioembolization for colorectal cancer liver metastases: a prospective cohort study on circulating angiogenic factors and treatment response. EJNMMI Res 2016;6:92.
14. Alsultan AA, Barentsz MW, Smits MLJ, Koopman M, Lam MGEH, Rosenbaum CENM. Angiogenesis in 90Y-radioembolization of colorectal liver metastases. Semin Nucl Med 2019;49:204-210.
15. Sergio A, Cristofori C, Cardin R, Pivetta G, Ragazzi R, Baldan A, Girardi L, Cillo U, Burra P, Giacomin A, Farinati F. Transcatheter arterial chemoembolization (TACE) in hepatocellular carcinoma (HCC): the role of angiogenesis and invasiveness. Am J Gastroenterol 2008;103:914-921.
16. Shim JH, Park JW, Kim JH, An M, Kong SY, Nam BH, Choi JI, Kim HB, Lee WJ, Kim CM. Association between increment of serum VEGF level and prognosis after transcatheter arterial chemoembolization in hepatocellular carcinoma patients. Cancer Sci 2008;99:2037-2044.
17. Li X, Feng GS, Zheng CS, Zhuo CK, Liu X. Expression of plasma vascular endothelial growth factor in patients with hepatocellular carcinoma and effect of transcatheter arterial chemoembolization therapy on plasma vascular endothelial growth factor level. World J Gastroenterol 2004;10:2878-2882.
18. Suzuki H, Mori M, Kawaguchi C, Adachi M, Miura S, Ishii H. Serum vascular endothelial growth factor in the course of transcatheter arterial embolization of hepatocellular carcinoma. Int J Oncol 1999;14:1087-1090.
19. Rahbari NN, Reissfelder C, Mühlbayer M, Weidmann K, Kahlert C, Büchler MW, Weitz J, Koch M. Correlation of circulating angiogenic factors with circulating tumor cells and disease recurrence in patients undergoing curative resection for colorectal liver metastases. Ann Surg Oncol 2011;18:2182-2191.
20. van Hazel GA, Heinemann V, Sharma NK, Findlay MP, Ricke J, Peeters M, Perez D, Robinson BA, Strickland AH, Ferguson T, Rodríguez J, Kröning H, Wolf I, Ganju V, Walpole E, Boucher E, Tichler T, Shacham-Shmueli E, Powell A, Eliadis P, Isaacs R, Price D, Moeslein F, Taieb J, Bower G, Gebski V, Van Buskirk M, Cade DN, Thurston K, Gibbs P. SIRFLOX: Randomized phase III trial comparing first-line mFOLFOX6 (plus or minus bevacizumab) versus mFOLFOX6 (plus or minus bevacizumab) plus

selective internal radiation therapy in patients with metastatic colorectal cancer. J Clin Oncol 2016;34:1723-1731.

21. Wasan HS, Gibbs P, Sharma NK, Taieb J, Heinemann V, Ricke J, Peeters M, Findlay M, Weaver A, Mills J, Wilson C, Adams R, Francis A, Moschandreas J, Virdee PS, Dutton P, Love S, Gebski V, Gray A; FOXFIRE trial investigators; SIRFLOX trial investigators; FOXFIRE-Global trial investigators, van Hazel G, Sharma RA. First-line selective internal radiotherapy plus chemotherapy versus chemotherapy alone in patients with liver metastases from colorectal cancer (FOXFIRE, SIRFLOX, and FOXFIRE-Global): a combined analysis of three multicentre, randomised, phase 3 trials. Lancet Oncol 2017;18:1159-1171.

Original Article
Mol Imaging Radionucl Ther 2022;31:123-129 DOI:10.4274/mirt.galenos.2022.44154

The Value of ^{18}F-FDG PET/CT Imaging in the Evaluation of Interim Neoadjuvant Chemotherapy Response in Locally Advanced Breast Cancer

Lokal İleri Meme Kanserinde Neoadjuvan İnterim Kemoterapi Yanıtının Değerlendirilmesinde ^{18}F-FDG PET/BT Görüntülemenin Değeri

Gamze Tatar[1], Özlem Özkul[2], Göksel Alçın[3]

[1]*University of Health Sciences Turkey, İstanbul Bağcılar Training and Research Hospital, Clinic of Nuclear Medicine, İstanbul, Turkey*
[2]*University of Health Sciences Turkey, İstanbul Bağcılar Training and Research Hospital, Division of Medical Oncology, İstanbul, Turkey*
[3]*University of Health Sciences Turkey, İstanbul Training and Research Hospital, Clinic of Nuclear Medicine, İstanbul, Turkey*

Abstract

Objectives: Neoadjuvant chemotherapy (NAC) is the frequently used treatment option for locally advanced breast cancer (LABC). This study investigated the potential value of ^{18}fluorine-fluorodeoxyglucose (^{18}F-FDG) positron emission tomography/computed tomography (PET/CT) to estimate the pathological complete response (pCR) using maximum standardized uptake value (SUV_{max}) and change (ΔSUV_{max}) after 3-4 cycles of NAC. Additionally, it was established the relationship between PET/CT imaging findings and histopathological features in LABC patients whose treatment response was evaluated with interim PET/CT.

Methods: Patients were evaluated with pretreatment and interim PET/CT scans and operated after on NAC. Data on the age of patients, menopausal status, tumor placement, histopathological and molecular subgroups were noted. SUV_{max} and ΔSUV_{max} of the primary tumor and axillary lymph node (ALN) were calculated from PET/CT review.

Results: Pretherapy mean SUV_{max} of the primary tumor and ALNs were 8.13±4.25 and 7.22±3.58, respectively. The highest mean primary tumor ΔSUV_{max} and ALN ΔSUV_{max} values were observed to be human epidermal growth factor receptor 2 positivity ($p<0.001$). SUV_{max}-T, SUV_{max}-N, ΔSUV_{max}-T, and ΔSUV_{max}-N values were significantly correlated with the ki-67 index ($p<0.001$). ΔSUV_{max}-T and ΔSUV_{max}-N values of pCR (+) patients were statistically higher than the ΔSUV_{max}-T and ΔSUV_{max}-N values of pCR (-) patients ($p<0.001$).

Conclusion: An earlier and more accurate response to NAC can be performed using interim ^{18}F-FDG PET/CT imaging. ΔSUV_{max} levels of the breast tumor and ALNs may act as predictive for pCR in LABC patients receiving NAC.

Keywords: Neoadjuvant chemotherapy, ^{18}F-fluorodeoxyglucose, positron emission tomography, breast cancer

Öz

Amaç: Neoadjuvan kemoterapi (NAK) lokal ileri meme kanseri (LİMK) tedavisinde sıklıkla başvurulan tedavi seçeneğidir. Bu çalışmada, LİMK tanısı ile NAK alan hastalarda bazal ^{18}flor-florodeoksiglukoz (^{18}F-FDG) pozitron emisyon tomografisi/bilgisayarlı tomografi (PET/BT), maksimum

Address for Correspondence: Gamze Tatar MD, University of Health Sciences Turkey, İstanbul Bağcılar Training and Research Hospital, Clinic of Nuclear Medicine, İstanbul, Turkey
Phone: + 90 212 440 40 00 **E-mail:** gamze_tatar@hotmail.com ORCID ID: orcid.org/0000-0002-4187-755X
Received: 31.01.2022 **Accepted:** 20.03.2022

standart alım değerinin (SUV_{maks}) ve 3-4 kür NAK sonrası SUV_{maks} değişiminin (ΔSUV_{maks}) patolojik tam yanıtı (pTY) öngörmedeki potansiyel değerini belirlemek, ikincil olarak PET/BT ile ara tedavi yanıtı değerlendirilen LİMK hastalarında görüntüleme bulgularıyla histopatolojik özellikler arasındaki ilişkiyi değerlendirmek amaçlandı.

Yöntem: Hastalar tedavi öncesi ve interim tedavi sonrası ^{18}F-FDG PET/BT görüntüleme ile değerlendirildi ve NAK sonrası opere edildi. Hastaların yaşı, menopoz durumu, tümör lokalizasyonu, histopatolojik ve moleküler alt tipi ile ilgili veriler kaydedildi. PET/BT görüntülerinden primer tümör ve aksiller lenf nodları (ALN) için SUV_{maks} ve ΔSUV_{maks} hesaplandı.

Bulgular: Primer tümör ve ALN'nin tedavi öncesi ortalama SUV_{maks} değerleri sırasıyla; 8,13±4,25 ve 7,22±3,58 idi. En yüksek ortalama primer tümör ΔSUV_{maks} ve ALN ΔSUV_{maks} değerlerinin insan epidermal büyüme faktör reseptörü 2 pozitifliğinde olduğu gözlendi (p<0,001). Ki-67 ile SUV_{maks}-T, SUV_{maks}-N, ΔSUV_{maks}-T ve ΔSUV_{maks}-N değerleri arasında korelasyon görüldü (p<0,001). PCR (+) hastalarında ΔSUV_{maks}-T ve ΔSUV_{maks}-N değerleri, pCR (-) hastalardan istatistiksel olarak daha yüksekti (p<0,001).

Sonuç: İnterim ^{18}F-FDG PET/BT görüntüleme ile daha erken ve daha doğru NAK yanıtı değerlendirilebilir. Primer tümör ve ALN ΔSUV_{maks} değerleri, NAK uygulanan LİMK hastalarında pTY için prediktör görev üstlenebilir.

Anahtar kelimeler: Neoadjuvan kemoterapi, ^{18}F-florodeoksiglukoz, pozitron emisyon tomografisi, meme kanseri

Introduction

Breast cancer (BC) ranks first among women's cancers in the world (1). Locally advanced breast cancer (LABC) is found in approximately one-third of patients at the time of diagnosis (2). The accepted multidisciplinary treatment approach in LABC includes preoperative neoadjuvant chemotherapy (NAC), followed by surgery and adjuvant systemic and local treatment steps (3). NAC is currently the first-line therapy for LABC and is increasingly preferred in early-stage patients. The advantages of NAC include enabling breast-conserving surgery (BCS) by shrinking the breast lesion, eliminating micrometastasis, evaluating drug resistance, and estimating the prognosis.

Positron emission tomography (PET) integrated with computed tomography (CT), is a hybrid modality that provides the three-dimensional distribution and quantitative volume of positron-emitting radionuclides in the human body, which has been widely used in the field of oncology in recent years (4). ^{18}Fluorine-fluorodeoxyglucose (^{18}F-FDG) is the most preferred radiopharmaceutical in oncological PET studies to demonstrate its increased glycolytic activity in cancer cells (5). Evaluation of treatment response and determination of chemosensitivity in the NAC patient group in the early period is important in terms of changing the treatment regimen, discontinuing unnecessary treatments and preventing possible drug toxicity and side effects.

^{18}F-FDG PET/CT is a useful method for NAC response by evaluating decreased glucose metabolism in BC tissue. With the antitumor effect of chemotherapy, cellular glycolysis decreases before the appearance of shrinkage in the tumor (6). In this study, we aimed to evaluate the potential contribution of ^{18}F-FDG PET/CT in predicting the pathological complete response (pCR) using maximum standardized uptake value (SUV_{max}) and change (ΔSUV_{max}) after 3-4 cycles of NAC in patients with LABC. Second, it was determined the relationship between PET/CT imaging findings and histopathological features in LABC patients whose treatment response was evaluated with interim PET/CT.

Materials and Methods

Patients

A total of 48 female patients [aged 29-68 years; mean ± standard deviation (SD): 49.4±9.5] diagnosed with LABC were evaluated retrospectively between October 2020 and September 2021 with ^{18}F-FDG PET/CT imaging performed before and after interim NAC.

Each study participant signed the informed consent forms. The University of Health Sciences Turkey, Istanbul Training and Research Hospital, Clinical Research Ethics Committee approved (number: 2916, date: 10.09.2021) the study and Helsinki Declaration rules were followed to conduct this study.

^{18}F-FDG PET/CT Imaging Protocol

Since the serum glucose level was below 150 mg/dL, ^{18}F-FDG was injected intravenously at a dose of 3.7 MBq/kg. PET/CT imaging was obtained using a Discovery St PET/CT (General Electric, Milwaukee, WI, USA) scanner with routine imaging protocol. With the patient's arms up, firstly CT scan was acquired with 2 mm section thickness in the craniocaudal direction between the vertex-upper thighs, and then a PET scan was received in 7-9 bed positions at the same interval, in the caudocranial direction.

Image Analysis

A semi-quantitative analysis method was used to evaluate PET/CT images by measuring the SUV_{max} for the primary breast tumor and axillary lymph nodes (ALNs) with increased ^{18}F-FDG uptake on visual examination. Pre-treatment tumor SUV_{max} (SUV_{max}-T) and ALN SUV_{max} (SUV_{max}-N) values were calculated using the software with

"region of interest" drawn on the most metabolically active areas on attenuation-corrected PET/CT images. SUV_{max}-T and SUV_{max}-N values were measured from the region of the first lesions in the interim scan. Also, ΔSUV_{max} (%) was calculated using the baseline and interim SUV_{max} values according to the formula: (interim SUV_{max}-baseline SUV_{max}) / (baseline SUV_{max}) x100.

Pathological Evaluation and Treatment Protocol

Patients were graded according to the modified Scarff-Bloom-Richardson classification. In immunohistochemical analysis, estrogen receptor (ER) and progesterone receptor (PR) status were scored and accepted as positive if high (10%). Furthermore, human epidermal growth factor receptor type-2 (HER2) was classified with scores of 0, 1+, 2+ intense, and 3+ based on the maximum staining intensity and stain distribution. 3+ score is accepted as HER2 positive. When the score was 2+, gene amplification of the fluorescent *in situ* hybridization method was used to determine HER2 positivity. Patients were classified into luminal A, luminal B, triple-negative, and HER2-positive molecular subtypes. The high ki-67 index represents the ≥15 values.

All patients included in the study received adriamycin 60 mg/m^2 and cyclophosphamide 600 mg/m^2 every 21 days for 3-4 cycles as a NAC protocol. After the interim evaluation PET/CT, NAC was continued with paclitaxel 80 mg/m^2 every 7 days for 12 weeks. In addition, trastuzumab (4 mg/kg as a loading dose, followed by 2 mg/kg) and pertuzumab (840 mg as a loading dose, followed by 420 mg) were given intravenously to HER2-positive patients. All patients underwent surgery after NAC.

The pCR was determined for the primary tumor and ALNs from surgical materials based on the Miller-Payne system (6). The Miller-Payne system has 5 grades and grade 5 indicates the pCR in the tumor means no invasive carcinoma but ductal carcinoma *in situ* may be present, and grades 1-4 define the pathological response rates relative to the tumor reduction ratio. We classified patients' pathological responses into two groups as pCR (+) vs pCR (-). For this study, Miller-Payne grade 5 responders were grouped as pCR (+), and partial responders or non-responders as pCR (-).

Statistical Analysis

Statistical analysis was performed by Macintosh Statistical Software (v27.0, IBM, Armonk, NY, USA) in this study. All descriptive data were expressed as mean, median, and SD. Mann-Whitney U and Kruskal-Wallis tests were used for variables with non-normal distribution. Comparison of numerical variables between groups was performed Student's t-test. The relationship between ki-67 and SUV parameters was assessed by Pearson correlation analysis. p less than 0.05 was considered significant.

Results

Histopathology was invasive ductal carcinoma in 45 (93.75%) cases and invasive lobular carcinoma (ILC) in three (6.25%) cases. The tumor was in the right-sided breast in 26 (54.1%) patients and the left-sided breast in 22 (45.9%) patients. Of 48 patients, 14 (29.2%) were ER negative, 34 (70.8%) were ER positive, 17 (35.4%) were PR negative, 31 (64.6%) were PR positive. Nine (18.8%) of the patients were in luminal A, 25 (52%) were in luminal B, 8 (16.7%) were in the HER2 positive, and 6 (12.5%) were in the triple-negative molecular subgroup. ALN metastasis was negative in four (8.3%) patients at diagnosis. Sixteen patients (33.3%) were in clinical stage 2 and 33 (66.7%) were in stage 3 before treatment. The study patients and tumor characteristics are summarized in Table 1.

The mean diameter of the primary tumor was 4.75±3.04 cm, the mean ALN size was 2.2±1.3 cm, and the ki-67 index was 42.77%±26.46%. Mean SUV_{max} levels of baseline breast tumor and ALN metastases were calculated as 8.13±4.25 and 7.22±3.58, respectively. Tumor and ALN SUV_{max} and ΔSUV_{max} levels of the three patients with

Table 1. Patients and characteristics of breast cancer

Variables	Number (n)	Percentage (%)
Menopause status		
Premenopausal	31	64.6
Postmenopausal	17	35.4
Histopathology		
IDC	45	93.75
ILC	3	6.25
Axillary lymph node metastasis		
Positive	44	91.6
Negative	4	8.4
Histological grade		
Grade 1	2	4.2
Grade 2	25	52
Grade 3	21	43.8
Surgical treatment		
BCS + SLNB	10	20.8
BCS + axillary dissection	8	16.7
MRM + SLNB	6	12.5
MRM + axillary dissection	24	50

IDC: Invasive ductal carcinoma, ILC: Invasive lobular carcinoma, BRC: Breast-conserving surgery, SLNB: Sentinel lymph node biopsy, MRM: Modified radical mastectomy

the initial diagnosis of ILC were 4.1±0.87 and 4.2±0.5, -42.40±21.27 and -41.51±18.05, respectively. The number of patients with pCR (+) for the primary tumor and ALN was 18 (37.5%) and 21 (47.7%), respectively. Total (breast & axilla) pCR (+) was obtained in 17 (35.4%) patients (Figure 1).

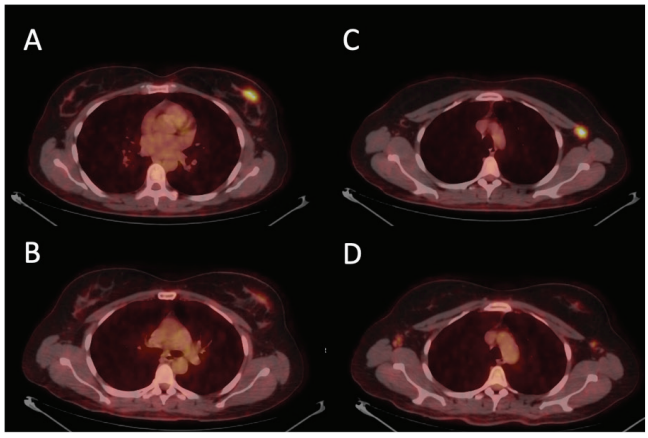

Figure 1. Thirty two-year-old woman with luminal B type invasive ductal left-sided breast cancer and axillary metastases achieved pCR at the end of NAC. Primary tumor SUV_{max} was 5.4 in baseline ^{18}F-FDG PET/CT (A). SUV_{max} was measured as 3.4 in interim evaluation PET/CT (B). Before and after interim treatment values of SUV_{max}-N were measured as 6.1 (C) and 2.9 (D), respectively

^{18}F-FDG: ^{18}Fluorine-fluorodeoxyglucose, NAC: Neoadjuvant chemotherapy, SUV_{max}: Maximum-standardized uptake value, PET/CT: Positron emission tomography/computed tomography, pCR: Pathological complete response

Relationship Between Histopathologicalc Features, pCR, and ^{18}F-FDG PET Analysis

The mean baseline SUV_{max}-T was statistically lower in the luminal A than in the triple-negative, HER2 positive, and luminal B groups (p=0.046, p<0.001, p=0.008), respectively. The mean baseline SUV_{max}-T was statistically higher in HER2 positives than in the luminal B group (p=0.017). The highest mean ΔSUV_{max}-T and ΔSUV_{max}-N were seen in HER2 positivity (p<0.01), but there was no significant difference in SUV_{max}-T levels of the positive and triple-negative groups (p=0.297). Additionally, SUV_{max}-T, SUV_{max}-N, ΔSUV_{max}-T, and ΔSUV_{max}-N levels had a highly significant correlation with the ki-67 index (Table 2).

Significant differences were seen between the SUV_{max} levels of pCR (+) and pCR (-) patients. ΔSUV_{max}-T was significantly higher in the pCR (+) group for the primary tumor than in the pCR (-) group (p<0.001). For ALNs, interim SUV_{max}-N was lower in the pCR (+) group than in the pCR (-) group (p=0.016). In the evaluation of all groups, SUV_{max}-N levels of pCR (+) patients were statistically higher than the SUV_{max}-N values of pCR (-) patients (p<0.001). The relationship between PET/CT parameters and pCR is shown in Table 3.

Discussion

PET/CT imaging in oncology practice, to clinical and pathological factors, has the importance of being a non-invasive method that provides timely determination of the response to therapy. PET/CT has an advantage over anatomical screening tools in demonstrating the metabolic nature of cancer by calculating the metabolic PET parameters before and in the interim period of NAC (7). Studies have documented that ^{18}F-FDG PET/CT images obtained interim, or at the end of NAC can estimate the response to therapy (8,9).

The value of radionuclide activity in breast lesions is related to tumor heterogeneity and molecular subgroups. Higher tracer accumulation has been found in negative ER status or triple-negative cases compared with positive ER status (10). In our study, it was shown that baseline SUV_{max} was higher in HER2 positive and triple-negative cases compared to luminal groups, which supports the published research (Figure 2). Also, studies showing a significant relation between SUV_{max} and the ki-67 levels or lymphatic and vascular invasion are available in the literature (11,12,13). Like studies on this subject, a statistically significant correlation was found between the ki-67 index and baseline SUV_{max}-T, SUV_{max}-N, ΔSUV_{max}-T, and ΔSUV_{max}-N.

Significant differences were observed in SUV_{max} values of specific molecular subgroups. The highest ΔSUV_{max}-T was seen in the HER2 positive and luminal B groups, and the highest ΔSUV_{max}-N in the HER2-positive and triple-negative groups in the study (Figure 3). In research, the mean breast ΔSUV_{max} level was found to be -73%±32% in HER2 positivity with more intense uptake values for the total breast & axilla, and -52%±33% in HER2 negativity (14). Similarly, the highest ΔSUV_{max}-T and ΔSUV_{max}-N levels were found in HER2-positive patients in our study.

The metabolic response of the primary malignancy to therapy is considered as a measure for assessing NAC response. Pathological CR is defined as the negativity of invasive cancer in the breast and axilla, which is seen in 10-40% of patients (15). In this study, pCR (+) was obtained in 35.4% of the patients and the most significant parameters for the pCR (+) were determined by ΔSUV_{max}-T and ΔSUV_{max}-N. Can et al. (16) investigated the prognostic role of PET/CT in the evaluation of newly diagnosed BC patients with ALN metastases, and reported pCR rates after neoadjuvant therapy as 37.2%, 42.2%, and 28.9% for breast, axilla, and breast & axilla, respectively. In a study evaluating the response to NAC with PET/CT in 32

Table 2. Histopathological analysis and ^{18}F-FDG PET/CT parameters

Molecular subgroup	**n**	**%**	**SUV_{max}-T**	**ΔSUV_{max}-T**	**SUV_{max}-N**	**ΔSUV_{max}-N**
Luminal A	9	18.7	3.5±0.7	-20.7±23.9	3.4±1.3	-21.7±8.0
Luminal B	25	52.0	7.8±3.3	-47.0±17.8	6.7±2.6	-44.6±18.6
HER2 positive	8	16.7	14.1±3.2	-59.7±6.5	11.0±3.5	-51.9±11.8
Triple-negative/BL*	6	12.5	8.3±2.6	-32.5±14.6	9.7±2.8	-45.3±10.3
p	**-**	**-**	**<0.001**	**<0.001**	**<0.001**	**0.003**
ER	-	-	-	-	-	-
Positive	34	70.8	7.3±4.3	-40.8±22.8	6.3±3.4	-38.0±19.2
Negative	14	29.2	9.9±3.4	-46.1±17.0	9.4±2.8	49.8±11.4
p	**-**	**-**	**0.052**	**0.008**	**0.005**	**0.013**
PR	-	-	-	-	-	-
Positive	31	64.6	7.6±4.2	-42.2±23.5	6.9±3.2	-42.6±19.0
Negative	17	35.4	8.9±4.2	-42.2±23.5	7.6±4.2	-39.3±16.5
p			0.339	**0.041**	0.547	0.549
Ki-67 index	-	-	-	-	-	-
High	9	18.8	3.5±0.7	-20.7±23.9	3.4±1.3	-21.7±8.0
Low	39	81.2	9.1±4.0	-47.3±17.4	8.1±3.3	-46.2±16.3
r	-	-	0.669	-0.509	0.602	-0.652
p	**-**		**<0.001**	**<0.001**	**<0.001**	**<0.001**

*Basal-like, ER: Estrogen receptor, PR: Progesterone receptor, T: Tumor, N: Axillary nodal metastasis, SUV_{max}: Maximum standardized uptake value; mean ± standard deviation values are given, ΔSUV_{max}: Change maximum standardized uptake value, ^{18}F-FDG: ^{18}Fluorine-fluorodeoxyglucose, PET/CT: Positron emission tomography/computed tomography, HER2: Human epidermal growth factor receptor type-2

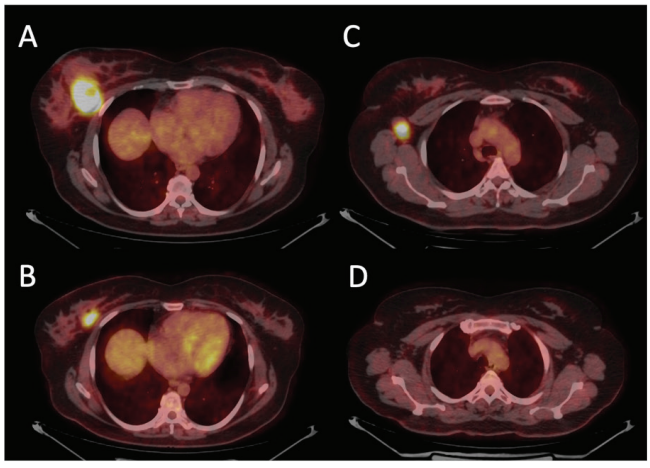

Figure 2. Fifty four-year-old patient with HER2 positive right-sided breast tumor and axillary metastases showed pCR in the axilla after NAC. Primary tumor SUV_{max} values were 11.0 and 4.9 in the fusion PET/CT images performed at baseline (A) and interim NAC (B). The partial metabolic response was detected in the primary tumor on interim treatment evaluation PET/CT. The baseline SUV_{max}-N value was 8.4 (C). The complete metabolic response was observed after NAC (D)

HER2: Human epidermal growth factor receptor type-2, pCR: Pathological complete response, NAC: Neoadjuvant chemotherapy, SUV_{max}: Maximum-standardized uptake value, PET/CT: Positron emission tomography/computed tomography

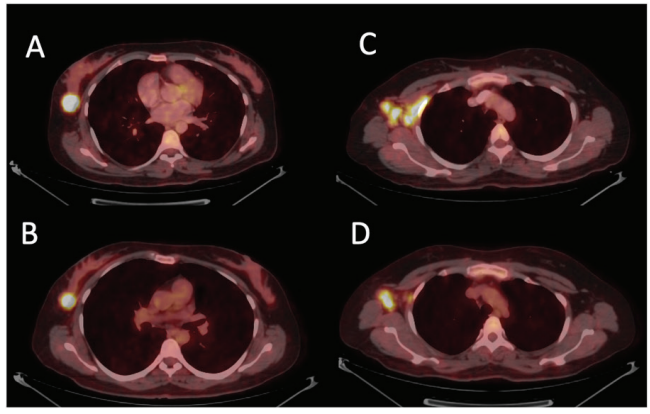

Figure 3. Forty one-year-old woman with triple-negative right-sided breast tumor and ALN metastases, whose pCR could not be obtained after NAC, had a primary tumor SUV_{max} value of 13.2 in the baseline PET/CT scan (A). SUV_{max} was measured as 11.8 in the interim evaluation (B). Under the partial metabolic response, the pre-treatment (C) and interim treatment (D) SUV_{max}-N were 12.3 and 8.5, respectively

ALN: Axillary lymph node, pCR: Pathological complete response, NAC: Neoadjuvant chemotherapy, SUV_{max}: Maximum-standardized uptake value, PET/CT: Positron emission tomography/computed tomography

BC patients, pCR was seen in 17 patients (43.8%) (17). Additionally, mean ΔSUV_{max} measured on PET/CT imaging after NAC was shown to be more prognostic in patients

Table 3. PET/CT parameters and pCR analysis			
	pCR (+)	pCR (-)	p
Baseline SUV_{max}-T	9.8±3.9	7.1±4.1	0.034
Interim SUV_{max}-T	4.1±1.2	4.0±2.0	0.773
ΔSUV_{max}-T	-55.1±9.2	-34.75±22.8	<0.001
Baseline SUV_{max}-N	8.5±3.0	6.9±3.4	0.119
Interim SUV_{max}-N	3.3±0.7	4.5±1.9	0.016
ΔSUV_{max}-N	-57.4±7.3	-31.8±12.5	<0.001

pCR: Pathological complete response, T: Tumor, N: Axillary lymph node metastasis, SUV_{max}: Maximum-standardized uptake value (mean values ± standard deviation), ΔSUV_{max}: Change maximum standardized uptake value, PET/CT: Positron emission tomography/computed tomography

with pCR (+) (18). In another study of luminal group B cancers, the authors showed no difference between patients' pathological responses for baseline SUV_{max}, but a higher ΔSUV_{max}-T was reported for pCR (+) (19).

BC comprises various subtypes in terms of tumor nature, therapy options, and clinical outcomes. The heterogeneous feature is also seen in the metabolic behavior of the tumor. In a prospective study evaluating triple-negative patients, the median baseline SUV_{max}-T did not differ significantly among the patients with and without pCR, while ΔSUV_{max}-T was found to be more significant in the patients with pCR (+) (20). In our study, the mean ΔSUV_{max}-T was higher in patients with pCR (+) groups than in patients with non-pCR. In another study, in which the metabolic and pathological response evaluation was performed separately for the breast and axilla with triple-negative and HER2 group patients, ΔSUV_{max}-T was determined as the strongest estimator of pCR in the primary tumor and ΔSUV_{max}-N was the most predictive of the total pCR (21).

Accurately revealing the response to NAC also affects surgical planning. The evaluation of response with anatomical imaging, which traditionally uses size-based criteria, has limitations. Anatomical and metabolic evaluation with PET/CT overcomes many of these limitations and plays an indispensable place in the assessment of NAC response in BC. Additionally, response to NAC in ALNs may affect the decision for axillary dissection. Colfry et al. (22) emphasized that axillary dissection may be unnecessary in LABC with complete response after NAC in their study, and they recommended its application, especially in unresponsive patients. In our study, pCR (+) was not established in 62.5% (30/48) of breast tumors and 52.2% (23/44) of axillary metastases after the NAC strategy. Only 17 cases (35.4%) achieved pCR (+) in both primary breast tumors and ALN metastases. Low ^{18}F-FDG uptake was observed in primary breast tumor ± ALN metastases of patients who did not respond to treatment, and this situation was primarily evaluated about the histopathological type (ILC) of the tumor. Similarly, Schwarz-Dose et al. (23) found high response rates in HER2 positive patients at post-treatment examination and low pCR rates after NAC in tumors with low glucose metabolism.

Study Limitations

The heterogeneity and the limited number of the patient population, with its retrospective design, can be considered the limitations of our study, and this may have weakened some of the statistical analysis.

Conclusion

An earlier and more accurate response to NAC could be performed with interim ^{18}F-FDG PET/CT imaging. PET/CT may also detect unresponsive patients in the early period and allow changes in treatment plans. Additionally, ΔSUV_{max} levels of primary tumor and ALN can be used to predict pCR in LABC patients receiving NAC.

Ethics

Ethics Committee Approval: The University of Health Sciences Turkey, Istanbul Training and Research Hospital, Clinical Research Ethics Committee approved (number: 2916, date: 10.09.2021) the study and Helsinki Declaration rules were followed to conduct this study.

Informed Consent: Each study participant signed the informed consent forms.

Peer-review: Externally peer-reviewed.

Authorship Contributions

Surgical and Medical Practices: G.T., Ö.Ö., G.A., Concept: G.T., Ö.Ö., G.A., Design: G.T., Ö.Ö., G.A., Data Collection or Processing: G.T., Ö.Ö., G.A., Analysis or Interpretation: G.T., Ö.Ö., G.A., Literature Search: G.T., Ö.Ö., G.A., Writing: G.T., Ö.Ö., G.A.

Conflict of Interest: No conflict of interest was declared by the authors.

Financial Disclosure: The authors declared that this study has received no financial support.

References

1. Bray F, Ferlay J, Soerjomataram I, Siegel RL, Torre LA, Jemal A. Global cancer statistics 2018: GLOBOCAN estimates of incidence and mortality worldwide for 36 cancers in 185 countries. CA Cancer J Clin 2018;68:394-424.
2. Tryfonidis K, Senkus E, Cardoso MJ, Cardoso F. Management of locally advanced breast cancer-perspectives and future directions. Nat Rev Clin Oncol 2015;12:147-162.
3. Heil J, Kuerer HM, Pfob A, Rauch G, Sinn HP, Golatta M, Liefers GJ, Vrancken Peeters MJ. Eliminating the breast cancer surgery paradigm

after neoadjuvant systemic therapy: current evidence and future challenges. Ann Oncol 2020;31:61-71.

4. Becker J, Schwarzenböck SM, Krause BJ. FDG PET hybrid imaging. Recent Results Cancer Res 2020;216:625-667.
5. Hofman MS, Hicks RJ. How we read oncologic FDG PET/CT. Cancer Imaging 2016;16:35.
6. Ogston KN, Miller ID, Payne S, Hutcheon AW, Sarkar TK, Smith I, Schofield A, Heys SD. A new histological grading system to assess response of breast cancers to primary chemotherapy: prognostic significance and survival. Breast 2003;12:320-327.
7. Lei L, Wang X, Chen Z. PET/CT imaging for monitoring recurrence and evaluating response to treatment in breast cancer. Adv Clin Exp Med 2016;25:377-382.
8. Akdeniz N, Kömek H, Küçüköner M, Kaplan MA, Urakçi Z, Oruç Z, Işikdoğan A. The role of basal 18F-FDG PET/CT maximum standard uptake value and maximum standard uptake change in predicting pathological response in breast cancer patients receiving neoadjuvant chemotherapy. Nucl Med Commun 2021;42:315-324.
9. Tian F, Shen G, Deng Y, Diao W, Jia Z. The accuracy of 18F-FDG PET/CT in predicting the pathological response to neoadjuvant chemotherapy in patients with breast cancer: a meta-analysis and systematic review. Eur Radiol 2017;27:4786-4796.
10. Arslan E, Çermik TF, Trabulus FDC, Talu ECK, Başaran Ş. Role of 18F-FDG PET/CT in evaluating molecular subtypes and clinicopathological features of primary breast cancer. Nucl Med Commun 2018;39:680-690.
11. Qu YH, Long N, Ran C, Sun J. The correlation of 18F-FDG PET/CT metabolic parameters, clinicopathological factors, and prognosis in breast cancer. Clin Transl Oncol 2021;23:620-627.
12. Erol M, Önner H, Eren Karanis Mİ. Evaluation of the histopathological features of early-stage invasive ductal breast carcinoma by 18fluoride-fluorodeoxyglucose positron emission tomography/computed tomography. Mol Imaging Radionucl Ther 2021;30:129-136.
13. Surov A, Meyer HJ, Wienke A. Associations between PET parameters and expression of Ki-67 in breast cancer. Transl Oncol 2019;12:375-380.
14. Cheng J, Wang Y, Mo M, Bao X, Zhang Y, Liu G, Zhang J, Geng D. 18F-fluorodeoxyglucose (FDG) PET/CT after two cycles of neoadjuvant therapy may predict response in HER2-negative, but not in HER2-positive breast cancer. Oncotarget 2015;6:29388-29395.
15. von Minckwitz G, Untch M, Blohmer JU, Costa SD, Eidtmann H, Fasching PA, Gerber B, Eiermann W, Hilfrich J, Huober J, Jackisch C, Kaufmann M, Konecny GE, Denkert C, Nekljudova V, Mehta K, Loibl S. Definition and impact of pathologic complete response on prognosis after neoadjuvant chemotherapy in various intrinsic breast cancer subtypes. J Clin Oncol 2012;30:1796-1804.
16. Can C, Akdeniz N, Kömek H, Gündoğan C, Urakçı Z, Işıkdoğan A. The prognostic role of baseline 18F-FDG PET/CT SUVmax and SUVmax change in patients with node-positive breast cancer receiving neoadjuvant chemotherapy. Rev Esp Med Nucl Imagen Mol (Engl Ed) 2022;41:3-10.
17. Kitajima K, Miyoshi Y, Yamano T, Odawara S, Higuchi T, Yamakado K. Assessment of tumor response to neoadjuvant chemotherapy in patients with breast cancer using MRI and FDG-PET/CT-RECIST 1.1 vs. PERCIST 1.0. Nagoya J Med Sci 2018;80:183-197.
18. Akimoto E, Kadoya T, Kajitani K, Emi A, Shigematsu H, Ohara M, Masumoto N, Okada M. Role of 18F-PET/CT in predicting prognosis of patients with breast cancer after neoadjuvant chemotherapy. Clin Breast Cancer 2018;18:45-52.
19. Pahk K, Kim S, Choe JG. Early prediction of pathological complete response in luminal B type neoadjuvant chemotherapy-treated breast cancer patients: comparison between interim 18F-FDG PET/CT and MRI. Nucl Med Commun 2015;36:887-891.
20. Humbert O, Riedinger JM, Charon-Barra C, Berriolo-Riedinger A, Desmoulins I, Lorgis V, Kanoun S, Coutant C, Fumoleau P, Cochet A, Brunotte F. Identification of biomarkers including 18FDG-PET/CT for early prediction of response to neoadjuvant chemotherapy in triple-negative breast cancer. Clin Cancer Res 2015;21:5460-5468.
21. van Ramshorst MS, Teixeira SC, Koolen BB, Pengel KE, Gilhuijs KG, Wesseling J, Rodenhuis S, Valdés Olmos RA, Rutgers EJ, Vogel WV, Sonke GS, Vrancken Peeters MT. Additional value of 18F-FDG PET/CT response evaluation in axillary nodes during neoadjuvant therapy for triple-negative and HER2-positive breast cancer. Cancer Imaging 2017;17:15.
22. Colfry AJ 3rd, Zhang X, Fuhrman GM. Response to neoadjuvant chemotherapy in the breast predicts axillary nodal status. Am Surg 2012;78:693-697.
23. Schwarz-Dose J, Untch M, Tiling R, Sassen S, Mahner S, Kahlert S, Harbeck N, Lebeau A, Brenner W, Schwaiger M, Jaenicke F, Avril N. Monitoring primary systemic therapy of large and locally advanced breast cancer by using sequential positron emission tomography imaging with [18F]fluorodeoxyglucose. J Clin Oncol 2009;27:535-541.

Original Article
Mol Imaging Radionucl Ther 2022;31:130-138 DOI:10.4274/mirt.galenos.2021.27880

Comparison of the Diagnostic Performance of Myocardial Perfusion Scintigraphy with and Without Attenuation Correction

Atenüasyon Düzeltmeli ve Düzeltmesiz Miyokard Perfüzyon Sintigrafisinin Tanısal Performansının Karşılaştırılması

Sira Vachatimanont, Sasitorn Sirisalipoch, Maythinee Chantadisai

Chulalongkorn University and King Chulalongkorn Memorial Hospital, Department of Radiology, Division of Nuclear Medicine, Bangkok, Thailand

Abstract

Objectives: Myocardial perfusion scintigraphy (MPS) is an important diagnostic test for detecting of coronary artery stenosis (CAS); however, tissue attenuation can lead to a difference in accuracy. We evaluated the diagnostic accuracy of attenuation-corrected (AC) and non-attenuation-corrected (NC) MPS for the detection of CAS.

Methods: We retrospectively recruited patients who underwent invasive coronary angiography within 10 months after Tc-99m sestamibi MPS. The AC and NC perfusion images were analyzed separately, and each myocardial segment was scored based on relative uptake from 0 to 4. The summed stress score (SSS), summed rest score (SRS), and summed difference score (SDS) were calculated. The diagnostic performances were analyzed using the area under the curve (AUC) of the receiver operating characteristic curve.

Results: From 117 patients, significant coronary stenosis was present in 66 patients (56%). The SSS and SRS obtained from NC-images were higher than those from AC, supporting the presence of attenuation artifacts in NC images. The AUC of SSS and SDS were significantly higher than those of SRS in both AC- and NC-images, but no significant difference was found between the AUC of SSS, and those of SDS. The optimal cut-offs were >12 for AC-SSS, >15 for NC-SSS, >4 for AC-SDS and >3 for NC-SDS. There was no statistically significant difference in the sensitivity, specificity, positive predictive value, negative predictive value, and accuracy among AC-SSS, NC-SSS, AC-SDS, and NC-SDS.

Conclusion: NC-based Tc-99m-sestamibi MPS promised comparable accuracy to AC images by using different cut-off values for diagnosis.

Keywords: Coronary artery disease, myocardial perfusion imaging, single photon emission computed tomography, attenuation correction, diagnostic performance, accuracy

Öz

Amaç: Miyokardiyal perfüzyon sintigrafisi (MPS), koroner arter darlığının (CAS) saptanması için önemli bir tanı testidir; ancak doku atenüasyonu doğrulukta bir farklılığa yol açabilir. Atenüasyon düzeltmeli (AC) ve düzeltmesiz (NC) MPS'nin CAS tespiti için tanısal doğruluğunu değerlendirmeyi amaçladık.

Yöntem: Tc-99m-sestamibi MPS'den sonraki 10 ay içinde invaziv koroner anjiyografi yapılan hastaları geriye dönük olarak inceledik. AC ve NC perfüzyon görüntüleri ayrı ayrı analiz edildi ve her bir miyokardiyal segment, 0 ila 4 arasındaki rölatif tutuluma dayalı olarak puanlandı. Toplam stres skoru (SSS), toplam dinlenme skoru (SRS) ve toplam fark skoru (SDS) hesaplandı. Tanılama performansları, alıcı işlem karakteristiği eğrisinin eğri altındaki alanı (AUC) kullanılarak analiz edildi.

Bulgular: Yüz on yedi hastadan 66 hastada (%56) belirgin koroner darlık mevcuttu. NC görüntülerinden elde edilen SSS ve SRS, AC'den elde edilenlerden daha yüksekti ve NC görüntülerinde atenüasyon artefaktlarının varlığını destekledi. Hem AC hem de NC görüntülerinde SSS ve SDS'nin AUC'si SRS'ninkinden önemli ölçüde daha yüksekti, ancak SSS'nin AUC'si ile SDS'ninkiler arasında anlamlı bir fark bulunmadı. Optimum kesim değerler AC-SSS için >12, NC-SSS için >15, AC-SDS için >4 ve NC-SDS için >3 idi. AC-SSS, NC-SSS, AC-SDS ve NC-SDS arasında duyarlılık, özgüllük, pozitif öngörü değeri, negatif tahmini değer ve doğruluk açısından istatistiksel olarak anlamlı bir fark yoktu.

Sonuç: NC tabanlı Tc-99m-sestamibi MPS, tanı için farklı kesim değerleri kullanarak AC görüntülerle karşılaştırılabilir doğruluk vaat etti.

Anahtar kelimeler: Koroner arter hastalığı, miyokardiyal perfüzyon görüntüleme, tek foton emisyonlu bilgisayarlı tomografi, atenüasyon düzeltmesi, tanısal performans, doğruluk

Address for Correspondence: Maythinee Chantadisai MD, Division of Nuclear Medicine, Department of Radiology, Faculty of Medicine, Chulalongkorn University, King Chulalongkorn Memorial Hospital, The Thai Red Cross Society, Bangkok, Thailand **Phone:** +66 2 256 4000 **E-mail:** aueng_tw45@hotmail.com
ORCID ID: orcid.org/0000-0003-1691-3958 **Received:** 25.06.2021 **Accepted:** 10.11.2021

Introduction

Non-invasive cardiac tests are crucial steps for the diagnosis of coronary artery stenosis in patients with an intermediate pretest probability of coronary artery disease (CAD) to optimize the use of invasive coronary angiography (ICA) (1). One of the commonly used non-invasive tests is the stress/rest Tc-99m-sestamibi myocardial perfusion scintigraphy (MPS) which can be safely performed in patients with limited physical activities, or impaired renal function (2,3,4).

Several myocardial perfusion scanning techniques and image processing protocols have been used to enhance the diagnostic performance of MPS. Attenuation correction, commonly performed using computed tomography (CT), promises to reduce attenuation artifacts caused by radiation absorption of the overlying tissue and thus significantly improve the specificity of the test (5). Semiquantitative interpretation has been proposed to reduce inter-observer variability and to standardize the method of interpretation. Seventeen-segment model of left ventricular myocardium is generally suggested owing to good representation of myocardial volume and vascular territories (6). A five-point scale for scoring of each segment based on perceived abnormality compared to either normal subject or maximum myocardial uptake is commonly performed (7,8).

In this study, we aimed to compare the diagnostic accuracy of attenuation-corrected (AC) and non-attenuation-corrected (NC) MPS for the diagnosis of coronary artery stenosis using ICA as a reference standard, and define the appropriate cut-off scoring values in both types of image interpretation.

Materials and Methods

Study Design and Subjects

Patients who were suspected of CAD and had indications for MPS were sent to the division of nuclear medicine to perform 2-day adenosine-stress/rest Tc-99m-sestamibi MPS. Patients who underwent those scans from January 2013 to December 2016 and underwent ICA within 10 months after MPS were retrospectively included. Patients who had prior coronary artery bypass graft were excluded because it altered the normal distribution of vascular supply, which may affect the image interpretation. Patients who had no CT attenuation for MPS for any reason were also excluded. A body mass index greater than 25 was used as the cut-off for obesity in our protocol. The study was conducted in accordance with the Declaration of Helsinki. The protocol was approved and the requirement for informed consent was waived by the Institutional Review Board of the Faculty of Medicine, Chulalongkorn University (COA no: 611/2017, IRB no: 366/60).

Imaging Procedures

On the first day, the patient was injected with Tc-99m-sestamibi 21-30 mCi at the 4th minute of total six-minute infusion of adenosine rate 140 mg/kg/min. After that, the patient took a high fat diet reduced interfering tracer activity in the liver. Then, the single photon emission computed tomography (SPECT) images were acquired approximately 1 h after radiotracer injection using a dual-head gamma camera SPECT/CT system (Symbia T6, Siemens, Erlangen, Germany) with low-energy ultra-high-resolution collimator. The data was acquired in 50 seconds/projections for 64 projections with matrix size 64x64 and zoom factor of 1.45. Low-dose CT centered at the heart was performed for attenuation correction. On the second day, the resting SPECT and CT images were acquired using the same amount of radiotracer activity and the same scanning protocol.

Image Processing

Emission data were reconstructed into short axis, horizontal long axis, vertical long axis and 17-segment polar map images with iterative reconstruction protocol using commercially available QPS (Cedar-Sinai medical center, Los Angeles, California) software. For AC images, the co-registration was properly checked by the researcher in every case before image processing. Processed SPECT images were displayed in GE multichrome color scale (9).

Semiquantitative Interpretation

AC and NC images were interpreted in a random order by the consensus of 2 experienced nuclear medicine physicians blinded to patients' medical history and ICA results. If there was disagreement between the two readers even after the discussion, a third nuclear medicine physician will give an additional comment/opinion, and a consensus was formed. The third interpreter was also blinded to the ICA results and the clinical information about the patients. Each myocardium segment was scored from 0 to 4 based on relative uptake compared to the segment of maximum uptake; score 0 represented maximum uptake while score 4 represented no uptake. For per-person analysis, the sum of scores in all segments of stress images represented summed stress score (SSS) and the sum of scores in all segments of rest images represented summed rest score (SRS). The summed difference score (SDS) was calculated by subtracting SRS from SSS. For vascular territory analysis, the summed scores are the sum of scores in all segments corresponding to the territory of each of the 3 major coronary arteries.

Invasive Coronary Angiography

The ICA was performed and interpreted by experienced board-certified interventional cardiologists using visual assessment as a routine clinical practice. The presence of significant CAD was defined when there was a stenosis of the left main coronary artery ≥50%, and/or any other coronary artery ≥70%. In patients who had previous percutaneous coronary intervention (PCI) with or without stent, the cut-off to define the diseased vessel was ≥50% re-stenosis in left main coronary artery, or ≥70% re-stenosis in other coronary arteries.

Statistical Analysis

Diagnostic performances were assessed using the area under the curve (AUC) of the receiver operating characteristic (ROC) curve. Comparison of AUC was performed by Delong's non-parametric methods (10). UL index, a statistical method for defining cut-offs using the shortest distance from the upper left corner to the ROC curve, was used to determine optimum cut-offs. These cut-off values were further used for the calculation of sensitivity, specificity, positive predictive value (PPV), negative predictive value (NPV), accuracy, positive and negative likelihood ratios (LR+ and LR-). Proportions and likelihood ratios were compared using chi-square tests and agreement between AC and NC scores was determined by intraclass correlation coefficient (ICC). Territories of each main coronary artery for per-vascular-territory analyses were in accordance with the American Society of Nuclear Cardiology (ASNC) Guidelines (11). The analysis was performed by SPSS for Windows version 22 and the Compbdt R package (12). P value <0.05 was considered statistically significant.

Results

Clinical Characteristics

One hundred and seventeen subjects were eligible (63 men and 54 women; mean age 69.5 years). Clinical characteristics are displayed in Table 1. CAD was present in 66 patients (56%). Most of the patients had a single vessel territory (45%) and the detailed pattern of coronary artery stenosis is shown in Table 2. Most of the patients with CAD had hypertension (n=57, 86%), and dyslipidemia (n= 91, 78%). Thirty-two patients received prior PCI (27%), and most of them had recent CAD in the current analysis (n=25, 78%). The median interval between MPS and ICA was 2 months (interquartile range 1-3 months), and the maximum interval was 10 months in 1 patient.

Per-person Analysis of The Diagnostic Performance of MPS and Optimal Cut-offs

ROC curves comparing the diagnostic performance between AC and NC scores are provided in Figure 1. There were no statistically significant differences between AC-SSS (AUC: 0.765) and NC-SSS (AUC: 0.780, p value=0.624), AC-SRS (AUC: 0.664) and NC-SRS (AUC: 0.659, p value=0.866), and AC-SDS (AUC: 0.690) and NC-SDS (AUC: 0.702, p value=0.771). For subgroup analysis based on sex, and obesity status, there was no statistically significant difference between AC-SSS (AUC: 0.801) and NC-SSS (AUC: 0.780) in the female subgroup (p value=0.668),

Table 1. Baseline patient characteristics

Characteristic	All patients, n (%)	Patients with CAD, n (%)	Patients without CAD, n (%)	p value
Disease status	117	66 (56)	51 (44)	-
Age (mean ± SD), year	69.5±12.0	69.8±13.4	69.2±10.1	0.806
Interval between MPS and ICA (mean ± SD), month	2.2±2.1	2.2±2.0	2.1±2.2	0.799
Sex				
Male	63 (54)	41 (62)	22 (43)	0.042
Female	54 (46)	25 (38)	29 (57)	0.042
Co-morbidity				
Hypertension	98 (84)	57 (86)	41 (80)	0.538
Diabetes	48 (41)	31 (47)	17 (33)	0.194
Dyslipidemia	91 (78)	58 (88)	33 (65)	0.006
Obesity	15 (13)	7 (11)	8 (16)	0.592
End-stage renal disease	4 (3)	2 (3)	2 (4)	1.000
Smoking	10 (9)	9 (14)	1 (2)	0.057

CAD: Coronary artery disease, MPS: Myocardial perfusion scan, ICA: Invasive coronary angiography, SD: Standard deviation

as well as those parameters in the male subgroup (AUC: 0.742 vs. 0.764, p value=0.588). There was also no statistically significant difference between AC-SSS (AUC: 0.764) and NC-SSS (AUC: 0.797) in non-obese subgroup (p value=0.284), as well as those parameters in the obese subgroup (AUC: 0.866 vs. 0.688, p value=0.228).

Each pair of AUCs was compared, aiming to determine the best AUC for CAD diagnosis. In the AC group, the AUC of AC-SSS was significantly higher than that of AC-SRS (p value=0.005), while there was no statistically significant difference between the AUC of AC-SSS and those of AC-SDS (p value=0.057). In the NC group, the AUC of NC-SSS was also significantly higher than that of NC-SRS (p value <0.001), while there was no statistically significant difference between the AUC of NC-SSS and that of NC-SDS (p value=0.107).

Due to the high AUC of SSS and SDS in both AC and NC images, the diagnostic performance of MPS was analyzed based on those data. The optimum cut-off values were more than 12 for AC-SSS, >15 for NC-SSS, >4 for AC-SDS and >3 for NC-SDS. The sensitivity, specificity, PPV, NPV and accuracy of AC-SSS were 61%, 82%, 82%, 62%, and 70%, respectively, and the parameters for NC-SSS were 79%, 67%, 75%, 71%, and 74%, accordingly. The diagnostic parameters of AC-SDS, and NC-SDS are demonstrated in Table 3. There were no statistically significant differences among the diagnostic parameters of AC-SSS vs. NC-SSS, AC-SDS vs. NC-SDS, AC-SSS vs. AC-SDS, or NC-SSS vs. NC-SDS as detailed in Table 3.

The LR+ and LR- of AC-SSS, NC-SSS, AC-SDS, and NC-SDS were 3.39, 0.48, 2.39, 0.31, 2.26, 0.52, and 1.96 and 0.60, respectively. There were no statistically significant differences in LR+ and LR- of AC-SSS vs. NC-SSS (p=0.200 for LR+ and p=0.060 for LR-), AC-SDS vs. NC-SDS (p=0.878 for LR+ and p=0.517 for LR-), AC-SSS vs. AC-SDS (p=0.145 for LR+ and p=0.624 for LR-), and NC-SSS vs. NC-SDS (p=0.676 for LR+ and p=0.141 for LR-).

Table 2. Pattern of coronary artery stenosis

Disease involvement	Subjects	
	Number	Percentage
Single vessel territory	30	46%
Double vessels territories	12	18%
Triple vessels territories	24	36%

Per-vascular Territory Analysis of the Diagnostic Performance of MPS and Optimal Cut-offs

In the left anterior descending territory, there is no statistical significance between AC-SSS (AUC: 0.782) and NC-SSS (AUC: 0.760). The optimum cut-off values are SSS >7 for AC (sensitivity 63%, specificity 87%, PPV 81%, NPV 73%, accuracy 76%) and SSS>6 for NC (sensitivity 70%, specificity 78%, PPV 73%, NPV 75%, accuracy 74%).

In the left circumflex (LCX) territory, there was no statistical significance between AC-SSS (AUC: 0.745) and NC-SSS (AUC: 0.713). The optimum cut-off values are SSS >2 for AC (sensitivity 67%, specificity 68%, PPV 42%, NPV 86%, accuracy 68%) and SSS >5 for NC (sensitivity 70%, specificity 59%, PPV 37%, NPV 85%, accuracy 62%).

In the right coronary (RCA) territory, there is no statistical significance between AC-SSS (AUC: 0.776) and NC-SSS (AUC: 0.774). The optimum cut-off values are SSS >2 for AC (sensitivity 69%, specificity 77%, PPV 60%, NPV 83%, accuracy 74%) and SSS >8 for NC (sensitivity 64%, specificity 86%, PPV 69%, NPV 83%, accuracy 79%).

Agreements of Each Score Obtained From AC and NC Images

There was significant difference between SSS obtained from NC and AC images, with a mean difference of 5.8 (NC-SSS was higher than AC-SSS, p value <0.001), and a significant difference between SRS obtained from NC and AC images was also observed (mean difference of 5.8, NC-SRS was higher than AC-SRS, p value <0.001). This resulted in no difference between SDS obtained from the NC and AC images (p value=0.952).

On the per-vascular-territory basis, there was a significant difference in SSS obtained from NC and AC images in LCX, and RCA territories (mean difference of 2.4, and 3.3,

Table 3. Diagnostic parameters of Tc-99m sestamibi MPS based on different criteria

Criteria	Sensitivity	Specificity	Accuracy	PPV	NPV
AC-SSS >12	61% (49-72)	82% (72-93)	70% (62-78)	82% (71-92)	62% (50-73)
NC-SSS >15	79% (69-89)	67% (54-80)	74% (66-82)	75% (65-86)	71% (58-84)
AC-SDS >4	62% (50-74)	73% (60-85)	67% (58-75)	75% (63-86)	60% (47-72)
NC-SDS >3	68% (57-79)	69% (56-81)	68% (60-77)	74% (63-85)	62% (50-75)

Data in parentheses are 95% confidence intervals. There was no statistical significance between each pair of the parameters (p value >0.05). AC: Attenuation-corrected, NC: Non-attenuation-corrected, MPS: Myocardial perfusion scan, PPV: Positive predictive value, NPV: Negative predictive value, SSS: Summed stress score, SDS: Summed difference score

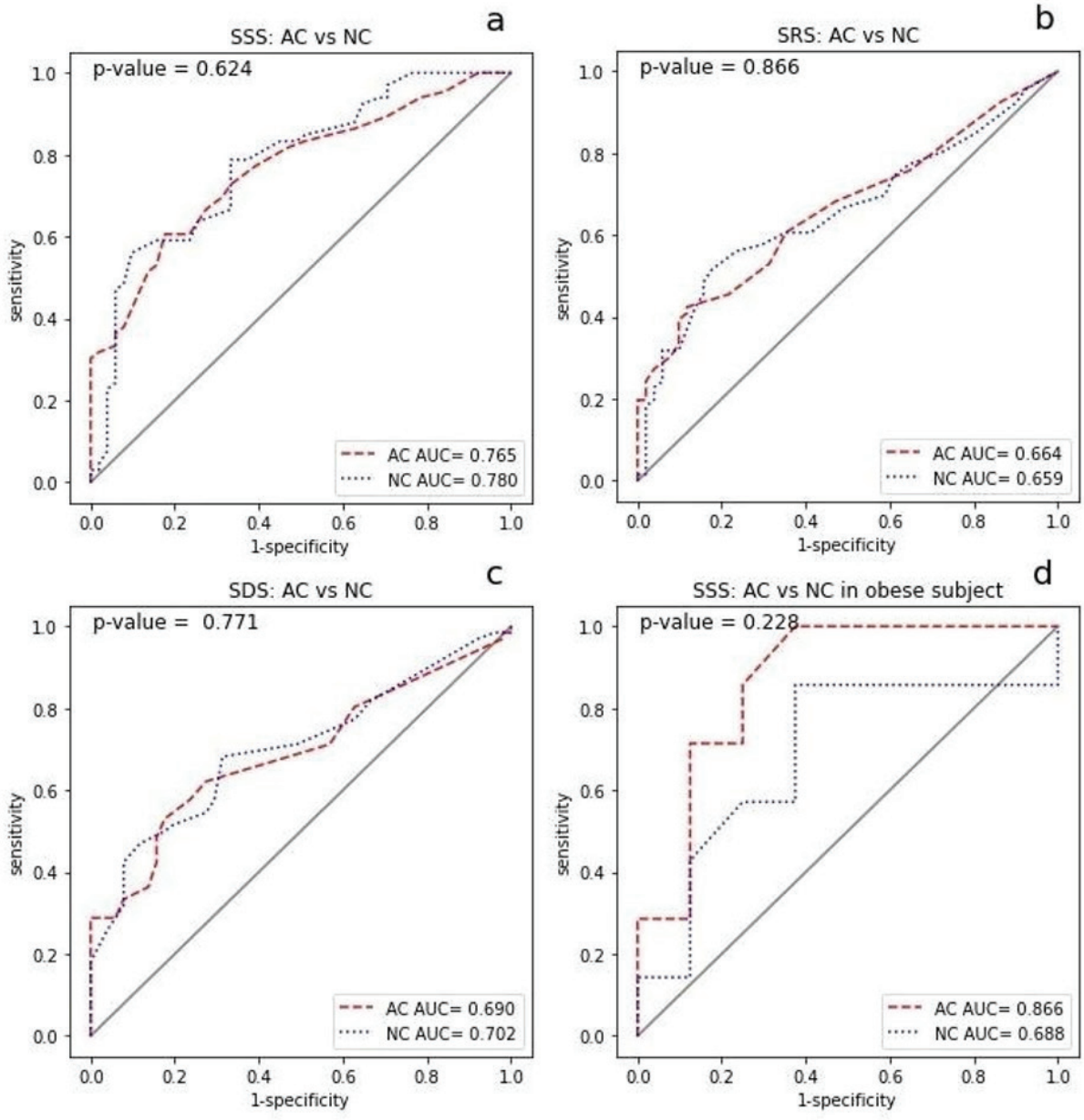

Figure 1. ROC curves comparing diagnostic performance between AC and NC scores of SSS (a), SRS (b), SDS (c) and SSS in obesity subgroup (d). (Created using Matplotlib version 3.3.3, https: matplotlib.org)
ROC: Receiver operating characteristic, AC: Attenuation-corrected, NC: Non-attenuation-corrected, SSS: Summed stress score, SRS: Summed rest score, SDS: Summed difference score

respectively, p value <0.001, Figure 2). These differences were also observed when interpreted by NC-SRS, and AC-SRS in both LCX and RCA territories (mean difference of 2.2, and 3.3, respectively, p value <0.001, Figure 3), which was not proved, but probably due to the breast and the diaphragmatic attenuation, respectively. There was no statistically significant difference between NC-SDS, and AC-SDS on per-vascular-territory basis (Figure 4).

Excellent agreements between AC-SSS, and NC-SSS (ICC: 0.9), AC-SRS, and NC-SRS (ICC: 0.9), and AC-SDS, and NC-SDS (ICC: 0.8) were observed.

Discussion

Our results demonstrated good diagnostic performance of Tc-99m-sestamibi stress-rest protocol either with or without

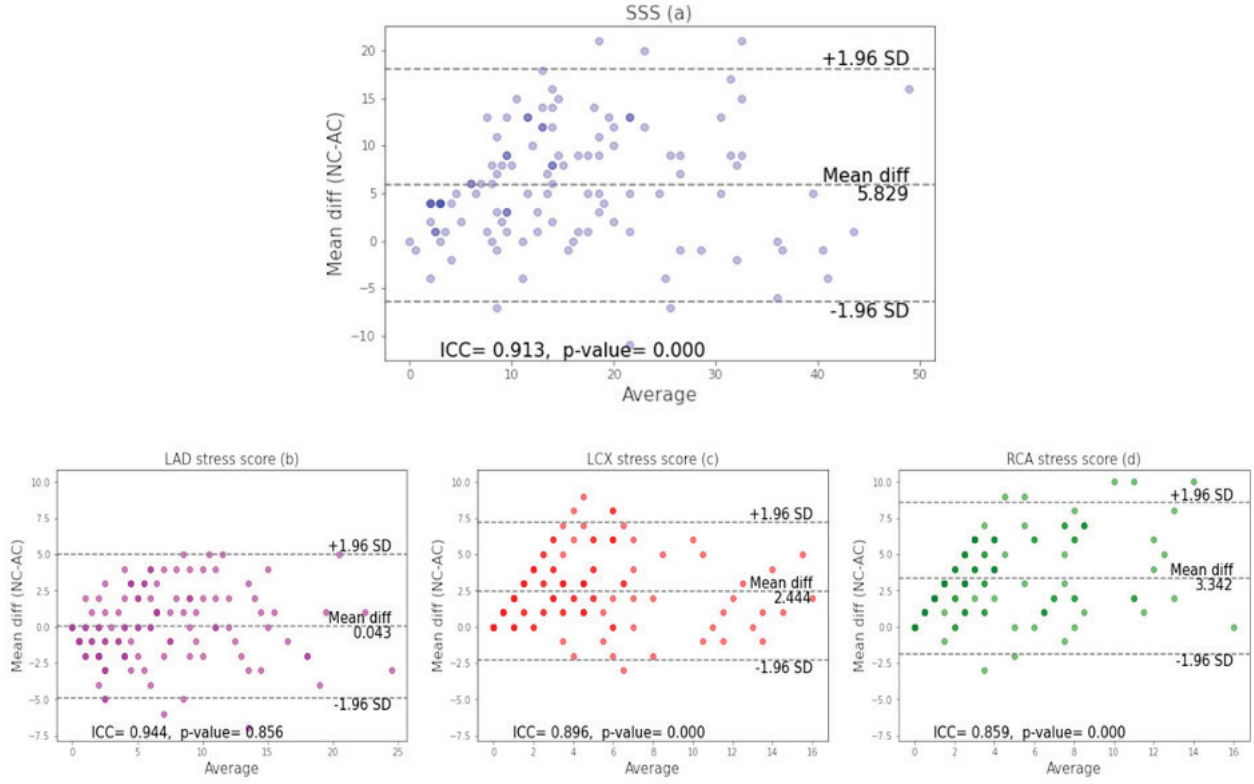

Figure 2. Agreements between stress scores. There were significant differences between AC and NC of SSS (a) and stress scores in LCX (c) and RCA (d) territories. No significant difference in seen in LAD territory (b)
AC: Attenuation-corrected, NC: Non-attenuation-corrected, SSS: Summed stress score, LCX: Left circumflex, LAD: Left anterior descending, RCA: Right coronary

attenuation correction for the diagnosis of coronary artery stenosis using ICA as a gold standard. The previously reported accuracy of MPS in several studies ranged from 63 to 94% (13,14,15). Our protocol provided good accuracy of MPS in both AC-SSS (70%) and NC-SSS images (74%). The reported superiority of AUC of SSS and SDS over SRS reaffirmed the significance of stress myocardial perfusion imaging for the diagnosis of coronary artery stenosis.

In subgroup analysis, we found no significant difference between the diagnostic performance of AC-, and NC-images in both male, and female subgroups, which concordant with the prior study by Wolak et al. (16). The difference cut-off values were due to difference interpretation methods as we defined all scores based on the relative uptake of one segment to the area of maximum uptake in the individual image. In our study, the AUC of AC-images of obese patients was notably higher than those of NC-images (AUC: 0.866 vs. 0.688), even without a statistically significant (p value=0.228). This might be consistent with Thompson et al.'s (17) conclusion that AC was particularly helpful in obese patients, but the failure to reach statistical significance in our study might be due to the small number of obese patients (n=15).

Even without a statistically significant difference, our results showed that AC-SSS offered slightly higher specificity (82%) compared to NC-SSS (67%). This was concordant with several prior studies (6,11,17). Recent meta-analysis by Huang et al. (5) revealed the pooled sensitivity and specificity of MPS using AC images of 84% and 80% and those from NC were 80% and 68%, respectively. The lower specificity of NC images was potentially caused by attenuation artifacts, which were more obvious without the correction process. The mean difference of 5.8 between AC-SSS and NC-SSS, as well as between AC-SRS, and NC-SRS found in the current study supported the presence of attenuation artifacts in NC images on both stress and rest images, especially in LCX, and RCA territories, when analyzed on per-vascular-territory basis. The presence of an attenuation artifact could also explain the larger difference between AC and NC cut-off values on per-vascular territory analysis in LCX and RCA territories.

We did not find inferior diagnostic performance of NC MPS in the diagnosis of CAD within the RCA territory, which

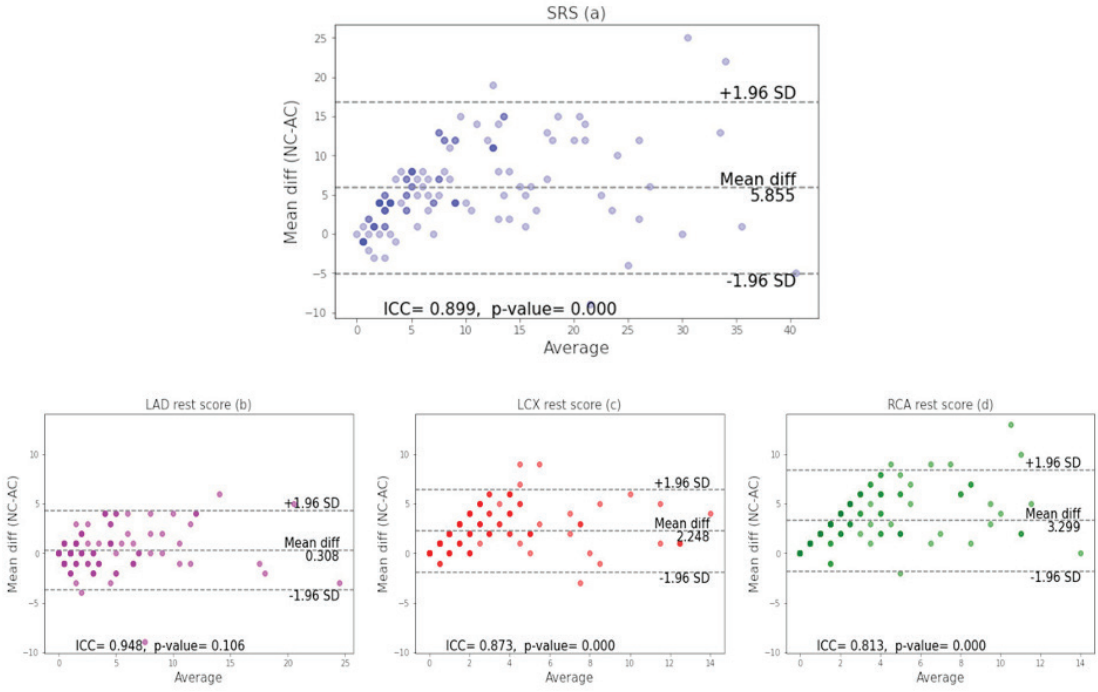

Figure 3. Agreements between rest scores. Similar to stress scores, there were significant differences between AC and NC of SRS (a) and rest scores in LCX (c) and RCA (d) territories. No significant difference in seen in LAD territory (b)

AC: Attenuation-corrected, NC: Non-attenuation-corrected, SRS: Summed rest score, LCX: Left circumflex, RCA: Right coronary, LAD: Left anterior descending

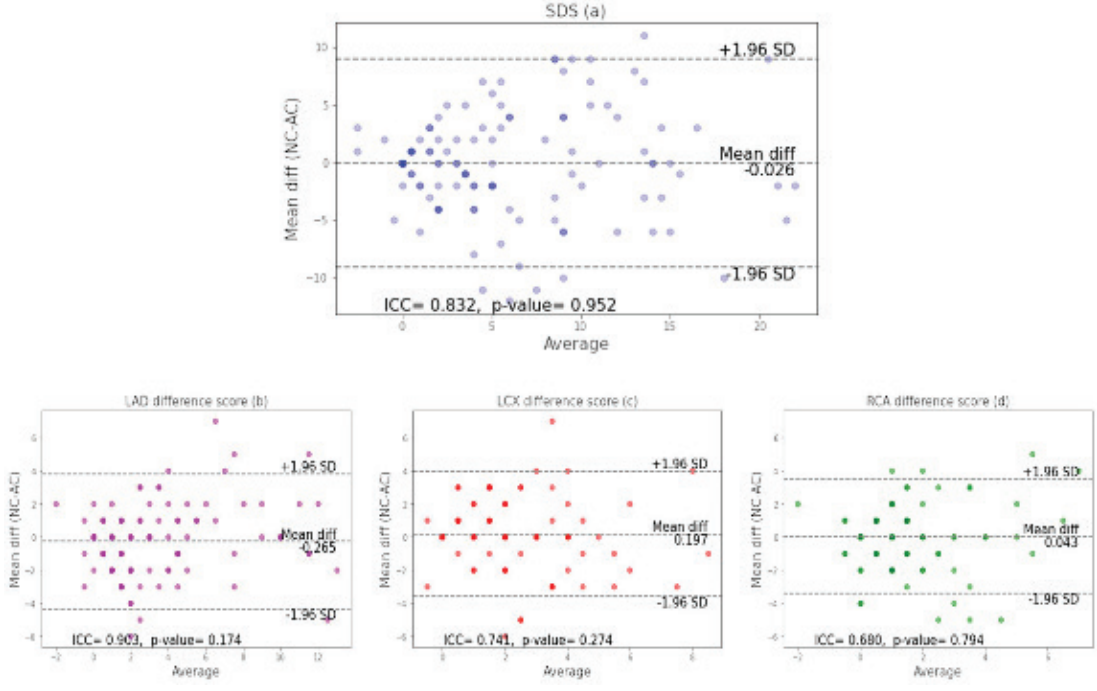

Figure 4. Agreements between difference scores. Contrary to stress and rest scores. No significant difference in either SDS (a) or territories of LAD (b), LCX (c) and RCA (d)

SDS: Summed difference score, LCX: Left circumflex, RCA: Right coronary, LAD: Left anterior descending

had been reported in past studies. This absence could be a result of using standardized criteria based on tracer uptake, difference cut-offs used, interpreters being experienced, or a combination of the aforementioned factors (18). It should also be noted that the current study population had a notably high rate of RCA stenosis (38/66 patients, 58% of the study population). It is widely accepted that the detection of RCA stenosis is a problematic for MPS. A diagnosis based on either AC-SDS or NC-SDS could eliminate the interference from attenuation artifacts. Some prior data also showed higher false positive rates in NC images, however, masking of true defects by attenuation correction in AC could lead to lower sensitivity when using AC images (7,19,20). Generally, the ASNC recommends the use of attenuation correction when available to optimize image quality and improve the diagnostic utility of MPS (11).

Study Limitations

Limitation of our study was a slightly long interval between MPS and ICA in 1 patient. Nevertheless, the progression of coronary stenosis was generally insidious (21). Our method using the semi-quantitative assessment might have limitation in the assessment of multi-vessel diseases, however, the dynamic Tc-99m-sestamibi MPS for quantitative assessment of myocardial blood flow was not widely performed because of the low count sensitivity of the conventional SPECT scanner (22). Another potential weakness in our study was MPS may exhibit defects in the absence of stenoses when MPS was performed after angioplasty or stenting thus the specificity of MPS following PCI might be limited (23). Apart from CAD diagnosis, the parameters from the MPS were found to have prognostic value in the long-term period in patients having CAD regardless of ICA findings; for examples, abnormal MPS, especially in AC images, was associated with higher number of cardiac events, worsening survival rate and increased rate of hospital admission (24,25,26). Our studies still lacked of long term follow up to assess those outcomes, which could be the topic of interest for further research.

Conclusion

In conclusion, using a semiquantitative method based on relative tracer uptake with a standard 17-segment model, NC-images based Tc-99m-sestamibi MPS either by SSS, or SDS promised fairly good diagnostic accuracy comparable to AC images with different cut-off values.

Acknowledgment

The authors thank Dr. Tawatchai Chaiwatanarat for facilitation of the administrative process and Dr. Suphot Srimahachota for coordination with clinical departments.

Ethics

Ethics Committee Approval: Institutional Review Board of the Faculty of Medicine, Chulalongkorn University (COA no: 611/2017, IRB no: 366/60).

Informed Consent: The informed consent are waived by the ethic committee.

Peer-review: Externally and internally peer-reviewed.

Authorship Contributions

Surgical and Medical Practices: S.V., Concept: S.S., S.V., Design: S.V., M.C., Data Collection or Processing: S.S., M.C., Analysis or Interpretation: S.S., M.C., Literature Search: S.V., Writing: S.V., M.C.

Conflict of Interest: No conflict of interest was declared by the authors.

Financial Disclosure: The authors declared that this study has received no financial support.

References

1. Task Force Members, Montalescot G, Sechtem U, Achenbach S, Andreotti F, Arden C, Budaj A, Bugiardini R, Crea F, Cuisset T, Di Mario C, Ferreira JR, Gersh BJ, Gitt AK, Hulot JS, Marx N, Opie LH, Pfisterer M, Prescott E, Ruschitzka F, Sabaté M, Senior R, Taggart DP, van der Wall EE, Vrints CJ; ESC Committee for Practice Guidelines, Zamorano JL, Achenbach S, Baumgartner H, Bax JJ, Bueno H, Dean V, Deaton C, Erol C, Fagard R, Ferrari R, Hasdai D, Hoes AW, Kirchhof P, Knuuti J, Kolh P, Lancellotti P, Linhart A, Nihoyannopoulos P, Piepoli MF, Ponikowski P, Sirnes PA, Tamargo JL, Tendera M, Torbicki A, Wijns W, Windecker S; Document Reviewers, Knuuti J, Valgimigli M, Bueno H, Claeys MJ, Donner-Banzhoff N, Erol C, Frank H, Funck-Brentano C, Gaemperli O, Gonzalez-Juanatey JR, Hamilos M, Hasdai D, Husted S, James SK, Kervinen K, Kolh P, Kristensen SD, Lancellotti P, Maggioni AP, Piepoli MF, Pries AR, Romeo F, Rydén L, Simoons ML, Sirnes PA, Steg PG, Timmis A, Wijns W, Windecker S, Yildirir A, Zamorano JL. 2013 ESC Guidelines on the management of stable coronary artery disease: the task force on the management of stable coronary artery disease of the European Society of Cardiology. Eur Heart J 2014;34:2949-3003.
2. Notghi A, Low CS. Myocardial perfusion scintigraphy: past, present and future. Br J Radiol 2011;84 Spec No 3(Spec Iss 3):S229-S236.
3. Beller GA, Watson DD. Risk stratification using stress myocardial perfusion imaging: don't neglect the value of clinical variables. J Am Coll Cardiol 2004;43:209-212.
4. Srimahachota S, Limpijankit T, Boonyaratavej S, Tepmongkol S, Udayachalerm W, Suithichaiyakul T, Ngarmukos P. Detection of restenosis after percutaneous transluminal coronary angioplasty using the exercise treadmill test and technetium 99m-sestamibi scintigraphy. J Med Assoc Thai 2001;84:307-313.
5. Huang JY, Huang CK, Yen RF, Wu HY, Tu YK, Cheng MF, Lu CC, Tzen KY, Chien KL, Wu YW. Diagnostic performance of attenuation-corrected myocardial perfusion imaging for coronary artery disease: a systematic review and meta-analysis. J Nucl Med 2016;57:1893-1898.
6. Hendel RC, Corbett JR, Cullom SJ, DePuey EG, Garcia EV, Bateman TM. The value and practice of attenuation correction for myocardial perfusion SPECT imaging: a joint position statement from the American Society of

Nuclear Cardiology and the Society of Nuclear Medicine. J Nucl Cardiol 2002;9:135-143.

7. Benkiran M, Mariano-Goulart D, Bourdon A, Sibille L, Bouallègue FB. Is computed tomography attenuation correction more efficient than gated single photon emission computed tomography analysis in improving the diagnostic performance of myocardial perfusion imaging in patients with low prevalence of ischemic heart disease? Nucl Med Commun 2015;36:69-77.
8. Huang R, Li F, Zhao Z, Liu B, Ou X, Tian R, Li L. Hybrid SPECT/CT for attenuation correction of stress myocardial perfusion imaging. Clin Nucl Med 2011;36:344-349.
9. Siennicki J, Kuśmierek J, Kovacevic-Kuśmierek K, Bieńkiewicz M, Chiżyński K, Płachcińska A. The effect of image translation table on diagnostic efficacy of myocardial perfusion SPECT studies. Nucl Med Rev Cent East Eur 2010;13:64-69.
10. DeLong ER, DeLong DM, Clarke-Pearson DL. Comparing the areas under two or more correlated receiver operating characteristic curves: a nonparametric approach. Biometrics 1988;44:837-845.
11. Dorbala S, Ananthasubramaniam K, Armstrong IS, Chareonthaitawee P, DePuey EG, Einstein AJ, Gropler RJ, Holly TA, Mahmarian JJ, Park MA, Polk DM, Russell R 3rd, Slomka PJ, Thompson RC, Wells RG. Single photon emission computed tomography (SPECT) myocardial perfusion imaging guidelines: instrumentation, acquisition, processing, and interpretation. J Nucl Cardiol 2018;25:1784-1846.
12. Roldán-Nofuentes JA. Compbdt: an R program to compare two binary diagnostic tests subject to a paired design. BMC Med Res Methodol 2020;20:143.
13. Slart RHJA, Que TH, van Veldhuisen DJ, Poot L, Blanksma PK, Piers DA, Jagers PL. Effect of attenuation correction on the interpretation of 99mTc-sestamibi myocardial perfusion scintigraphy: the impact of 1 year's experience. Eur J Nucl Med Mol Imaging 2003;30:1505-1509.
14. Elhendy A, van Domburg RT, Bax JJ, Nierop PR, Valkema R, Geleijnse ML, Kasprzak JD, Liqui-Lung AF, Cornel JH, Roelandt JR. Dobutamine-atropine stress myocardial perfusion SPECT imaging in the diagnosis of graft stenosis after coronary artery bypass grafting. J Nucl Cardiol 1998;5:491-497.
15. Elhendy A, Geleijnse ML, Roelandt JR, van Domburg RT, Nierop PR, Bax JJ, Kasprzak JD, el-Said GM, Ibrahim MM, Fioretti PM. Dobutamine 99Tcm-MIBI SPET myocardial perfusion scintigraphy in the prediction of restenosis after percutaneous transluminal coronary angioplasty in patients unable to perform an exercise stress test. Nucl Med Commun 1997;18:122-128.
16. Wolak A, Slomka PJ, Fish MB, Lorenzo S, Berman DS, Germano G. Quantitative diagnostic performance of myocardial perfusion SPECT with attenuation correction in women. J Nucl Med 2008;49:915-922.
17. Thompson RC, Heller GV, Johnson LL, Case JA, Cullom SJ, Garcia EV, Jones PG, Moutray KL, Bateman TM. Value of attenuation correction on ECG-gated SPECT myocardial perfusion imaging related to body mass index. J Nucl Cardiol 2005;12:195-202.
18. DePasquale EE, Nody AC, DePuey EG, Garcia EV, Pilcher G, Bredlau C, Roubin G, Gober A, Gruentzig A, D'Amato P. Quantitative rotational thallium-201 tomography for identifying and localizing coronary artery disease. Circulation 1988;77:316-327.
19. Sharma P, Patel CD, Karunanithi S, Maharjan S, Malhotra A. Comparative accuracy of CT attenuation-corrected and non-attenuation-corrected SPECT myocardial perfusion imaging. Clin Nucl Med 2012;37:332-338.
20. Utsunomiya D, Tomiguchi S, Shiraishi S, Yamada K, Honda T, Kawanaka K, Kojima A, Awai K, Yamashita Y. Initial experience with X-ray CT based attenuation correction in myocardial perfusion SPECT imaging using a combined SPECT/CT system. Ann Nucl Med 2005;19:485-489.
21. Shea S, Sciacca RR, Esser P, Han J, Nichols AB. Progression of coronary atherosclerotic disease assessed by cinevideodensitometry: relation to clinical risk factors. J Am Coll Cardiol 1986;8:1325-1331.
22. Slomka PJ, Berman DS, Germano G. Absolute myocardial blood flow quantification with SPECT/CT: is it possible? J Nucl Cardiol 2014;21:1092-1095.
23. Georgoulias P, Valotassiou V, Tsougos I, Demakopoulos N. Myocardial Perfusion SPECT imaging in patients after percutaneous coronary intervention. Curr Cardiol Rev 2010;6:98-103.
24. Pazhenkottil AP, Ghadri JR, Nkoulou RN, Wolfrum M, Buechel RR, Küest SM, Husmann L, Herzog BA, Gaemperli O, Kaufmann PA. Improved outcome prediction by SPECT myocardial perfusion imaging after CT attenuation correction. J Nucl Med 2011;52:196-200.
25. Heller GV, Herman SD, Travin MI, Baron JI, Santos-Ocampo C, McClellan JR. Independent prognostic value of intravenous dipyridamole with technetium-99m sestamibi tomographic imaging in predicting cardiac events and cardiac-related hospital admissions. J Am Coll Cardiol 1995;26:1202-1208.
26. Milvidaite I, Kulakiene I, Vencloviene J, Kinduris S, Jurkiene N, Grizas V, Navickas R, Slapikas R. Prognostic value of myocardial perfusion abnormalities for long-term prognosis in patients after coronary artery bypass grafting. Indian J Nucl Med 2014;29:222-226.

Interesting Image
Mol Imaging Radionucl Ther 2022;31:139-141 DOI:10.4274/mirt.galenos.2022.64497

Almost Complete Response with a Single Administration ^{225}Ac-DOTATATE in a Patient with a Metastatic Neuroendocrine Tumor of Unknown Primary

Primeri Bilinmeyen Metastatik Nöroendokrin Tümörlü Hastaya Tek Doz ^{225}Ac-DOTATATE Uygulaması Sonrası Tam/Tama Yakın Yanıt

Nalan Alan Selçuk[1], Emre Demirci[1], Meltem Ocak[2], Türkay Toklu[1], Selçuk Ergen[3], Levent Kabasakal[4]

[1]*Yeditepe University Faculty of Medicine, Department of Nuclear Medicine, İstanbul, Turkey*
[2]*İstanbul University Faculty of Pharmacy, Department of Pharmaceutical Technology, İstanbul, Turkey*
[3]*Yeditepe University Faculty of Medicine, Department of Medical Oncology, İstanbul, Turkey*
[4]*İstanbul University-Cerrahpaşa, Cerrahpaşa Faculty of Medicine, Department of Nuclear Medicine, İstanbul, Turkey*

Abstract

Neuroendocrine tumors (NETs) are being seen increasingly frequently, and the only known curative treatment method is surgical resection. Peptide receptor radionuclide therapy (PRRT) is a treatment option that the most contributes to progression-free survival and overall survival in metastatic cases.β-emitting radionuclides are traditionally used for PRRT. Nowadays, alpha particle-emitting radionuclides are being developed, with advantages in terms of very high energy and a short path length, which should theoretically show higher efficacy. In this case; in a patient with NET diagnosis who had multiple (>50) lesions in the abdomen, almost all the lesions disappeared with a single dose application. This paper aims to present a case in which we observed the efficacy of ^{225}Ac-DOTATATE treatment, which is an alpha treatment.

Keywords: ^{225}Ac targeted alpha therapy, neuroendocrine tumors, peptide receptor radionuclide therapy

Öz

Nöroendokrin tümörler (NET) son yıllarda giderek artan hızda ortaya çıkmakta olup bilinen tek küratif tedavi yöntemi cerrahi rezeksiyondur. Peptid reseptör radyonüklid tedavisi (PRRT) ise metastatik olgularda progresyonsuz sağkalımı ve genel sağkalıma en çok katkı sağlayan bir tedavi seçeneğidir. Ancak PRRT'de en sık tercih edilen ^{177}Lu radyonükliti bir beta partikül yayıcısıdır. Son zamanlarda radyobiyolojik özellikleri daha güçlü olan, yüksek enerjili ve kısa menzil avantajı sunan 225Ac gibi alfa ışını yayan radyonüklidler ile PRRT'nin yapılması gündeme gelmiştir. Bu olguda; batın içerisinde çok sayıda (>50) lezyonları olan NET tanılı hastada tek doz uygulamayla lezyonların neredeyse tamamı tedavi sonrasında saptanmamıştır. Bu yazının amacı bir alfa tedavi olan ^{225}Ac-DOTATATE tedavisinin etkinliğini gözlediğimiz olguyu sunmaktır.

Anahtar kelimeler: ^{225}Ac hedeflendirilmiş alfa tedavisi, nöroendokrin tümörler, peptid reseptör radyonüklid tedavisi

Address for Correspondence: Levent Kabasakal Prof. MD, İstanbul University-Cerrahpaşa, Cerrahpaşa Faculty of Medicine, Department of Nuclear Medicine, İstanbul, Turkey
Phone: +90 532 366 79 08 **E-mail:** lkabasakal@tsnn.org ORCID ID: orcid.org/0000-0002-4050-1972
Received: 30.07.2021 **Accepted:** 07.01.2022

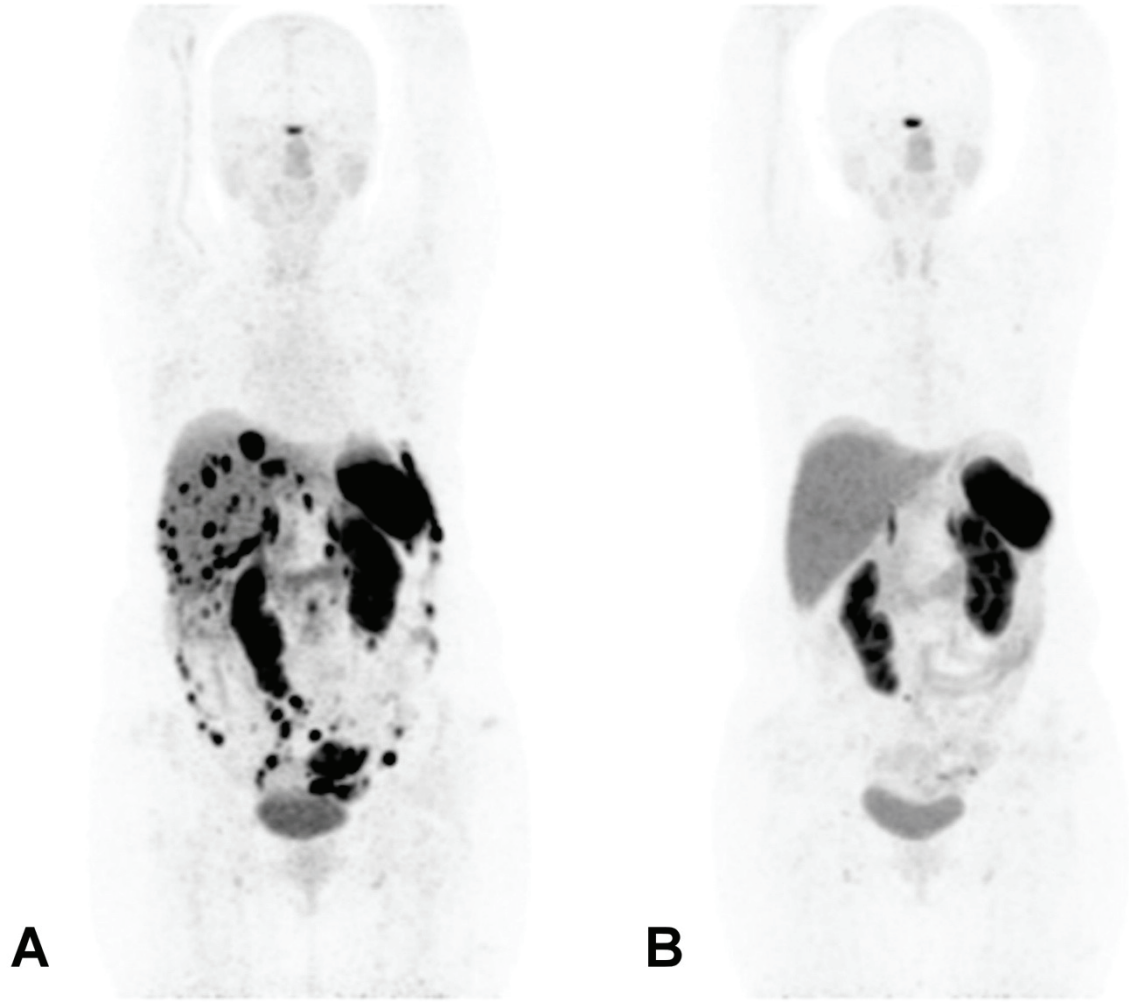

Figure 1. A 46-year-old woman was admitted to an oncology clinic with epigastric pain and weakness five years ago. Magnetic resonance imaging showed a retroperitoneal mass lesion along with peritoneal carcinomatosis. Resection of the retroperitoneal tumor revealed a metastatic neuroendocrine tumor of an unknown primary site (WHO grade 2). After carboplatin and etoposide treatment, thermal ablation and hyperthermic intraperitoneal chemotherapy, which to control the disease for 4 years, the recurrence was observed based on up-to-date [^{68}Ga]Ga-DOTATATE PET/CT scan examination (somatostatin receptor positive more than 50 lesions in abdomen, liver and peritoneal space). For this purpose, the patient was referred to our department for ^{177}Lu DOTATATE treatment. After several investigations with consideration the specific conditions of the patient, a single administration of 10 MBq [^{225}Ac] Ac-DOTATATE was administered to the patient as treatment. The radiopharmaceutical was injected slowly for 5 minutes. To lower radiation-absorbed doses of the kidney, an amino acid solution started 30-60 minutes before treatment and maintained for 4 hours according to the recommendations of current peptide receptor radionuclide therapy (PRRT) guidelines. The patient had a slow onset of abdominal pain which was resolved after corticosteroid treatment. The results of the post therapy [^{68}Ga]Ga-DOTATATE positron emission tomography/computed tomography scan, which was performed 3 months after the therapy, showed almost complete response. All lesions in the abdomen with the exception of 5 mm lymph node in the paraaortic area disappeared.

Among the various therapeutic options, PPRT such as radioactive labeling DOTATATE conjugate molecule is highly effective and a well-tolerated therapy, improving progression-free survival and probably overall survival (1). Despite the multiple treatment options in NET, a considerable number of patients are found to be non-responders to the available therapy options. In this group, the use of high linear energy transfer (LET) alpha-emitting radioisotopes such as ^{225}Ac and ^{213}Bi instead of low LET beta-emitting radioisotopes like 90Y and 177Lu is a promising option (2,3,4). Although there are not enough studies on this topic in the literature, limited studies have shown that ^{225}Ac-DOTATATE is a promising treatment option, which adds a new dimension in patients especially who are refractory to ^{177}Lu-DOTATATE (5). Our case was the first case who received actinium in the first step and almost complete response at a single dosage in the PubMed.

Ethics

Informed Consent: Obtained from the patient.

Peer-review: Externally and internally peer-reviewed.

Authorship Contributions

Surgical and Medical Practices: L.K., N.A.S., E.D., Concept: L.K., Design: N.A.S., E.D., Data Collection or Processing: E.D., T.T., M.O., S.E., Analysis or Interpretation: T.T., M.O., Literature Search: T.T., M.O., Writing: L.K., N.A.S., E.D., T.T., M.O.

Conflict of Interest: No conflict of interest was declared by the authors.

Financial Disclosure: The authors declared that this study received no financial support.

References

1. Bodei L, Kidd M, Paganelli G, Grana CM, Drozdov I, Cremonesi M, Lepensky C, Kwekkeboom DJ, Baum RP, Krenning EP, Modlin IM. Long-term tolerability of PRRT in 807 patients with neuroendocrine tumours: the value and limitations of clinical factors. Eur J Nucl Med Mol Imaging 2015;42:5-19.
2. Navalkissoor S, Grossman A. Targeted alpha particle therapy for neuroendocrine tumours: the next generation of peptide receptor radionuclide therapy. Neuroendocrinology 2019;108:256-264.
3. Nayak TK, Norenberg JP, Anderson TL, Prossnitz ER, Stabin MG, Atcher RW. Somatostatin-receptor-targeted alpha-emitting 213Bi is therapeutically more effective than beta(-)-emitting 177Lu in human pancreatic adenocarcinoma cells. Nucl Med Biol 2007;34:185-193.
4. Ocak M, Toklu T, Demirci E, Selçuk N, Kabasakal L. Post-therapy imaging of 225Ac-DOTATATE treatment in a patient with recurrent neuroendocrine tumor. Eur J Nucl Med Mol Imaging 2020;47:2711-2712.
5. Ballal S, Yadav MP, Bal C, Sahoo RK, Tripathi M. Broadening horizons with 225Ac-DOTATATE targeted alpha therapy for gastroenteropancreatic neuroendocrine tumour patients stable or refractory to 177Lu-DOTATATE PRRT: first clinical experience on the efficacy and safety. Eur J Nucl Med Mol Imaging 2020;47:934-946.

Interesting Image
Mol Imaging Radionucl Ther 2022;31:142-144 DOI:10.4274/mirt.galenos.2021.65882

"Picture-in-Picture" Artifact in Post-therapeutic ^{131}I Whole-body Survey: Deceiving Spot View but Unraveling Whole-body Scanning

Tedavi Sonrası ^{131}I Tüm Vücut Taramada "Resim-İçinde-Resim" Artefaktı: Spot Görüntülemedeki Yanıltıcılığın Tüm Vücut Görüntülemede Ortaya Çıkarılması

Mohsen Qutbi[1], Reyhane Ahmadi[2]

[1]*Department of Nuclear Medicine, Taleghani Educational Hospital, School of Medicine, Shahid Beheshti University of Medical Sciences, Tehran, Iran*
[2]*Department of Nuclear Medicine and Molecular Imaging, Farshchian Heart Center, School of Medicine, Hamadan University of Medical Sciences, Hamadan, Iran*

Abstract

Artifacts originated from imaging hardware or instrumentation may be, on some occasions, confusing and peculiar to both physicians and technicians. Various artifacts from a variety of sources have been reported. In this note, we intend to describe a new one with an interesting pattern in whole-body scanning, which is strikingly different from its pattern in static spot view, in a patient presented for post-therapeutic ^{131}I survey after total thyroidectomy.

Keywords: Post-therapeutic ^{131}I survey, "Picture-in-Picture" artifact, whole-body scanning

Öz

Görüntüleme donanımı veya enstrümantasyonundan kaynaklanan artefaktlar, bazı durumlarda kafa karıştırıcı ve hem doktorlara hem de teknisyenlere özgü olabilir. Çeşitli kaynaklardan çeşitli artefaktlar bildirilmiştir. Bu notta, total tiroidektomi ardından tedavi sonrası ^{131}I incelemesi için başvuran bir hastada, tüm vücut taramasında statik spot görünümdeki paterninden çarpıcı şekilde farklı olan ilginç bir paterni tanımlamayı amaçlıyoruz.

Anahtar kelimeler: Tedavi sonrası ^{131}I tarama, "Resim-İçinde-Resim" artefaktı, tüm vücut taraması

Address for Correspondence: Mohsen Qutbi Asst. Prof., Department of Nuclear Medicine, Taleghani Educational Hospital, School of Medicine, Shahid Beheshti University of Medical Sciences, Tehran, Iran
Phone: +982123031250 **E-mail:** mohsen.qutbi@gmail.com ORCID ID: orcid.org/0000-0002-8347-605X
Received: 16.03.2021 **Accepted:** 02.06.2021

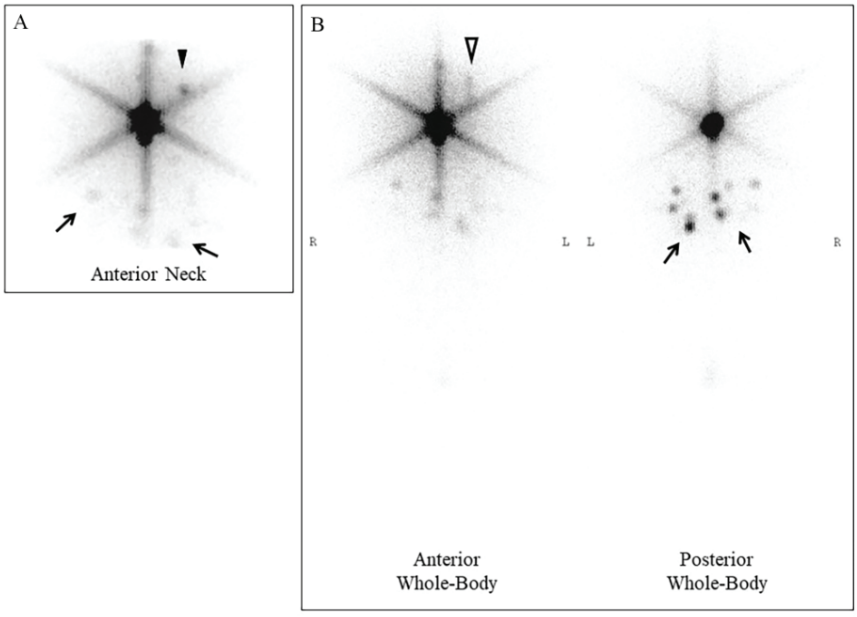

Figure 1. A 40-year-old woman with a recent diagnosis of papillary thyroid carcinoma is referred for radioiodine therapy after undergoing total thyroidectomy. One week later, a post-therapeutic whole-body ^{131}I scan was performed. In static spot view (A), considerable uptake of thyroid tissue remnant was observed in the thyroid bed. Also, a small iodine-avid focus was noticed above and right to the thyroid bed. This finding, initially, gave the impression of a metastatic cervical lymph node (shown by solid arrowhead). However, after performing the anterior whole-body projection (B, left), the mentioned finding is reshaped and transformed to a short vertical line (indicated by open arrowhead), appearing as smudging or smearing of the spot vertically, which makes the diagnosis of a metastatic cervical lymph node less likely. This pattern is in contrast to other active foci scattered in the patient's chest, most prominently visualized in the posterior projection (B, right), which disclose a constant pattern in both spot view and whole-body scanning, attributable to rib metastasis (arrows in A and B, right).

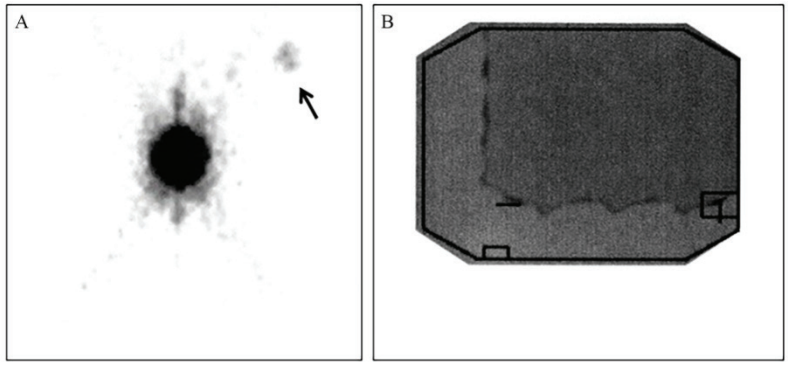

Figure 2. We thought the finding described in Figure 1 could result from the error occurred erratically in the camera in use in our laboratory, which was recognized in other scans performed recently as well (1,2). We, again, carried out quality control testing using a point source placed on the table of the gamma camera. A one-minute image was acquired (A). The static image of the point source revealed a hot spot in the center with its corresponding reproduced image (indicated by arrow) with much less intensity located above and right to the original hot spot, to confirm the pattern which was observed in spot view of the neck. The intrinsic uniformity test performed as a routine weekly task, demonstrated the described pattern in the flood image (B) as a smaller reproduced image superimposed on the right upper corner of the main image. Artifacts from a variety of sources of error may impose serious challenges for interpreting physicians. One such source of error is issues related to imaging instrumentation. Although not occurring very often owing to regular quality control testing in nuclear medicine laboratories, they may be confusing to the interpreter in terms of diversity and complexity of the pattern of artifacts originated from imaging hardware or instrumentation (3,4,5,6). One such artifact with an interesting appearance in nuclear medicine images, is the one which is named and coined as "Picture-in-Picture" artifact. The mechanism by which this artifact occurs lies behind an error in an item of hardware of the gamma camera detector, i.e., digital event processor electronic board, which is responsible for positioning the signals transmitted from photomultiplier tubes. Each event is recorded as a point with values of x and y, in an imaginary Cartesian coordinate system which corresponds point-by-point to a matrix with predefined size in the camera computer memory set by the operator before acquiring images. This process of event localization and positioning does not work properly in this specific flaw of the mentioned electronic board and therefore, the result is a reproduction of the main image. The pattern is particularly striking in images with an intense hot spot against a lower-activity background (1,7).

Ethics

Informed Consent: Written Informed consent was obtained from the patient before performing the scanning.

Peer-review: Externally peer-reviewed.

Authorship Contributions

Concept: M.Q., Design: M.Q., R.A., Data Collection or Processing: M.Q., R.A., Analysis or Interpretation: M.Q., R.A., Literature Search: M.Q., R.A., Writing: M.Q., R.A.

Conflict of Interest: No conflict of interest was declared by the authors.

Financial Disclosure: The authors declared that this study received no financial support.

Reference

1. Qutbi M, Soltanshahi M, Gorzi SK, Shiravand Y, Edalat Haghi SM, Khosravi A, Asli IN. "Picture-in-Picture" artifact: introduction and characterization of a hitherto unrecognized imaging artifact in creating perfusion defects in myocardial perfusion single-photon emission computed tomography. Indian J Nucl Med 2021;36:69-72.
2. Qutbi M, Asadi A, Asli IN. Coexisting sources of false-positive reflux on a direct radionuclide cystography scan. J Nucl Med Technol 2019;47:177-178.
3. IAEA Quality Control Atlas for Scintillation Camera Systems. Vienna, International Atomic Energy Agency; 2003.
4. Quality Assurance for SPECT Systems. Vienna, International Atomic Energy Agency; 2009.
5. O'Connor MK. Instrument- and computer-related problems and artifacts in nuclear medicine. Semin Nucl Med 1996;26:256-277.
6. Zanzonico P. Routine quality control of clinical nuclear medicine instrumentation: a brief review. J Nucl Med 2008;49:1114-1131.
7. ADAC Laboratories. Matador electronics overview manual, 9202-0104 Rev A. In: Vertex Matador Field Service Kit. Milpitas, CA: ADAC Laboratories; 1997.

Interesting Image
Mol Imaging Radionucl Ther 2022;31:145-147 DOI:10.4274/mirt.galenos.2021.40326

Unusual Uptake of [^{131}I] in a Tenosynovial Giant Cell Tumour Relapse in a Patient with Differentiated Thyroid Cancer

Diferansiye Tiroid Kanserli Bir Hastada Tenosinovyal Dev Hücreli Tümör Nüksünde Olağandışı [^{131}I] Tutulumu

Francisco Manuel Cañete Sánchez, Leonardo Gabriel Romero Robles, Xavier Louis Boulvard Chollet, María Mangas Losada, Puy Garrastachu, Antonio Cabrera Villegas, Rafael Ramírez Lasanta, Roberto Delgado Bolton

University Hospital San Pedro and Centre for Biomedical Research of La Rioja (CIBIR), Department of Nuclear Medicine, Logroño, Spain

Abstract

A 77-year-old woman with follicular thyroid cancer underwent total thyroidectomy and subsequent Iodine-131 remnant ablation. She had a history of a wide tenosynovial giant cell tumor (TGCT) of the right wrist and hand that had been resected thirteen years ago. Post-therapeutic scintigraphy and single photon emission computed tomography showed mild uptake on the distal right forearm, wrist and hand. Magnetic resonance imaging and posterior histopathology confirmed a relapse of TGCT. No radioiodine adverse effects were reported after a one-year follow-up. As far as we know, this report is the first in the literature to a TGCT visualized on post-therapy radioiodine scan.

Keywords: Giant cell tumor of tendon sheath, thyroid neoplasms, scintigraphy, magnetic resonance imaging

Öz

Foliküler tiroid kanserli 77 yaşında bir kadına total tiroidektomi ve ardından İyot-131 remnant ablasyonu uygulandı. On üç yıl önce rezeke edilmiş sağ el bileği ve elde geniş tenosinovyal dev hücreli tümör (TGCT) öyküsü vardı. Tedavi sonrası sintigrafi ve tek foton emisyon tomografisi distal sağ önkol, el bileği ve elde hafif tutulum gösterdi. manyetik rezonans görüntüleme ve posterior histopatoloji, TGCT'nin relapsını doğruladı. Bir yıllık takipten sonra hiçbir radyoiyodin yan etkisi bildirilmemiştir. Bildiğimiz kadarıyla bu rapor, tedavi sonrası radyoiyot taramasında görüntülenen bir TGCT'nin literatürdeki ilk raporudur.

Anahtar kelimeler: Tendon kılıfının dev hücreli tümörü, tiroid neoplazmaları, sintigrafi, manyetik rezonans görüntüleme

Address for Correspondence: Francisco Manuel Cañete Sánchez MD, University Hospital Puerta del Mar, Department of Nuclear Medicine, Cádiz, Andalucía, Spain
Phone: +34-956-003-008 **E-mail:** francisco.canete.sanchez.sspa@juntadeandalucia.es ORCID ID: orcid.org/0000-0001-7282-8534
Received: 16.10.2020 **Accepted:** 01.04.2021

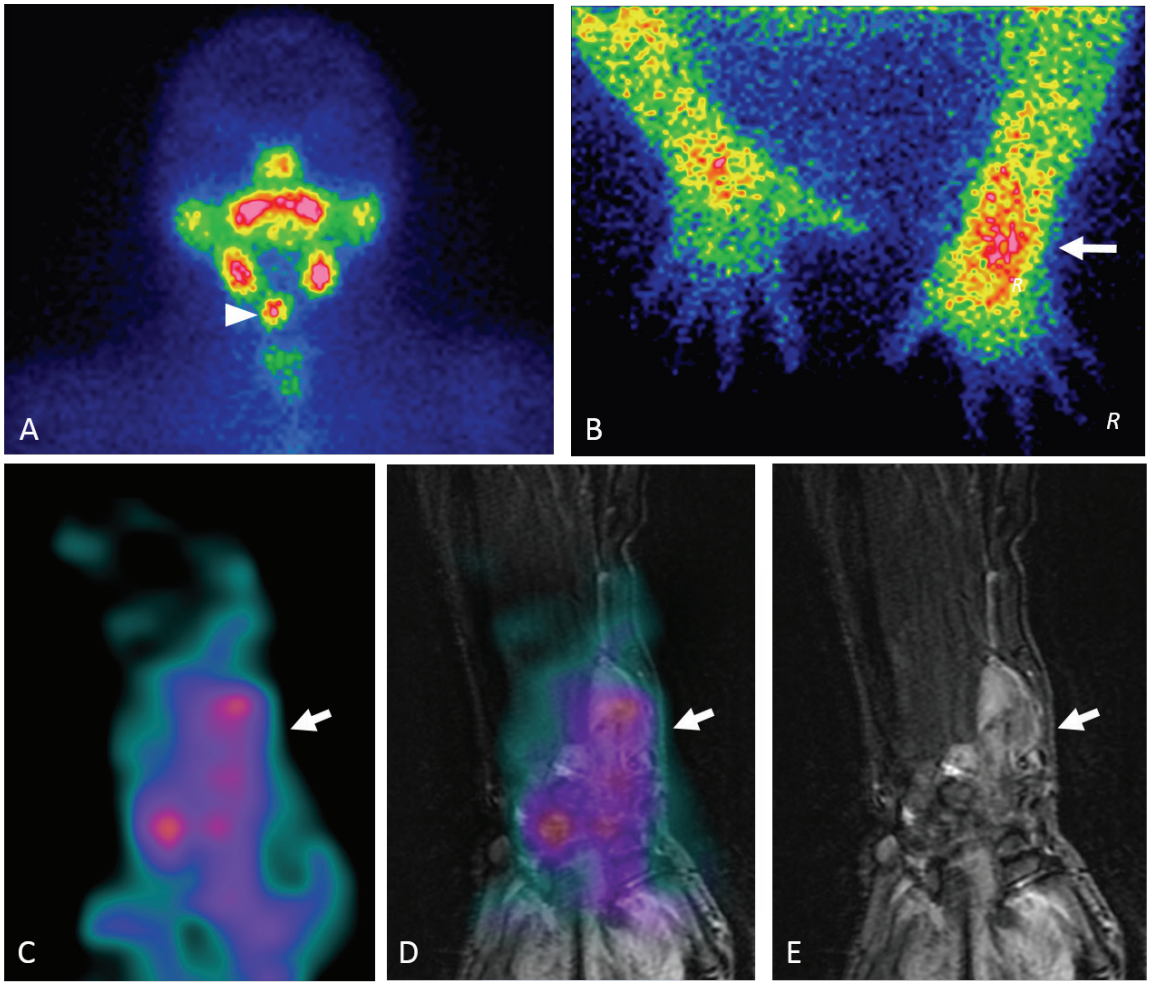

Figure 1. Seventy seven year-old woman with a history of wide tenosynovial giant cell tumor (TGCT) of the right wrist and hand that had been resected thirteen years ago, who did not follow the surveillance for this tumour. Following the diagnosis of a well-differentiated follicular thyroid carcinoma, the patient underwent total thyroidectomy and subsequent Iodine-131 [^{131}I] remnant ablation, receiving an activity of 3.7 GBq. Five days after [^{131}I] administration, the post-therapy scan showed mild uptake in the thyroid remnant and a more intense focus of uptake, probably secondary to a thyroglossal duct remnant (A, arrowhead). To assess the possibility of a TGCT relapse, we did a palmar planar image of both forearms, wrists and hands (B), which showed mildly increased uptake in the distal third of the radial forearm, wrist and metacarpal spaces (B, arrow) a more evident in the single photon emission computed tomography (SPECT) images (C, arrow). Subsequent magnetic resonance imaging (MRI) and fused SPECT/MRI images (D: Coronal SPECT-MRI; E: Coronal MRI) revealed increased signal on fat suppression with short-time inversion recovery (STIR) coronal sequence concordant with the increased uptake in SPECT (arrows in D and E). The histological examination was consistent with the TGCT. The patient did not present with any clinical side effect secondary to radioiodine treatment, or any clinical sign or symptom in the right upper limb after one-year follow-up. TGCT is an orphan, mono-articular and potentially locally aggressive disease that occurs in a localized form, which involves a discrete section of the synovium, or in a diffuse form, which involves the entire synovium (1,2,3). The diffuse type has high recurrence rates and poor functional outcomes (1,2,4). TGCT is characterized by hypervascular neoplastic proliferation of the synovium with deposition of macrophages, multinucleated giant cells and hemosiderin (3). The proposed reasons for iodine increased uptake in non-thyroid tumors are an expression of sodium iodide symporter, augmented vascularity and enhanced capillary permeability, which can be caused by inflammation secondary to the tumor (5,6,7). MRI is the most distinctive imaging technique in diagnosing and treating TGCT (1,2,3,8). It reflects the existence of hemosiderin-laden tissue that applies a paramagnetic effect decreasing T1 and T2 relaxation times, leading to low to intermediate signal intensity in T1 and T2 weighted spin-echo sequences. On STIR sequences, the effect is overstated because of increased magnetic susceptibility deriving in areas of very high signal intensity (3,8). The main treatment modality is resection for naïve and relapsed TGCT. Radiation therapy and targeted therapies, mainly with monoclonal antibody inhibiting colony-stimulating factor 1 receptor (pexidartinib) are promising, and both should be considered especially in case of relapse (1,2,3,4,8). However, in our patient's case, watchful waiting was finally decided, mostly because of age, relative good mobility, and the stability of the tumor on serial MRI. A considerable number of cases of unexpected radioiodine uptake have been reported and some of which were in the limbs (6). To our knowledge, this report is the first in the literature of a TGCT visualized in the post-therapy radioiodine scan.

Ethics

Informed Consent: Consent form was filled out by the patient.

Peer-review: Externally peer-reviewed.

Authorship Contributions

Concept: F.M.C.S., L.G.R.R., R.D.B., Design: F.M.C.S., L.G.R.R., X.L.B.C., R.D.B., Data Collection or Processing: F.M.C.S., L.G.R.R., R.D.B., Literature Search: F.M.C.S., L.G.R.R., X.L.B.C., R.D.B., Writing: F.M.C.S., L.G.R.R., X.L.B.C., M.M.L., P.G., A.C.V., R.R.L., R.D.B.

Conflict of Interest: No conflict of interest was declared by the authors.

Financial Disclosure: The authors declared that this study received no financial support.

References

1. Gouin F, Noailles T. Localized and diffuse forms of tenosynovial giant cell tumor (formerly giant cell tumor of the tendon sheath and pigmented villonodular synovitis). Orthop Traumatol Surg Res 2017;103:S91-S97.
2. Mastboom MJL, Verspoor FGM, Hanff DF, Gademan MGJ, Dijkstra PDS, Schreuder HWB, Bloem JL, van der Wal RJP, van de Sande MAJ. Severity classification of tenosynovial giant cell tumours on MR imaging. Surg Oncol 2018;27:544-550.
3. Jain JK, Vidyasagar JV, Sagar R, Patel H, Chetan ML, Bajaj A. Arthroscopic synovectomy in pigmented villonodular synovitis of the knee: clinical series and outcome. Int Orthop 2013;37:2363-2369.
4. Mastboom MJL, Palmerini E, Verspoor FGM, Rueten-Budde AJ, Stacchiotti S, Staals EL, Schaap GR, Jutte PC, Aston W, Gelderblom H, Leithner A, Dammerer D, Takeuchi A, Thio Q, Niu X, Wunder JS; TGCT Study Group, van de Sande MAJ. Surgical outcomes of patients with diffuse-type tenosynovial giant-cell tumours: an international, retrospective, cohort study. Lancet Oncol 2019;20:877-886.
5. Liu Z, Xing M. Induction of sodium/iodide symporter (NIS) expression and radioiodine uptake in non-thyroid cancer cells. PLoS One 2012;7:e31729.
6. Oh JR, Ahn BC. False-positive uptake on radioiodine whole-body scintigraphy: physiologic and pathologic variants unrelated to thyroid cancer. Am J Nucl Med Mol Imaging 2012;2:362-385.
7. Anh BC. Physiologic and false positive pathologic uptakes on radioiodine whole body scan. 12 Chapters on Nuclear Medicine. InTech; 2011.
8. Bassetti E, Candreva R, Santucci E. Giant cell tumor of the flexor tendon of the wrist: US and MRI evaluation. Case report. J Ultrasound 2011;14:37-39.

Interesting Image
Mol Imaging Radionucl Ther 2022;31:148-150 DOI:10.4274/mirt.galenos.2021.60590

A Rare Case of Primary Cardiac Diffuse Large B-cell Lymphoma Imaged with ^{18}F-FDG PET/CT

^{18}F-FDG PET/BT ile Görüntülenen Nadir Bir Primer Kardiyak Diffüz Büyük B-hücreli Lenfoma Olgusu

Seval Erhamamcı[1], Nesrin Aslan[2]

[1]Başkent University Faculty of Medicine, Başkent University İstanbul Hospital, Department of Nuclear Medicine, İstanbul, Turkey
[2]Neolife Medical Center, Clinic of Nuclear Medicine, İstanbul, Turkey

Abstract

Primary cardiac lymphoma is an extremely rare malignancy. A few reports about the findings of ^{18}fluorine-fluorodeoxyglucose (^{18}F-FDG) positron emission tomography/computed tomography (PET/CT) imaging has been presented. We report a rare case of a 70-year-old male with diagnosed primary intracardiac diffuse large B-cell lymphoma referred for ^{18}F-FDG PET/CT imaging for initial staging. The scan revealed an abnormal hypermetabolic gross tumoral lesion involving the right atrium and auricula. After completing three cycles of chemotherapy, post-treatment ^{18}F-FDG PET/CT showed complete response.

Keywords: Primary cardiac tumor diffuse large B-cell lymphoma, ^{18}F-FDG, PET/CT

Öz

Primer kardiyak lenfoma oldukça nadir görülen bir malignitedir. ^{18}Flor-florodeoksiglukoz (^{18}F-FDG) pozitron emisyon tomografisi/bilgisayarlı tomografi (PET/BT) görüntüleme bulguları hakkında birkaç bildiri sunulmuştur. Başlangıç evreleme amacıyla ^{18}F-FDG PET/BT görüntüleme için gönderilen primer intrakardiyak diffüz büyük B-hücreli lenfoma tanısı almış 70 yaşında nadir bir erkek hastayı sunduk. Görüntüleme sağ atrium ve aurikulayı kapsayan anormal hipermetabolik büyük tümör lezyonunu ortaya çıkardı. Üç kür kemoterapi tamamlandıktan sonra, tedavi sonrası ^{18}F-FDG PET/BT tam yanıt gösterdi.

Anahtar kelimeler: Primer kardiyak tümörler, diffüz büyük B-hücreli lenfoma, ^{18}F-FDG, PET/BT

Address for Correspondence: Seval Erhamamcı Assoc. Prof., Başkent University Faculty of Medicine, Başkent University İstanbul Hospital, Department of Nuclear Medicine, İstanbul, Turkey
Phone: +90 216 554 15 00 **E-mail:** sevaler@yahoo.com ORCID ID: orcid.org/0000-0001-5016-4650
Received: 10.05.2020 **Accepted:** 17.01.2021

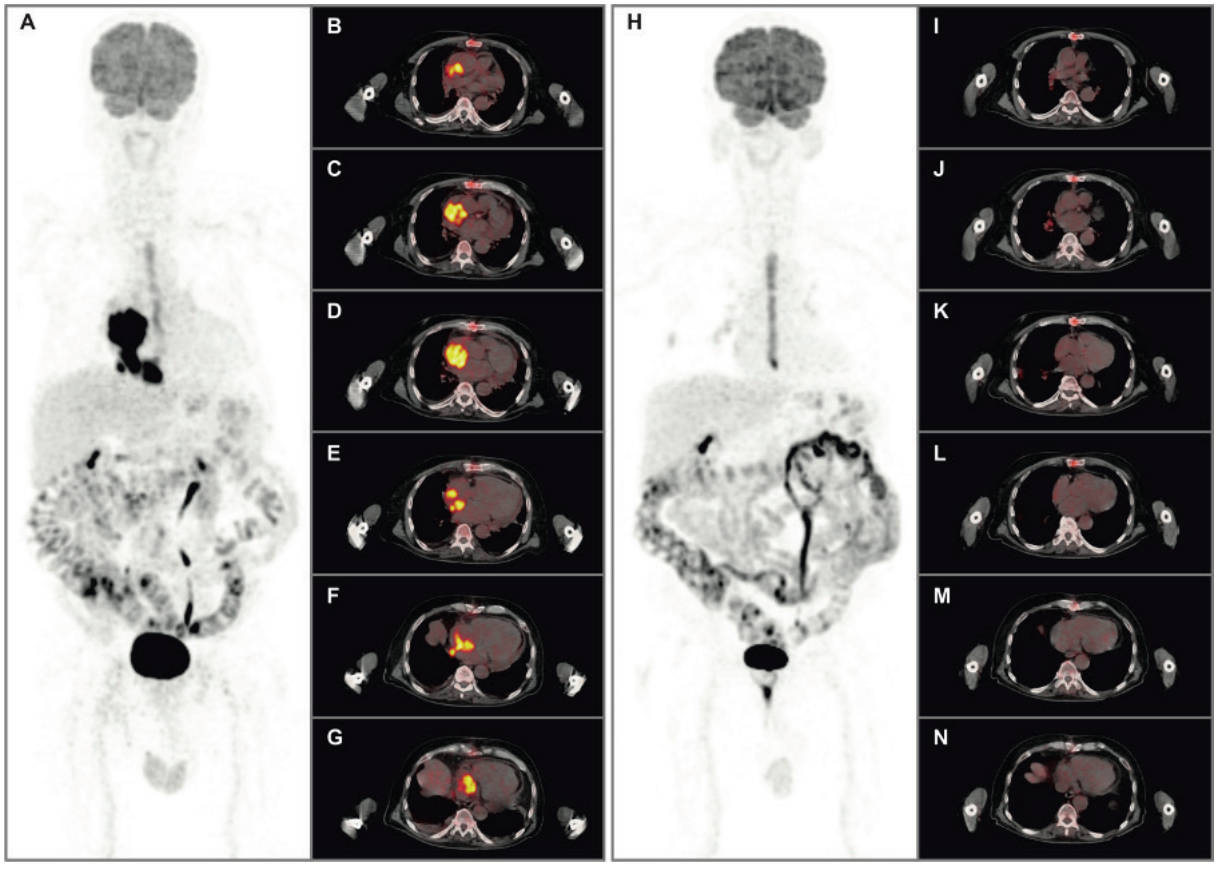

Figure 1. A 70-year-old male was admitted order to investigate dyspnea and weakness. Computed tomography (CT) imaging of the thorax revealed a large soft tissue mass in the right atrium (RA). He underwent excisional biopsy of the mass in the RA with histopathological result of diffuse large B-cell lymphoma (DLBCL). For initial staging, ^{18}fluorine-fluorodeoxyglucose (^{18}F-FDG) positron emission tomography (PET)/CT imaging was requested. The scan MIP (A) and transaxial fused (B, C, D, E, F, G) images demonstrated intense ^{18}F-FDG uptake with an maximum standardized uptake value (SUV_{max}) of 26.6 in an irregular gross tumoral lesion, approximately 6 cm in diameter, in the RA and auricula. Mild pericardial effusion without ^{18}F-FDG uptake and bilateral pleural effusion without ^{18}F-FDG uptake was seen. Linear increased ^{18}F-FDG uptake in the sternum was observed due to thoracotomy. There were no other findings elsewhere in the body, which suggested a metastatic disease. The patient underwent three cycles of combination chemotherapy with rituximab, cyclophosphamide, doxorubicin, vincristine and prednisone (R-CHOP). To therapy response early evaluation, post-treatment ^{18}F-FDG PET/CT MIP (H) and transaxial fused (I, J, K, L, M, N) images revealed complete resolution of the tumoral lesion and, pericardial and pleural effusion compared with baseline scan. Newly developed slightly hypermetabolic activities were seen in the right lung hilar lymph nodes, in the right lower lobe superior segment and on the right upper lobe bronchus level, which may be due to an infectious or inflammatory etiology. Primary cardiac lymphoma (PCL) is an extremely rare malignancy, comprising about 1% of primary cardiac tumors, which is accompanied by a poor prognosis, unless it is timely diagnosed and treated (1,2). PCL is most commonly reported to be a DLBCL, and the RA and right ventricle are the two most frequently involved sites (1,2). ^{18}F-FDG PET/CT imaging has become an essential method for staging and treatment response evaluation of lymphomas (3). A few reports have been presented about the ^{18}F-FDG PET/CT findings of PCLs due to its rare presentation, and most of the information comes from case reports and case series (4,5,6). specific findings of ^{18}F-FDG PET/CT imaging of primary cardiac DLBCL is reported to be the combination of a large right-sided cardiac mass, a large pericardial effusion and a high SUVmax value, compared with other cardiac malign and benign tumors (4,5,6). This case had a gross tumoral lesion with high SUVmax located in the RA, consistent with previous reports. However, the patient had mild pericardial effusion without ^{18}F-FDG uptake. Furthermore, after three chemotherapy cycles, the patient showed a good response to treatment and considered to have a better prognosis with a lower recurrence rate.

Ethics

Informed Consent: Written informed consent was obtained.

Peer-review: Externally and internally peer-reviewed.

Authorship Contributions

Concept: S.E., Design: S.E., Data Collection or Processing: S.E., N.A., Analysis or Interpretation: S.E., N.A., Literature Search: S.E., Writing: S.E.

Conflict of Interest: No conflict of interest was declared by the authors.

Financial Disclosure: The authors declared that this study received no financial support.

References

1. Petrich A, Cho SI, Billett H. Primary cardiac lymphoma: an analysis of presentation, treatment, and outcome patterns. Cancer 2011;117:581-589.
2. Coulier B, Colin GC, Tourmous H, Floris N, Van Eeckhout P, Scavée C. Imaging features of primary cardiac lymphoma. Diagn Interv Imaging 2018;99:115-117.
3. Cheson BD. PET/CT in lymphoma: current overview and future directions. Semin Nucl Med 2018;48:76-81.
4. Kikuchi Y, Oyama-Manabe N, Manabe O, Naya M, Ito YM, Hatanaka KC, Tsutsui H, Terae S, Tamaki N, Shirato H. Imaging characteristics of cardiac dominant diffuse large B-cell lymphoma demonstrated with MDCT and PET/CT. Eur J Nucl Med Mol Imaging 2013;40:1337-1344.
5. Kaida H, Kumode T, Kimura M, Ishii K. 18F-FDG PET/CT finding of primary cardiac lymphoma. Clin Nucl Med 2020;45:319-321.
6. Castelli JB, Alexandre L, Futuro G, Scanavacca M, Soares Júnior J. Primary cardiac lymphoma detected by 18F-FDG PET scan: a case report. J Nucl Cardiol 2011;18:974-977.

Interesting Image
Mol Imaging Radionucl Ther 2022;31:151-153 DOI:10.4274/mirt.galenos.2021.80775

A Rare Case of Pulmonary Alveolar Microlithiasis with Diffuse Lung Uptake on Bone Scintigraphy

Kemik Sintigrafisinde Diffüz Akciğer Tutulumu Olan Nadir Bir Pulmoner Alveolar Mikrolitiazis Olgusu

Ahmet Eren Şen, Özlem Şahin, Zeynep Aydın, Buğra Kaya, Çağlagül Erol

Necmettin Erbakan University, Meram Faculty of Medicine, Department of Nuclear Medicine, Konya, Turkey

Abstract

Pulmonary alveolar microlithiasis is a rare disease characterized by accumulating intraalveolar small calcium phosphate stones. The disease is slow and does not show any signs in the early stages, but the shortness of breath, cough, and right heart failure may develop as it progresses. Methylene diphosphonate used in bone scintigraphy shows high uptake of calcium deposits in the alveoli and causes diffuse increased radiopharmaceutical uptake in the lungs.

Keywords: Pulmonary alveolar microlithiasis, MDP, bone scintigraphy

Öz

Pulmoner alveolar mikrolitiazis intraalveoler küçük kalsiyum fosfat taşlarının birikmesi ile karakterize nadir görülen bir hastalıktır. Hastalık yavaş seyirlidir ve ilk dönemlerinde bulgu vermese de ilerledikçe nefes darlığı, öksürük ve sağ kalp yetersizliği gelişebilmektedir. Kemik sintigrafisinde kullanılan metilendifosfonat alveollerdeki kalsiyum depozitlerinde yüksek tutulum göstererek akciğerlerde diffüz artmış radyofarmasötik tutulumuna sebep olur.

Anahtar kelimeler: Pulmoner alveolar mikrolitiazis, MDP, kemik sintigrafisi

Address for Correspondence: Ahmet Eren Şen MD, Necmettin Erbakan University, Meram Faculty of Medicine, Department of Nuclear Medicine, Konya, Turkey
Phone: +90 332 223 77 74 **E-mail:** ahmeterensen.aes@gmail.com ORCID ID: orcid.org/0000-0001-7628-7640
Received: 11.12.2020 **Accepted:** 31.01.2021

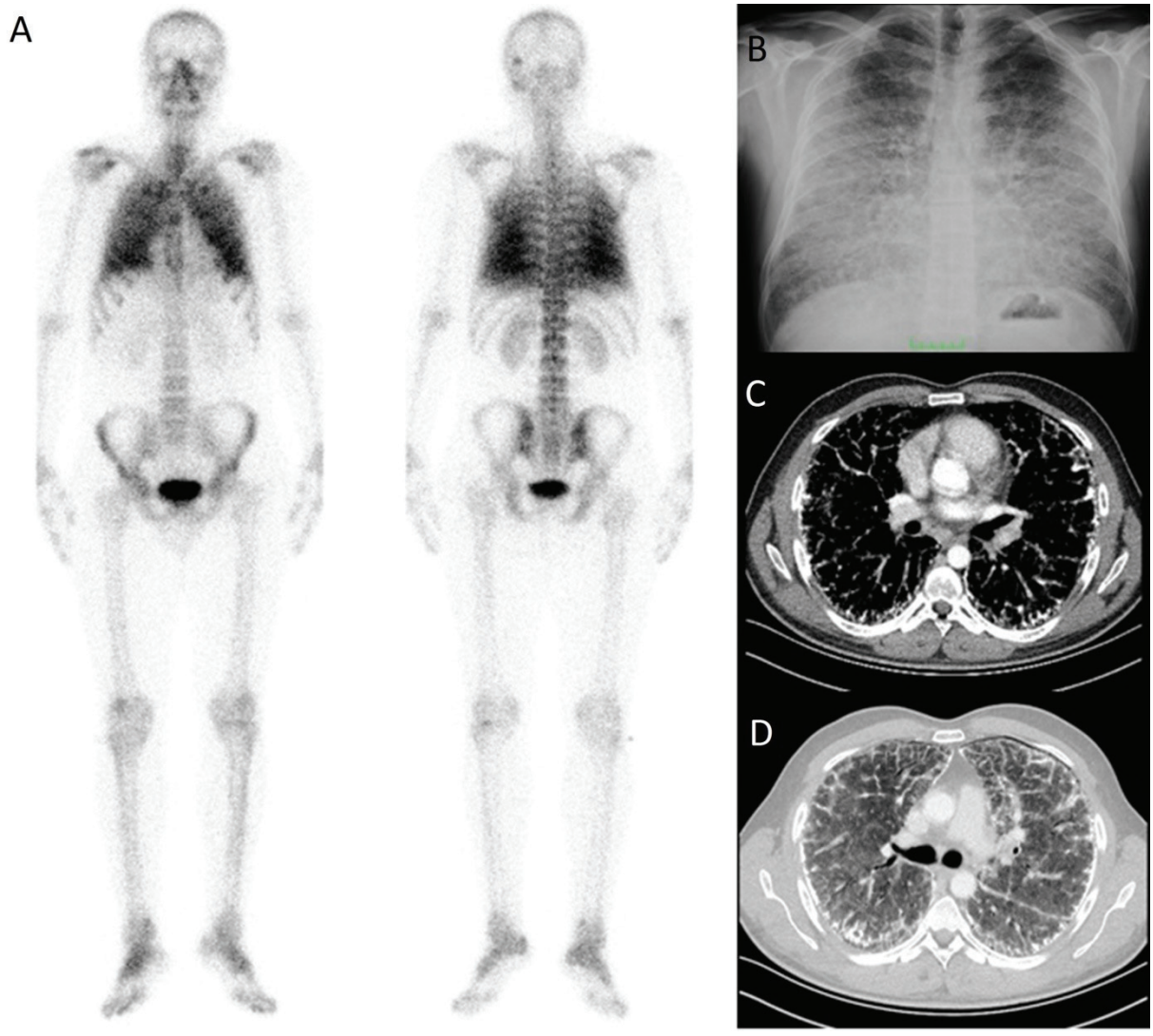

Figure 1. Twenty eight years old male patient was admitted to the outpatient clinic of chest disease with cough and dyspnea complaints for several months. was diagnosed with pneumoconiosis was suspected on the posteroanterior (PA) chest X-ray performed seven years before the military service. The patient could not be accurately diagnosed and did not undergo further examination. A bilateral, diffuse, micronodular pattern erasing the heart shadow was observed on the PA chest radiograph (B). Contrast-enhanced thorax-computed tomography (CT) showed diffuse ground-glass densities, septal thickening, and occasionally clustered high-density opacities in both peripheral parenchymas (C, D). Tc-99m methylene diphosphonate (MDP) whole-body bone scintigraphy was performed considering pulmonary alveolar microlithiasis (PAM). Scintigraphy showed diffuse increased radioactivity uptake in both lungs, consistent with PAM (A). PAM is a rare disease characterized by intraalveolar, widespread, large numbers of calcium and phosphate-rich microliths reaching 3 mm in size. The majority of cases in the literature have been reported in Turkey, China, Japan, India, and Italy. Although the disease has been known for nearly 90 years, its etiology has not been fully elucidated. In addition to being known as an autosomal recessive disorder, sporadic cases have been reported (1,2,3,4,5,6,7). Diagnosis is usually made at an advanced stage since it is slow, and the clinical findings are minimal. In the following years, shortness of breath, cough, pulmonary fibrosis, and pulmonary heart disease (cor pulmonale) may develop. Serum calcium and phosphorous levels are normal in these patients (1,2). Microlith can be identified in sputum, bronchoalveolar lavage, and transbronchial biopsy specimens (1,3). Symptoms are less severe in these patients than in radiological findings (2). In the PA chest radiography, the appearance of common thin calcific micronodules called sandstorm in both lungs may be observed (1). Thorax CT may show microcalcification, ground-glass opacities, parenchymal bands, prominent fissure, and paraseptal emphysema (8). CT findings may be similar to those of miliary histoplasmosis, interstitial lung disease, pneumoconiosis, pulmonary amyloidosis, and military tuberculosis. In case of doubt in the diagnosis, Tc-99m MDP bone scintigraphy may be performed. Tc-99m MDP bone scintigraphy shows widespread radioactivity involvement in the lungs. In the presence of scintigraphic findings, the need for biopsy may be eliminated. This specific finding assists the clinician in the differential diagnosis of PAM (1,2,3).

Ethics

Informed Consent: Written informed consent was obtained.

Peer-review: Externally peer-reviewed.

Authorship Contributions

Surgical and Medical Practices: A.E.Ş., Z.A., Concept: Ö.Ş., Design: Ö.Ş., B.K., Data Collection or Processing: A.E.Ş., Ç.E., Analysis or Interpretation: Ö.Ş., B.K., Literature Search: A.E.Ş., Z.A., Ç.E., Writing: A.E.Ş., Ö.Ş., B.K.

Conflict of Interest: No conflict of interest was declared by the authors.

Financial Disclosure: The authors declared that this study received no financial support.

References

1. Kashyap S, Mohapatra PR. Pulmonary alveolar microlithiasis. Lung India 2013;30:143-147.
2. Alkhankan E, Yamin H, Bukamur H, Alkhankan F, Shweihat Y, Zeid F. Pulmonary alveolar microlithiasis diagnosed with radiography, CT, and bone scintigraphy. Radiol Case Rep 2019;14:775-777.
3. Arpağ H, Sayan M, Atilla N, Bozkuş F, Bahar AY, Kahraman H, Tokur M. A case of pulmonary alveolar microlithiasis diagnosed by transbronchial biopsy. Turk Thorac J 2017;18:134-136.
4. Simon CT, Lewis TC, Neemuchwala F, Arteta M, Rabah R. Pulmonary alveolar microlithiasis: a case report with a novel mutation in the SLC34A2 gene and review of the literature. Human Pathology: Case Reports 2018;13:33-35.
5. Ferreira Francisco FA, Pereira e Silva JL, Hochhegger B, Zanetti G, Marchiori E. Pulmonary alveolar microlithiasis. State-of-the-art review. Respir Med 2013;107:1-9.
6. Castellana G, Castellana G, Gentile M, Castellana R, Resta O. Pulmonary alveolar microlithiasis: review of the 1022 cases reported worldwide. Eur Respir Rev 2015;24:607-620.
7. Basu S, Shah M, Joshi JM, Lad S. Imaging calcific concretions of pulmonary alveolar microlithiasis with PET: insight into disease pathophysiology. Clin Nucl Med 2012;37:707-708.
8. Tanrıkulu AÇ, Dağlı AC, Şenyiğit A, Nazaroğlu H, Babayiğit C. Pulmonary alveolar microlithiasis: radiologic findings of eight cases in Turkey. Turkiye Klinikleri J Med Sci 2010;30:713-720.

Interesting Image
Mol Imaging Radionucl Ther 2022;31:154-156 DOI:10.4274/mirt.galenos.2021.95914

Mesenteric Panniculitis Appears as Metastatic Disease on ^{18}F-FDG-PET/CT Scan

^{18}F-FDG-PET/BT Görüntülemesinde Metastaz Düşündüren Mezenterik Pannikülit Olgusu

Özgül Ekmekçioğlu[1], Selim Bakan[2], Kerim Sönmezoğlu[3]

[1]*University of Health Sciences Turkey, Şişli Hamidiye Etfal Training and Research Hospital, Clinic of Nuclear Medicine, İstanbul, Turkey*
[2]*İstanbul University-Cerrahpaşa, Cerrahpaşa Faculty of Medicine, Department of Radiology, İstanbul, Turkey*
[3]*İstanbul University-Cerrahpaşa, Cerrahpaşa Faculty of Medicine, Department of Nuclear Medicine, İstanbul, Turkey*

Abstract

Mesenteric panniculitis is a rare benign inflammatory process involving mesenteric adipose tissue and the pathogenesis is still unknown. It may present ^{18}Fluorine-fluorodeoxyglucose (^{18}F-FDG) uptake and appear like a malign tumor or metastatic disease. We report a case of 47 year-old woman with serous ovarian adenocarcinoma demonstrating intense ^{18}F-FDG uptake and hyperdense nodularity in mesenteric fatty tissue on post-chemotherapy positron emission tomography/computed tomography imaging. The serum tumor marker (CA-125) level was within the normal range. A correlative magnetic resonance imaging highlighted the diagnosis of mesenteric panniculitis that was also confirmed by clinical follow-up.

Keywords: Mesenteric panniculitis, PET/CT, ovary carcinoma

Öz

Mezenterik pannikülit mezenterik yağlı dokunun nadir görülen ve benign karakterli enflamatuvar hastalığı olup patogenezi halen tam olarak bilinmemektedir. ^{18}Flor-florodeoksiglukoz (^{18}F-FDG) tutulumu gösterip, malignite veya metastatik hastalık gibi görünebilir. Seröz tipte over adenokarsinom tanısı bulunan 47 yaşında kadın hastanın kemoterapi sonrası pozitron emisyon tomografisi/bilgisayarlı tomografi görüntülemesinde mezenterik yağlı dokuda hiperdens nodüler görünüm ve ^{18}F-FDG tutulumu saptandı. Serum tümör marker (CA-125) normal düzeyde bulunan olguda, sonrasında yapılan manyetik rezonans görüntülemesinde mezenterik pannikülit tanısı takipte ve klinik olarak da doğrulandı.

Anahtar kelimeler: Mezenterik pannikülit, PET/BT, over kanseri

Address for Correspondence: Özgül Ekmekçioğlu MD, University of Health Sciences Turkey, Şişli Hamidiye Etfal Training and Research Hospital, Clinic of Nuclear Medicine, İstanbul, Turkey
Phone: +90 212 373 52 14 **E-mail:** ozgulek@gmail.com ORCID ID: orcid.org/0000-0002-3313-8087
Received: 13.11.2020 **Accepted:** 13.02.2021

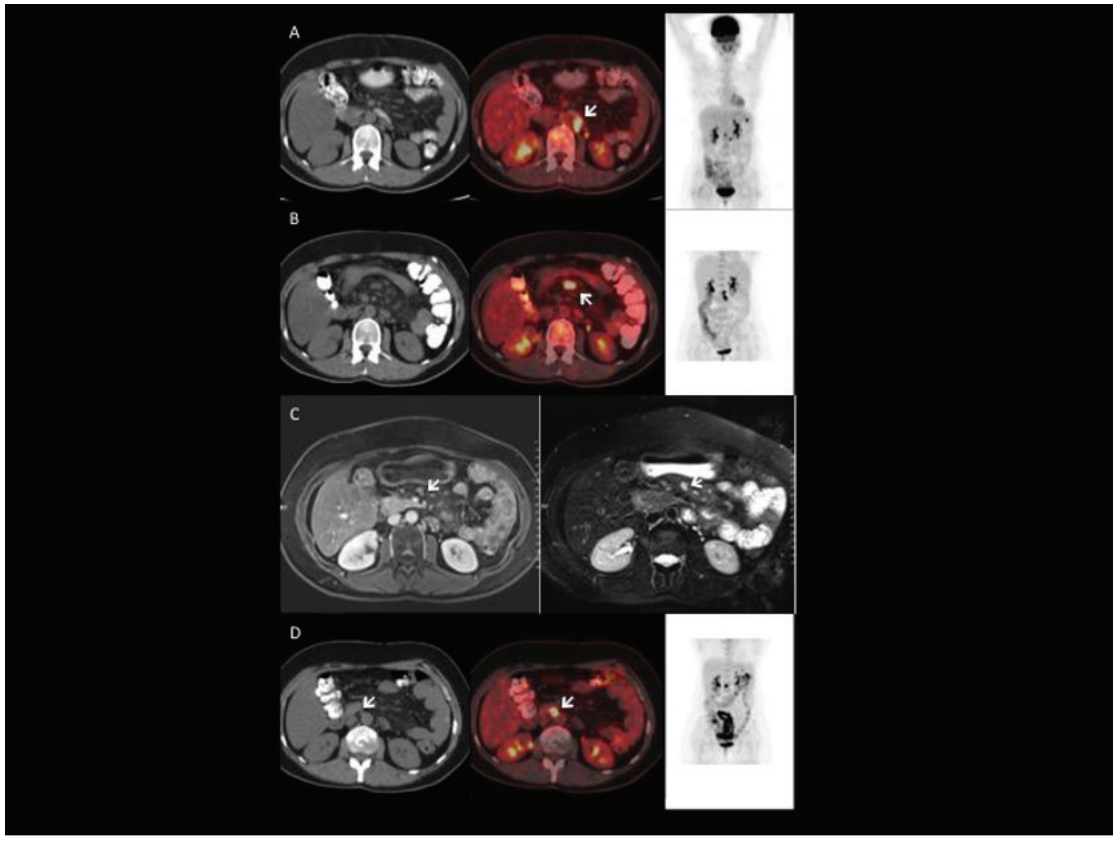

Figure 1. The first positron emission tomography/computed tomography (PET/CT) scan was performed for restaging purposes due to increased (CA-125) level (70 U/mL) is shown in the upper row.There were several enlarged lymph nodes with intense ^{18}Fluorine-fluorodeoxyglucose (^{18}F-FDG) uptake in the left aortic and interaortocaval regions [maximum standardized uptake value (SUV_{max}:11.6)] of the abdomen (A). Post-therapeutic PET/CT study done after 8 cycles of chemotherapy is seen in the second row and showed complete metabolic regression of all metastatic lesions seen on the previous scan. However, a few new lesions with intense ^{18}F-FDG accumulation were observed in the mesenteric region (SUV_{max}: 13.4) (B), despite normal ranged tumor markers at that time. To provide further lesion characterization, a magnetic resonance imaging (MRI) was performed and revealed hyperintense nodular lesions in the superior mesenteric region on T2 weighted fat saturated images, all of which also demonstrated contrast enhancement with no vessel invasion on T1 weighted fat saturated post-contrast images. These findings were suggestive of mesenteric panniculitis, rather than malignancy (C) (1). After one year clinical follow-up without any treatment and any severe clinical problem, PET/CT scan was repeated as CA-125 levels increased up to 192 U/mL and showed multiple hypermetabolic lymphadenopathies (SUV_{max}: 21.6) in the interaortocaval area and some hypermetabolic implants in the peritoneal surfaces of the abdomen, suggesting recurrent disease. On the contrary, mesenteric ^{18}F-FDG uptake that was detected on previous PET/CT scan due to panniculitis was completely resolved, as reported in the most cases in other reports (D) (2).

The etiology of mesenteric panniculitis is still unknown but the history of abdominal trauma or surgical operation has been reported. Other causes may also be responsible (3,4). The CT findings are reported to vary depending on the stage of the disease but even mesenteric vessels are displaced and surrounded by the involved fat, there is no vessel invasion. Thereby MRI will be more useful for evaluation of vessel invasion and differential diagnosis (5,6). In a study, a group of 19 patients with a history of different malignancies was investigated by ^{18}F-FDG-PET/CT study for the recent diagnosis of mesenteric panniculitis on abdominal CT imaging. Among these, 11 patients with no ^{18}F-FDG uptake in the abdomen had no active malignancy during follow-up, whereas 7 of 8 patients who had increased ^{18}F-FDG uptake were associated with tumor involvement. Therefore, it was concluded that ^{18}F-FDG PET/CT scan can be used to differentiate malignant involvement in patients with mesenteric panniculitis (7). However, there was one patient in that study, who was diagnosed with rectal carcinoma, with no tumor involvement and false positive ^{18}F-FDG uptake, similar to our case. Another case with non-Hodgkin lymphoma has also demonstrated false ^{18}F-FDG uptake that was compatible with mesenteric panniculitis (8). In conclusion, it should be kept in mind that increased ^{18}F-FDG uptake in mesenteric region might be related to inflammatory lesions like panniculitis.

Ethics

Informed Consent: It was obtained from the patient.

Peer-review: Externally and internally peer-reviewed.

Authorship Contributions

Surgical and Medical Practices: K.S., S.B., Concept: Ö.E., S.B., K.S., Design: Ö.E., K.S., Data Collection or Processing: Ö.E., Analysis or Interpretation: S.B., K.S., Literature Search: Ö.E., Writing: O.E.

References

1. Biscaldi E, Romairone E, Rollandi GA. Regarding six cases of mesenteric panniculitis: US, spiral CT, magnetic resonance. Radiol Med 2002;103:511-518.
2. Delgado Plasencia L, Rodríguez Ballester L, López-Tomassetti Fernández EM, Hernández Morales A, Carrillo Pallarés A, Hernández Siverio N. Paniculitis mesentérica: experiencia en nuestro centro [Mesenteric panniculitis: experience in our center]. Rev Esp Enferm Dig 2007;99:291-297.
3. Emory TS, Monihan JM, Carr NJ, Sobin LH. Sclerosing mesenteritis, mesenteric panniculitis and mesenteric lipodystrophy: a single entity? Am J Surg Pathol 1997;21:392-398.
4. Pahuja D, Eustace M, Chadha P. Mesenteric panniculitis: an unusual initial presentation of systemic lupus erythematosus (SLE). Internet J Rheumatol 2005;2:1-5.
5. Mata JM, Inaraja L, Martin J, Olazabal A, Castilla MT. CT features of mesenteric panniculitis. J Comput Assist Tomogr 1987;11:1021-1023.
6. Kobayashi S, Takeda K, Tanaka N, Hirano T, Nakagawa T, Matsumoto K. Mesenteric panniculitis: MR findings. J Comput Assist Tomogr 1993;17:500-502.
7. Zissin R, Metser U, Hain D, Even-Sapir E. Mesenteric panniculitis in oncologic patients: PET-CT findings. Br J Radiol 2006;79:37-43.
8. Sideras PA, Patil V, Li Z, Heiba S, Kostakoglou L. PET-CT of mesenteric panniculitis: a potential confounder of lymphoma. Radiography 2015;21:51-53.

Interesting Image
Mol Imaging Radionucl Ther 2022;31:157-159 DOI:10.4274/mirt.galenos.2021.87487

Multiple Subcutaneous ^{18}F-FDG-avid Granulomas Due to Enoxaparin Injection

Enoksaparin Enjeksiyonuna Bağlı Gelişen Yoğun ^{18}F-FDG Tutan Multipl Subkütan Granülomlar

Özge Erol Fenercioğlu, Nurhan Ergül, Ediz Beyhan, Rahime Şahin, Tevfik Fikret Çermik

University of Health Sciences Turkey, İstanbul Training and Research Hospital, Clinic of Nuclear Medicine, İstanbul, Turkey

Abstract

A 67-year-old female patient with metastatic gastric adenocarcinoma was referred to ^{18}fluorine-fluorodeoxyglucose (^{18}F-FDG) positron emission tomography/computed tomography (PET/CT) for restaging. PET/CT revealed liver metastasis and the patient received six-cycles of chemotherapy. On control ^{18}F-FDG PET/CT the liver lesion disappeared but newly formed multiple foci of increased uptake in the subcutaneous adipose tissues of the abdominal wall were detected. The uptake was related to nodular lesions resulting from an idiosyncratic reaction to enoxaparin and from local trauma through repeated injections.

Keywords: Enoxaparin, granuloma, ^{18}F-FDG PET/CT

Öz

Metastatik mide adenokarsinomu tanılı 67 yaşında kadın hastaya yeniden evreleme amacıyla ^{18}flor-florodeoksiglukoz (^{18}F-FDG) pozitron emisyon tomografisi/bilgisayarlı tomografi (PET/BT) çekimi yapıldı. PET/BT'de karaciğer metastazı saptandı ve hasta altı kür kemoterapi aldı. Kontrol ^{18}F-FDG PET/BT'de karaciğer lezyonu kayboldu, ancak karın duvarında subkütan yağlı dokularda yeni oluşan çok sayıda artmış ^{18}F-FDG tutulum odağı tespit edildi. Artmış tutulum, enoksaparine bağlı reaksiyondan kaynaklanan nodüler lezyonlarla ve ayrıca tekrarlanan enjeksiyonlara bağlı lokal travmayla ilişkili bulundu.

Anahtar kelimeler: Enoksaparin, granülom, ^{18}F-FDG PET/BT

Address for Correspondence: Nurhan Ergül Assoc. Prof., University of Health Sciences Turkey, İstanbul Training and Research Hospital, Clinic of Nuclear Medicine, İstanbul, Turkey
Phone: +90 505 886 08 11 **E-mail:** nurhanergul@yahoo.com ORCID ID: orcid.org/0000-0002-8214-9743
Received: 07.10.2020 **Accepted:** 15.02.2021

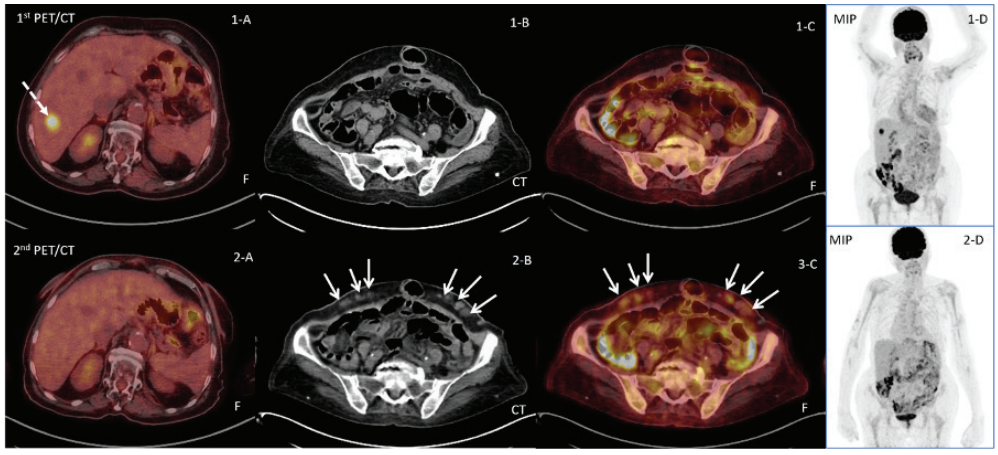

Figure 1. A 67-year-old female patient with metastatic gastric adenocarcinoma was admitted to our hospital for restaging ^{18}fluorine-fluorodeoxyglucose (^{18}F-FDG) positron emission tomography/computed tomography (PET/CT). The patient had undergone total gastrectomy (T2N2M0) 18 months earlier and then received radiotherapy. PET/CT revealed one ^{18}F-FDG-avid metastatic lesion in the liver (1st PET/CT; dashed arrow). After six-cycles of chemotherapy, the second PET/CT imaging was performed for therapy response. In this imaging, metastatic lesion disappeared in the liver, but PET/CT demonstrated newly formed multiple focal increased uptakes of ^{18}F-FDG in the subcutaneous adipose tissues of the abdominal wall with the largest dimension of 2.1 cm and the highest maximum standardized uptake value of 4.5 (2nd PET/CT; arrows).

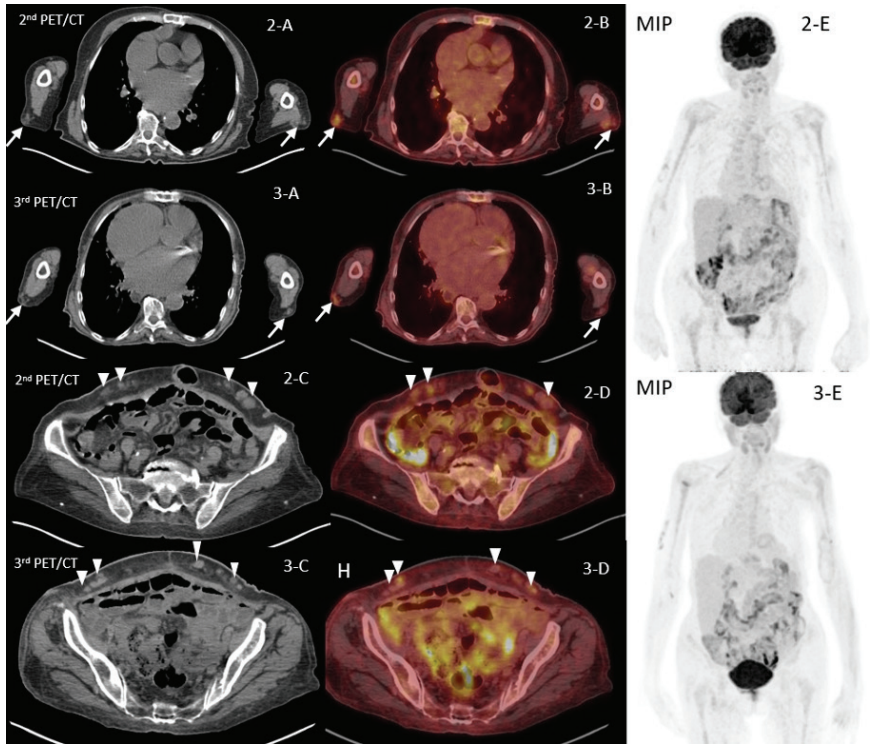

Figure 2. The patient continued to receive chemotherapy and after 7 months, a third follow-up 18F-FDG was performed. There were no new metastatic lesion in whole body, however the subcutaneous hypermetabolic lesions remained existed on the anterior abdominal wall (arrowheads) and bilateral arms (arrows) at different localizations from the second PET/CT related to continuing enoxaparin injection. Subcutaneous metastasis from gastric cancer is a rare manifestation, with a reported incidence of 0.8-1.0% (1). The most commonly reported origins of cutaneous metastasis are lung, breast and colon cancer, melanoma, squamous cell carcinoma of the oral cavity and renal cell carcinoma (2). The patient had a history of mitral valve replacement and switched from injection therapy with heparin to enoxaparin between the first and second PET/CT imaging. Although these nodules can simulate metastasis, in this case, since the liver lesion was disappeared after chemotherapy, the increased 18F-FDG uptake at the subcutaneous injection sites was not evaluated in favor of metastasis. These nodular lesions may result from an idiosyncratic reaction to enoxaparin and from local trauma through repeated injections as a promoting factor (3). A careful and detailed clinical history is needed to prevent misdiagnosis in PET/CT evaluation.

Ethics

Informed Consent: The written and verbal consent has been received before the PET/CT scan.

Peer-review: Externally peer-reviewed.

Authorship Contributions

Surgical and Medical Practices: Ö.E.F., N.E., E.B., R.Ş., T.F.Ç., Concept: Ö.E.F., N.E., E.B., R.Ş., T.F.Ç., Design: Ö.E.F., N.E., E.B., R.Ş., T.F.Ç., Data Collection or Processing: Ö.E.F., N.E., E.B., R.Ş., T.F.Ç., Analysis or Interpretation: Ö.E.F., N.E., E.B., R.Ş., T.F.Ç., Literature Search: Ö.E.F., N.E., E.B., R.Ş., T.F.Ç., Writing: Ö.E.F., N.E., E.B., R.Ş., T.F.Ç.

Conflict of Interest: No conflict of interest was declared by the authors.

Financial Disclosure: The authors declared that this study received no financial support.

References

1. Kawai S, Nishida T, Hayashi Y, Ezaki H, Yamada T, Shinzaki S, Miyazaki M, Nakai K, Yakushijin T, Watabe K, Iijima H, Tsujii M, Nishida K, Takehara T. Choroidal and cutaneous metastasis from gastric adenocarcinoma. World J Gastroenterol 2013;19:1485-1488.
2. Alcaraz I, Cerroni L, Rütten A, Kutzner H, Requena L. Cutaneous metastases from internal malignancies: a clinicopathologic and immunohistochemical review. Am J Dermatopathol 2012;34:347-393.
3. Val D, Val-Bernal J. Subcutaneous infiltrative nodule at the injection site of low-molecular weight heparin simulating malignancy. Am J Dermatopathol 2014;36:397-401.

Interesting Image
Mol Imaging Radionucl Ther 2022;31:160-162 DOI:10.4274/mirt.galenos.2021.16013

Two Cases of Acrometastasis from Lung Cancer Revealed on ^{18}F-FDG PET/CT

^{18}F-FDG PET/BT ile Gösterilen Akciğer Kanserine Bağlı İki Akrometastaz Olgusu

Rahime Şahin, Özge Erol Fenercioğlu, Ediz Beyhan, Nurhan Ergül, Tevfik Fikret Çermik

University of Health Sciences Turkey, İstanbul Training and Research Hospital, Clinic of Nuclear Medicine, İstanbul, Turkey

Abstract

We present 2 cases of acrometastases that manifest as the first signs of underlying lung cancer. The first case is 37 year-old-man misdiagnosed and treated as having a traumatic fracture at the left thumb. The second case is a 77 year-old-man who received treatment for soft tissue infection at left hand for 4 weeks. In both cases ^{18}fluorine-fluorodeoxyglucose positron emission tomography/computed tomography demonstrated primary malignant lesions in the lungs consistent with primary lung cancer with acrometastases.

Keywords: Acrometastasis, lung carcinoma, bone metastasis, PET/CT, ^{18}F-FDG-PET

Öz

Altta yatan akciğer kanserinin ilk bulgusu olarak ortaya çıkan iki akrometastaz olgusu sunuyoruz. İlk olgu sol el baş parmağında travmaya bağlı kırık teşhisiyle bir süre tedavi almış olan 37 yaşında erkek hastadır. İkinci olgu sol elinde yumuşak doku enfeksiyonu tanısıyla 4 hafta tedavi almış olan 77 yaşında erkek hastadır. Her iki olguya ait akral metastazların primer kaynağının akciğer olduğu ^{18}flor-florodeoksiglukoz pozitron emisyon tomografisi/bilgisayarlı tomografi ile gösterildi.

Anahtar kelimeler: Akrometastaz, akciğer kanseri, kemik metastazı, PET/BT, ^{18}F-FDG-PET

Address for Correspondence: Rahime Şahin MD, University of Health Sciences Turkey, İstanbul Training and Research Hospital, Clinic of Nuclear Medicine, İstanbul, Turkey
Phone: +90 212 459 60 00 **E-mail:** rahimesahin@yahoo.com ORCID ID: orcid.org/0000-0002-5062-4538
Received: 30.11.2020 **Accepted:** 03.03.2021

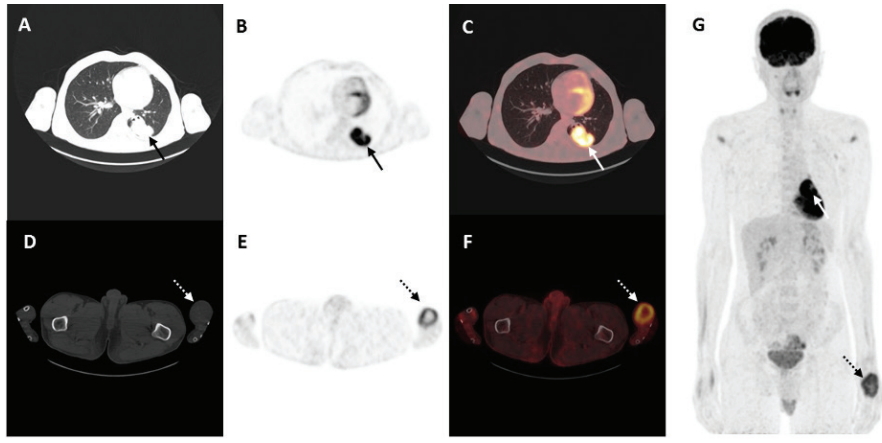

Figure 1. A 37 year-old-man presented with pain and swelling of his left thumb. He previously had a plaster cast treatment for two months considered as a traumatical fracture. His pain got persistent and the mass at the left thumb grew gradually. According to the radiological features, biopsy was planned suspicion of bone metastasis. In tissue samples taken from the first metacarpal bone and related soft tissue, histopathology showed a high-grade neuroendocrine tumor metastasis, likely originating from the lung. The patient was referred to ^{18}fluorine-fluorodeoxyglucose (^{18}F-FDG) positron emission tomography/computed tomography (PET/CT) to search for the underlying primary tumor. There was a mass lesion in the posterobasal segment of the left lung 4.3x3.6 cm size with intense ^{18}F-FDG uptake, consistent with primary lung cancer (arrow). The metastatic lesion at the left first metacarpal region also showed intense uptake (dash arrow). There was no other pathological hypermetabolic focus at any point of the body.

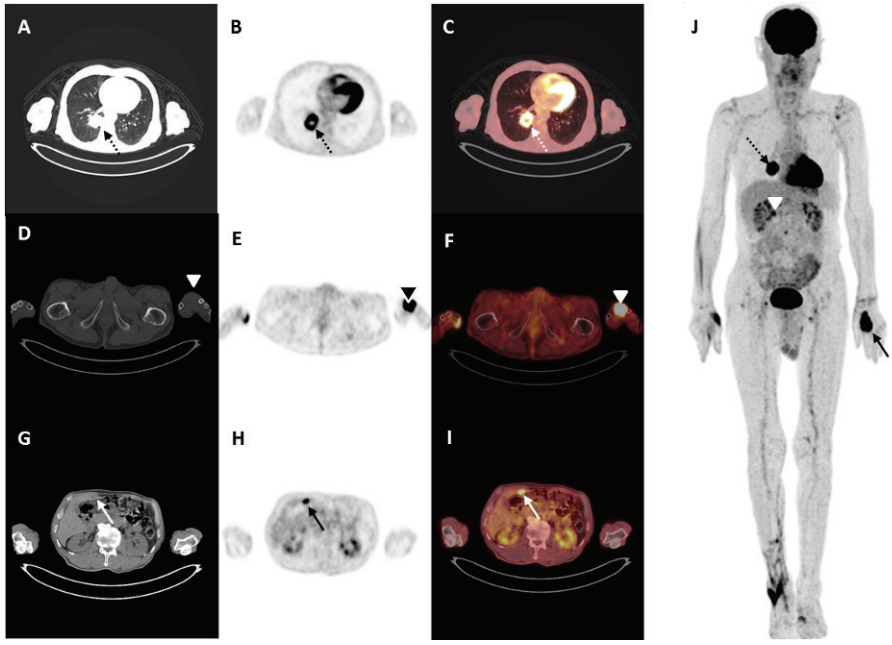

Figure 2. A 77 year-old-man presented with an open wound and a mass lesion on his left hand mimicking a soft tissue infection. Because the enlarging mass did not respond to any treatment, the patient underwent open biopsy. Histopathology revealed metastasis from squamous cell lung cancer. The patient was referred to ^{18}F-FDG PET/CT for diagnosis and staging. PET/CT demonstrated the primary malign tumor in the inferior lobe of the right lung 3.4x4.1 cm size with intense ^{18}F-FDG uptake (dash arrow). In addition to the metastatic lesion at the second metacarpal region of the left hand, PET/CT showed metastases in the right hand thumb region (arrow head) and left lobe of the liver (arrow) with intense ^{18}F-FDG uptake. The accumulation on the right foot ankle was related to the injection site. Acrometastasis is the first sign of cancer in approximately 25% of cases and is a common finding in diffuse metastatic disease . Early diagnosis enables early treatment and positively affects the patient's quality of life (1). Acrometastasis as the first manifestation of an occult neoplasm, can be mistaken for more common benign lesions, resulting in inappropriate management (2). Main symptoms are heat, redness, swelling, tenderness, and intermittent pain in the extremity (3,4). Osteomyelitis, gouty arthritis, pyogenic granuloma, tuberculous dactylitis, and primary skin malignancies should be considered in the differential diagnosis. acrometastasis is most commonly caused by lung, kidney, breast and colon cancers, in turn (4). The mean survival time of patients with acrometastasis is 7 months, reflecting a poor prognosis (4). Since acrometastases are rare, no standard treatment protocol has yet been established. Because the prognosis is poor, treatment is planned palliative; such as ideal tumor resection, preservation of hand functions, elimination of pain and rapid recovery (5).

Ethics

Informed Consent: The written and verbal constant has been obtained before the PET/CT scan.

Peer-review: Externally peer-reviewed.

Authorship Contributions

Surgical and Medical Practices: R.Ş., Ö.E.F., E.B., N.E., T.F.Ç., Concept: R.Ş., Ö.E.F., E.B., N.E., T.F.Ç., Design: R.Ş., Ö.E.F., E.B., N.E., T.F.Ç., Data Collection or Processing: R.Ş., Ö.E.F., E.B., N.E., T.F.Ç., Analysis or Interpretation: R.Ş., Ö.E.F., E.B., N.E., T.F.Ç., Literature Search: R.Ş., Ö.E.F., E.B., N.E., T.F.Ç., Writing: R.Ş., Ö.E.F., E.B., N.E., T.F.Ç.

References

1. Muñoz-Mahamud E, Combalia A, Carreño A, Arandes JM. Five cases of acrometastasis to the hand from a carcinoma and review of the literature. Hand Surg Rehabil 2017;36:12-16.
2. Long LS, Brickner L, Helfend L, Wong T, Kubota D. Lung cancer presenting as acrometastasis to the finger: a case report. Case Rep Med 2010;2010:234289.
3. Machado V, San-Julian M. Prognosis and treatment of acrometastases: observational study of 35 cases treated in a single institution. Rev Esp Cir Ortop Traumatol (Engl Ed) 2019;63:49-55.
4. Stomeo D, Tulli A, Ziranu A, Perisano C, De Santis V, Maccauro G. Acrometastasis: a literature review. Eur Rev Med Pharmacol Sci 2015;19:2906-2915.
5. Mavrogenis AF, Mimidis G, Kokkalis ZT, Karampi ES, Karampela I, Papagelopoulos PJ, Armaganidis A. Acrometastases. Eur J Orthop Surg Traumatol 2014;24:279-283.

Interesting Image
Mol Imaging Radionucl Ther 2022;31:163-165 DOI:10.4274/mirt.galenos.2021.42650

Imaging Features of Breast Plasmacytoma

Meme Plazmositomunun Görüntüleme Özellikleri

Şeyma Babaoğlu[1], Necdet Poyraz[1], Buğra Kaya[2], Sıddıka Fındık[3], Sinan Demircioğlu[4]

[1]*Necmettin Erbakan University, Meram Faculty of Medicine, Department of Radiology, Konya, Turkey*
[2]*Necmettin Erbakan University, Meram Faculty of Medicine, Department of Nuclear Medicine, Konya, Turkey*
[3]*Necmettin Erbakan University, Meram Faculty of Medicine, Department of Pathology, Konya, Turkey*
[4]*Necmettin Erbakan University, Meram Faculty of Medicine, Department of Hematology, Konya, Turkey*

Abstract

Extramedullary plasmacytoma (EMP) occurs as a result of abnormal proliferation of plasma cells outside the bone marrow. Breast plasmacytomas are rare. Radiologically, they can be confused with benign and malignant lesions of the breast. It is important to be able to diagnose EMP in the breast since the treatment strategy is different from that of other lesions and allows for the diagnosis and early treatment of multiple myeloma (MM) relapse. We report imaging and clinicopathological findings of an EMP case in which a 65-year-old patient with MM in remission presented with breast masses.

Keywords: PET/CT, plasmacytoma, breast, ultrasonography, mammography

Öz

Ekstramedüller plazmositom (EMP), plazma hücrelerinin kemik iliği dışında anormal proliferasyonu sonucu meydana gelir. Meme plazmositomu nadir görülür. Radyolojik olarak memenin benign ve malign lezyonlarıyla karışabilmektedir. Memede EMP tanısını koyabilmek önemlidir, çünkü diğer lezyonlarla tedavi stratejisi farklıdır ve multipl miyelom (MM) relapsının tanınıp erken tedavisine olanak sağlar. Bu yazıda 65 yaşında MM tanılı hastanın meme lezyonuyla prezente olduğu EMP olgusunun görüntüleme ve klinikopatolojik bulguları sunulmuştur.

Anahtar kelimeler: PET/BT, plazmositom, meme, ultrasonografi, mamografi

Address for Correspondence: Şeyma Babaoğlu MD, Necmettin Erbakan University, Meram Faculty of Medicine, Department of Radiology, Konya, Turkey
Phone: +90 554 666 83 39 **E-mail:** seymababaoglu@hotmail.com ORCID ID: orcid.org/0000-0002-4788-4734
Received: 06.02.2021 **Accepted:** 17.03.2021

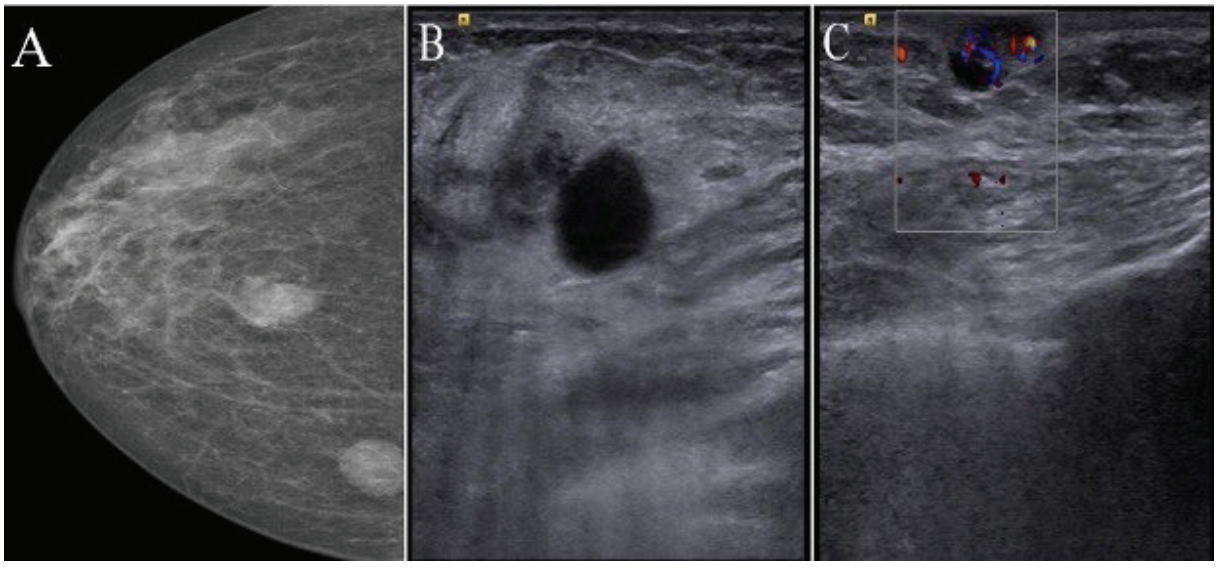

Figure 1. A 65-year-old female patient diagnosed with multiple myeloma (MM), who was followed up in remission, was admitted to the hospital with a complaint of mass in the right breast. In the mammography (A), two well-circumscribed, oval-shaped lesions with equal density to the fibro-glandular tissue were observed in the upper inner quadrant of the right breast. Ultrasonography (US) showed (B) a well-circumscribed markedly hypoechoic (pseudo-cystic appearance) 9x10 mm and 3x2 mm lesions with posterior acoustic enhancement (C). Color Doppler US showed increased vascularity in these lesions. US findings of breast plasmacytoma; in line with our case, are circumscribed margin, pseudo-cystic appearance and internal vascularity in Doppler US. Microcalcification and lymphadenopathy were not expected findings (1,2). However, the US imaging findings are variable and not specific, therefore, US-guided core needle breast biopsy was performed for histopathological diagnosis (3).

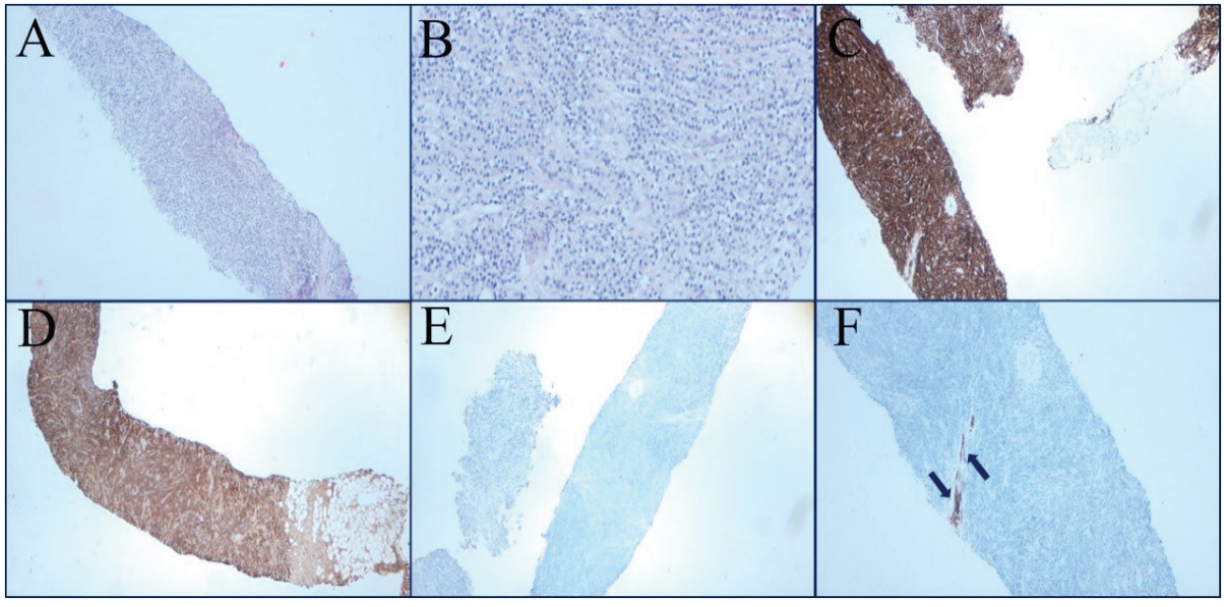

Figure 2. Histopathological analysis. Microscopy revealed plasma cell infiltration (A x40, B x100, hematoxylin-eosin stain). Tumor cells were positive for immunohistochemical CD-138 and kappa (C and D, x20). Lambda and pancytokeratin were negative (E and F, x20). The breast ductus between tumor cells appeared as positive (F, arrows). The pathology result was compatible with extramedullary plasmacytoma (EMP).

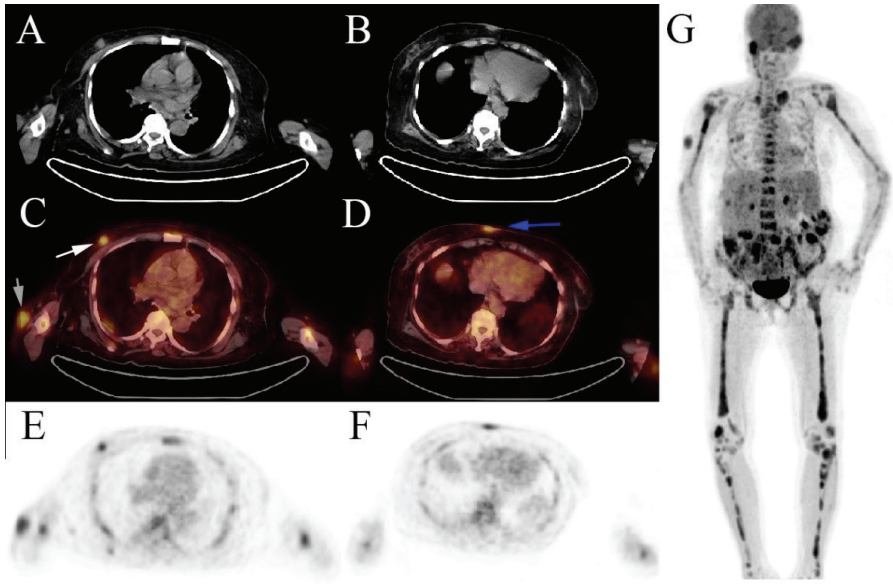

Figure 3. Positron emission tomography/computed tomography (PET/CT) has been found to be useful in detecting extramedullary involvement and disease extension in MM (4,5). The International Myeloma Working Group recommends ^{18}fluorine-fluorodeoxyglucose (^{18}F-FDG)-PET combined with CT or magnetic resonance imaging to monitor treatment response and detect extramedullary involvement (1,2,6). In our patient, in axial CT (A, B), fusion PET/CT (C, D) and PET images in ^{18}F-FDG PET/CT nodular lesions in soft tissue density in the right breast (E, F) showed ^{18}F-FDG uptake [white arrow, maximum standardized uptake value (SUV_{max}): 3.8; blue arrow, SUV_{max}: 3.6]. In addition, in axial sections (A, B, C, D, E, F) nodular lesion in the right arm and pleural thickening in the posterior part of the right hemithorax showed increased activity. In PET maximum intensity projection image (G), ^{18}F-FDG uptake in other areas (bilateral maxilla retrobulbar, bilateral proximal clavicular and common bone marrow) was also monitored. ^{18}F-FDG PET/CT whole-body screening ensured that lesions in other areas were shown. EMP in the breast is rare, although its frequency is not clear, with 63 cases corresponding to approximately 15 cases per year reported in 1928 and 2009 (1,3). The average incidence age is 53 and the vast majority of patients are women (7). Although 90% of EMP cases occur in the head and neck area, they are most commonly seen in the upper respiratory tract or oral cavity. It is important to distinguish breast plasmacytoma from benign and malignant breast lesions since its treatment is not surgical but through chemotherapy and/or local radiotherapy (2,8). Therefore, knowing the imaging features allows for accurate diagnosis and treatment.

Ethics

Informed Consent: It has received institutional ethics approval.

Peer-review: Externally and internally peer-reviewed.

Authorship Contributions

Surgical and Medical Practices: S.D., S.F., Concept: B.K., Design: N.P., Data Collection or Processing: Ş.B., Analysis or Interpretation: N.P., B.K., S.F., S.D., Literature Search: Ş.B., Writing: Ş.B.

Conflict of Interest: No conflict of interest was declared by the authors.

Financial Disclosure: The authors declared that this study received no financial support.

References

1. Eden JK, Borgen R, Haq R, Dobrashian R. A rare imaging case of bilateral plasmacytoma of the breast. BJR Case Rep 2020;6:20190131.
2. Park YM. Imaging findings of plasmacytoma of both breasts as a preceding manifestation of multiple myeloma. Case Rep Med 2016;2016:6595610.
3. Surov A, Holzhausen HJ, Ruschke K, Arnold D, Spielmann RP. Breast plasmacytoma. Acta Radiol 2010;51:498-504.
4. Lu YY, Chen JH, Lin WY, Liang JA, Wang HY, Tsai SC, Kao CH. FDG PET or PET/CT for detecting intramedullary and extramedullary lesions in multiple myeloma: a systematic review and meta-analysis. Clin Nucl Med 2012;37:833-837.
5. Durie BG, Waxman AD, D'Agnolo A, Williams CM. Whole-body (18) F-FDG PET identifies high-risk myeloma. J Nucl Med 2002;43:1457-1463.
6. Rajkumar SV, Dimopoulos MA, Palumbo A, Blade J, Merlini G, Mateos MV, Kumar S, Hillengass J, Kastritis E, Richardson P, Landgren O, Paiva B, Dispenzieri A, Weiss B, LeLeu X, Zweegman S, Lonial S, Rosinol L, Zamagni E, Jagannath S, Sezer O, Kristinsson SY, Caers J, Usmani SZ, Lahuerta JJ, Johnsen HE, Beksac M, Cavo M, Goldschmidt H, Terpos E, Kyle RA, Anderson KC, Durie BG, Miguel JF. International Myeloma Working Group updated criteria for the diagnosis of multiple myeloma. Lancet Oncol 2014;15:e538-e548.
7. Binesh F, Vahedian HA, Shabani M, Zare S, Shahcheraghi SH. Extramedullary plasmacytoma of the breast: A case report and literature review. Acta Med Iran 2018;56:204-207.
8. Lee HS, Kim JY, Kang CS, Kim SH, Kang JH. Imaging features of bilateral breast plasmacytoma as unusual initial presentation of multiple myeloma: case report and literature review. Acta Radiol Short Rep 2014;3:2047981614557666.

Interesting Image
Mol Imaging Radionucl Ther 2022;31:166-168 DOI:10.4274/mirt.galenos.2021.48243

Metabolic Activity of Neurogenic Heterotopic Ossification on ^{18}F-FDG PET/CT Matching with Ongoing Osteoblastic Activity on Bone Scan

^{18}F-FDG PET/BT'de Nörojenik Heterotopik Ossifikasyonun Metabolik Aktivitesi ile Kemik Taramasında Devam Eden Osteoblastik Aktivite Eşleşmesi

Matthieu Dietz, Jeremie Tordo

Hospices Civils de Lyon, Department of Nuclear Medicine, Lyon, France

Abstract

A 54-year-old man, with previous history of neurogenic heterotopic ossification (HO) in muscles around the left hip following a spinal cord injury ten months earlier, was referred to our nuclear medicine center for an ^{18}fluorine-fluorodeoxyglucose (^{18}F-FDG) positron emission tomography/computed tomography (PET/CT) to rule out a spondylodiscitis. No sign of spondylodiscitis was found on ^{18}F-FDG PET/CT, but images revealed an increased ^{18}F-FDG uptake in HO areas, matching with ongoing osteoblastic activity on a following bone scan.

Keywords: Heterotopic ossification, bone scan, ^{18}F-FDG PET/CT

Öz

On ay önce omurilik yaralanmasını takiben sol kalça çevresindeki kaslarda nörojenik heterotopik ossifikasyon (HO) öyküsü olan 54 yaşında bir erkek hasta, spondilodiskiti ekarte etmek için ^{18}flor-florodeoksiglukoz (^{18}F-FDG) pozitron emisyon tomografisi/bilgisayarlı tomografi (PET/BT) için nükleer tıp merkezimize sevk edildi. ^{18}F-FDG PET/BT'de spondilodiskit belirtisi bulunmadı, ancak görüntüler, sonraki kemik taramasında devam eden osteoblastik aktivite ile eşleşen, HO alanlarında ^{18}F-FDG tutulumunun arttığını ortaya koydu.

Anahtar kelimeler: Heterotopik ossifikasyon, kemik taraması, ^{18}F-FDG PET/BT

Address for Correspondence: Matthieu Dietz MD, Hospices Civils de Lyon, Department of Nuclear Medicine, Lyon, France
Phone: +41795569161 **E-mail:** matthieu.dietz@chu-lyon.fr ORCID ID: orcid.org/0000-0001-6041-2531
Received: 29.12.2020 **Accepted:** 10.04.2021

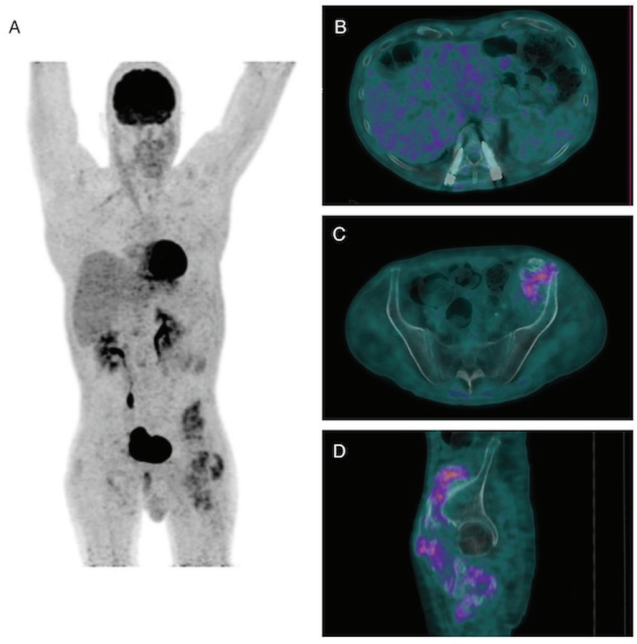

Figure 1. A 54-year-old man was referred to our nuclear medicine center for a combined ^{18}fluorine-fluorodeoxyglucose (^{18}F-FDG) positron emission tomography/computed tomography (PET/CT) to rule out a spondylodiscitis. He had a previous history ten months earlier of a thoracolumbar fracture complicated with paraplegia, treated with anterolateral decompression and fixation. He presented unexplained persistent lumbar pain and C-reactive protein level above the normal range after two successfully treated obstructive pyelonephritis, and a suspicion of spondylodiscitis was waived. The patient was known to present heterotopic ossification (HO) associated with the spinal cord injury with multiple areas of dense calcifications in the muscles around the left hip, as the anterior compartment of the thigh and iliopsoas muscle. No sign of spondylodiscitis was found on ^{18}F-FDG PET/CT (maximum intensity projection ^{18}F-FDG PET/CT image A, axial fused PET/CT image B), but images revealed a diffuse increased ^{18}F-FDG uptake in a few of HO areas (axial and sagittal fused PET/CT images C and D).

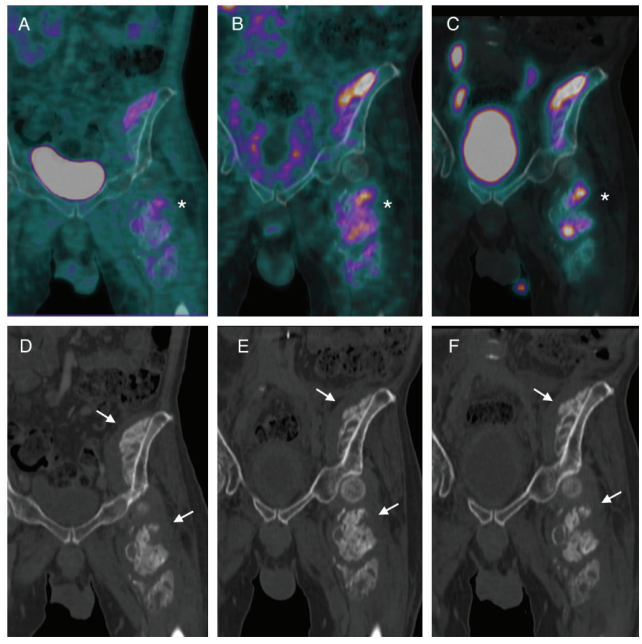

Figure 2. A complementary 3-phase bone scan was secondly performed. The bone scan showed extra-osseous extensive accumulations of technetium-99m (Tc-99m) hydroxymethylene diphosphonate matching with increased ^{18}F-FDG uptake areas. Coronal fused PET/CT image (A), coronal fused single photon emission computed tomography/CT images on soft-tissue phase (B) and on delayed phase (C), showing a matching tracer uptake between the two modalities in HO areas around the left hip (asterisks). On CT images, multiple areas of dense calcifications were seen (arrows, coronal CT images D, E, and F). HO is a diverse pathologic process, defined as the formation of extraskeletal bone in muscle and soft tissues, usually between the muscle and the joint capsule. The reported incidence of HO in patients with spinal cord injury is approximately 20% (1). Such development of neurogenic HO generally occurs within a few months after spinal cord injury and progresses over a period of years (2). Clinically, neurogenic HO may cause severe pain during the process of formation and adversely affecting quality of life (3). Three-phase bone scanning is a highly sensitive method for the assessment of progression, maturation process and extent of HO. An increased vascularity on angiographic flow and soft-tissue phases is the earlier sign. Then occurs Tc-99m methyl diphosphonate (MDP) accumulation on delayed-phase, which is often seen 4 to 6 weeks earlier than ossification (4). Three-phase bone scanning could be required for the clinical management of HO. Indeed, conservative treatment such as medication or local radiotherapy could be performed over surgical excision in case of high Tc-99m MDP accumulation (5). ^{18}F-FDG uptake in HO, suggestive of active inflammation, is known as a pitfall of ^{18}F-FDG PET/CT imaging. The concern, especially in early cases is that the imaging findings on FDG PET/CT could mimic that of aggressive sarcomas (6,7,8). Elucidating the antecedent history becomes important in making the current diagnosis in these patients.

Ethics

Informed Consent: A written informed consent was obtained.

Peer-review: Externally peer-reviewed.

Authorship Contributions

Concept: J.T., Design: J.T., Data Collection or Processing: M.D., J.T., Analysis or Interpretation: M.D., J.T., Literature Search: M.D., Writing: M.D., J.T.

Conflict of Interest: No conflict of interest was declared by the authors.

Financial Disclosure: The authors declared that this study received no financial support.

References

1. Wittenberg RH, Peschke U, Bötel U. Heterotopic ossification after spinal cord injury. Epidemiology and risk factors. J Bone Joint Surg Br 1992;74:215-218.
2. Meyers C, Lisiecki J, Miller S, Levin A, Fayad L, Ding C, Sono T, McCarthy E, Levi B, James AW. Heterotopic ossification: a comprehensive review. JBMR Plus 2019;3:e10172.
3. Cipriano CA, Pill SG, Keenan MA. Heterotopic ossification following traumatic brain injury and spinal cord injury. J Am Acad Orthop Surg 2009;17:689-697.
4. Freed JH, Hahn H, Menter R, Dillon T. The use of three-phase bone scan in the early diagnosis of heterotopic ossification (HO) and in the evaluation of Didronel therapy. Paraplegia 1982;20:208-216.
5. Lin Y, Lin WY, Kao CH, Tsai SC. Easy interpretation of heterotopic ossification demonstrated on bone SPECT/CT. Clin Nucl Med 2014;39:62-63.
6. Koob M, Durckel J, Dosch JC, Entz-Werle N, Dietemann JL. Intercostal myositis ossificans misdiagnosed as osteosarcoma in a 10-year-old child. Pediatr Radiol 2010;40:S34-37.
7. Clarençon F, Larousserie F, Babinet A, Zylbersztein C, Talbot JN, Kerrou K. FDG PET/CT findings in a case of myositis ossificans circumscripta of the forearm. Clin Nucl Med 2011;36:40-42.
8. Costelloe CM, Murphy WA Jr, Chasen BA. Musculoskeletal pitfalls in 18F-FDG PET/CT: pictorial review. AJR Am J Roentgenol 2009;193:WS1-WS13.

Interesting Image
Mol Imaging Radionucl Ther 2022;31:169-171 DOI:10.4274/mirt.galenos.2021.22590

Increased ^{18}F-FDG Uptake in the Axillary Lymph Nodes of the Vaccinated Side Associated with COVID-19 Vaccination

COVID-19 Aşılaması ile İlişkili Aşılı Tarafın Aksiller Lenf Nodlarında Artan ^{18}F-FDG Tutulumu

Yoichi Otomi[1], Saho Irahara[1], Hiroaki Inoue[2], Takayoshi Shinya[1], Hideki Otsuka[1], Masafumi Harada[1]

[1]*Tokushima University, Department of Radiology, Tokushima, Japan*
[2]*Tokushima University, Department of Thoracic and Endocrine Surgery and Oncology, Tokushima, Japan*

Abstract

A 50-year-old female patient underwent ^{18}fluorine-fluorodeoxyglucose (^{18}F-FDG) positron emission tomography/computed tomography (PET/CT) following modified radical mastectomy for cancer of the left breast. Ten days before the PET/CT, the coronavirus disease-2019 (COVID-19) vaccine was injected intramuscularly into the right deltoid muscle. Increased ^{18}F-FDG uptake of maximum standardized uptake value (11.0) was observed in the lymph nodes of the right axilla, which had not been observed in the previous PET/CT. The size of the oval-shaped lymph nodes was up to approximately 11×9 mm; however, it was larger than that observed on the previous PET/CT. We contemplate that the increased ^{18}F-FDG uptake was a reactive change in the lymph nodes associated with the COVID-19 vaccine.

Keywords: COVID-19, vaccination, ^{18}F-FDG PET/CT

Öz

Elli yaşında kadın hastaya sol meme kanseri nedeniyle modifiye radikal mastektomi sonrası ^{18}flor-florodeoksiglukoz (^{18}F-FDG) pozitron emisyon tomografisi/bilgisayarlı tomografi (PET/BT) uygulandı. PET/BT'den 10 gün önce, koronavirüs hastalığı-2019 (COVID-19) aşısı sağ deltoid kas içine enjekte edildi. Daha önceki PET/BT'de izlenmeyen, sağ aksilla lenf nodlarında maksimum standardize alım değeri (11,0) ^{18}F-FDG tutulumu artışı gözlendi. Oval şekilli lenf nodlarının boyutu yaklaşık olarak 11x9 mm'ye kadardı; ancak önceki PET/BT'de gözlemlenenden daha büyüktü. Artan ^{18}F-FDG tutulumunun, COVID-19 aşısıyla ilişkili olarak lenf nodlarındaki reaktif bir değişiklik olduğunu düşünüyoruz.

Anahtar kelimeler: COVID-19, aşı, ^{18}F-FDG PET/BT

Address for Correspondence: Yoichi Otomi MD, Tokushima University, Department of Radiology, Tokushima, Japan
Phone: +81-88-633-7173 **E-mail:** otomi.yoichi@tokushima-u.ac.jp ORCID ID: orcid.org/0000-0002-8960-3662
Received: 02.04.2021 **Accepted:** 12.05.2021

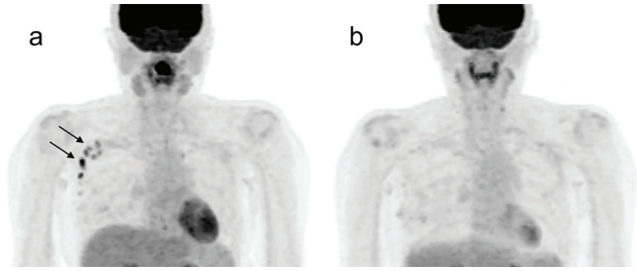

Figure 1. ^{18}Fluorine-fluorodeoxyglucose (^{18}F-FDG) positron emission tomography (PET) maximum intensity projection image of a 50-year-old female patient. ^{18}F-FDG PET/computed tomography (CT) performed 2 years and 10 months after surgery for cancer of the left breast shows several lymph nodes in the right axilla with increased ^{18}F-FDG uptake (arrows) (a). Ten days before the ^{18}F-FDG PET/CT was performed, the patient received the coronavirus disease-2019 (COVID-19) vaccine (Comirnaty, Pfizer-BioNTech), injected intramuscularly into the right deltoid muscle. The reactive change was considered to have been caused by the vaccine. No increased uptake in the axillary lymph nodes was seen on the ^{18}F-FDG PET/CT performed previously (1 year and 10 months after surgery) (b).

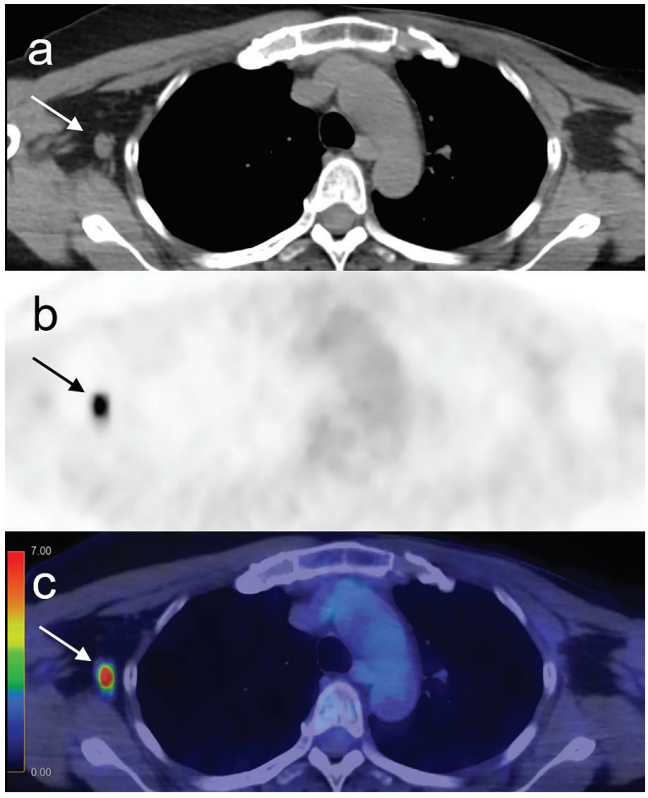

Figure 2. Axial CT (a), ^{18}F-FDG PET (b), ^{18}F-FDG PET/CT fusion image (c) at the axillary level. Lymph nodes with increased ^{18}F-FDG uptake [maximum standardized uptake value (SUV_{max}) 11.0] are seen in the right axilla (arrows). These lymph nodes were oval-shaped, and the hilum was seen in the largest of these lymph nodes. Their size was up to approximately 11×9 mm, which was larger than that observed on the ^{18}F-FDG PET/CT performed a year ago. Some studies have reported that COVID-19 vaccination increases the ^{18}F-FDG uptake in the axillary lymph nodes on the vaccinated side (1,2,3,4,5,6). To date, ^{18}F-FDG uptake in the lymph nodes has been reported to have a SUV_{max} of 4.5 and 9.4 (1,2); however, it was even higher in this case (SUV_{max} 11.0). Similar findings have been reported for influenza vaccinations (7,8). It is necessary to appropriately interpret these findings after injection of the influenza vaccine to avoid confusion with lymph node metastasis or lymphoproliferative diseases, such as malignant lymphoma. The same would also apply to the COVID-19 vaccination. Especially when the vaccine is injected intramuscularly on the ipsilateral side of the cancerous breast, it might be difficult to distinguish the reactive changes due to vaccination from metastasis of the breast cancer in the ^{18}F-FDG PET/CT images. Therefore, patients with breast cancer should be vaccinated in the deltoid muscle contralateral to the cancerous breast. In addition, when interpreting the ^{18}F-FDG PET/CT findings in patients who have received the COVID-19 vaccine, it should be noted that vaccination might cause increased uptake in the axillary lymph nodes on the vaccinated side. It is expected that the chances of interpretation of ^{18}F-FDG PET/CT images of patients who have been vaccinated against COVID-19 will increase rapidly. Hence, it is important to confirm the patient's recent vaccination history, site of vaccination, and the period since vaccination before the examination.

Ethics

Informed Consent: Written informed consent of the patient was obtained.

Peer-review: Externally peer-reviewed.

Authorship Contributions

Surgical and Medical Practices: Y.O., S.I., H.I., Concept: Y.O., S.I., Design: Y.O., S.I., Data Collection or Processing: Y.O., S.I., H.I., Analysis or Interpretation: Y.O., T.S., H.O., M.H., Literature Search: Y.O., S.I., Writing: Y.O.

Conflict of Interest: No conflict of interest was declared by the authors.

Financial Disclosure: The authors declared that this study received no financial support.

References

1. Johnson BJ, Van Abel KM, Ma DJ, Johnson DR. 18F-FDG-avid axillary lymph nodes after COVID-19 vaccination. J Nucl Med 2021;62:1483-1484.
2. Avner M, Orevi M, Caplan N, Popovtzer A, Lotem M, Cohen JE. COVID-19 vaccine as a cause for unilateral lymphadenopathy detected by 18F-FDG PET/CT in a patient affected by melanoma. Eur J Nucl Med Mol Imaging 2021;48:2659-2660.
3. Ahmed N, Muzaffar S, Binns C, Ilyas MW, Usmani S. COVID-19 Vaccination Manifesting as Incidental Lymph Nodal Uptake on 18F-FDG PET/CT. Clin Nucl Med 2021;46:435-436.
4. Nawwar AA, Searle J, Hagan I, Lyburn ID. COVID-19 vaccination induced axillary nodal uptake on [18F]FDG PET/CT. Eur J Nucl Med Mol Imaging 2021;48:2655-2656.
5. Xu G, Lu Y. COVID-19 mRNA vaccination-induced lymphadenopathy mimics lymphoma progression on FDG PET/CT. Clin Nucl Med 2021;46:353-354.
6. Eifer M, Eshet Y. Imaging of COVID-19 vaccination at FDG PET/CT. Radiology 2021;299:E248.
7. Panagiotidis E, Exarhos D, Housianakou I, Bournazos A, Datseris I. FDG uptake in axillary lymph nodes after vaccination against pandemic (H1N1). Eur Radiol 2010;20:1251-1253.
8. Thomassen A, Lerberg Nielsen A, Gerke O, Johansen A, Petersen H. Duration of 18F-FDG avidity in lymph nodes after pandemic H1N1v and seasonal influenza vaccination. Eur J Nucl Med Mol Imaging 2011;38:894-898.